Institut fur Nutzpflanzenwissenschaften und Ressourcenschutz (INRES)

Towards improved process representation for modelling CO_2 and H_2O fluxes of crops

Dissertation

zur Erlangung des Grades

Doktor der Agrarwissenschaften (Dr. agr.)

der Landwirtschaftlichen Fakultät

der

Rheinischen Friedrich-Wilhelms-Universität Bonn

vorgelegt von:

Thuy Huu Nguyen

aus Thai Binh, Vietnam

Bonn 2022

Referent: Prof. Dr. Frank Ewert
Korreferent: Prof. Dr. Matthias Langensiepen
Tag der mündlichen Prüfung: 22.02.2022
Angefertigt mit Genehmigung der Landwirtschaftlichen Fakultät der Universität Bonn

Acknowledgment

My PhD study involved many people whom I could not mention all names, help, and contribution in a single page of the paper.

First and foremost, I would like to express my heartfelt appreciation to Prof. Dr. Frank Ewert for accepting to be my first supervisor, for giving me fruitful ideas, burning discussion, helpful comments, and for assisting me to edit this thesis with an aim of its successful completion. My special thanks are to him for his confirmation in financial support, opportunities for networking and exchanging with other researchers.

I also wish to thank Prof. Dr. Matthias Langensiepen for his initial ideas in the research proposal, his support in the collection of field data, and relevant technical issues as well as constructive comments to former versions of the manuscripts. Without his support, completing this thesis would not have been possible.

I would like to sincerely acknowledge Dr. Hubert Hüging for his kindness, enthusiastic and technical support, and understanding throughout my PhD. I appreciated his hard work for the preparations of the field experiments, the long days of help to deal with sap flow installations as well as for traveling and management assistance. My fieldwork and data collection would not have been possible without his support.

The joined project could not be successfully fulfilled without the responsive and hard work from colleagues of the TR32 sub-projects B4 and B6. I would like to thank Prof. Jan Vanderborght, Prof. Andrea Schnepf, and Normen Hermes for their support and work on the rhizotrone facilities. My special thanks to Prof. Schnepf for accepting the responsibility as member of my TR32 doctoral committee. My great acknowledgment to Prof. Vanderborght for his constructive comments and helpful work on the modeling activities and the manuscript of my first paper. I also thank Miriam Zörner, Shehan Morandage, and Gaochao Cai for their work on irrigation and sheltering applications, soil and root data collection, and data provision.

My sincere appreciation goes to (Deutsche Forschungsgemeinschaft – DFG) for providing financial support for my studies in Germany. I would like to express my special thanks to TR32 staff, especially Prof. Dr. Clemens Simon, Dr. Insa Thiele-Eich, Mrs. Monica Faller, Mrs. Kremana Offenberg, and Mrs. Nadine Heinrich for their help, enthusiasm, and care regarding the funding issues and organizing research activities. Special gratitude to colleagues who worked on the Selhausen test site at the FZ Jülich, especially to Dr. Alexander Graf for his LICOR 8100 and technical help in CO_2 flux measurement and weather data provision.

I am grateful to Dr. Thomas Gaiser, Dr. Sabine Seidel, Dr. Cho Miltin Mboh, Dr. Heidi Webber, Dr. Amit Srivastava, Dr. Ixchel Hernandez, and Dr. Hella Ahrends for their comments and English revision of my chapters/thesis. My many thanks are to Moritz Kupisch, Anja Stadler for their helpful hand-on training in measurements and data processing. Technical support in the lab from Mrs. Petra Weber, Mrs. Sandra Damn was strongly appreciated. I also want to extend my thanks to Gunther Krause and Andreas Enders for their technical help in SIMPLACE. Many thanks devote to LAP colleagues, especially Mrs. Christine Tilly and Prof. Michael Frei, for their help. I enjoyed the work with my student assistants both in the lab and in the field, my appreciations go to David Bergmann, Julia Hackländer, Robin Cowper, Lucas Elizabeth, Moritz Kastrop, Izabela Kucharski, Marian Weigel, Sebastian Kneckt, Samira Bauerfeind, Kathrin Segbert, Clemens Stephany, Stephan Himmer, and John Bimi.

Summary

Exchange rates of CO_2 and H_2O between vegetation and the atmosphere are strongly linked by stomatal functions and leaf area growth. Crops under drought stress show different responses, such as stomatal regulations (short-term responses) and canopy adjustments (i.e., the change of leaf area). Stomatal behaviors are related to leaf water potential (Ψ_{leaf}) which can be grouped into two broad categories: anisohydric and isohydric. Anisohydric plants, such as winter wheat, keep their stomata open for longer time periods, independent from changes in the soil water supply, thereby inducing variable Ψ_{leaf}. Plants continue to transpire under drought resulting in a lower Ψ_{leaf} as compared to those grown under non-limited soil water conditions. Isohydric plants, such as maize, show a strong stomatal control of transpiration to maintain Ψ_{leaf} at a certain threshold. Much research has aimed at obtaining a better eco-physiological understanding of stomatal behavior as well as improved modeling of relevant processes to better understand stomatal regulation during water stress. However, such modeling activities are generally limited to the leaf level. Crop models and land surface models which are scaling leaf processes to the canopy level and simulating physiological processes of crop growth and yield. These models are used to predict gas fluxes at field and larger scales. However, their water flux modules are often simplified. Complex processes, such as stomatal regulations and associated underlying mechanisms (i.e., hydraulic signal), are considered in simplistic ways which require improvements. A better understanding of the crop-specific responses (e.g., winter wheat and maize) to variable water stress across different growing seasons and soil types is necessary in order to improve understandings in crop management, irrigation systems, crop water use efficiency, and yield. Further, using this knowledge for improving soil-plant models and crop models towards more accurate simulations of CO_2 and H_2O gas fluxes and crop yields, will allow for more reliable predictions of food production under variable weather conditions and climate change.

Data was collected at a field characterized by two contrasting soil types (stony and silty) and different water regimes (irrigated, rainfed, and drought) near the Research Center Jülich, Germany in 2015, 2016, 2017, and 2018. This thesis analysed and presented a unique and comprehensive data set on leaf water status, leaf and canopy CO_2 and H_2O gas fluxes and associated dynamic crop growth processes (leaf area, root growth, and crop biomass) for winter wheat and maize obtained under a wide range of soil water conditions. The first aim of this thesis was to gain a better understanding of the relationships between soil water availability and stomatal responses for different crops at various scales (leaf and canopy) through modelling studies and field experiments. The second aim was to use this knowledge

to potentially advance and improve the modelling of gas fluxes and crop growth by including a new modeling modul for simulating stomatal regulations (isohydric and anisohydric) and associated underlying mechanisms (plant hydraulic conductance) in an existing crop model. The thesis comprises three studies based on three main hypotheses. The first study hypothesized that the the consideration of plant hydraulic conductance (K_{plant}) in the model can improve the simulation of CO_2 and H_2O fluxes, and crop growth (biomass, roots and leaf area index) for winter wheat. The second study hypothesized that this improved model (optimized for simulating the anisohydric behaviour of winter wheat) is generic enough to simulate the effects of fluctuating soil water availability, resulting from variable water supply and changing weather conditions, on the gas fluxes and crop growth of maize (isohydric behaviour). The third hypothesis (tested in the third study using detailed field observations) was that both winter wheat and maize are not limited in terms of their photosynthetic capacity and light use efficiency due to their different adaptive responses under drought stress.

In the first study, an existing crop model (LINTULCC2) using a tipping bucket water balance model approach and operating at a daily time step was modified to create a hourly subroutine for the simulations of diurnal changes in assimilation and stomatal conductance. The modified corresponding shoot model was then coupled with the root growth module (SLIMROOT) and a physically-based water balance model (HILLFLOW 1D), and tested using different root water uptake (RWU) models (Feddes and Couvreur) using an hourly time step. Hereby, two coupled models: HILLFLOW–Couvreur's RWU–SLIMROOT–LINTULCC2 (Co) and HILLFLOW–Feddes' RWU–SLIMROOT–LINTULCC2 (Fe). While the Feddes RWU model does not consider K_{plant}, the Couvreur approach explicitly estimates K_{plant} from root hydraulic conductance and total root length, which, in turn, depends on root growth. In this approach the water potential gradient from soil to root to leaf is simulated and the stomatal regulation is captured by using the critical leaf water potential threshold ($\Psi_{threshold}$ = - 2 MPa) in order to account for the anisohydric behavior of winter wheat. A model intercomparison was performed for the two different RWU approaches using field measurements of gas fluxes and crop growth observations for winter wheat in 2016 as validation data. Both approaches showed a relatively similar performance in simulating dry matter, LAI, root growth, RWU, gross assimilation rate, and soil water content. However, the Feddes model predicted more severe drought stress and lower plant growth for the silty soil compared with the results for plants grown on the stony soil, which is opposite to the observed growth patterns. The Couvreur model better captured the difference in growth due to differences in soil type and water treatments. The coupled model

Co provided realistic simulations of the dynamics and magnitude of K_{plant} over the growing season. The explicit consideration of K_{plant} improved simulation results, thereby confirming the first hypothesis.

For the second study, the two coupled models (using Feddes - Fe and Couvreur - Co approaches) applied in the first study were further modified to additionally include the C_4 photosynthesis pathway. The two coupled models (Fe and Co) were tested for maize using data of crop growth, CO_2 gas fluxes, and sap flow observed in 2017 and 2018 under contrasting water supplies and evaporative demands. Both models were able to simulate the temporal dynamics of biomass, leaf area index, transpiration, soil water dynamic, and canopy water potential at a high level of accuracy (confirming the second hypothesis). The Couvreur model incorrectly simulated water stress in the earlier crop growing stages, but it captured water stress and crop growth at the later growing periods more accurately as compared to the Feddes approach. Considering more specific crop properties such as root segment hydraulic conductance, critical leaf hydraulic head the Couvreur model becomes more error-prone in comparison to the Feddes model if the dynamic root growth and total root system conductance (thus, the whole-plant hydraulic conductance) were inadequately simulated.

The third study investigated the diurnal and seasonal dynamics of leaf water potential and CO_2 and H_2O gas exchange at leaf and canopy levels as well as crop growth patterns of winter wheat and maize in 2016, 2017, and 2018 under a wide range of soil water and weather conditions. More specifically, stomatal regulation and morphological changes (i.e. leaf area and crop size) in response to drought stress were examined. Water deficit strongly reduced photosynthesis and transpiration rates at both leaf and canopy levels as well as biomass growth. Winter wheat showed an anisohydric stomatal response (variable Ψ_{leaf}), while the Ψ_{leaf} level of maize was maintained and ranged from -1.6 to -2 MPa. The study further illustrated that the reduction of leaf area plays an important role in regulating transpiration and assimilation rates for both wheat and maize. Isohydric behaviour upon water deficit was not necessarily associated with the limitation of the photosynthetic capacity of maize because of its special leaf anatomy and physiological advantages of the C_4 photosynthetic pathway thereby confirming the third hypothesis.

In summary, in this thesis, the integration and implementation of routines for simulating diurnal changes in stomatal conductance in a crop model, the comprehensive assessment of simulation results and the aquisition, analysis and integration of field data provided new

insights into processes of plant-water relation and growth. Presented data and gained knowledge provided a useful basis for further improvements of dynamic crop models, soil-plant models, and land surface models in simulating CO_2 and H_2O gas flux exchange and crop growth under drought stress. This related to the findings that: (i) the coupled model with the inclusion of K_{plant} allowed adequate simulation of gas fluxes and crop growth for both maize and winter wheat under soil water and evaporative fluctuation; (ii) the use of critical Ψ_{leaf} thresholds as a proxy for stomatal regulations allowed for a realistic representation of anisohydric and isohydric stomatal behaviour for modelling applications; (iii) field data and simulation results confirmed that a value of -1.6 to -2 MPa for Ψ_{leaf} can be used as critical Ψ_{leaf} threshold for winter wheat and maize. Results from this thesis highlighted that two-way feedbacks between growth and root water uptake, inclusion of plant hydraulic conductance, and stomatal functions are very important for predicting the crop response to different soil water conditions in different soils. For soil-vegetation-atmosphere models and process-based crop simulation models, this implied that besides the simulation of stomatal regulations, the representation of photosynthesis mechanisms, leaf and canopy/ root growth as well as morphological adjustments are required. Results of gas flux and crop growth simulations highlighted the need for further research on the effects of the within-field variability of soil characteristics on dynamic root growth and root distribution and corresponding model improvements for reliable estimations of root hydraulic conductance and gas fluxes under drought stress. This especially requires improvements in the simulation of root growth and total root hydraulic conductance, as well as dynamic changes in leaf area. The coupled model developed within this thesis marks a promising approach that should be tested for a wider range of crops, soils, and climate conditions in order to be applied for modeling studies at larger spatial scales.

Zusammenfassung

Die Austauschraten von CO_2 und H_2O zwischen der Vegetation und der Atmosphäre sind stark mit den Funktionen der Stomata und dem Wachstum der Blattfläche verbunden. Pflanzen unter Trockenstress zeigen verschiedene Reaktionen, wie z. B. stomatäre Regulierungen (kurzfristige Reaktionen) und Anpassungen des Kronendachs (d. h. die Veränderung der Blattfläche). Das stomatäre Verhalten steht im Zusammenhang mit dem Wasserpotential der Blätter (Ψ_{leaf}), das in zwei große Kategorien eingeteilt werden kann: anisohydrisch und isohydrisch. Anisohydrische Pflanzen, wie z. B. Winterweizen, halten ihre Spaltöffnungen über längere Zeiträume offen, unabhängig von Änderungen der Bodenwasserversorgung, was zu einem variablen Ψ_{leaf} führt. Die Pflanzen transpirieren bei Trockenheit weiter, was zu einem geringeren Ψ_{leaf} im Vergleich zu den Pflanzen führt, die unter nicht begrenzten Bodenwasserbedingungen angebaut werden. Isohydrische Pflanzen, wie z. B. Mais, zeigen eine starke stomatäre Kontrolle der Transpiration, um das Ψ_{leaf} auf einem bestimmten Grenzwert zu halten. Viele Forschungsarbeiten zielen darauf ab, ein besseres öko-physiologisches Verständnis des stomatären Verhaltens zu erlangen sowie die Modellierung relevanter Prozesse zu verbessern, um die stomatäre Regulation bei Wasserstress besser zu verstehen. Allerdings sind solche Modellierungsaktivitäten im Allgemeinen auf die Blattebene beschränkt. Erntemodelle und Landoberflächenmodelle, die Blattprozesse auf die Baumkronenebene skalieren und physiologische Prozesse des Pflanzenwachstums und -ertrags simulieren. Diese Modelle werden zur Vorhersage von Gasflüssen auf Feld- und größeren Skalen verwendet. Ihre Wasserflussmodule sind jedoch oft vereinfacht. Komplexe Prozesse, wie z.B. die stomatäre Regulation und die damit verbundenen zugrundeliegenden Mechanismen (z.B. das hydraulische Signal), werden auf vereinfachende Weise berücksichtigt, was Verbesserungen erfordert. Ein besseres Verständnis der pflanzenspezifischen Reaktionen (z.B. Winterweizen und Mais) auf variablen Wasserstress über verschiedene Vegetationsperioden und Bodentypen hinweg ist notwendig, um das Verständnis für Pflanzenmanagement, Bewässerungssysteme, Wassernutzungseffizienz und Ertrag zu verbessern. Darüber hinaus wird die Nutzung dieses Wissens zur Verbesserung von Boden-Pflanzen-Modellen und Pflanzenmodellen im Hinblick auf genauere Simulationen von CO_2- und H_2O-Gasflüssen und Ernteerträgen eine zuverlässigere Vorhersage der Nahrungsmittelproduktion unter variablen Wetterbedingungen und dem Klimawandel ermöglichen.

Die Daten wurden in den Jahren 2015, 2016, 2017 und 2018 auf Feldern in der Nähe des Forschungszentrums Jülich erhoben, die durch zwei kontrastierende Bodentypen (steinig und schluffig) und unterschiedliche Wasserregime (bewässert, regengespeist, und Trockenheit) gekennzeichnet sind. In dieser Arbeit wird ein einzigartiger und umfassender Datensatz zum Blattwasserstatus, den CO_2- und H_2O -Gasflüssen von Blättern und Kronen und den damit verbundenen dynamischen Pflanzenwachstumsprozessen (Blattfläche, Wurzelwachstum, und Pflanzenbiomasse) für Winterweizen und Mais präsentiert und analysiert, der unter einer großen Bandbreite von Bodenwasserbedingungen gewonnen wurde. Das erste Ziel dieser Arbeit war es, durch Modellierungsstudien und Feldexperimente ein besseres Verständnis der Beziehungen zwischen Bodenwasserverfügbarkeit und stomatären Reaktionen bei verschiedenen Pflanzen auf verschiedenen Ebenen (Blatt und Baumkrone) zu gewinnen. Das zweite Ziel bestand darin, dieses Wissen zu nutzen, um die Modellierung der Gasflüsse und des Pflanzenwachstums zu verbessern, indem ein neues Modellierungsmodul zur Simulation der stomatären Regulierung (isohydrisch und anisohydrisch) und der zugrundeliegenden Mechanismen (hydraulische Leitfähigkeit der Pflanzen) in ein bestehendes Pflanzenmodell aufgenommen wird. Die Arbeit umfasst drei Studien, die auf drei Haupthypothesen beruhen. In der ersten Studie wurde die Hypothese aufgestellt, dass die Berücksichtigung der hydraulischen Leitfähigkeit der Pflanzen (K_{plant}) im Modell die Simulation der CO_2- und H_2O-Flüsse und des Pflanzenwachstums (Biomasse, Wurzel- und Blattflächenindex) für Winterweizen verbessern kann. In der zweiten Studie wurde die Hypothese aufgestellt, dass dieses verbesserte Modell (das für die Simulation des anisohydrischen Verhaltens von Winterweizen optimiert wurde) generisch genug ist, um die Auswirkungen der schwankenden Bodenwasserverfügbarkeit, die sich aus der variablen Wasserversorgung und den wechselnden Wetterbedingungen ergibt, auf die Gasflüsse und das Pflanzenwachstum von Mais (isohydrisches Verhalten) zu simulieren. Die dritte Hypothese (die in der dritten Studie anhand detaillierter Feldbeobachtungen getestet wurde) lautete, dass sowohl Winterweizen als auch Mais aufgrund ihrer unterschiedlichen Anpassungsreaktionen unter Trockenstress in ihrer photosynthetischen Kapazität und Lichtnutzungseffizienz nicht eingeschränkt sind.

In der ersten Studie wurde ein bestehendes Kulturpflanzenmodell (LINTULCC2), das einen Kippschalen-Wasserhaushaltsmodell-Ansatz verwendet und mit einem täglichen Zeitschritt arbeitet, modifiziert, um eine stündliche Subroutine für die Simulationen der täglichen Änderungen der Assimilation und der stomatären Leitfähigkeit zu erstellen. Das modifizierte entsprechende Sprossmodell wurde dann mit dem Wurzelwachstumsmodul (SLIMROOT) und

einem physikalisch basierten Wasserhaushaltsmodell (HILLFLOW 1D) gekoppelt und mit verschiedenen Wurzelwasseraufnahmemodellen (RWU) (Feddes und Couvreur) mit einem stündlichen Zeitschritt getestet. Dabei wurden zwei gekoppelte Modelle: HILLFLOW-Couvreur's RWU-SLIMROOT-LINTULCC2) (Co) und HILLFLOW-Feddes' RWU-SLIMROOT-LINTULCC2 (Fe). Während das Feddes RWU-Modell K_{plant} nicht berücksichtigt, schätzt der Couvreur-Ansatz K_{plant} explizit aus der hydraulischen Leitfähigkeit der Wurzeln und der Gesamtwurzellänge, die wiederum vom Wurzelwachstum abhängt. In diesem Ansatz wird der Wasserpotentialgradient vom Boden über die Wurzel zum Blatt simuliert und die stomatäre Regulation durch die Verwendung der kritischen Blattwasserpotentialschwelle ($\Psi_{threshold}$ = -2 MPa) erfasst, um das anisohydrische Verhalten von Winterweizen zu berücksichtigen. Ein Modellvergleich wurde für die beiden unterschiedlichen RWU-Ansätze durchgeführt, wobei Feldmessungen der Gasflüsse und Beobachtungen des Pflanzenwachstums für Winterweizen im Jahr 2016 als Validierungsdaten verwendet wurden. Beide Ansätze zeigten eine relativ ähnliche Leistung bei der Simulation von Trockenmasse, LAI, Wurzelwachstum, RWU, Bruttoassimilationsrate und Bodenwassergehalt. Allerdings sagte das Feddes-Modell für den schluffigen Boden stärkeren Trockenstress und geringeres Pflanzenwachstum voraus, verglichen mit den Ergebnissen für Pflanzen, die auf dem steinigen Boden angebaut wurden, was den beobachteten Wachstumsmustern entgegengesetzt ist. Das Couvreur-Modell erfasste die Wachstumsunterschiede aufgrund von Unterschieden im Bodentyp und der Wasserbehandlung besser. Das gekoppelte Modell Co lieferte realistische Simulationen der Dynamik und der Größenordnung von Kplant über die Wachstumsperiode. Die explizite Berücksichtigung von Kplant verbesserte die Simulationsergebnisse und bestätigte damit die erste Hypothese.

Für die zweite Studie wurden die beiden gekoppelten Modelle (mit den Ansätzen Feddes - Fe und Couvreur - Co), die in der ersten Studie angewendet wurden, weiter modifiziert, um zusätzlich den C_4-Photosyntheseweg einzubeziehen. Die beiden gekoppelten Modelle (Fe und Co) wurden für Mais unter Verwendung von Daten des Pflanzenwachstums, der CO_2-Gasflüsse und des Saftflusses getestet, die in den Jahren 2017 und 2018 unter kontrastierenden Wasserversorgungen und Verdunstungsanforderungen beobachtet wurden. Beide Modelle waren in der Lage, die zeitliche Dynamik von Biomasse, Blattflächenindex, Transpiration, Bodenwasserdynamik und Kronenwasserpotenzial mit hoher Genauigkeit zu simulieren (was die zweite Hypothese bestätigt). Das Couvreur-Modell simulierte den Wasserstress in den früheren Wachstumsstadien der Pflanzen falsch, aber es erfasste den

Wasserstress und das Pflanzenwachstum in den späteren Wachstumsperioden genauer als der Feddes-Ansatz. Unter Berücksichtigung spezifischerer Pflanzeneigenschaften wie der hydraulischen Leitfähigkeit des Wurzelsegments und der kritischen Blatthydraulik wird das Couvreur-Modell im Vergleich zum Feddes-Modell fehleranfälliger, wenn das dynamische Wurzelwachstum und die Gesamtleitfähigkeit des Wurzelsystems (also die hydraulische Leitfähigkeit der gesamten Pflanze) unzureichend simuliert wurden.

Die dritte Studie untersuchte die tägliche und saisonale Dynamik des Blattwasserpotenzials und des CO_2- und H_2O-Gasaustauschs auf Blatt- und Kronenhöhe sowie die Wachstumsmuster von Winterweizen und Mais in den Jahren 2016, 2017 und 2018 unter einer Vielzahl von Bodenwasser- und Wetterbedingungen. Insbesondere wurden die stomatäre Regulation und morphologische Veränderungen (d.h. Blattfläche und Pflanzengröße) als Reaktion auf Trockenstress untersucht. Wasserdefizit reduzierte die Photosynthese- und Transpirationsraten sowohl auf Blatt- als auch auf Kronenhöhe sowie das Biomassewachstum stark. Winterweizen zeigte eine anisohydrische stomatäre Reaktion (variables Ψ_{leaf}), während das Ψ_{leaf}-Niveau von Mais beibehalten wurde und von -1.6 bis -2 MPa reichte. Die Studie zeigte weiter, dass die Reduzierung der Blattfläche eine wichtige Rolle bei der Regulierung der Transpirations- und Assimilationsraten sowohl für Weizen als auch für Mais spielt. Das isohydrische Verhalten bei Wasserdefizit war aufgrund der speziellen Blattanatomie und der physiologischen Vorteile des C_4-Photosynthesewegs nicht unbedingt mit der Einschränkung der Photosynthesekapazität von Mais verbunden, was die dritte Hypothese bestätigt. Zusammenfassend lässt sich sagen, dass in dieser Arbeit die Integration und Implementierung von Routinen zur Simulation der täglichen Änderungen des stomatären Leitwerts in einem Pflanzenmodell, die umfassende Bewertung der Simulationsergebnisse und die Erfassung, Analyse und Integration von Felddaten neue Einblicke in die Prozesse der Pflanzen-Wasser-Beziehung und des Wachstums lieferten. Die präsentierten Daten und gewonnenen Erkenntnisse lieferten eine nützliche Grundlage für weitere Verbesserungen von dynamischen Pflanzenmodellen, Boden-Pflanzen-Modellen und Landoberflächenmodellen bei der Simulation des CO_2- und H_2O Gasflussaustausches und des Pflanzenwachstums unter Berücksichtigung von Trockenstress. Dies bezog sich auf die Erkenntnisse, dass: (i) das gekoppelte Modell mit der Einbeziehung von K_{plant} eine adäquate Simulation der Gasflüsse und des Pflanzenwachstums sowohl für Mais als auch für Winterweizen unter Bodenwasser- und Verdunstungsschwankungen ermöglichte; (ii) die Verwendung von kritischen Ψ_{leaf}-Schwellenwerten als Proxy für stomatäre Regulierungen eine realistische Darstellung des anisohydrischen und isohydrischen stomatären Verhaltens für Modellierungsanwendungen

ermöglichte; (iii) Felddaten und Simulationsergebnisse bestätigten, dass ein Wert von -1.6 bis -2 MPa für Ψ_{leaf} als kritische Ψ_{leaf}-Schwelle für Winterweizen und Mais verwendet werden kann. Die Ergebnisse dieser Arbeit haben gezeigt, dass die wechselseitigen Rückkopplungen zwischen Wachstum und Wasseraufnahme durch die Wurzeln, die Einbeziehung der hydraulischen Leitfähigkeit der Pflanzen und die stomatären Funktionen sehr wichtig für die Vorhersage der Reaktion der Pflanzen auf unterschiedliche Bodenwasserbedingungen in verschiedenen Böden sind. Für Boden-Vegetation-Atmosphäre-Modelle und prozessbasierte Pflanzensimulationsmodelle bedeutete dies, dass neben der Simulation der stomatären Regulationen auch die Darstellung von Photosynthesemechanismen, Blatt- und Kronenwachstum sowie morphologische Anpassungen erforderlich sind. Die Ergebnisse der Gasfluss- und Pflanzenwachstumssimulationen verdeutlichten den Bedarf an weiterer Forschung zu den Auswirkungen der feldinternen Variabilität der Bodeneigenschaften auf das dynamische Wurzelwachstum und die Wurzelverteilung sowie entsprechende Modellverbesserungen für zuverlässige Abschätzungen der hydraulischen Leitfähigkeit der Wurzeln und der Gasflüsse unter Trockenstress. Dies erfordert insbesondere Verbesserungen bei der Simulation des Wurzelwachstums und der gesamten hydraulischen Leitfähigkeit der Wurzeln sowie der dynamischen Veränderungen der Blattfläche. Das in dieser Arbeit entwickelte gekoppelte Modell stellt einen vielversprechenden Ansatz dar, der für ein breiteres Spektrum von Kulturpflanzen, Böden und Klimabedingungen getestet werden sollte, um für Modellierungsstudien auf größeren räumlichen Skalen eingesetzt werden zu können.

Contents

List of Abbreviations

ABA	Abscisic acid
Co	Couvreur RWU model
CLM	Community land surface model
DAS	Day after sowing
DM	Crop dry matter or dry biomass
DOY	Day of the year
ET	Evapotranspiration
ETP	Potential evapotranspiration
Fe	Feddes RWU model
LAI	Leaf area index
LUE	Light use efficiency
LSM	Land surface model
LWP	Leaf water potential
NRLD	Normalized root length density
PAW	Plant available water
RLD	Root length density
RWU	Root water uptake
SF	Sap flow
SVAT	Soil-vegetation-atmospheric transfer model
SWB	Soil water balance
VPD	Vapour pressure deficit
WUE	Water use efficiency

List of Symbols

$AMAX_{shaded}$	Light saturated photosynthesis rate of shaded leaf	mM m^{-2} s^{-1}
$AMAX_{sun}$	Light saturated photosynthesis rate of sunlit leaf	mM m^{-2} s^{-1}
C_a	Ambient concentration of CO_2	mM mol^{-1}
C_i	Intercellular concentration of CO_2	mM mol^{-1}
fwat	Water stress factor	(-)
g_s	Leaf stomatal conductance	mol m^{-2} s^{-1}
k	Light extinction coefficient	(-)
KC25	CO_2 turnover rate per gram of Rubisco at 25 °C	μM g^2 s^{-1}
KMC25	Michaelis-Menten constant for CO_2 at 25 °C	μM m^{-2} s^{-1}
KMO25	Michaelis-Menten constant for O_2 at 25 °C	mM m^{-2} s^{-1}
O_2	Atmospheric oxygen concentration	μM mol^{-1}
T_{plant}	Actual transpiration	mm h^{-1}
T_{pot}	Potential transpiration	mm h^{-1}
$TRLD_{doy}$	Total length of the root system below a unit surface area	m m^{-2}
$T_{threshold}$	Transpiration rate when plant is under water stress	mm h^{-1}
β	Constant fraction to upscale root to whole plant hydraulic conductance	(-)
Γ*	CO_2 compensation point	μM mol^{-1}
θ_{fc}	Soil water content at field capacity from soil layer i	m^3 m^{-3}
θ_i	Soil water content at soil layer i	m^3 m^{-3}
θ_{wp}	Soil water content at wilting point from soil layer i	m^3 m^{-3}
K_{comp}	Sompensatory hydraulic conductance per unit root length per surface area	d^{-1} cm^{-1} cm^{-2}
K_{plant}	Whole plant hydraulic conductance	d^{-1}
K_{rs}	Root hydraulic conductance	d^{-1}
$K_{rs,\ normalized}$	Root hydraulic conductance per unit root length per surface area	d^{-1} cm^{-1} cm^{-2}
Ψ_{leaf}	Leaf hydraulic head (in Chapter 2)	m (or MPa)
Ψ_c	Canopy hydraulic head (in Chapter 3)	m (or MPa)
Ψ_m	Soil pressure head	m (or MPa)
Ψ_{sr}	Root zone hydraulic head	m (or MPa)
$\Psi_{threshold}$	Critical leaf hydraulic head threshold when plant is under water stress	m (or MPa)

List of Figures

List of Tables

1 Chapter: General introduction and objectives

General need for understanding and modeling crop gas fluxes

With a predicted world population of 9.8 billion people by 2050 (UN, 2017) feeding more people with limited water is becoming increasingly challenging, particularly in regions with water scarcity (Water, 2012; IPCC 2007). Soil water is one of the most important environmental variable that affects gas fluxes related to photosynthetic gases (CO_2) and transpiration (H_2O), and crop yield (Chaves et al., 2003; Aroca, 2012). The exchange process of CO_2 and H_2O between crops and their surrounding atmosphere is not only important for production of biomass and yield but also influences the soil-vegetation-atmosphere system (i.e. gas and heat flux partitioning), thereby affecting atmospheric conditions at larger scales. Optimizing irrigation and crop water use efficiency are important strategies to enhance crop yield per unit area and reduce water consumption. In this context, quantifying gas fluxes (photosynthesis and transpiration) at both leaf and canopy scales is essential in understanding water flow and carbon exchange capacity in the soil-vegetation-atmospheric system. The collection of such data will support efficient irrigation, crop practices, and breeding procedures for drought resistance under different climate and soil water conditions. It will facilitate improvements and prediction skills of mechanistic crop models through representing more eco-physiological crop characteristics (LINTULCC2 model Rodriguez et al., 2000; GECROS model (Yin and van Laar, 2006), also see the review from Boote, 2003; Siad et al., 2019)) as well as the improvement of land surface model schemes [such as the Community Land Model (CLM) (Oleson et al., 2013; Sulis et al., 2015) and see the review from Verheof and Egea et al., (2014)]. Such improvements are critical for more accurate crop growth processes predictions and more realistic simulations of soil-vegetation-atmosphere-transfer processes, and, in consequence, for more realiable weather predictions, climate change projections, and weather forecasts.

1.1 Crop responses to drought stress

The amount and rate of gas exchange with the atmosphere and, thus, water withdrawal from the soil depends on crop physiological characteristics (Hay and Porter, 2006; Baldocchi, 1994), soil water availability, root water uptake capacity (Thorup-Kristensen et al., 2009; Rich and Watt, 2013), and evaporative demand of the atmosphere (Buckley et al., 2003). When soil water is depleted, crops show a wide range of strategies to cope with this, including short- and long-term physiological and/or morphological (structural) adaptations, which affect and regulate the amount of gas exchange with the atmosphere (Chaves et al., 2003; Tardieu and Parent, 2017).

Stomata are essential in preventing excessive water loss when the plant is under water stress and the root may be damaged and lose contact with surrounding soil (Tyree and Sperry, 1988; Brodribb and McAdam, 2011b). Although there has been a recent increase in knowledge about the role of mesophyll conductance in regulating photosynthesis during periods of water stress (Keenan et al., 2010; Niinemets et al., 2009; Flexas et al, 2004), the importance of stomatal regulation as a physiological response of plants to soil water depletion is undisputed (Demour et al., 2011). Stomatal adjustments often occur at short-time periods (seconds to hours). The risk-avoiding strategy refers to isohydric plants (such as maize and poplar), which close their stomata to maintain leaf water potential (Ψ_{leaf}) at a certain level to reduce severe water loss. Some species such as winter wheat and sunflower, however, keep their stomata fully open and allow Ψ_{leaf} to decrease during soil drying and increasing evaporative demand. Thus, a much lower Ψ_{leaf} under drought is observed as compared to well-watered plants (anisohydric plants) (Tardieu and Simonneau, 1998). However, there is evidence that a clear distinction between those two stomatal regulations is difficult. A continuum between the two strategies was observed in many grapevine (Schultz, 2003, Rogiers et al., 2012, Zhang et al., 2012) or tree species (*Eucalyptus gomphocephala*, see Franks et al., 2007), but also in major agricultural food crops, such as winter wheat (Galle et al., 2014). A like-anisohydric behavior was observed under high evaporative demand for some species but this can change to a like-isohydric behavior under lower evaporative demand. Franks et al., (2007) defined the third mode an isohydrodynamic where the difference between midday and predawn Ψ_{leaf} remains constant across seasons, while the Ψ_{leaf} could vary following evaporative demand and soil water conditions.

These stomatal behaviors can be explained through several underlying mechanisms and their interactions, however, they have not been fully understood yet (Tardieu, 2016). The hydraulics of the root and shoot systems create a direct linkage between root water potential, transpiration flow, and leaf water potential (Schultz, 2003; Franks et al., 2007). The long-distance hydraulic signal, thus, links plant water potential and stomatal closure (Christmann et al., 2013). In addition, plants also developed a non-hydraulic mechanism to regulate stomata. The phytohormone, such as abscisic acid (ABA) can be produced in water-stressed roots (Gowing et al., 1990; Davies and Zhang, 1991; Tardieu and Simonneau, 1998; Wilkinson and Davies, 2002) or shoots (Christmann et al., 2007, Christmann et al., 2013) and then be transported through the xylem to regulate stomata movements. The interaction of such hydraulic and non-hydraulic signals in regulating stomata has also been reported (Tardieu and Davies, 1993; Tardieu and Simonneau, 1998). The weak relationship of stomatal conductance to leaf water status (see the analysis of the global dataset for trees in Martínez-Vilalta and

Garcia-Forner, 2017; Martnez-Vilalta et al., 2014) suggests that a deeper understanding of stomatal regulations is required to better understand the applicability and suitability of the concept of anisohydric and isohydric plants. This is important not only for the explanation of drought effects on assimilation and transpiration of crops but also for the adequate representation of stomatal regulation for different crop functional types in crop models and land surface models (Roman et al., 2015; Verhoef and Egea, 2014).

In addition to short-term regulations of stomata, crops have also developed diverse long-term adaptation strategies and mechanisms (at day, week, and seasonal scales) in response to variable soil water availability (Ramalho and Chaves, 1991; Rodrigues et al., 1995; Chaves et al., 2000; Chaves et al., 2003; Aroca, 2012). Anisohydric plants such as winter wheat have similar leaf stomatal conductance and transpiration rates regardless of daytime and field conditions. However, their growth characteristics (i.e. increasing number of tillers and green leaf area) show responses to low soil water availability, which in turn affects the gas fluxes (i.e., transpiration rates) at the canopy scale (Jamieson et al., 1998; Ewert, 2004; Kupisch et al., 2015, Damour et al., 2010; Kadam et al., 2015). In addition to stomatal closure, leaf rolling in maize has been associated with a reduction in transpiration rates to save water loss (Moulia, 1994; Baret et al., 2018). Some maize cultivars can reduce the amount of assimilates allocated to lateral root growth, thereby minimizing lateral root branching density (Zhan et al., 2015). Alternatively, assimilation can be devoted to deeper root growth which, in turn, allows crops to access water in the lower layers and thereby improves the tolerance of plants such as maize to water stress (Lynch, 2013; Zhan et al., 2015). The resistance to drought depends not only on differences in stomatal control but also on plant development stages and growth rates. For instance, a plant with faster leaf growth will cause a faster depletion of soil water, therefore, resulting in earlier stomatal closure (Tardieu and Simonneau, 1998). Under high soil moisture levels, anisohydric poplar has a clear advantage because of its faster growth and higher photosynthesis rate, which may favor higher biomass production. In contrast, isohydric poplar has higher water use efficiency and can survive under water-limited conditions (Attia et al., 2015).

1.2 Modeling stomatal functions in response to drought stress

1.2.1 Some plant-water relation terminologies

The water gradient from soil to root to leaf and canopy creates the continuum pathway. The driver for this transport is the difference in water potential (a measure of the energy state of water) between the atmosphere and the soil. The energy of the plant (or soil) water or water

potential can be either stated as total water pressure (Ψ in [MPa], energy per volume) or as the hydraulic head (in [m], energy per weight). The hydraulic heads refer to total water potentials expressed in length units while pressure heads are hydraulic heads minus the gravitational potential. A pressure head of -100 m approximates a pressure of -1 MPa. The use of these terms is not consistent across research disciplines. For instance, in the context of hydrological processes and models, researchers refer to leaf or soil hydraulic heads, while plant ecophysiologists often apply the terms leaf or soil water potential. Similarly, stomatal resistance (conductance) is often expressed in s m^{-1} (m s^{-1}) in physics while biologists and agronomists often describe this term in mol H_2O m^{-2} s^{-1}. Both units can be converted and used depending on contexts and disciplines.

1.2.2 SVAT and crop models

Before describing existing modeling approaches on stomatal functions, several underlying concepts are described in the following in order to support the understanding of these approaches and their use for simulating gas fluxes (transpiration and photosynthesis). The soil-plant-atmosphere continuum (SPAC) is an important concept which emphasizes the interrelationships of soil, plant, and atmospheric factors in determining plant water status (van Honert, 1948). The representation of the water flow through the SPAC closely resembles that for the flow of electricity in a conducting system. Therefore, it is often termed the Ohm's law analog (Jones and Sutherland, 1991). A second important concept is the soil-vegetation-atmosphere transfer (hereby SVAT) or soil-plant-atmosphere transfer schemes/models which are designed to describe fluxes of heat, water vapor, and CO_2 between a multi-component vegetated land surface and the atmosphere (Jones et al., 1996; Calvet et al., 1998). The SVAT concept might take into account physiological properties of the vegetation components, in particular, leaf area index (LAI) and stomatal conductance. The model of stomatal conductance has been included in the SVAT scheme in different ways (see Damour et al., 2011; Verhoef and Egea et al., 2014). The SVAT model can be used as a stand-alone modeling tool at the field scale (Calvet et al., 1998; Olioso et al., 1996; Verhoef and Allen, 2000; Wang and Leuning, 2000; Wang et al., 2007) or can be employed as a module of hydrological models and land surface models for a comprehensive understanding and simulation of the interaction between meteorological and hydrological processes (Noilhan and Mahfouf, 1996; Kucharik and Brye, 2003; Oleson et al., 2013; Aroca, 2002). Lastly, crop models, which focus on simulating dynamic crop growth processes (i.e. phenology, root, and shoot growth) and yield prediction under a wide range of conditions at diverse temporal and spatial scales (van Ittersum et al., 2003; Boote, 2013). Most current SVAT schemes and

hydrological models do not parameterize vegetation as a dynamic component. For instance, the seasonal evolution of LAI is most often prescribed and monthly LAI values are kept constant in each year (Aroca, 2002). Dynamic root growth is often still poorly represented in SVAT schemes that are implemented in land surface models. For instance, the CLM 4.5 model (Oleson et al., 2013) considers root growth over soil depth but not over time. Therefore, crop models have been used to inform and supplement the root dynamics to improve the water uptake and soil flux simulation (Wöhling et al., 2013; Gayler et al., 2013) or LAI growth (Lee et al., 2014). However, the detailed characteristics and roles of stomatal function and the interrelationship within continuum pathways have been rarely considered in the crop model community. An overview on the state of art of crop models, SVATs, and land surface models with respect to their representation of stomatal regulations and associated underlying mechanisms is given in Table 1.1.

Table 1.1 General overview and comparison of crop models, SVAT models, and soil-plant models

Processes	**Crop models**	**SVAT models**	**Land surface models**	**Soil-plant models (i.e in soil physics)**
Photosynthesis/biomass	Yes, mainly based on radiation use efficiency concept (Monteith 1977; Goudriaan and van Laar, 1978)	Yes, often biochemical photosynthesis (Farquhar et al., 1980)	Yes, often biochemical photosynthesis (Farquhar et al., 1980)	No
Coupled photosynthesis-stomatal conductance model	Rarely	Often	Rarely	No
Stomatal conductance/functions	Rarely	Often, diverse approaches	Often, diverse approaches	Rarely, indirect
Signals (hydraulic and chemicals)	Rarely	Often	Rarely	Few models
Anisohydric + isohydric stomatal regulations Examples:	No	Rarely Olioso et al., 1996; Tuzet et al., 2003; Wang et al., 2007	Rarely Sulis et al., 2019	Few models Couvreur et al., 2012; Huber et al., 2014
LAI	Yes, dynamic	Yes (static or as input)	Yes (static or as input)	Yes (static, or as input)
Root growth	Yes, dynamic	Yes (static or as input)	Yes (static or as input)	Yes (static, or as input)
Root water uptake (RWU)	Mainly tipping bucket	Feddes' RWU or van den Honert model	Feddes' RWU or van den Honert model	van den Honert model
Soil water balance (SWB)	Mainly tipping bucket	Mainly physically based model (Richard equation)	Mainly physically based model (Richard equation)	Physically-based model (Richard equation)
Temporal discretization	Mostly daily	Second to daily	Second to monthly	Second to daily
Spatial discretization of soil profile	Several layers, coarse	Millimeter to meter	Millimeter to meter	Millimeter to centimeter
Application scales	Field to global	Field	Regional, global	Sub-soil
Application purposes	Crop growth and yield prediction	Understand the flux evolution and simulating soil-plant-atmosphere interactions	Simulating gas exchange between land surface and atmosphere, component of weather forecast models	Simulating dynamic soil-plant and soil-root processes and interactions

1.3 Modeling water flux, photosynthesis, and stomatal conductance

In terms of structure and complexity, crop growth models consist of a combination of empirical and mechanistic approaches for simulating photosynthesis (Boote, 2013, Yin and van Laar, 2005). Process-based models have been developed that use the biochemical photosynthese model (Farquhar, 1980). In these approaches, the net leaf assimilation rate depends on both Rubisco kinetics to CO_2 and O_2 and electron transport rate which is influenced by photon flux and temperature. Some of these models have been developed for the field scale (LINTULCC2 Rodriguez et al., 2001; GECROS from Yin and van Laar, 2005) or as components of land surface models operating at larger scales (Kucharik and Brye, 2003; CLM4.5 from Oleson et al., 2013)). The main common feature of these mechanistic models is that they simulate photosynthesis using the Farquhar equation (Farquhar, 1980) and a type of empirical Ball and Berry equation (Ball et al., 1987) or a modified version of this equation (Leuning 1990, 1995) to simulate stomatal conductance (LINTULCC2 Rodriguez et al., 2001; IBIS from Kucharik and Brye, 2003; CLM4.5 from Oleson et al., 2013). Another similarity in these crop models is that the response of stomata to low water availability is implicitly accounted for using an empirical "water stress factor". Timing and magnitude of water stress are typically derived from actual and potential transpiration rates, which depend on soil water availability and root water uptake (Rodriguez et al., 2001; Yin and van Laar, 2005) or simply from soil water content (Wang and Leuning, 1998) and the soil water potential (Verhoef and Allen, 2000; Kucharik et al., 2000; Oleson et al., 2013). These approaches, thus, neglect processes such as root to shoot signaling mechanisms that control stomatal behaviors. Especially, the empirical nature of these models makes it difficult to apply them for predicting changes under future environmental conditions (i.e. climate change scenarios) or for more complex environments (i.e. a wide range of soil water conditions) (Verhoef and Egea, 2014; Egea et al., 2011; Damour et al., 2010), or for different plant-specific characteristics or species.

Water stress factors are based on simulated soil water balances (SWB) and root water uptake (RWU), with SWB and RWU estimates being dependant on whether a conceptual or physically based approach is used (van Ittersum, 2003). The hydrological and land surface modeling community commonly applies a physically-based simulation approach (Richards equation; Richard 1931). However, most crop models apply conceptual RWU and water balance (tipping bucket) models at a daily resolution. The cascaded tipping bucket approach mimics the water flow without explicitly considering the energy potential of soil water. To overcome these shortcomings hydrological models have been coupled with crop growth models for an improved simulation of crop growth and water uptake dynamics (see Siad et al., 2019 for a

recent review). Examples are interfaces between the Feddes RWU model and HYDRUS 1D water balance model (Simunek et al., 2009) with the DSSAT crop model (Shelia et al., 2018) to simulate soybean yields or the coupling between HYDRUS 1D and the WOFOST crop model to simulate maize yields (Li et al., 2012; Yang et al., 2017) or wheat (Zhou et al., 2012). These studies however did not consider changes in the root and plant hydraulic conductance or stomatal regulations for simulating crop responses to water stress and neglected compensatory root water uptake. Since stomata regulate the transpiration rate and thus leaf water status (Sperry 2000; Tardieu et al., 2015), a realistic simulation of the leaf water potential and associated stomatal regulations requires simulations of the soil water potential and, more specifically, the difference between the water potential of the soil at the root surface and the water potential of the water in the root xylem (Tardieu et al., 2017; Courveur et al., 2012). This cannot be achieved using either the tipping bucket method or Feddes' RWU. Models such as those based on the Feddes approach require calibration data for different crop types and growing seasons and can only indirectly simulate the effects of changes in the root and plant hydraulic conductance (Cai et al., 2018; Vandoorne et al., 2012; Wesseling et al., 1991). Further, the daily time step used in tipping bucket approaches poses another limitation to crop models to capture the true diurnal course of the energy flux by introducing additional errors because of the non-linear response of stomata to environmental factors (Boote, 2013; Tardieu and Parent, 2017).

1.4 Modeling anisohydric and isohydric responses to water stress

Many attempts have been made to improve the simulation of gas fluxes by explicitly considering contrasting stomatal behaviors when modeling stomatal conductance (Damour et al., 2010). For instance, "regulating signals" (hydraulic and/or chemical) at the leave level have been linked to a coupled stomatal conductance-photosynthesis model (Dewar 2002, Gutschick and Simmoneau 2000, Tuzet et al., 2003; Ahmadi et al., 2009; Verhoef and Egea 2014). Huntingford et al., (2015) developed a concept to include the ABA signal and leaf water potential in simulating stomatal conductance for tree plants at the canopy scale, however, it has not been tested for field data yet. Recently, detailed 3D root architecture models have been developed for incorporating signaling processes crtitical for simulating the interaction between plant water uptake and soil water dynamics (Courveur et al., 2014, van Dam et al., 2003; Huber et al., 2014). These models often use a greater modeling detail with respect to the temporal (water flux from second to longer time steps) and spatial resolution (millimeter, centimeter, and meter of soil profile). Also, in a recent effort, the hydraulic signal was included in a 1D RWU model which was deduced from a 3D model with hydraulic principles (Cai et al.,

2017, Cai et al., 2018). However, these studies did not explicitly consider photosynthesis and/ or stomatal functions, and their effect on crop growth. Few studies included the hydraulic signal and corresponding feedback mechanism in dynamic crop growth models (Claudio, 2003; Olioso et al., 1996; Wang et al., 2007). At the field scale this has been done for soybean (Olioso et al., 1996) and spring wheat (Jensen et al., 1993). Both studies applied a static root growth model where plant hydraulic conductance was kept constant during the growing season. Several studies compared the performance of physically-based RWU models (considering plant hydraulic resistance) for estimating the RWU with that of conventional approaches (i.e. Feddes model) (de Jong van Lier et al., 2008; 2013; Santos et al., 2017). However, there have been few comparisons on the predictive capacity of Couvreur's RWU model and Feddes's model based on field data, particularly with respect to the simulation of transpiration and photosynthesis fluxes, soil water, and crop growth. Recent examples are studies on winter wheat (Cai et al., 2018; Cai et al., 2017) where field-based data on root and aboveground biomass growth (LAI, crop height) has been used for an inverse modeling approach. Comparative assessments of a coupled root: shoot model using Couvreur and Feddes RWU models with respect to their results on CO_2 and H_2O gas exchange and crop growth have not been done before.

1.5 Objectives

This study aims to bridge the gap between commonly applied conceptual modeling approaches and physically-based approaches implemented in hydrological and soil physical models by coupling a root: shoot model with an SWB model that explicitly accounts for plant hydraulic conductance and associated stomatal regulations. The advanced 1D RWU uptake model from Couvreur was introduced as a sink term into the physically-based SWB model (HILLFLOW 1D, Bronstert and Plate, 1997) which has been already implemeted in the SIMPLACE modeling framework (simplace.net, Enders et al., 2010). The resulting model was then linked with the SLIMROOT root growth model (Addiscott and Whitmore, 1991) and the crop growth model LINTULCC2 (Rodriguez et al., 2000) with the latter component providing all subroutines required for simulating assimilation (coupled photosynthesis- stomatal conductance model), phenology, assimilate partitioning, leaf growth, hereby Co:<HIFLLOW 1D-Couvreur-SLIMROOT- LINTULCC2>.

In the coupled model with Couvreur approach, the hydraulic signal is the only signal that controls stomatal closure. This assumption is commonly applied for SVAT models (Damour et al., 2010). Nevertheless, it might lead to an oversimplification of real-world processes where several additional factors are involved in the regulatation of plant stomatal behavior (Tardieu,

2017). Chemical signals such as abscisic acid (Zhang and Davies, 2000), pH (Wilkinson et al., 1998), strigolactones (Visentin et al., 2016) also affect the leaf water status. However, the sources of chemical signals, for instance ABA, either due to water stress in roots or shoots, and its transport within the plant systems are difficulties to capture and would require the introduction of several parameters. Moreover, disentangling effects from several chemicals involved in the water stress responses is challenging (Tardieu and Parent, 2017). The effects of ABA can be captured by coupling Ball-Berry-Leuning model equations with the Tardieu and Simmoneau model (Dewar 2002). However, it is still difficult to extrapolate at the field or larger scales due to the lack of accurate measurement of ABA at these scales.

In the coupled model with Couvreur approach, the whole plant hydraulic conductance (K_{plant}) is explicitly derived from the total root length. Thus, K_{plant} is changing over the growing season following the root development. For the sake of simplification, K_{plant} is assumed to be constant during the course of single days and was upscaled from root hydraulic conductance based on a constant fraction. In fact, xylem embolism could cause a hydraulic loss in the continuum pathway (Cochard, 2002; Tyree, 1988). The oscillation of hydraulic conductance is controled by the circadian rhythms of plasma membrane aquaporin and protein content in the root (Caldeira et al., 2014; Tardieu et al., 2015).

We use the (critical) leaf water potential thresholds to characterize the stomatal regulations. The critical leaf water potential threshold is the leaf water potential value at which the stomatal conductance begins to decrease markedly (Turner, 1974; Jones and Sutherland, 1991; Olioso et al., 1996; Tuzet et al., 2003). This approach is employed in many SVAT models (Olioso et al., 1996; Tuzet et al., 2003). In the work from Couvreur et al., (2012); Couvreur et al., (2014); Cai et al., (2017); Cai et al., (2018), the Couvreur model did not explicitly simulate the stomatal conductance. However, it assumes that stomatal conductance is not influenced by Ψ_{leaf} as long as the Ψ_{leaf} is above a critical leaf hydraulic threshold ($\Psi_{threshold}$). The Ψ_{leaf} is kept constant by changing stomatal conductance when the $\Psi_{thresholds}$ are reached. Contrastingly, in our study, stomatal conductance is explicitey simulated. The stomatal responses to water stress are considered using a water stress function which, in turn, is determined by the $\Psi_{threshold}$.

The first overall aim of this thesis is to contribute to an improved understanding of the relationships between soil water availability and stomatal responses for different crops through modeling and field experiments. The second overall aim is to improve an existing crop model with respect to the simulation of gas fluxes and crop growth by implementing equations that allow for stomatal regulations and associated underlying mechanisms.

To achieve the two main objectives, three hypotheses will be tested:

(a) The first hypothesis is that consideration of plant hydraulic conductance can improve the simulation of CO_2 and H_2O fluxes, and crop growth in biomass, roots, and leaf area index in winter wheat. To test this hypothesis, several topics will be particularly addressed:

- **(a1)** to analyze and compare the predictive quality of a crop growth model coupled with a RWU model that considers plant hydraulics (Couvreur RWU model) and a model that does not consider plant hydraulics (Feddes RWU model);
- **(a2)** to compare the simulated plant hydraulic conductances for variable growing conditions with direct estimates of these conductances from field measurements; and
- **(a3)** to analyze the sensitivity of simulated RWU and crop growth to the Couvreur RWU and root growth model parameters (root hydraulic conductance, critical leaf hydraulic threshold, and specific weight of seminal and lateral roots)

(b) The second hypothesis is that the coupled model with the Couvreur RWU model is generic enough to simulate the effects of soil water availability on the CO_2 and H_2O gas fluxes and crop growth of maize with varying weather conditions (including different levels of evaporative demand/ potential evapotranspiration (ETP) and vapor pressure deficit (VPD)). The objectives of this study are:

- **(b1)** to analyze the sensitivity of aboveground biomass growth and RWU to plant-water relation model parameters (seminal and lateral specific root lengths, $\Psi_{thresholds}$, root hydraulic conductance parameters)
- **(b2)** to compare the predictive capacity of the coupled models with and without the inclusion of K_{plant} (Couvreur and Feddes RWU models, respectively) for simulating maize crop growth and corresponding CO_2 and H_2O gas fluxes observed under different water treatments and within different growing seasons characterized by contrasting weather conditions at the field scale.

(c) The third hypothesis is that winter wheat and maize are not limited in photosynthesis capacity and light use efficiency due to their different adaptive responses under drough stress. The research questions addressed are:

- **(c1)** what are the stomatal strategies of winter wheat and maize under different water supply conditions in the field?
- **(c2)** how do photosynthesis and transpiration at leaf and canopy levels as well as crop growth rate and LAI differ among different water regimes?

- **(c3)** what is the relative contribution of short-term stomatal regulation vs longer-term (morphological) adjustments (i.e. LAI) to gas exchange and crop biomass production?

1.6 Overview of the experimental setup, measurement, and outline of thesis

The study area was located in Selhausen in North Rhine-Westphalia, Germany (50°52'N, 6°27'E). The research field was characterized by a strong gradient in gravel content and slightly inclined with a slope of around 4°. Within the field, two experimental research sites had been established: one on the upslope with stony soil (F1) and one on the downslope with silty soil (F2). The upslope soil contains up to 60% gravel by weight while at the downslope site the gravel content was approximately 4% and the soil texture was silty. The study was performed from 2015 to 2018. The experimental set-up has been slightly changed during the observation period with spring wheat (*Triticum aestivum cv.* Scirocco) tested in 2015, winter wheat (*Triticum aestivum cv.* Ambello*)* in 2016, and silage maize (*Zea may* cv. Zoey) tested in 2017 and 2018. In 2015 and 2016, at both sites, three different water treatments were tested, resulting in sheltered plots (F1P1 and F2P1), rainfed plots (F1P2 and F2P2), and irrigated plots (F1P3 and F2P3) (Table 1.2). In 2017, on the upslope site, only two water treatments were tested: rainfed plots (F1P1/F1P2 and F2P1/F2P2) and irrigation (F1P3 and F2P3) (Table 1.2). Silage maize (*Zea may* cv. Zoey) was sown on 4th May 2017 with a density of 10.66 seeds m^{-2} for all treatments. In 2018, using the same cultivar and sowing density plants were sown on 8th May 2018 on the upslope rainfed (F1P2), upslope irrigated (F1P3), downslope rainfed (F2P2), and downslope irrigated (F2P3) plots. One of the rainfed downslope plots (F2P1) was sown using a higher density of 16 seed m^{-2} and one of the upslope rainfed plots (F1P1) was sown two weeks after the other plots on 22nd May 2018 (Table 1.2).

Table 1.2 Summary of experimental set-up, growing seasons, and crop managements

Years	Soil types	Water treatments	Plot names	Phenology	Sowing density	Fertilizer applications
2015	Stony	Sheltered	F1P1	Sowing: 17/03/15 Emergence: 21/03/15 Anthesis: 08/06/15 Harvest: 30/07/15	350-370 seed m^{-2}	08/05/15: 100 kg N + 60 kg K_2O + 30 kg P_2O_5 16/06/15: 80 kg N
		Rainfed	F1P2			
		Irrigated	F1P3			
	Silty	Sheltered	F2P1			
		Rainfed	F2P2			
		Irrigated	F2P3			
2016	Stony	Sheltered	F1P1	Sowing: 26/10/15 Emergence: 11/11/15 Anthesis: 03/06/16 Harvest: 26/07/16	350-370 seed m^{-2}	03/15/16: 80 kg N + 60 kg K_2O + 30 kg P_2O_5 02/05/16: 60 kg N 07/06/16: 50 kg N
		Rainfed	F1P2			
		Irrigated	F1P3			
	Silty	Sheltered	F2P1			
		Rainfed	F2P2			
		Irrigated	F2P3			
2017	Stony	Rainfed	F1P1	Sowing: 04/05/17 Emergence: 09/05/17 Tasseling: 09/07/17 Silking: 14/07/17 Harvest: 16/09/17	75cm x 12.5cm; 10.66 plants m^{-2}	09/05/17: 100 kg N + 40kg P_2O_5; 06/07/17: 80 kg N + 40 kg K_2O
		Rainfed	F1P2			
		Irrigated	F1P3			
	Silty	Rainfed	F2P1			
		Rainfed	F2P2			
		Irrigated	F2P3			
2018	Stony	Rainfed	F1P1	Sowing: 22/05/18 Emergence: 26/05/18 Tasseling: 21/07/18 Silking: 23/07/18 Harvest: 02/09/18	75cm x 12.5cm; 10.66 plants m^{-2}	22/05/18: 100 kg N; 30/05/18: 40 kg P_2O_5 + 40 kg K_2O 27/06/18: 80 kg N
		Rainfed	F1P2	Sowing: 08/05/18 Emergence: 13/05/18 Tasseling: 09/07/18 Silking: 11/07/18 Harvest: 22/08/18		
		Irrigated	F1P3			
	Silty	Rainfed	F2P1		75cm x 8.3cm; 16 plants m^{-2}	
		Rainfed	F2P2		75cm x 12.5 cm; 10.66 plants m^{-2}	
		Irrigated	F2P3			

The diurnal and seasonal data of gas fluxes at leaf and canopy scales (leaf stomatal conductance and photosynthesis, leaf water potential, sap flow, canopy gas exchange) were collected for all water treatments. In addition, data on the dynamic crop growth (phenology, crop height, dry biomass, and leaf area index) has been obtained (see Table 1.3). The data set is complemented by observations on the dynamics of the soil water content, soil water potential, soil temperature, and root growth (root counts and root lengths) in different soil depths provided within the framework of the TR32 program.

Table 1.3 Overview of data collection and measurements

	2015	2016	2017	2018
1. Gas fluxes				
Canopy gas chamber (diurnal course)	x	x	x	x
Leaf gas exchange & water potential (diurnal course)	x	x	x	x
Sap flow/transpiration (diurnal course)	x	x	x	x
Soil respiration (diurnal course)			x	x
2. Crop growth				
Phenology	x	x	x	x
Stem/tiller number	x	x	x	x
Height	x	x	x	x
Aboveground dry matter (different organs)	x	x	x	x
Leaf area index	x	x	x	x
Chlorophyll		x	x	x
C:N content	x	x	x	x

This dissertation is composed of five chapters, including the introduction (**Chapter 1**). **Chapters 2** to **4** present the main results of the study. **Chapters 2** and **3** focus on the modeling studies for winter wheat and maize, respectively. **Chapter 4** analyzes field data on leaf water status, gas exchange, and crop growth characteristics for both crops in more detail. **Chapter 2** focusses on the simulation of winter wheat dynamics (data from 2016). In this chapter, plant hydraulic conductance, derived from the dynamic root growth over the growing season (SLIMROOT root growth model), was introduced into an existing crop model (LINTULCC2). The coupling between the Couvreur RWU model, the physically-based water balance model (HILLFLOW 1D) with the root: shoot model enabled the simulation of the water potential movement within the continuum pathway. This newly coupled model (Co: <HILLFLOW 1D-Couvreur RWU-SLIMROOT-LINTULCC2>) was compared with the model based on the Feddes RWU approach (Fe: <HILLFLOW 1D-Feddes RWU-SLIMROOT-LINTULCC2>) in predicting transpiration and photosynthesis, and crop growth of field-grown winter wheat in different soil types and water treatments. In **Chapter 3,** the performance of both modeling approaches was evaluated for maize, using CO_2 and H_2O gas exchange observations (data from 2017 and 2018) obtained for a broad spectrum of soil water availability and evaporative demands as well as different soil characteristics. **Chapter 4** focuses on a detailed assessment and analysis of the measured data from soil to leaf to canopy for both crop species obtained under contrasting environmental conditions and water treatments. In a first step, the diurnal and seasonal variations of leaf water potential and gas exchange at leaf

levels and measured gas fluxes at canopy levels are described and analyzed for both crops. Secondly, crop growth data (LAI, biomass, tiller number, crop height, and stem diameter) and related canopy CO_2 and H_2O gas flux data are presented. The relative roles of short-term (leaf water potential and stomatal conductance) and long-term responses (i.e., change of leaf area) to water stress in regulating CO_2 and H_2O gas fluxes and crop growth of two crops under different soil moisture are discussed. Finally, **Chapter 5** discusses to which extent the introduction of the newly coupled model which allows for the consideration of isohydric and anisohydric behavior and $K_{plant,}$ improves the simulation of wheat and maize growth and yield. An integrated discussion of how the results from the measurements (**Chapter 4**) compare with the insights gained from the modeling studies (**Chapter 2 and 3**) about the importance/need to distinguish between isohydric and anisohydric is provided. **Chapter 5** further identifies the most important limitations of the study and remaining knowledge gaps that require further research.

Due to the extreme spatial heterogeneity of the spring wheat canopy in 2015, which was caused by birds and poor germination, the data from this year was not included in the results and discussion. Chapter 2 presents data from winter wheat grown in two different soil types (which can be described as stony and silty) and under three water treatments (sheltered, rainfed, and irrigated) (green color, Table 1.4). Chapter 3 is based on data for maize grown on stony soil (irrigated and rainfed plots in 2017 and irrigated and rainfed plots with normal sowing dates, and the rainfed plot with the late sowing date in 2018). Chapter 4 presented data for plants grown on the stony soil: winter wheat (2016), maize (2017), and maize (2018) (Table 1.4).

Table 1.4 Summary of water treatment and soil types used in each chapter (green color)

Years	Soil types	Water treatments	Plot names	Chapter 2	Chapter 3	Chapter 4
2016	Stony	Sheltered	F1P1	F1P1		2016P1
		Rainfed	F1P2	F1P2		2016P2
		Irrigated	F1P3	F1P3		2016P3
	Silty	Sheltered	F2P1	F2P1		
		Rainfed	F2P2	F2P2		
		Irrigated	F2P3	F2P3		
2017	Stony	Rainfed	F1P1			2017P1
		Rainfed	F1P2		2017F1P2	2017P2
		Irrigated	F1P3		2017F1P3	2017P3
	Silty	Rainfed	F2P1			
		Rainfed	F2P2			
		Irrigated	F2P3			
2018	Stony	Rainfed	F1P1		2018F1P1	2018P1
		Rainfed	F1P2		2018F1P2	2018P2
		Irrigated	F1P3		2018F1P3	2018P3
	Silty	Rainfed	F2P1			
		Rainfed	F2P2			
		Irrigated	F2P3			

2 Chapter: Comparison of root water uptake models in simulating CO_2 and H_2O fluxes and growth of wheat

Abstract.

Stomatal regulation and whole plant hydraulic signaling affect water fluxes and stress in plants. Land surface models and crop models use a coupled photosynthesis-stomatal conductance modelling approach. Those models estimate the effect of soil water stress on stomatal conductance directly from soil water content or soil hydraulic potential without explicit representation of hydraulic signals between the soil and stomata. In order to explicitly represent stomatal regulation by soil water status as a function of the hydraulic signal and its relation to the whole plant hydraulic conductance, we coupled the crop model LINTULCC2 and the root growth model SLIMROOT with Couvreur's root water uptake model (RWU), and the HILLFLOW soil water balance model. Since plant hydraulic conductance depends on the plant development, this model coupling represents a two-way coupling between growth and plant hydraulics. To evaluate the advantage of considering plant hydraulic conductance and hydraulic signaling, we compared the performance of this newly coupled model with another commonly used approach that relates root water uptake and plant stress directly to the root zone water hydraulic potential (HILLFLOW with Feddes' RWU model). Simulations were compared with gas flux measurements and crop growth data from a wheat crop grown under three water supply regimes (sheltered, rain-fed and irrigated) and two soil types (stony and silty) in Western Germany in 2016. The two models showed a relatively similar performance in simulation of dry matter, LAI, root growth, RWU, gross assimilation rate, and soil water content. The Feddes model predicts more stress and less growth in the silty soil than in the stony soil, which is opposite to the observed growth. The Couvreur model better represents the difference in growth between the two soils and the different treatments. The newly coupled model (HILLFLOW–Couvreur's RWU–SLIMROOT–LINTULCC2) was also able to simulate the dynamics and magnitude of whole plant hydraulic conductance over the growing season. This demonstrates the importance of two-way feedbacks between growth and root water uptake for predicting the crop response to different soil water conditions in different soils. Our results suggest that a better representation of the effects of soil characteristics on root growth is needed for reliable estimations of root hydraulic conductance and gas fluxes, particularly in heterogeneous fields. The newly coupled soil-plant model marks a promising approach but requires further testing for other scenarios regarding crop, soil, and climate.

2.1 Introduction

Soil water status is amongst the key factors that influence photosynthesis, evapotranspiration and growth processes (Hsiao, 1973). Accurate estimation of crop water stress responses is important for predictions of crop growth, yield, and water use by crop models and land surface models (Egea et al., 2011).

Crop models and land surface models lump the effects of soil water deficit on stomatal regulation and crop growth in so-called 'stress factors' (Verhoef and Egea, 2014; Mahfouf et al., 1996). Crop water stress is strongly influenced by soil water availability which in turn depends on the distribution of water and of roots in the root zone and the transpiration rate or total root water uptake. Adequate representations in simulation models of root water uptake (hereby RWU) and root distributions (Gayler et al., 2013; Wöhling et al., 2013; Zeng et al., 1998; Desborough, 1997) are therefore needed. Most macroscopic RWU models estimate the water uptake as a function of potential transpiration (i.e. the transpiration of the crop when water is not limiting) and average moisture content or soil water pressure head and rooting densities (Feddes et al., 2001; van Dam, 2000). However, in this representation of RWU, crucial relations between RWU model parameters and root and plant hydraulic conductances, which translate soil water pressure head to water hydraulic heads in the shoot to which stomata respond, are lost. Note that hydraulic heads refer to total water potentials expressed in length units, and pressure heads to the hydraulic head minus the gravitational potential or elevation. For instance, the water stress factor calculated by the Feddes model (Feddes et al., 1978) based on the soil water pressure heads involves indirect linkages between the root zone water pressure head and the hydraulic head in the shoot in the sense that the water stress factors are adapted when potential transpiration rate changes. Such models like the Feddes approach represent indirectly the role of the root and plant hydraulic conductance and thus require calibration for different crop types and growing seasons (Cai et al., 2018; Vandoorne et al., 2012; Wesseling et al., 1991). The conductance of the root system is an important feature of the root system and different approaches to include it in RWU models were published (Quijano and Kumar, 2015; Vadez, 2014, Kramer and Boyer, 1995; Peterson and Steudle, 1993). Plant hydraulic conductance determines leaf water potentials which have a significant impact on stomatal conductance, leaf gas exchange, and leaf growth (Tardieu et al., 2014; Trillo and Fernández, 2005; Sperry, 2000; Zhao et al., 2005; Gallardo et al., 1996). Recently, some one-dimensional macroscopic RWU models based on hydraulic principles have been developed to represent water potential gradients from soil to root (de Jong van Lier et al., 2008) and within the root system (Couvreur et al., 2014). The latter approach simplified a

physically based description of water flow in the coupled soil-root system accounting for the root system hydraulic properties and architecture to simple linear equations between soil water pressure heads, leaf water hydraulic head, root water uptake profiles and transpiration rate that can be solved directly. It thereby avoids computation of time consuming numerical solutions of ordinary differential equations for the water flow and balance in the root system that are coupled with the non-linear soil water balance partial differential equation. It uses a stomatal regulation model assuming that stomatal conductance is not influenced by the leaf water hydraulic head as long as the leaf hydraulic head is above a critical leaf hydraulic threshold. Leaf water hydraulic head is kept constant by changing stomatal conductance when the critical leaf hydraulic threshold is reached. The Couvreur model also allows presenting the different stomatal regulations [i.e. isohydric and anisohydric in Tardieu and Simonneau, (1998)] (Couvreur et al., 2014, 2012).

Recently, inverse modelling routines using datasets of root density, leaf area, and soil water content and potential permitted the quantification of root-related parameters of Couvreur's model (root hydraulic conductivity). Sap flow measurements were used to validate simulated RWU by the parameterized model (Cai et al., 2018; Cai et al., 2017). These studies demonstrated the close relation between the root system conductance and root growth as part of overall plant growth and its response to water stress pointing at a two-way coupling between root-water uptake and plant growth. This implies that the parameterization of root water uptake needs to be coupled to plant growth, which in turn is influenced by water stress and other factors. Plant hydraulic conductance was introduced in crop models for several field crops such as soybean (Olioso et al., 1996), winter wheat (Wang et al., 2007), or for model testing (Tuzet et al., 2003). However, plant hydraulic conductance in these studies was kept constant without reference to dynamic root growth. To our knowledge, the effect of a two-way coupling between a RWU model accounting for whole plant hydraulic regulation and a crop growth model has not been studied yet. It is unclear whether such a coupled model improves the simulation of crop growth and development, CO_2 and H_2O fluxes.

In this study, we coupled the Couvreur's RWU model (Couvreur et al., 2014; Couvreur et al., 2012) with the existing crop growth model LINTULCC2 (Rodriguez et al., 2001) to consider the whole plant hydraulic conductance from root to shoot. The dynamics of root and shoot growth under varying soil water availability are explicitly represented by the coupled model. The overall aim of the study was to investigate whether consideration of plant hydraulic conductance can improve the simulation of CO_2 and H_2O fluxes, and crop growth in biomass, roots, and leaf area index of the same crop that is grown in two different soils and for three different water application regimes. To achieve this aim, three objectives were addressed: (i)

analyse and compare the predictive quality of a crop growth model coupled with a RWU model that considers plant hydraulics (Couvreur RWU model) and a model that does not consider plant hydraulics (Feddes RWU model), (ii) compare the simulated plant hydraulic conductances for the different growing conditions with direct estimates of these conductances from measurements, and (iii) analyse the sensitivity of RWU and crop growth to the Couvreur RWU and root growth model parameters (root hydraulic conductance, critical leaf hydraulic threshold, and specific weight of seminal and lateral root).

2.2 Materials and Methods

2.2.1 Location and experimental set-up

The study area was located in Selhausen in North Rhine-Westphalia, Germany (50°52'N, 6°27'E). The study field is slightly inclined with a slope of around 4° and characterized by a strong gradient in stone content along the slope (Stadler et al., 2015). Two rhizotrones were set up in the field: the upper site with stony soil (hereby F1) contains up to 60% gravel by weight while in the lower site with silty soil (hereby F2) the gravel content was approximately 4%. At each study site the effects of three different water treatments on growth and fluxes were investigated (sheltered – P1, rainfed – P2, and irrigated – P3) (Fig. 2.1). Each treatment was 3.25 m wide and 7 m long. The treatments bordered each other along 7-m-long side. Further information on the field experiment and set-up are presented in Cai et al., (2016), Stadler et al., (2015), and Cai et al., (2018). Irrigation was applied two times: on 22 May and 26 May 2016 in the irrigated plots (F1P3 and F2P3) during the growing season using dripper lines. The dripper lines (Model T-Tape 510-20-500, Wurzelwasser GbR, Münzenberg, Germany) were installed with 0.3-m intervals and parallel to crop rows. The non-transparent plastic shelter was manually covered (11 times) during rainfall and removed when rain stopped to induce water stress. On the sheltered days, radiation was assumed to be zero for the sheltered plots. Winter wheat (*Triticum aestivum* cv. Ambello) was sown with a density of 350-370 seed m^{-2} on 26 October 2015 and harvested on 26 July 2016 in both the stony (F1) and silty (F2) parts of the field. Fertilizers were applied at a rate of 80 kg N + 60 kg K_2O + 30 kg P_2O_5 per hectare on 15 March 2016. Nitrogen was further added on 2 May and 7 June 2016 with 60 and 50 kg N per hectare, respectively. Weeds and pests were controlled according to standard agronomic practice.

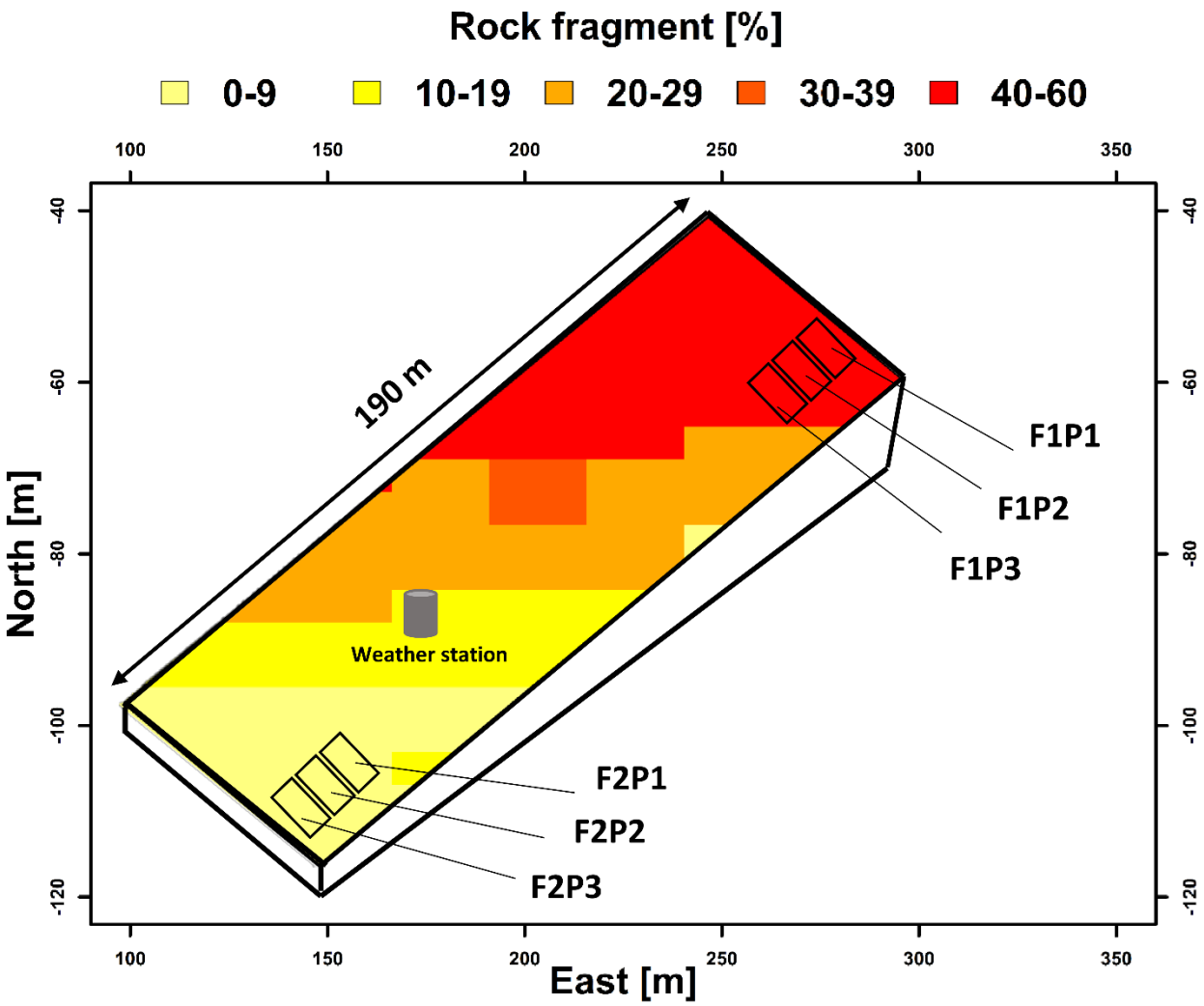

Figure 2.1: Description of the location of field experiment and set up of water treatments in the stony soil (F1) and silty soil (F2). P1, P2, and P3 are the sheltered, rainfed, and irrigated plots, respectively. Rock fragments are gravels with weathered granites.

2.2.2 Measurements

2.2.2.1 Soil water measurement and root growth

Soil water content and soil water potential were measured hourly by home-made time domain reflectometer (TDR) probes (Cai et al., 2016), tensiometers (T4e, UMS GmbH), and dielectric water potential sensors (MPS-2 matric potential and temperature sensor, Decagon Devices), respectively. Sensors were installed at 10, 20, 40, 60, 80 and 120 cm depth. Root measurements were taken with a digital camera (Bartz Technology Corporation) repeatedly from both left and right sides at 20 locations along 7 m-long horizontally installed minirhizotubes (clear acrylic glass tubes with outer and inner diameters of 64 and 56 mm, respectively). The calibration of the sensors, root growth observation, and post processing of the data were described in detail in Cai et al., (2016) and Cai et al., (2017).

2.2.2.2 Sap flow, leaf water hydraulic head, and gas fluxes measurement

Five, three, and five sap flow sensors (SAG3) (Dynamax Inc., Houston, USA) were installed in the irrigated, rainfed and sheltered treatments, respectively, at the beginning of wheat anthesis when stem diameters ranged between 3-5 mm. Vertical and horizontal temperature gradients, (dT) of each sensor were recorded at 10 minute intervals with a CR1000 data logger and two AM 16/32 multiplexers (Campbell Scientific, Logan, Utah). Sensor heat inputs were controlled by voltage regulators controlled by the CR1000 data logger. The raw signal data was aggregated to 30 minutes intervals and sap flow was calculated following Langensiepen et al., (2014). The number of tillers per square meter was counted every two weeks during the operation period of sap flow sensors (26 May – 23 July 2016). Tiller numbers were used to upscale the sap flow of single tiller (g h^{-1}) to canopy transpiration rate (mm h^{-1} or mm d^{-1}).

Leaf stomatal conductance and leaf water hydraulic head was measured every two weeks from 7 AM to 8 PM under clear and sunny conditions from tillering (20 April) to the beginning of maturation (29 June 2016). Stomatal conductance to water vapor of three to four upmost fully developed leaves were measured using a LICOR 6400 XT device (Licor Biosciences, Lincoln, Nebraska, USA) with a reference CO_2 concentration of 400 ppm, flow rate of 500 (µmol s^{-1}), and using real-time records of photosynthetic active radiation, vapor pressure deficit, and leaf temperature provided by the instrument. Then the leaves were quickly detached by a sharp knife to measure leaf water pressure head with a digital pressure chamber (SKPM 140/ (40-50-80), Skye Instrument Ltd, UK).

Plant hydraulic conductance in crop species can be estimated by measuring the transpiration and the root zone and leaf water hydraulic heads (Tsuda and Tyree, 2000). In our study, we calculated the conductance according to Ohm's law by dividing the hourly sap flow by the difference between effective root-zone hydraulic head and leaf hydraulic head. The effective root zone hydraulic head was calculated based on hourly measured soil water hydraulic head and measured root length density (cm cm^{-2}) at six depths (10, 20, 40, 60, 80, and 120 cm) in the soil profile following Eqs. (8) and (10) (see Section 2.3.4). During one measurement day, 6 hourly values of the conductance were obtained from measurements between 11 AM to 4 PM. The average and standard deviation of these hourly measurements were calculated for each measurement day. Yet, the hydraulic conductance can vary within short time periods due to the role of aquaporins (Maurel et al., 2008; Javot and Maurel, 2002; Henzler et al., 1999) or ABA regulation (Parent et al., 2009), and xylem cavitation (Sperry et al., 1998). We assumed however a constant plant hydraulic conductance during the day.

Canopy gas exchange was measured hourly on the same days when leaf water pressure heads were measured with a closed chamber system (Langensiepen et al., 2012). CO_2 concentration was derived with a regression approach by Langensiepen et al., (2012). Because we were interested in comparing measured with calculated hourly instantaneous gross assimilation by the newly coupled root: shoot model (LINTULCC2 with other subroutines), the total soil respiration (i.e. heterotrophic organisms and root respiration) was subtracted from the instantaneous canopy CO_2 exchange rate measured by the closed chamber. The total soil respiration was calculated based on measured soil temperature, soil water content at 10 cm soil depth, and leaf area index from crop using the fitted parameters derived from the same field and soil types (Prolingheuer et al., 2010). The calculated total soil respiration was compared and validated with the measured values in the same field in the previous years from Stadler et al., (2015).

2.2.2.3 Crop growth

Crop growth information was collected bi-weekly from 20 April until harvest 26 July 2016. Leaf area index and crop biomass were measured by harvests of two rows (1 m each) for each treatment. Leaves were separated into green leaves and brown leaves, and the brown and green leaf area was measured using a leaf area meter (LI-3100C, Licor Biosciences, and Lincoln, Nebraska, USA). The aboveground biomass was measured using the oven drying method. Samples were first weighed in total, then separated into different plant organs (green leaf, brown leaf, stem, ear, and grain) and weighed. Subsamples were afterward extracted from these samples, weighed, dried in an oven at 105 °C for 48 hours and weighed again for determining dry matter. At the end of growing season, four replicates of one square meter of plants were harvested from the plots to determine grain yield and harvest index.

2.2.3 Model description

2.2.3.1 Description of the original LINTULCC crop model

We used the crop model LINTULCC2 (Rodriguez et al., 2001). LINTULCC2 couples photosynthesis to stomatal conductance and can perform a detailed calculation of leaf energy balances (Rodriguez et al., 2001) (see Appendix 2A). This model was validated and compared with different crop models for spring wheat and used to simulate the effects of elevated CO_2 and drought conditions (Ewert et al., 2002; Rodriguez et al., 2001). LINTULCC2 calculates phenology, leaf growth, assimilate partitioning, and root growth following the procedure outline in Rodriguez et al., (2001).

In LINTULCC2, the assimilation rate of the sunlit and shaded leaf is calculated using the biochemical model of Farquhar and Caemmerer (1982). Stomatal conductance (g_s) was calculated according to the model of Leuning (Leuning, 1995) for sunlit and shaded leaves separately. In LINTULCC2 CO_2 uptake is calculated as a function of CO_2 demand by photosynthesis, and the ambient concentration of CO_2, using the iterative methodology proposed by Leuning (1995) (Appendix 2A). For the sake of simplification, in LINTULCC2, the internal leaf CO_2 concentration, C_i, is initially assumed as 0.7 times the atmospheric CO_2 concentration C_a (Vico and Porporato, 2008; Rodriguez et al., (2001); Jones, 1992). Then, the light saturated photosynthetic rate of sunlit and shaded leaves (AMAXsun, and AMAXshade, μM CO_2 m^{-2} s^{-1}), and the quantum yield for sunlit and shaded leaves (EFFsun, and EFFshade, μM CO_2 MJ^{-1}), are calculated iteratively (Farquhar et al., 1980; Farquhar, 1982). This iterative loop ends when the difference in calculated internal CO_2 mole fraction between two consecutive loops is < 0.1 μmol mol^{-1} (Appendix 2A). Based on a fraction of sunlit (and shaded) leaf area and leaf area index (LAI), the leaf stomatal resistance of sunlit and shaded leaves was integrated over the canopy leaf area to the canopy resistance (r_s) (Appendix 2B).

The canopy resistance, crop height, and calculated crop albedo (depending on both crop and soil water content of the surface layer) and the surface energy balance were used to calculate potential crop evapotranspiration (ETP – mm h^{-1}) using the Penman-Monteith equation (Allen et al., 1998) (see Appendix 2B). The obtained potential surface evapotranspiration is then split into evaporation and potential transpiration using:

$$T_{pot} = ETP(1 - e^{-kLAI}) \quad (1)$$

where k is the light extinction coefficient [0.6 in this study (Faria et al., 1994; Mo and Liu, 2001; Rodriguez et al., 2001)].

T_{pot} (mm h^{-1}) represents by definition the transpiration of the crop that is not limited by the root zone water hydraulic head. In section 2.3.4 it is explained how the actual transpiration, T_{plant} (mm h^{-1}), is calculated as a function of the potential transpiration and the root zone soil water pressure head. The ratio T_{plant} /T_{pot} defines the water stress factor fwat, which is used in the photosynthesis model:

$$\text{fwat} = \frac{T_{plant}}{T_{pot}} \quad (2)$$

Originally, LINTULCC2 runs at daily time steps (which allows for the within day variations in temperature, radiation and vapor pressure deficit). LINTULCC2 requires daily maximum and minimum temperature, actual vapor pressure, rainfall, wind speed, and global radiation. In order to capture the diurnal response of stomata, we modified the time step of the

photosynthesis and stomatal conductance subroutine from daily to hourly, while daily time steps were kept in the remaining subroutines (phenology, leaf growth, and biomass partition).

2.2.3.2 Root growth model

Root growth was simulated using SLIMROOT (Addiscott and Whitmore, 1991). The vertical extension of the seminal roots and the distribution of the lateral roots within the soil profile depend on the root biomass, the soil bulk density, the soil water content calculated by Hillflow1D (Bronstert and Plate, 1997), and the soil temperature computed by STMPsim (Williams and Izaurralde, 2005). The supply of assimilates from the shoot (RWTR) (g m^{-2} d^{-1}) is given by a partitioning table based on the thermal time (van Laar et al., 1997)) that is used to calculate the vertical penetration of seminal and lateral roots. The assimilate allocation for seminal root growth (ASROOT) is constrained by daily supply of assimilates from the shoot RWRT (g m^{-2} d^{-1}) and the demand of assimilates from seminal roots ($ASROOT_{demand}$).

$$ASROOT = \min(ASROOT_{demand}, RWRT) \quad (3)$$

$ASROOT_{demand}$ is a function of the number of seminal roots per square meter (NSROOT) which depends on the number of emerged plants per square meter and the number of seminal roots per plant; the specific weight of seminal root WSROOT (g m^{-1}); and the daily elongation rate of seminal roots RSROOT (m d^{-1}):

$$ASROOT_{demand} = RSROOT * WSROOT * NSROOT \quad (4)$$

RSROOT depends on the soil temperature and is constrained by a maximal elongation rate, $RSROOT_{max}$ and the soil temperature depend rate which is an empirical function of the soil temperature of the deepest layer where roots are growing, TBOTLAYER (K) (Jamieson and Ewert, 1999):

$$RSROOT = min(RSROOT_{max}, TBOTLAYER * RTFAC) \quad (5)$$

where RTFAC is the temperature factor driving the penetration of seminal roots (m K^{-1} d^{-1}) and TBOTLAYER (K) the soil temperature of the deepest layer where roots are growing. When soil temperature is below or equal to 0°C, no seminal growth occurs. The maximum daily elongation rate of seminal roots, $RSROOT_{max}$ was set at 0.03 m d^{-1} for wheat according to Watt et al., (2006).

The daily increment in seminal root length (SRLIR - m m^{-2} d^{-1}) is defined as:

$$SRLIR = ASROOT/WSROOT \quad (6)$$

Lateral roots are simulated when the root biomass supplied by the shoot is greater than the assimilate demand of seminal roots (RWRT > $ASROOT_{demand}$). Lateral root biomass is distributed stepwise from the top layer to the deepest soil layer with seminal roots.

Roots start to die after anthesis. Since the specific weight of the roots of cereal crops varies with soil strength (Colombi et al., 2017; Lipiec et al., 2016; Hernandez-Ramirez et al., 2014; Merotto Jr and Mundstock, 1999), we chose different specific weights for the stony (F1) and silty soil (F2) from the range that was observed by Noordwijk and Brouwer (1991) and Jamieson and Ewert (1999) in soils with different soil strength (Appendix 2C).

2.2.3.3 Physically based soil water balance model

HILLFLOW 1D was chosen for calculating the water pressure heads in the soil and how they change with depth and time as a function of the precipitation, soil evaporation, RWU, and water percolation at the bottom of the simulated soil profile (Bronstert and Plate, 1997). HILLFLOW 1D calculates soil water content and water fluxes by numerically solving the Darcy equation for unsaturated water flow in porous media (Bronstert and Plate, 1997). The relations between soil water hydraulic head, water content and hydraulic conductivity are described by the Mualem-van Genuchten functions (van Genuchten, 1980). The parameters of these functions, i.e. the soil hydraulic parameters, for the different soil layers and the two sites were taken from (Cai et al., 2018) (Appendix 2D). In this study, a soil depth of 1.5 m vertically discretized into 50 layers was considered. A free drainage bottom boundary and a mixed flux-matric potential boundary at the soil surface were implemented. The mixed upper boundary condition prescribes the flux at the soil surface by the precipitation and evaporation rates as long as the soil water pressure heads are not above or below critical heads. When these heads are reached, the boundary conditions are switched to constant pressure head boundary conditions.

2.2.3.4 Feddes' and Couvreur's root water uptake models

The Feddes RWU model (Feddes et al., 1978) (See Appendix 2E) was already built in the HILLFLOW 1D model (Bronstert and Plate, 1997). We implemented the Couvreur RWU model (Couvreur et al., 2014a; Couvreur et al., 2012) into HILLFLOW. Both models, T_{plant} is calculated in both models from the sum of the simulated RWU in the different soil layers and used to calculate the water stress factor (fwat) following Eq. (2), which was used in the photosynthesis model. In the Feddes model, root water uptake from a soil layer is proportional to the normalized root density, NRLD (m^{-1}), in that layer and is multiplied by a stress function α that depends on the soil water pressure head, ψ_m(m), in that soil layer and the potential transpiration rate (see Appendix 2E for the definition of α):

$$RWU_i = \alpha(\psi_{m,i}, T_{pot}) T_{pot} NRLD_i \Delta z_i \quad (7)$$

where NRLDi is calculated from the root length density, RLD (m m^{-3}) and discretized soil depth Δz_i (m) as:

$$NRLD_i = RLD_i / \sum_{i=1}^{N} RLD_i \, \Delta z_i \quad (8)$$

The parameters of the α stress functions model were taken from (Cai et al., 2018) (See Appendix 2C). According to Eq. (7), the reduction of water uptake in a given layer depends on the soil water pressure head in that layer only and does not influence the water uptake in other layers. This means that a reduced water uptake in dried out soil layers directly leads to a reduction of the total root water uptake and plant transpiration and is not compensated by increased uptake in other layers where there is still water available.

In the Couvreur model, the root water uptake in a given soil layer is related to the water potentials in the root system and root water uptake in other soil layers so that compensatory uptake is considered in this model. Root water uptake in a certain layer is obtained from:

$$RWU_i = T_{plant} NRLD_i \Delta z_i + K_{comp}(\psi_i - \psi_{sr}) NRLD_i \Delta z_i \quad (9)$$

where ψ_i (m) is the total hydraulic head (or hydraulic head which is the sum of the pressure head and gravitation potential heads) in layer i, ψ_{sr} (m) is the average hydraulic head in the root zone and K_{comp} (d^{-1}) is the root system conductance for compensatory uptake. The first term of Eq. (9) represents the uptake from that soil layer when the hydraulic head is uniform in the root zone and the second term represents the increase or decrease of uptake from the soil layer due to a respectively higher and lower hydraulic head in layer i than the average hydraulic head. The average root zone hydraulic head is calculated as the weighted average of the hydraulic heads in the different soil layers as:

$$\psi_{sr} = \sum_{i=1}^{N} \psi_i NRLD_i \, \Delta z_i \quad (10)$$

The plant transpiration rate is the minimum of the potential transpiration rate and the transpiration rate, $T_{threshold}$ (mm h^{-1}), when the hydraulic head in the leaves reaches a threshold value, $\psi_{threshold}$ (m) that triggers stomatal closure:

$$T_{plant} = \max(0, \min(T_{pot}, T_{threshold})) \quad (11)$$

$T_{threshold}$ is calculated from difference between the root zone hydraulic head and the threshold hydraulic head in the leaves $\psi_{threshold}$ that is multiplied by the plant hydraulic conductance, K_{plant} as:

$$T_{threshold} = K_{plant}(\psi_{sr} - \psi_{threshold}) \quad (12)$$

In our study, we used the a critical leaf hydraulic head, $\psi_{threshold}$ of – 200 m (equivalent to – 2 MPa) (Cochard, 2002; Tardieu and Simonneau, 1998). The original Couvreur model only considers the hydraulic conductance from the roots to the plant collar, K_{rs}, by assuming that the hydraulic resistance from plant collar to leaves is minor as compared to root system resistance. The shoot hydraulic resistance could be large in some crop plants (Gallardo et al., 1996) or in trees (Domec and Pruyn, 2008; Tsuda and Tyree, 1997). In order to simulate the leaf water hydraulic head, the whole plant hydraulic conductance (K_{plant}) needs to be used. The whole plant hydraulic conductance could be estimated from different components (i.e. soil to root, stem to leaf) following an approach from Saliendra et al., (1995) or a more complex attempt by Janott et al., (2011). Because hydraulic data from plant collar to leaf are rare and difficult to obtain and account for differing species characteristics and environmental conditions, for the sake of simplification, we derived K_{plant} (d^{-1}) from the root hydraulic conductance ($K_{rs,doy}$) assuming that K_{plant} is a constant fraction β of $K_{rs,doy}$ (d^{-1}):

$$K_{plant} = \beta\, K_{rs,doy} \quad (13)$$

We used the measured plant hydraulic conductance from sap flow, leaf water hydraulic head, soil water pressure head, and root observation (Section 2.2.1 above) in the lower rainfed plot to calibrate □ which was then applied for all plots (Appendix 2C). K_{plant} and K_{rs} in anisohydric wheat are influenced by soil water availability and crop development. We followed the approach of Cai et al., (2017) to estimate the root hydraulic conductance ($K_{rs,,doy}$) and compensatory root water uptake (K_{comp}) based on the total length of the root system below a unit surface area, $TRLD_{doy}$ ($m\ m^{-2}$), at a given day of year (DOY) (Eq. 14), which is the output from SLIMROOT:

$$TRLD_{doy} = \sum_{i}^{N} RLD_{i,doy}\, \Delta z_i \quad (14)$$

Assuming the same conductance for all root segments, the root system conductance scales with the TRLD:

$$K_{rs,\ doy} = K_{rs,\,normalized} TRLD_{doy} \quad (15)$$

where $K_{rs,\ normalized}$ ($d^{-1}\ cm^{-1}\ cm^2$) is the root system conductance per unit root length per surface area. For $K_{rs,\ normalized}$, we took the average value that was obtained by Cai et al., (2018) for the stony soil (F1) and silty soil (F2) sites: $0.2544\ 10^{-5}$ ($d^{-1}\ cm^{-1}\ cm^2$) (Appendix 2C).

Many studies included hydraulic conductance along the soil-plant-atmosphere pathway to simulate water transport (Verhoef and Egea, 2014; Wang et al., 2007; Tuzet et al., 2003; Olioso et al., 1996). However, root and plant hydraulic conductance in these studies were assumed constant. In our work, the plant hydraulic conductance varied following the shoot and root development in the growing season.

2.2.3.5 Coupling of water balance and root water uptake models with the crop model

We carried out a comprehensive comparison of the following modelling approaches for simulating CO_2 and H_2O fluxes and crop growth (Fig. 2.2):

- HILLFLOW 1D - Couvreur's RWU - SLIMROOT - LINTULCC2 (Co) ;
- HILLFLOW 1D - Feddes' RWU - SLIMROOT - LINTULCC2 (Fe)

The photosynthesis and stomatal conductance subroutines, RWU and HILLFLOW 1D water balance model, and evaporative demand (ETP) were run or specified with hourly time steps, while phenology, leaf growth, root growth, and biomass partitioning were updated daily. For a certain hourly time step $\Delta t_i = t_i - t_{i-1}$, different modules were solved in the following sequence. First, LINTULCC2 was used with a water stress factor fwat =1 to calculate the leaf and canopy resistance, and the potential transpiration rate. T_{pot} was then used in HILLFLOW 1D to calculate the soil water pressure head changes, water content changes, the actual transpiration, and fwat during the time step. LINTULCC2 was then run again using the fwat. The leaf conductance and assimilation rate were calculated. For the next time step, the same loop was run and hourly assimilation was accumulated to a daily value. Daily assimilation rates were used in modules that run with a daily time step. For instance, modules of LINTLCC2 that calculate assimilate partitioning which is used to calculate shoot (LAI) development and passed to SLIMROOT to simulate root development (Fig. 2.2). Before comparing these modelling approaches, we calibrated the original LINTULCC model using the data from the rainfed plots in the silty soil (F2P2). The model is firstly calibrated to make sure the model properly described the phenology. Two parameters (minimum thermal sum from sowing to anthesis and thermal sum from anthesis to maturity (°C d)) were used for phenology calibration based on information of sowing, anthesis, and maturity dates. The model was then calibrated using time series of LAI, biomass, and gross assimilation rate through the change of maximum carboxylation rate at 25 °C (VCMAX25), critical leaf area index (LAICR), and relative growth rate of leaf area during exponential growth (RGRL) parameters. The same crop parameters and soil parameters were applied for both model configurations (Appendix 2C, D). All presented flux data (soil water flux, gross assimilation rate, sap flow, stomatal conductance,

and leaf water pressure head) and the simulated outputs were converted from local time to coordinated universal time (UTC) to avoid the confusion in interpretation.

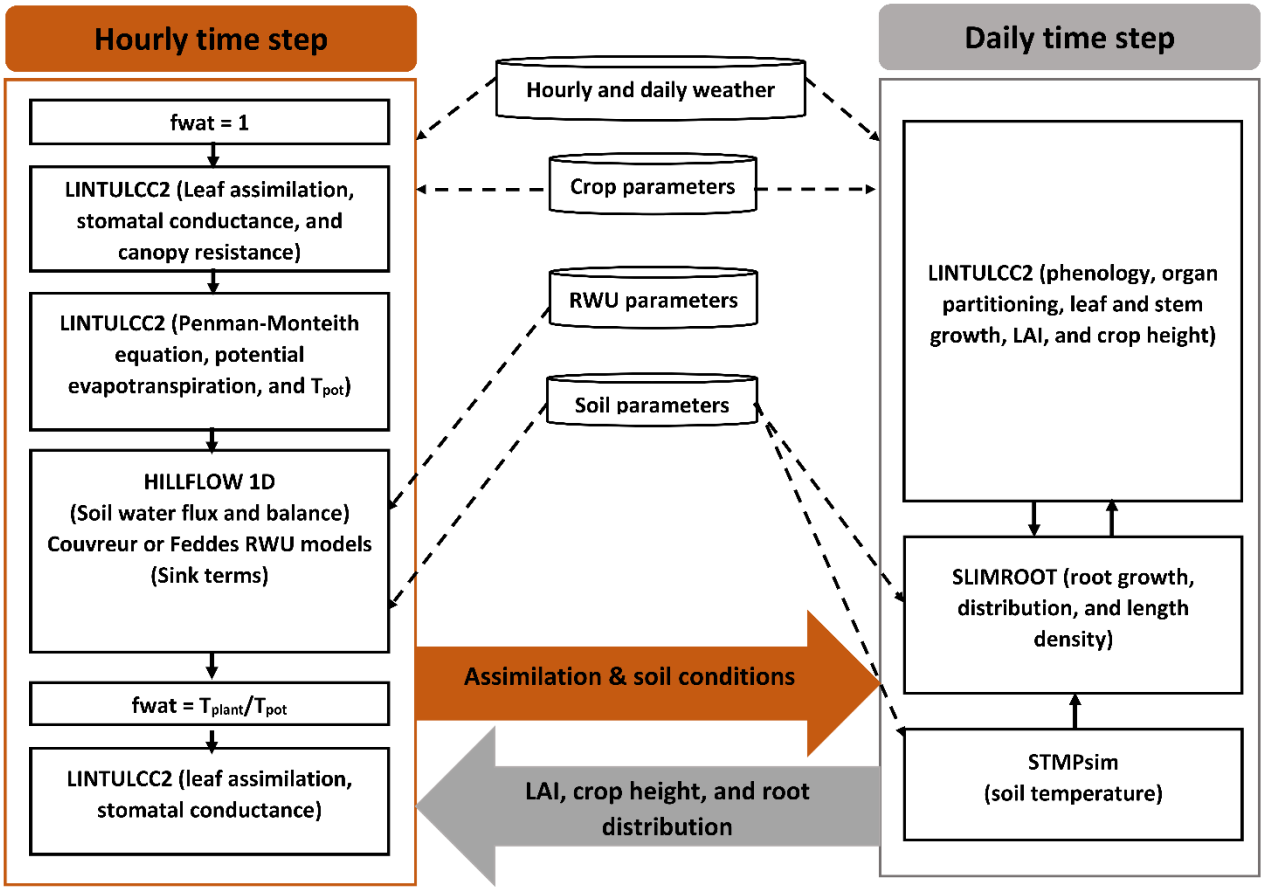

Figure 2.2: Description of the coupled root: shoot models in the study. The orange arrow indicates feedbacks from the hourly simulations to daily simulation while the grey arrow indicates feedbacks from the daily simulations to the hourly simulations. The dashed black arrows denote the weather input and parameters to the subroutines. The continuous black arrows indicate the links amongst the modelling subroutines.

2.2.4 Criteria for model comparison and evaluation

We analysed the performance of two modelling approaches following the approach from (Willmott, 1981): (i) correlation coefficient (r) (Eq. 16); (ii) the degree to which simulated values approached the observations or index of agreement (I) defined in Eq. (17). This value varies from 1 (for perfect agreement) to 0 (for no agreement); (iii) the root mean square errors (RMSE) was computed to characterize the difference between simulated value and observed data (Eq. 18);

$$r = \frac{\sum_{i=1}^{n}\left(Sim_i - \overline{Sim}\right)\left(Obs_i - \overline{Obs}\right)}{\sqrt{\left[\sum_{i=1}^{n}\left(Sim_i - \overline{Sim}\right)^2\right]\left[\sum_{i=1}^{n}\left(Obs_i - \overline{Obs}\right)^2\right]}} \quad (16)$$

$$I = 1 - \left[\frac{\sum_{i=1}^{n}(Sim_i - Obs_i)^2}{\sum_{i=1}^{n}\left(\left|Sim_i - \overline{Obs}\right| + \left|Obs_i - \overline{Obs}\right|\right)^2}\right] \quad (17)$$

$$RMSE = \sqrt{\frac{\sum_{i=1}^{n}(Sim_i - Obs_i)^2}{n}} \quad (18)$$

where Sim and Obs are simulated and measured variables; i is the index of a given variable; $\overline{Obs}$ and $\overline{Sim}$ is the mean of the simulated and measured data; and n is the number of observations;

2.2.5 Sensitivity analysis

The parameters of the SLIMROOT root growth model and the Couvreur RWU model were derived from literature data. However, these parameters are uncertain and vary between different wheat varieties. In order to evaluate the effect of these parameters on the simulated crop growth and root water uptake, we carried out a sensitivity analysis.

In a first set of simulations, the root length normalized root system conductivity $K_{rs,\ normalized}$ was varied from 0.1 to 40 times the $K_{rs,\ normalized}$ = 0.2554 10^{-5} cm d^{-1} that was estimated by Cai et al., (2018). The root system hydraulic conductance is related to the total root length, which depends on the specific weight of lateral and seminal roots. These two parameters are rarely reported, especially for field grown wheat (Noordwijk and Brouwer, 1991). The range of observed specific weight of lateral root in wheat was reported in the range of 0.00406 to 0.00613 g m^{-1} (Noordwijk and Brouwer, 1991). Huang et al., (1991) found that the specific weight of seminals root of winter wheat grown under controlled soil chamber conditions decreased from 0.023 to 0.0052 g m^{-1} when air temperature increased from 10 to 30°C. The values of 0.015 and 0.0035 g m^{-1} are often used for specific weights of seminal and lateral roots, respectively in crop growth simulations of wheat cultivars (Mboh et al., 2019; Jamieson and Ewert, 1999). In a second set of simulations, the specific weight of lateral roots was subjected to change from 0.002, 0.003, 0.0035, 0.004, 0.005, 0.006, and 0.007 g m^{-1} while specific weight of seminal roots was the same (0.015 g m^{-1}) for all simulations. For the third set of simulations, specific weight of lateral root was kept at 0.0035 g m^{-1} while the specific weights of seminal root varied from 0.005, 0.0075, 0.01, 0.0125, 0.015, 0.0175, 0.02, and 0.0225 g m^{-1}. In the last sensitivity exercise, the critical leaf hydraulic head threshold ($\psi_{threshold}$) was varied between -120 m and -260 m.

2.3 Results and discussion

In the first section, we discuss the performance of the two coupled root-shoot models with Couvreur RWU model (Co model) and Feddes RWU model (Fe model). The comparative analysis firstly focuses on simulating crop growth and root development under different water conditions and soil types. Next, the simulated transpiration reduction, soil water dynamics, RWU, and gross assimilation rate are presented and discussed. The K_{plant} is explicitly simulated by the Co model in the different soils and treatments and is compared with direct estimates of K_{plant} from measurements. In the second part, we discuss the sensitivity analysis of the Co model to understand the effects of changing $K_{rs,\ normalized}$, specific weight of seminal and lateral root, and $\Psi_{threshold}$ on the simulated biomass growth and RWU in different soils and under different water regimes.

2.3.1 Comparison of Couvreur and Feddes's RWU model

2.3.1.1 Root and shoot (biomass and LAI) growth

Fig. 2.3 shows the dry matter and LAI simulated by the Co and Fe model versus the measured data. The difference between the two samples of the two different rows for each sampling day indicated the heterogeneity in crop growth even within a small treatment plot. Biomass and LAI simulated by the Co and Fe models were in fair agreement with observations. The r^2 of Co and Fe models were 0.91 and 0.86, respectively, for biomass while 0.76 and 0.75, respectively, for LAI (Table 1). However, both models overestimated dry matter and LAI production in the irrigated and rainfed stony plots whereas biomass and LAI were underestimated in the sheltered silty plot. This suggests that water stress in the sheltered silty plot was overestimated. For the irrigated stony soil plot, in which the water content stayed high due to the frequent rainfall events and the additional irrigation, it is unlikely that the lower growth is due to water stress. The later start of the growth after the winter could be due to the effects of soil strength and lower soil temperature on crop development in the stony field that were not captured by the model. Soil hardness could constrain root growth while the higher stone content possibly resulted in slower warming up of the soil in spring than the silty soil which in turn slowed down root and crop development.

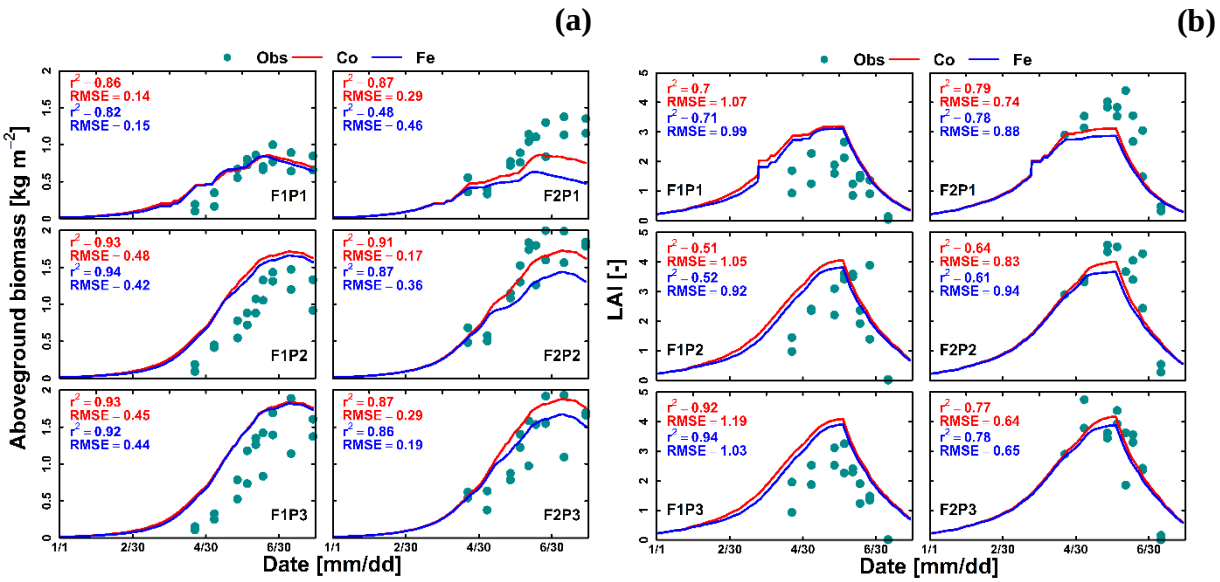

Figure 2.3: Comparison between observed (cyan dot) and simulated (a) above ground dry matter and (b) LAI by Couvreur (Co, solid red line), and Feddes (Fe, solid blue line) model at the sheltered (P1), rainfed (P2), and irrigated (P3) plots of the stony soil (F1) and the silty soil (F2). Note: crop germination was on 26th October 2015, data is shown here from 1 January to harvest 23 July 2016. RMSE in (a) is kg m^{-2} while RMSE in (b) is unit less.

Table 2.1 Quantitative and statistical measures of the comparison between two modelling approaches and the observed data for the 3 water treatments and 2 soil types. RMSE: root mean square error; r^2: correlation coefficient; I: agreement index; n samples: number of sample. Couvreur RWU model (Co) and Feddes RWU model (Fe).

Variables	Statistical	Co	Fe
Daily RWU (mm d^{-1})	RMSE	1.15	1.13
	r^2	0.62	0.66
	I	0.84	0.85
	n samples	312	312
Biomass (g m^{-2})	RMSE	303	336
	r^2	0.91	0.86
	I	0.84	0.81
	n samples	54	54
LAI (-)	RMSE	0.92	0.90
	r^2	0.76	0.75
	I	0.77	0.77
	n samples	54	54
Gross assimilation rate (µM m^{-2} s^{-1})	RMSE	6.34	7.26
	r^2	0.63	0.61
	I	0.86	0.83
	n samples	302	302

For the stony plots, the Fe and Co models gave similar results whereas for the silty soil, the Co model reproduced the biomass and LAI better than the Fe model. Although the statistical parameters (r^2 and RMSE) for the silty soil plots show only a slightly better fit of the Co than of the Fe model, there is a remarkable qualitative difference between the models. The Fe model simulated lower biomass and leaf area in the silty soil than in the stony soil, which is opposite to the observations. The Co model simulated similar biomass and LAI in the irrigated and rainfed plots of the silty and stony soils and higher biomass and LAI in the sheltered plot in silty soil than in the stony soil, which is in closer agreement with the observed differences in biomass and LAI between the two soils. The simulated effect of the soil type on the crop growth was qualitatively correct for the Co model but incorrect for the Fe model.

Fig. 2.4 displays the observed root length densities from minirhizotube observations and the simulated ones. Higher root length densities were observed and simulated in the silty soil than in the stony soil. The model simulated smaller root densities in the stony soil because a larger specific weight of the roots was considered for the stony than for the silty soil. The simulated root density profiles showed the highest root densities near the surface whereas the observed profiles, especially in the silty soil, showed higher densities in the deeper soil layers. The model simulated smaller root length densities in the sheltered than in the other plots of both the stony and silty soils. This is a consequence of the lower biomass growth that was simulated in the sheltered plots. For the stony soil, this corresponds with the observations that also showed lower root length densities in the sheltered than in the other plots. However, for the silty plot, the opposite was observed. For both the simulations and the observations, we compared the ratio of total root lengths in a certain plot and treatment to the total root length in rainfed stony plot F1P2 (Appendix 2F). In the stony plots the ratios of the observed total root length to the reference were close to 1 but the simulated total root length in the sheltered plot was smaller than one. The ratios of the total root lengths in the silty plot to the reference were for all plots larger than one. Nevertheless, the ratios of observed root lengths were larger (2.27 - 4.03) than those of the simulated ones (1.04 - 1.67). The observed ratios were larger for the sheltered plot than for the other plots in the silty soil whereas the opposite was simulated by the models. Predefined ratios of root and shoot biomass allocation for a given growth period and a source driven root growth (van Laar et al., 1997) in our models do not allow a shift in carbon allocation to root (for more root growth) in response to water stress. However, this should not be emphasized too much because the observed imaged root data from minirhizotubes for driving the root length might have potential errors and uncertainties (Cai et al., 2018).

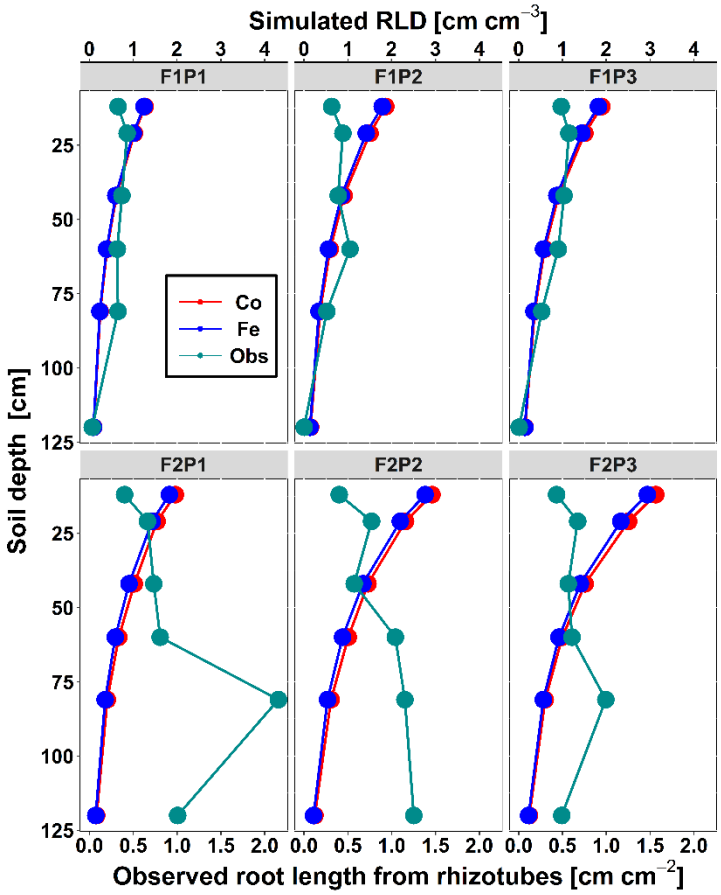

Figure 2.4: Comparison between observed root length from rhizotubes (cm cm^{-2}) (cyan line with dots) and simulated root length density (RLD) (cm cm^{-3}) from 10, 20, 40, 60, 80, and 120 cm soil depth at DOY 149 by Couvreur (Co, solid red) and Feddes (Fe, solid blue) model at the sheltered (P1) rainfed (P2), and irrigated (P3), of the stony soil (F1) and the silty soil (F2)

2.3.1.2 Transpiration reduction, soil water dynamic, RWU, and gross assimilation rate

Fig. 2.5a and 2.5b show the reduction of the transpiration compared to the potential transpiration, fwat, simulated by the Fe and Co models (mid of March until harvest) and Fig. 2.5c and 2.5d show the simulated potential and the simulated and measured actual transpiration rates from the end of April until harvest. The Fe model simulated more water stress than the Co model and a more pronounced and earlier stress in the silty than in the stony soil. As a consequence, the simulated transpiration rates by the Fe model were generally lower than the simulated ones by the Co model. According to the fwat factors, also the Couvreur model simulated more water stress in the silty soil than in the stony soil. The effect of fwat on the cumulative transpiration and growth depends also on the timing of the lower fwat values. At the beginning of the growing season when the LAI and potential transpiration are low, the impact of a lower fwat on the cumulative transpiration and growth is lower than later in

the growing season. These results are in contrast with findings by Cai et al., (2017) and Cai et al., (2018) who found that there was no water stress simulated in the silty soil in 2014 by the Co and Fe models. However, the studies from Cai et al., (2018) used the measured root distributions instead of the simulated ones from the root-shoot model. Therefore, in their simulations, the crop had more access to water in the deeper soil layers. Second, they used the Feddes-Jarvis model, which accounts for root water uptake compensation. This could explain why they did not simulate water stress in the silty plot with the Feddes model. Thirdly, weather conditions and irrigation applications were different in their study in 2014 (less dry) from our experimental season in 2016.

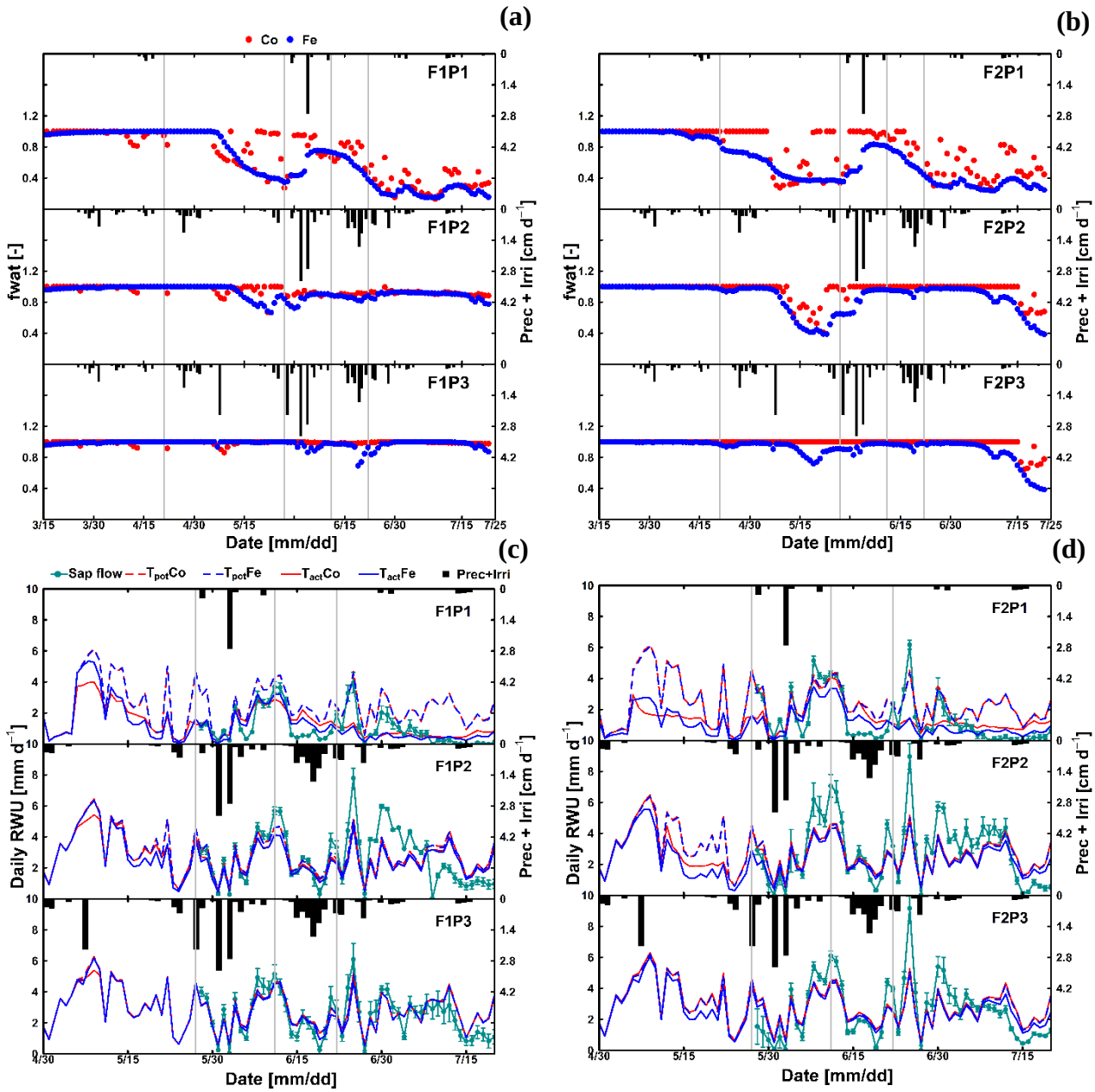

Figure 2.5: Daily transpiration reduction factor (fwat) (a, b) from 15 March to harvest 23 July 2016 and comparison between observed (cyan) and simulated root water uptake (RWU) and potential transpiration simulated (c, d) by Couvreur (Co, closed red), and Feddes (Fe, closed blue) from 30 April to 20 July 2016 model at the sheltered (P1), rainfed (P2), and irrigated (P3) plots of the stony soil (F1), and the silty soil (F2). Time series of precipitation (Prec) and irrigation (Irri) are given in the panels. Note: crop germination was on 26th October 2015. Vertical cyan bars represent the standard deviation of the flux measurements in the different stems. Vertical grey lines show days with the measured and simulated diurnal courses of root water uptake (RWU), leaf water pressure head (ψ_{leaf}), stomatal conductance (gs), and gross assimilation rate (Pg) as used in Figure 2.9.

According to Fig. 2.5c and 2.5d, during the time when sap flow could be measured (from end of May until harvest), the stress factors did not differ a lot between the Fe and Co models. For the rainfed and irrigated plots in the silty soil, the Fe model predicted a stronger reduction in transpiration near the end of the growing season than the Co model. This resulted in a smaller cumulative transpiration predicted by the Fe than by the Co model over the measurement period in these treatments (Fig. 2.6). Although this gives the impression that the Co model is better in agreement with the measurements in these treatments, Fig. 2.5d indicates that this is due to compensating errors. Both models underestimate the measured sap flow in the beginning of the measurement period and overestimate it towards the end, and the Co model overestimates more than the Fe model. This overestimation is due to an overestimation of the LAI by both models near the end of the growing season (Fig. 2.3b). The reduction of the transpiration in the sheltered plots of the two soils compared to the other treatments is predicted relatively well but the Fe model predicted more stress and a stronger reduction in transpiration than the Co model, especially in the silty soil. For this treatment, the Co model, which simulated less stress (larger fwat factors), predicted the cumulative transpiration and how it differed between the two soil types better than the Fe model.

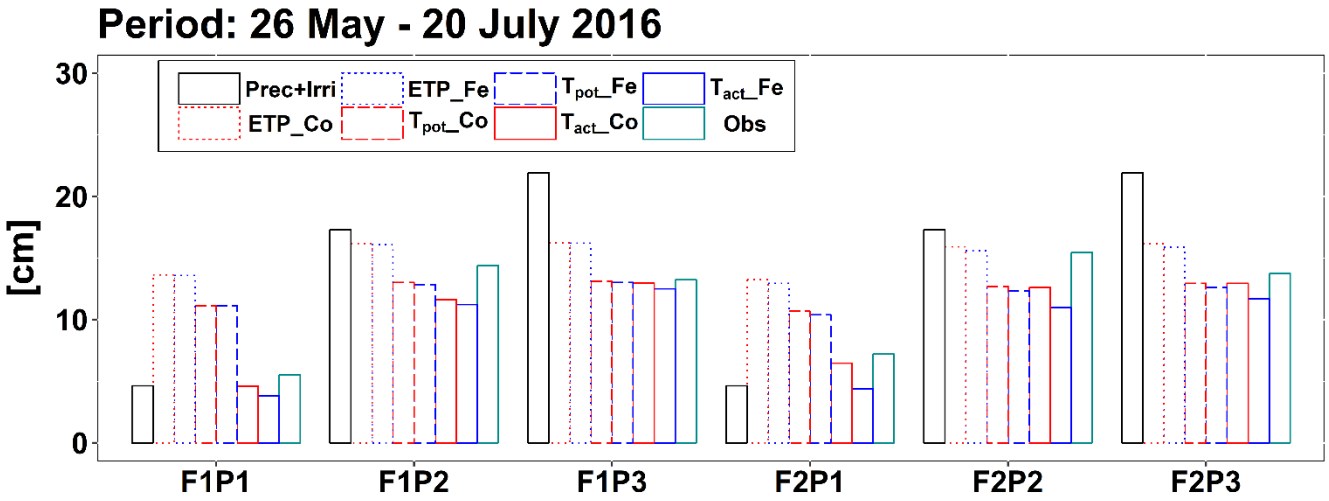

Figure 2.6: Cumulative precipitation and irrigation (Prec+Irri), potential evapotranspiration (ETP), potential transpiration (T_{pot}), actual transpiration (T_{act} or RWU) simulated by Couvreur (Co) and Feddes (Fe) model, and measured transpiration by sap flow sensors (Obs) from 26 May to 20 July 2016 at the sheltered (P1), rainfed (P2), and irrigated (P3) plots of the stony soil (F1), and the silty soil (F2).

Simulated transpiration in all treatments and both soils are plotted versus the sap flow measurements in Fig. 2.7. On average, the two models slightly underestimated measured T_{act} (Fig. 2.5c and 2.5d). This was also found in the study by Cai et al., (2018) where sap flow was measured in winter wheat in 2014. However, in their study, there was a rather constant offset

between the simulations and the sap flow data. One reason could be that in our study we used the simulated LAI values whereas Cai et al., (2018) used the measured LAI values. In the stony plots, the measured LAIs are overestimated by the simulations so that one would expect an overestimation of the transpiration by the model. The opposite holds true for the silty plot. The overestimation of the LAI at the end of growing season resulted in an overestimation of the transpiration in non-sheltered plots in both soil types. Because of the small size and hollow stem of wheat plants (Langensiepen et al., 2014), it is difficult to install the micro-sensors and measure the temperature variation for the thin wheat stem with high time frequency under ambient field conditions. In addition, the sap flow in a single tiller is also influenced by spatial variation in environmental conditions. The variability of stem development also results in a significant stem-to-stem variability in sap flow (Cai et al., 2018). The r^2 of simulated RWU from the Co and Fe models versus sap flow are 0.62 and 0.66, respectively (Table 1 and Fig. 2.7a) indicating that our coupled models have fair performance in RWU simulation. Measuring gas exchange with closed chamber concentration measurements can significantly alter the microclimatic conditions within the chamber, especially at times of high exchange rate. However using regression functions at the starting point of measurement intervals reduces absolute errors (Langensiepen et al., 2012). The simulated gross assimilation rate (Pg) from two models matched relatively well with the gross assimilation rate measured by a manually closed-canopy chamber with r^2 of 0.63 and 0.61 for Co and Fe, respectively (Table 2.1 and Fig. 2.7b).

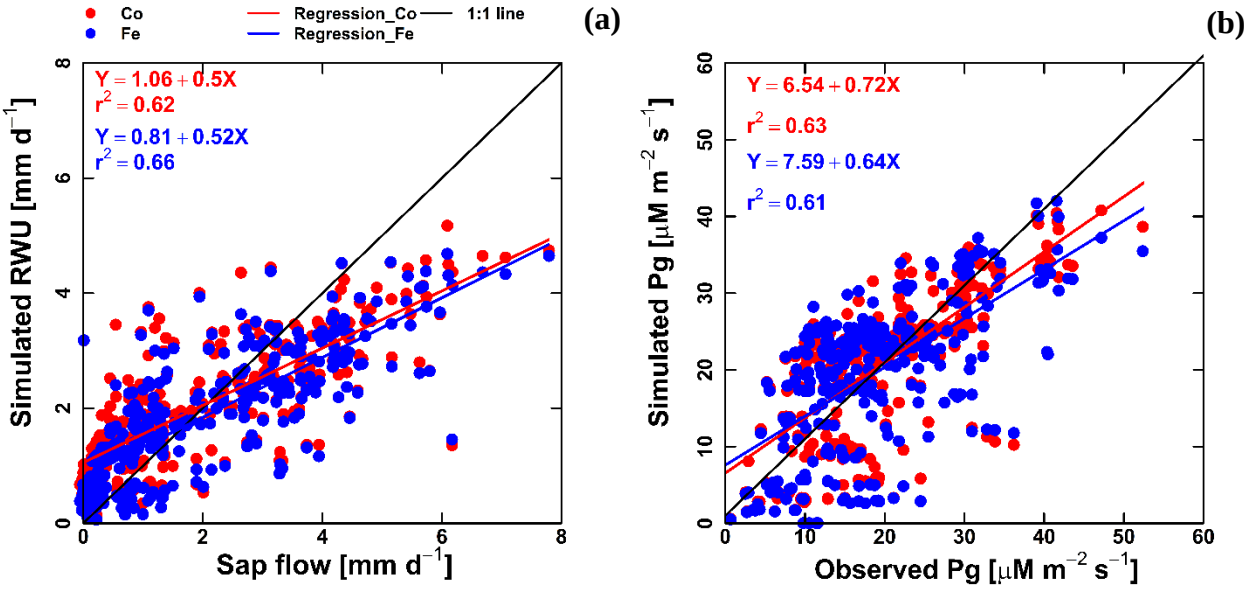

Figure 2.7: Correlation between observed and simulated (a) daily actual transpiration (or RWU) (b) hourly gross assimilation rate (Pg) from Couvreur (Co, red dot), and Feddes (Fe, blue dot) models of both fields (F1 and F2). Sap flow data was from 26 May until 20 July 2017 (n = 312). Gross assimilation rate from 08 measurement days (n = 302). RMSE in (a) is mm d^{-1} while RMSE in (b) is µM m^{-2} s^{-1}.

The method that we used for modelling the canopy resistance used in the Penman-Monteith has been reported for both short and tall crops (Dickinson et al., 1991; Kelliher et al., 1995; Irmak & Mutiibwa, 2010; Perez et al., 2006; Katerji et al., 2011; Srivastava et al., 2018). The fair agreement of RWU to sap flow in our study indicates the proper estimate of ETP based on the crop canopy resistance (with fwat = 1) in winter wheat. The direct calculation of crop canopy resistance in our work allows to capture physiological responses of the crop (stomatal conductance) to solar radiation, temperature, and vapor pressure deficit (Eqn. A5). In addition, this approach also avoids calculating grass reference evapotranspiration based on a constant canopy resistance.

The differences in simulated stress between the different models were more pronounced in May (Fig. 2.5) when no sap flow data were available. The Co model predicted less stress and more RWU than the Fe model in May, especially in the rainfed and irrigated plots of the silty soil. The larger stress simulated by the Fe model in the rainfed and irrigated silty plots resulted in a smaller increase in biomass that was simulated in May by the Fe than by the Co model (Fig. 2.3a). The measurements of growth in the silty soil do not suggest that there was water stress in these plots in the silty soil indicating that the Co model better simulated transpiration and growth for these cases than the Fe model. Another way to test the RWU simulated by the different models is to compare the simulated soil water contents (Fig. 2.8). The Co and Fe models were able to simulate both dynamics and magnitude of SWC in different soil depths and for different water treatments (average of RMSEs over all soil depths was 0.06 for both models, Appendix 2G). The Co and Fe models displayed lower water contents than the measured ones in the deeper layers at the late growing season (i.e. depth 80 and 120 cm) (Fig. 2.8). This could be due to the free drainage bottom boundary condition in the HILLFLOW water balance model, which implies that the water can only leave the soil profile but no water can flow in it. Capillary rise in the soil can keep the lower layers relatively wet (Vanderborght et al., 2010). In our simulation, the use of a soil depth of 1.5 m may not be deep enough to capture this effect. The simulated SWC were however very similar for both models. The larger RWU simulated by the Co than by the Fe model in the silty soil in May resulted in slightly lower simulated water contents by the Co model. But, the differences in simulated water contents by the two models were much smaller than the deviations from the observed water contents.

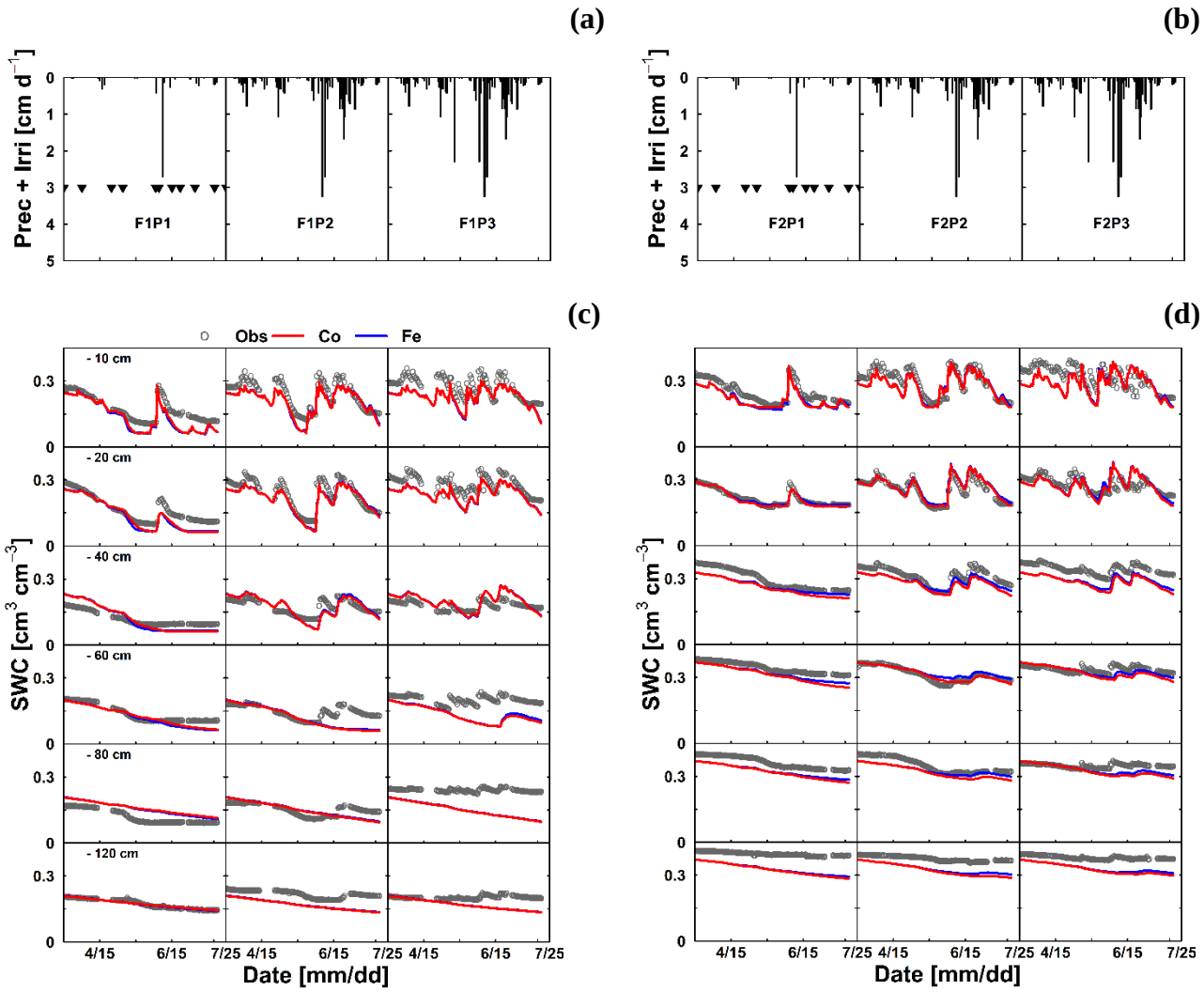

Figure 2.8: Illustrations of (a & b) time series of precipitation (Prec) and irrigation (Irri) and comparison between observed (black) and simulated soil water content (SWC) by the Couvreur (Co, solid red) and Feddes RWU model (Fe, solid blue) at six soil depths in at the sheltered (P1), rainfed (P2), and irrigated (P3) plots of (c) the stony soil (F1) (d) the silty soil (F2) from 15 March to 23 July 2016. Triangle symbols in the sheltered plots (F1P3 and F2P3) indicate the sheltered events.

For a few selected days, the diurnal course of T_{act} (or RWU), gross assimilation rate (Pg), stomatal conductance (gs), and leaf pressure head were measured. The measured and simulated data are shown in Fig. 2.9. Both Co and Fe models could mimic the daytime fluctuation of RWU and Pg in the sheltered plot of the stony soil, which is consistent with the adequate simulation of root growth (Fig. 2.4, F1P1) and SWC dynamics (Fig. 2.8c, F1P1). When the simulated ψ_{leaf} reached $\psi_{threshold}$ = - 200 m, the simulated RWU and Pg by the Co model showed a plateau (26 May in Fig. 2.9c, 2.9e, and 2.9i). The Co simulated better the diurnal courses of stomatal conductance as compared to the Fe, especially on a day with water stress (26 May, Fig. 2.9g and 2.9h). Using the leaf water pressure head threshold as an indication of water stress effects on stomata, Tuzet et al., (2003) and Olioso et al., (1996) also

reported a considerable drop of Pg and transpiration. The sharp drop of simulated RWU and Pg which is in contrast with measurement on the same day in the sheltered plot in silty soil illustrated that both models overestimated the water stress. This related to the underestimation of both root growth (Fig. 2.4, F2P1) and SWC (Fig. 2.8d, F2P1) in the deeper soil layers by two models.

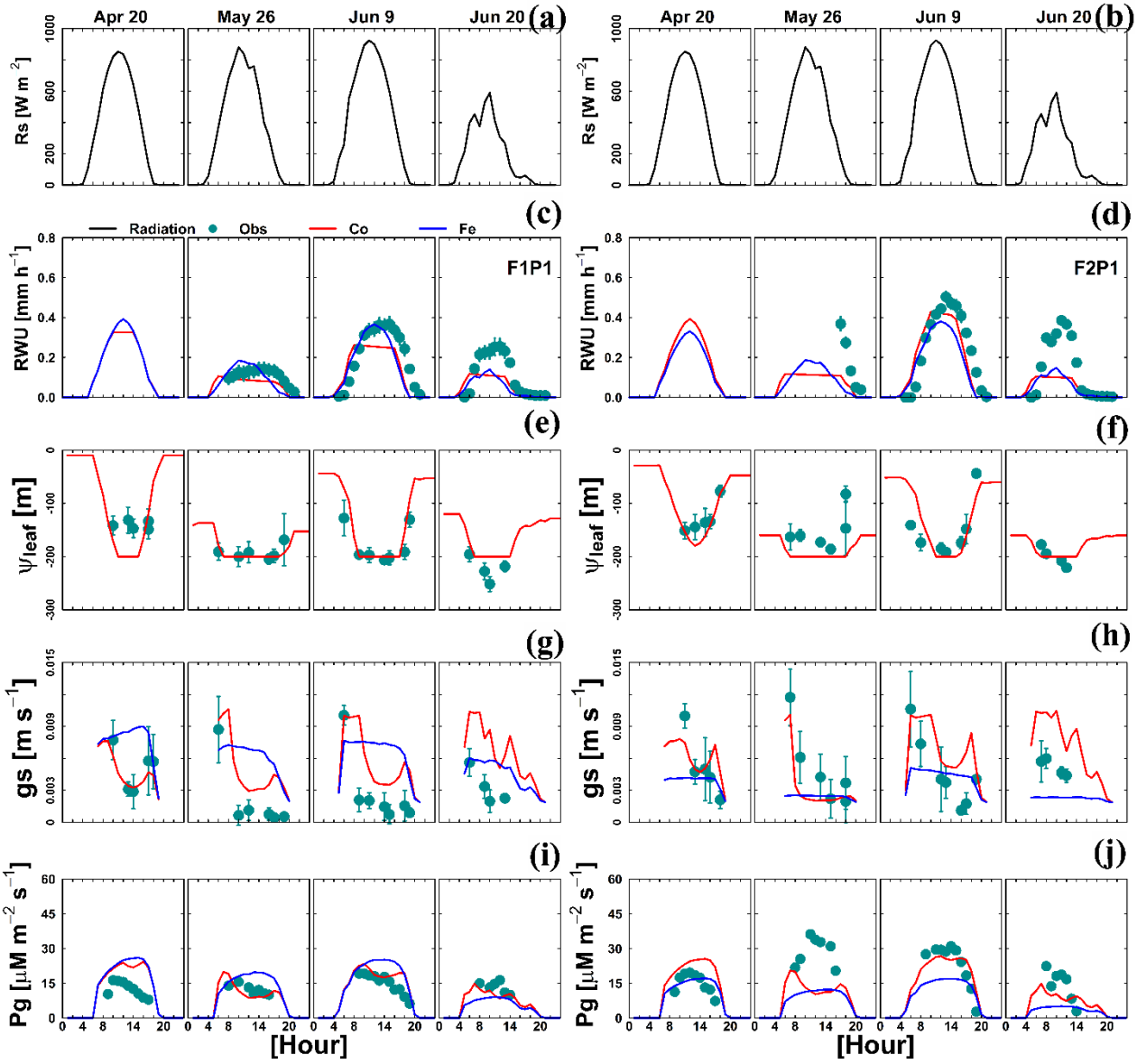

Figure 2.9: Diurnal courses of 4 selected measurement days: 20 April, 26 May, 9 June, and 20 June 2016 (a & b) global radiation (Rs) (c & d) actual transpiration (RWU), (e & f) leaf water pressure head (ψ_{leaf}), (g & h) stomatal conductance to water vapor (gs), and (i & j) gross assimilation rate (Pg) at the sheltered plot (P1) of the stony soil (F1) and the silty soil (F2). The cyan dots, solid red, and solid blue lines denote the observed, simulated values from the Couvreur model (Co), and Feddes (Fe), respectively. Sap flow sensors were installed on 26 May 2016 at 9 AM and 5 PM for F1P1 and F2P1, respectively. Simulated stomatal conductance are from sunlit leaves. The Feddes RWU model did not simulate leaf water pressure head.

2.3.1.3 Whole plant hydraulic conductance from Couvreur RWU model

The Couvreur RWU model considers the root hydraulic conductance which relies on absolute root length. The root hydraulic conductance is used to upscale to whole plant hydraulic conductance. The simulated K_{plants} reproduced the measured ones in the different treatments quite well (Fig. 2.10). Our measured K_{plant} ranged from 1.5 x 10^{-5} to 10.2 x 10^{-5} d^{-1} (Fig. 2.10). These values are in the same order of magnitude as values reported by Feddes and Raats, (2004) for ryegrass ranging from 6 x 10^{-5} to 20 x 10^{-5} d^{-1}. The simulated K_{plant} from our coupled root and shoot Co model followed the root growth and reached a maximum at around anthesis. K_{plant} reduces toward the end of the growing season due to root death. For the sheltered plot of the silty field, we would expect, based on the root density measurements (Fig. 2.4), the highest K_{plant} of all treatments. However, this was not observed in the field. Based on the measured total root lengths, we would also expect that K_{plant} of the sheltered plot in the stony soil should be similar to K_{plant} in the other plots of the stony soil. But, K_{plant} was clearly lower in the sheltered plot of the stony soil than in the other treatments in the stony soil. In the model simulations, the lower K_{plant} in the sheltered plots compared to the other plots in the same soil was due to a lower simulated total root length. Since the differences in observed total root lengths were smaller (stony soil) or opposite (silty soil) to the differences in simulated total root lengths, the smaller observed K_{plant} in the sheltered plots must have causes that are not considered in the model. A potential candidate is the resistance to water flow from the soil to the root in the soil, which increases considerably when the soil dries out, as was the case in the sheltered field plots.

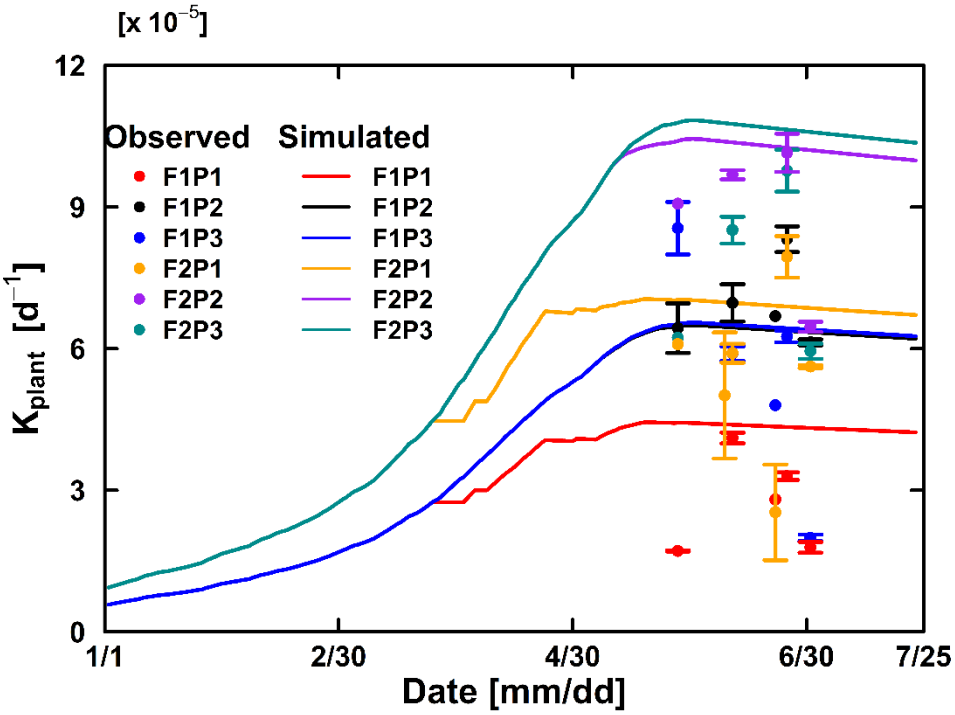

Figure 2.10: Comparison between observed (dot) and simulated plant hydraulic conductance (solid line) by the Couvreur (Co) model in the sheltered (P1), rainfed (P2), and irrigated (P3) plots of the stony soil (F1) and the silty soil (F2). The vertical bars represent the standard deviation of 6 hourly plant hydraulic conductance values at around midday (11 AM to 4 PM) in the measurement day. Note: crop germination was on 26th October 2015, data is showed here from 1 January 2016 to harvest 23 July 2016. Blue line was overlapped by the black line

The observed field data has been shown and compared with the simulated results from the two models in the above-mentioned (2.3.1.1, 2.3.1.2, and 2.3.1.3). The data were collected for both crop growth (root, LAI, and biomass) and gas fluxes at different scales (soil water flux and gas exchange from leaf to canopy) in two contrast soil types and under different water treatments. To our knowledge, this is the unique experimental set-up and dataset for understanding soil-plant processes as well as parameterizing and evaluating of soil-plant-atmospheric models. However, due to complex and costly construction of the underground minirhizotrone facilities, there were no replicates for plots in our study. LAI and aboveground biomass showed the large variability not only between water treatments but even in the same plot because of microclimate and soil heterogeneities. The variability of tiller development also considerably influences stem-to-stem variability of sap flow. In addition, the small size of plot did not allow having replicates for manual canopy chamber measurement because it might strongly disturb and alter crop growth, leaf gas exchange, and sap flow measurements of the surrounding areas. Nevertheless, despite of these shortcoming issues, the data illustrated the

difference and variability among water regimes in two soil types, and over measured dates that it is still valid for modelling comparison and validation in this study.

2.3.2 Effects of changing root hydraulic conductance and leaf water pressure head thresholds

We conducted three sets of simulations. In the first set of simulations $K_{rs,\ normalized}$ was subjected to change. Fig. 2.11 illustrates the sensitivity of Co model to $K_{rs,\ normalized}$ in terms of above-ground biomass at harvest and cumulative RWU (from 15 March to harvest) for the different water treatments and soil types. For the rainfed and irrigated plots, an increase in $K_{rs,\ normalized}$ does not lead to a substantial increase in RWU and above ground biomass. This is a trivial consequence of the fact that water is not (irrigated plots) or only slightly (rainfed plots) limited in these cases. For the stony soil, a decrease of $K_{rs,\ normalized}$ by a certain factor leads to a stronger decrease in RWU and biomass than in the silty soil. This indicates that in the stony soil, less water is 'accessible' so that a decrease in root water uptake capacity by the crop has a stronger impact on RWU and biomass production than in the silty soil. For the sheltered plots, RWU and biomass production increase with $K_{rs,\ normalized}$ suggesting that increasing the water uptake capacity by the plants would increase the uptake and growth. But, increasing $K_{rs,\ normalized}$ by the same factor had a smaller relative effect on the RWU and biomass production than decreasing $K_{rs,\ normalized}$.

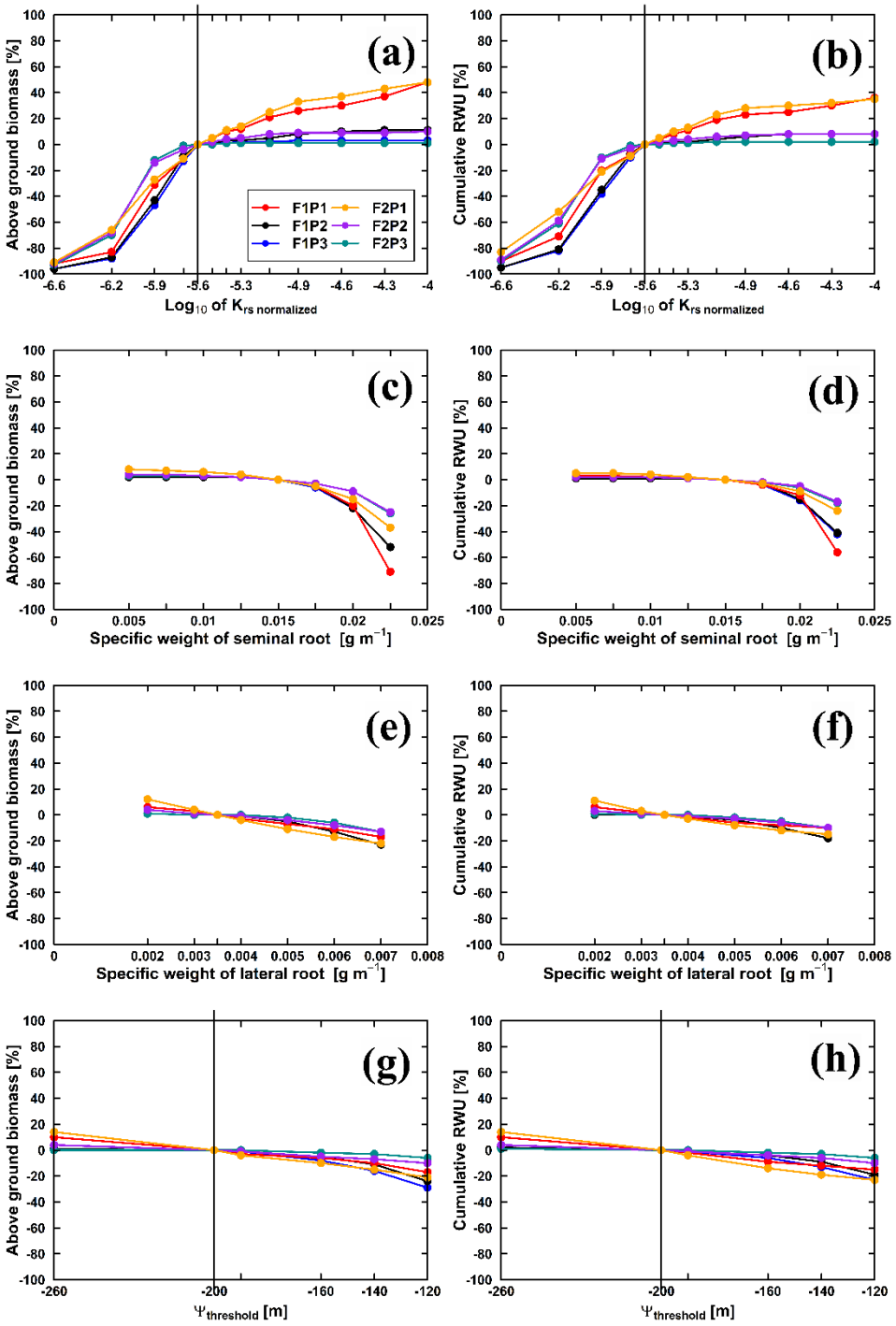

Figure 2.11: Relative changes of simulated (Co model) above ground biomass at harvest (a, c, e, and g) and cumulative RWU (b, d, f, and h) (from 15 March to harvest 23 July 2016) with the changing $K_{rs,\ normalized}$, specific weights of seminal and lateral root, and leaf pressure head threshold ($\Psi_{threshold}$) in the sheltered (P1), rainfed (P2), and irrigated (P3) plots of the stony soil (F1) and the silty soil (F2). Vertical lines in (a) and (b) indicates the original value $K_{rs,\ normalized}$ = 0.2554 10^{-5} (cm d^{-1}) while (g) and (h) indicates the $\Psi_{threshold}$ = - 200 m.

Decreasing the specific weight of lateral and seminal roots increases the specific root length and thus total root length of root system, total root system hydraulic conductance, and thus and whole plant hydraulic conductance. However, for the considered range of specific weights, there was only a minor increase of above dry biomass and RWU (Fig. 2.11c-f). Reducing the specific root length by increasing the specific weights of lateral and seminal roots caused a stronger reduction in biomass and RWU, especially for the seminal root in the stony soil. High values of $\Psi_{threshold}$ led to more water stress and a sharp decrease in stomatal conductance and photosynthesis when Ψ_{leaf} was limited to its thresholds (Fig. 2.11g & h). Our results suggested that $\Psi_{threshold}$ at -120 m or -140 m could overestimate the water stress while the $\Psi_{threshold}$ at -260 m could underestimate the stress.

The impact of the change of the root segment conductance, specific weight of roots, and the leaf pressure head threshold at which stomata close on RWU and above ground biomass is amplified by the positive feedback between the above ground biomass, the root biomass, the total root length, the root system hydraulic conductance, and finally K_{plant}. Considering these interactions and feedbacks is important to evaluate the impact of changing a certain property of the crop on its performance in different soils and under different conditions.

The impact of changing root system properties or stomatal sensitivity to water pressure head on root water uptake, stress, and crop growth cannot be assessed by a model that is not sensitive to these crop properties. Different to the Co model the Fe model is not sensitive to the total root length, the normalized root conductance, the specific root weight, and the leaf water hydraulic head at which stomata close. Therefore, the impact of introducing crop varieties with new properties cannot be assessed by this type of model. Only with the Co model the impact of the crop properties on growth and drought resilience can be studied.

2.4. Conclusion

We evaluated two different root water uptake modules of a coupled soil water balance and crop growth model. One root water uptake model was the often used Feddes model whereas the other, the Couvreur RWU model represents a “mechanistic” RWU that explicitly simulates the continuum in water potential from soil to root, and to leaf based on the whole plant hydraulic conductance. Overall, the measured biomass growth, LAI development, soil water contents, leaf water pressure heads, and transpiration rates were well reproduced by both models. But, the Fe model incorrectly predicted more water stress and less growth in the silty soil than in the stony soil whereas the opposite was observed. The Fe model does not account for the higher plant conductance in the silty soil where more roots were simulated than in the stony soil. In addition, the Fe model does not consider root water uptake compensation which

reduces water stress. In other words, the Feddes approach did not possess the flexibility as compared to Couvreur model in simulating RWU for different soil and water conditions.

Based on the absolute root length, the Co model was able to simulate K_{plant} in different soils and treatments. The simulated K_{plant} followed the root growth and reached a maximum at around anthesis. However, the observed K_{plant} was lower in the sheltered plots although the observed total root lengths in these plots were almost similar (stony soil) or larger (silty soil) as compared to the irrigated and rainfed plots. Moreover, the higher simulated K_{plant} in comparison to the observed values in the sheltered plots suggested that the newly coupled model needs to consider the declined hydraulic conductance of the root-soil interface due to decreased soil water pressure head. The formation of air gaps at soil-root interface due to the root shrinkage of roots and root-soil contact loosening (Carminati et al., 2009) could induce a strong increase of hydraulic resistance to radial water flow between soil and roots.

A mechanistic model that is based on plant hydraulics and links root system properties to RWU, water stress, and crop development can evaluate the impact of certain crop properties (change of root segment conductance, specific weights of root, or leaf pressure head thresholds) on crop performance in different environments and soils. The Co model could capture the positive feedbacks between the aboveground biomass, the root length, the total root system hydraulic conductance, and finally K_{plant}.

In this study, a higher total root length was simulated in the silty soil than in the stony soil because a higher specific root length was found for root growth in the silty soil. This can be considered as an extra relationship that requires attention in crop modelling. Crop growth models will need to consider soil specific calibration to account for differences in specific root length with soil. Alternatively, a more mechanistic description of root growth that predicts root specific length would reduce the amount of calibration in crop growth models. Another aspect in demand of improvement is the prediction of the root distribution with depth. In our simulations, highest root densities were simulated in the top soil whereas the observations showed higher densities in the deeper soil layers. Examples of detailed 3D root growth models that could improve the simulation of root distribution are given by Dunbabin et al., (2013). The coupling of a shoot model with a 3D root growth model that represents root system architecture simulated more accurate root distributions (at both top and subsoil layers) under drought conditions (Mboh et al., 2019). Nevertheless, simulating the third dimension of root growth would largely extend the parameter requirements which makes them more difficult for testing under the field.

Finally, the model did not consider changes in carbon allocation to the root system that are triggered by stress. Therefore, the model simulated less roots in the water stressed sheltered plot of the silty soil whereas more roots were observed in this plot compared with the other plots in this soil. A more mechanistic description of root: shoot partitioning of both carbon and nitrogen (Yin and Schapendonk, 2004) or carbon allocation as a function of soil water conditions (i.e. soil water potential in Kage et al., (2004) and Li et al., (1994)) would be needed to refine the prediction of responses of root development to water stress.

Future research should focus on testing the newly coupled model (HILLFLOW–Couvreur's RWU–SLIMROOT–LINTULCC2) for other wheat genotypes and crop types (isohydric like maize) and for a wider range of soil and climate conditions. Further improvements should particularly be targeted leaf area simulation. Improving the modelling of leaf growth should result in better simulations of LAI and more accurate estimates of energy fluxes at canopy level.

3 Chapter: Expansion and evaluation of two coupled root-shoot models in simulating CO_2 and H_2O fluxes and growth of maize

Abstract

Leaf stomata play an essential role in preventing excessive water loss when plants are under water stress. Leaf water hydraulic head (Ψ_{leaf}) and more specifically its critical thresholds ($\Psi_{threshold}$) characterizes stomatal control of transpiration, particularly for C_4 plants, but this physiological process has rarely been integrated into dynamic crop models. Two coupled models with Feddes root water uptake (RWU) and Couvreur RWU models were further extended by the C_4 photosynthesis model (a model that considers a complex combination of both biochemical and anatomical specialization, which provides an elevation of the CO_2 concentration at the site of Rubisco) in order to be applicable to maize. Model performance was evaluated with a comprehensive dataset including stomatal conductance, Ψ_{leaf}, sap flow, gross assimilation rate (Pg), soil water content (SWC), dry biomass, and leaf area index (LAI) from a two season maize experiment grown under contrasting environments and water regimes. For the Couvreur model, the RWU and dry biomass were more sensitive to the root hydraulic conductance parameters than to $\Psi_{thresholds}$ and root growth parameters. The agreement index (I) for the Couvreur model after calibration was 0.91, 0.80, 0.81, and 0.69 for biomass, LAI, RWU, and Pg, respectively. The Feddes model performed similarly for the same metrics. The Feddes model simulated accurately the plant water stress in the first 45 days of the growing season whereas the Couvreur model inaccurately predicted water stress which resulted in lower agreement with observations. The Feddes model showed the potential to be used for maize under water stress whereas the Couvreur model needs to be further evaluated and improved with an adequate estimation of root hydraulic conductance. A dynamic parameterization of normalized root system conductance and/or more accurate assimilate allocation to the roots, especially under drought stress, should be considered with this model in future studies for maize.

Keywords: anisohydric, crop modeling, drought, gas exchange, isohydric, maize

Abbreviations: ABA – abscisic acid; DAS – day after sowing; DM – dry matter; LAI – leaf area index; RWU – root water uptake; SWC – soil water content;

3.1 Introduction

Maize (*Zea mays*) is a major staple crop throughout the world. Drought stress, which negatively affects crop growth and yield production, is increasingly affecting several important maize cultivating regions (Daryanto et al., 2016). Given the importance of maize for global food security and increases in frequency and severity of drought events due to climate change (IPCC, 2007), field observations and modeling studies on how maize responds to water stress are necessary to facilitate predictions of crop growth, yield, and water use by crop models (Hammer et al., 2009) and land surface models (Sulis et al., 2015).

Maize has various responses to water stress, which are determined by the plant cultivar as well as the intensity, duration, and rate of progression of the imposed stress (Pinheiro and Chaves, 2011). This includes leaf rolling (Baret et al., 2018), change in root architecture such as reduced lateral root branching (Zhan et al., 2015), or increasing root: shoot ratio (Cai et al., 2017a). Stomatal control is considered an early and effective response to water stress under field conditions to prevent excessive water loss and desiccation (Tyree and Sperry, 1988; Brodribb and McAdam, 2011). Maize has been described as isohydric plants, which close their stomata to maintain leaf hydraulic head (Ψ_{leaf}) above critical levels. The hydraulic heads refer to total water potentials expressed in length units (i.e meter) while pressure heads are hydraulic heads minus the gravitational potential (i.e -1 MPa equal to -100 m). The second strategy is found in anisohydric plants which have a looser stomatal control with the result that Ψ_{leaf} will decrease in response to soil drying and/or increasing evaporative demand. Consequently, Ψ_{leaf} in anisohydric plants experiencing drought stress will be considerably lower than in well-watered plants (Tardieu and Simonneau, 1998). A continuum exists in the degree to which stomata regulate the Ψ_{leaf} for trees (Domec and Johnson, 2012; Klein, 2014; Sade et al., 2012; Frank et al., 2007; Meinzer et al., 2016) or in grape-vine (Schultz, 2003). Also, cultivars of grape vine show large differences in minimum Ψ_{leaf} indicating differing degrees of isohydric behavior (Coupel-Ledru et al., 2014). Comparing different herbaceous species, Turner et al., (1984) showed that there was a range from isohydric to increasingly anisohydric behavior in terms of the response to increasing vapor pressure deficit (VPD) under sufficient soil moisture. The Ψ_{leaf} from eucalyptus, a plant rather characterized as having anisohydric behavior, can decrease to very low values and vary with the fluctuations of soil moisture whereas the difference between soil water pressure head and midday Ψ_{leaf} is maintained constant over a season which is defined as “isohydrodynamic” (Franks et al., 2007).

Several underlying mechanisms are involved to explain those stomatal controls, which are still

in debate (Tardieu, 2016; Martinez-Vilalta and Garcia-Forner, 2017; Meinzer, 2002). For instance, stomatal closure responded to a decrease of leaf-specific hydraulic conductance and vice versa (Schultz, 2003). The avoidance of xylem embolism reduces hydraulic loss to ensure water movement in the continuum pathway (Cochard, 2002; Tyree and Sperry, 1988). The increase in cavitation resistance also maintained higher leaf water pressure head under water stress in maize (Cochard, 2002). Changes in root hydraulic conductance via the modulation of aquaporin activity play an important role in affecting root water uptake and maintain plant water status (Gambetta et al., 2017; Pawłowicz and Masajada, 2019; Champeyroux et al., 2019; Adiredjo et al., 2014). A decreasing soil water pressure head resulted in an increase of abscisic acid concentration in the roots (Dodd et al., 2010), which could increase the aquaporin activities that facilitates more effective root radial hydraulic conductance (Parent et al., 2012; McElrone et al., 2007).

Stomatal conductance can be modeled in many ways (Damour et al., 2010), at different scales (Table 3.1). Earlier empirical models related the effects of Ψ_{leaf} to stomatal conductance with a multiplicative approach [Jarvis type of equation (Jarvis, 1976)] (Olioso et al., 1996 with soybean; Jensen et al., 1993 for spring barley), which requires a high number of parameters to capture different environmental conditions (Damour et al., 2011). The semi-empirical Ball-Berry-Leuning equation (Leuning, 1995; Ball et al., 1987) related photosynthesis and stomatal conductance. However, this model initially did not consider the water stress or effects of Ψ_{leaf} on stomatal conductance. The Ball-Berry-Leuning models were further improved through inclusions of the “water stress factor” on the slope of photosynthesis and stomatal conductance relationship. The water stress factors were calculated from soil water content (Wang and Leuning, 1998) or soil water pressure head (Oleson et al., 2013), which is often used in dynamic crop models and many land surface models (Verhoef and Egea, 2014; Damour et al., 2010). Tuzet et al., (2003) introduced an empirical water stress factor on the Ball-Berry-Leuning stomatal conductance model. The water stress factor was below 1 if the simulated Ψ_{leaf} was below the reference Ψ_{leaf}. The reference Ψ_{leaf} in Tuzet’s study was defined as the value of Ψ_{leaf} below which the stomatal conductance begins to decrease drastically (Tuzet et al., 2003; Olioso et al., 1996; Jones and Sutherland, 1991). Plants with a high stomatal sensitivity to Ψ_{leaf} were then modeled with a higher reference Ψ_{leaf} (-1.2 MPa) (-1 MPa = -100 m). For species that are more tolerant to water stress, a lower reference Ψ_{leaf} was used (i.e. -1.9 or -2.6 MPa) (Tuzet et al., 2003). However, the Ψ_{leaf} was simulated with the assumed constant whole-plant hydraulic conductance. Moreover, the model from Tuzet did not separate the different canopy layers (i.e sunlit and shaded leaves), which can be the important feature when simulating CO_2 and H_2O gas exchange (De Pury and Farquhar, 1997; Wang and

Leuning 1998). Additionally, Tuzet's model considered soil profile as a single layer with homogeneous soil characteristics and a uniform root distribution which is not the case under field conditions (Vereecken et al., 2016; van Dam, 2000). Tardieu and Davies, (1993) proposed a stomatal conductance model involving the Ψ_{leaf} and xylem abscisic acid (ABA). The abscisic acid is originated and transported from the dehydrated roots to the leaf, where it regulates stomatal closure. Consideration of either hydraulic signal combined with ABA or only ABA allowed the model to simulate anisohydric and isohydric behavior (Tardieu and Simonneau, 1998; Tardieu et al., 2015). The models with hydraulic and chemical signals from Tardieu and Davies (Tardieu and Davies, 1993) were later simplified to a water stress factor/function, and then introduced into the slope of the coupled Ball-Berry-Leuning model (Dewar, 2002). A sensitivity analysis was conducted afterwards, showing that varied values of ABA and critical Ψ_{leaf} could mimic the range of stomatal responses of anisohydric and isohydric stomatal behaviors (Huber et al., 2014). The consideration of hydraulic/chemical signals for extending the Ball-Berry-Leuning equation has mainly been applied at leaf scale (Ahmadi et al., 2009; Gutschick and Simonneau, 2002; Dewar, 2002) or in theoretical studies (Huntingford et al., 2015; Verhoef and Egea, 2014) (Table 3.1). To our knowledge, modeling applications and performance evaluation of these models on simulating stomatal conductance, CO_2 and H_2O gas flux exchange, and crop growth processes are rarely done at the field scale.

Table 3.1 Summary of some common stomatal conductance models and their application scales

Order	Approaches	Water relation underlying mechanism	Applied scales	References (first use in plants)
1	Multiplicative model, environmental factors are independent	Hydraulic signal: Ψ_{leaf}, constant K_{plant}	Plant, field, landscapes	Jarvis, 1976 (spuce and Douglas fir) Jensen et al., 1993 (barley) Olioso et al., 1996 (soybean)
2	Hydraulic model	Hydraulic signal: Ψ_{leaf}, K_{plant}, and SWP	Plant	Tyree and Sperry, 1988; Jones and Sutherland, 1991 (trees)
3	Turgor regulation of guard cell (hydromechanical model	Hydraulic signal: SWP and guard cell water potential	Cell and leaf	Gao et al., 2002 Buckley et al., 2003
4	Hydraulic and chemical ABA control	Hydraulic and chemical signals: Ψ_{leaf} and ABA	Plant and pot	Tardieu and Davies, 1993; Tardieu and Simonneau, 1998; Tardieu et al., 2015 (maize)
5*	Hydraulic and chemical ABA control	Hydraulic and chemical signals: Ψ_{leaf} and ABA	Theoretical modeling studies	Huber et al., 2015
6	Coupled photosynthesis–stomatal conductance (A_n-g_s) model	No water stress was considered	Plant, field	Ball et al.,1987 (soybean) Leuning, 1995 (Eucalyptus grandis)
7	Modified (A_n- g_s) model with water stress functions of SWC or SWP	Water stress functions of SWC or SWP, neither Ψ_{leaf} nor K_{plant} and/or ABA	Plant, field, landscapes	Oleson et al., 2013; Kucharik and Brye, 2003 (varieties of trees, plant functional types), Rodriguez et al., 2001 (spring wheat); Wang and Leuning, 1998 (wheat)
8	Modified (A_n- g_s) model with water stress functions from Ψ_{leaf}	Hydraulic signals: Water stress functions of Ψ_{leaf}, constant K_{plant}	Theoretical modeling study with homogenous soil; field	Tuzet et al., 2003 (the applied crop was not specified)
9	Modified (A_n- g_s) model with water stress functions from Ψ_{leaf} and ABA	Hydraulic and chemical signals: Water stress functions of Ψ_{leaf} and ABA, constant K_{plant}	Leaf, theoretical modeling studies	Dewar, 2002 Verhoef and Egea, 2014; Ahmadi et al., 2009 (tomato); Gutschick and Simonneau, 2002 (sunflower); Huntingford et al., 2015 (tree)
10	Modified (A_n- g_s) model with water stress function (T_a/T_p)	Hydraulic signal: Ψ_{leaf}, dynamic K_{plant} based on root length	Field	Nguyen et al., 2020 (winter wheat)

Notes and abbreviations: A_n: net photosynthesis rate; g_s: leaf stomatal conductance; ABA: acid abscisic; K_{plant}: whole plant hydraulic conductance; T_a: actual transpiration; T_p: potential transpiration; SWC: soil water content; SWP: soil water pressure head; Ψ_{leaf}: leaf pressure head. The modified A_n-g_s models in the 7th, 8th, 9th, and 10th approaches were originated from the coupled A_n-g_s model in the 6th approach (so-called Ball-Berry-Leuning model). *This approach simulated transpiration reductions factor rather than explicitly simulated the g_s.

Further improvements consider that water stress is calculated from leaf hydraulic head and/or xylem ABA concentration, thus replacing the more empirical approaches often based on soil water content or soil water pressure head (i.e. theoretical modeling study (Verhoef and Egea, 2014) and recent modeling studies under the field-grown condition in winter wheat (Cai et al., 2017a; Cai et al., 2018; Sulis et al., 2019; Nguyen et al., 2020). Nguyen et al., (2020) coupled

the HILLFLOW soil water balance model (Bronstert and Plate, 1997), crop model LINTULCC2 (Rodriguez et al., 2001), root growth model SLIMROOT with Feddes's root water uptake (RWU) model) (Feddes et al., 1978) and Couvreur's RWU model (Couvreur et al., 2014; Couvreur et al., 2012). The Feddes RWU model is commonly used in hydrological models which does not consider the plant hydraulic conductance. The Couvreur model explicitly calculates the root hydraulic conductance (K_{rs}) based on the total length of the root system below a unit of surface area (i.e cm cm^{-2}). Leaf hydraulic head (Ψ_{leaf}) was explicitly simulated via extending K_{rs} to whole-plant hydraulic conductance (K_{plant}). The root water uptake approach by the Couvreur model is based on hydraulic principles that represented water dynamics within the root system. The model uses a stomatal regulation model, which assumes that stomatal conductance is not influenced by Ψ_{leaf} as long as the Ψ_{leaf} is above a critical leaf hydraulic threshold ($\Psi_{threshold}$). The Ψ_{leaf} is kept constant by changing stomatal conductance when the $\Psi_{thresholds}$ are reached. In theory, the coupled model with Couvreur's RWU model allows the reproduction of the different stomatal regulations i.e. isohydric and anisohydric by setting a $\Psi_{threshold}$. The coupled model with Couvreur RWU predicted better water stress than the Feddes model (Nguyen et al., 2020). The coupled model with Couvreur RWU also was able to simulate K_{plant}, gross photosynthesis, transpiration, and soil water dynamics for winter wheat. However, the water response dynamics and model comparisons for Couvreur-coupled and Feddes-coupled models, have not been parameterized and evaluated for maize. It is necessary to test the models for more crops and different weather conditions to build up larger experimental support for the models. We hypothesized that the coupled model with the Couvreur RWU model is generic enough to simulate the effects of soil water availability on the CO_2 and H_2O gas fluxes and crop growth of maize with varying weather conditions (including different levels of evaporative demand/ potential evapotranspiration (ETP) and vapor pressure deficit (VPD). The objectives of this study were: (i) to analyze the sensitivity of aboveground biomass growth and RWU of maize to changing plant-water related parameters (seminal and lateral specific root lengths, $\Psi_{thresholds}$, root hydraulic conductance parameters) (ii) to compare the predictive capacity of the coupled models with and without the inclusion of K_{plant} (Couvreur and Feddes RWU models) in simulating maize crop growth, CO_2, and H_2O gas fluxes under different water regimes and contrasting weather conditions at field scale. We used a comprehensive field dataset comprising measurements of CO_2 and H_2O gas flux from soil to leaf and dynamic crop growth (biomass and leaf area index).

3.2 Materials and Methods

3.2.1 Location and set-up of the field experiments

The field experiments were located in a farm near Jülich, Western Germany (50°52'N, 6°27'E). The site characterized with stony soil (hereby F1) with approx. 50-60% gravel by weight in the 10 cm topsoil. The study site was divided in two rainfed plots (namely P1, P2) and one irrigated (namely P3). Maize was grown during two seasons (2017 and 2018). Silage maize cultivar Zoey was sown on May 4th and May 8th during the 2017 and 2018 season, respectively, with a 10.66 seeds m^{-2} plant density for all treatments and soil types (Fig. 3.1a and Table 3.2). In 2018, the rainfed plot (F1P1) was seeded two weeks later, on May 22nd (Fig. 3.1a). Since the objective of this study was to analyze the performance of the coupled root: shoot model under different soil water conditions and evaporative demands, we selected datasets from irrigated and rainfed plots for two growing seasons, naming 2017F1P3, 2017F1P2, 2018F1P3, 2018F1P2, and 2018F1P1. Detailed information on crop management is described in Table 3.2.

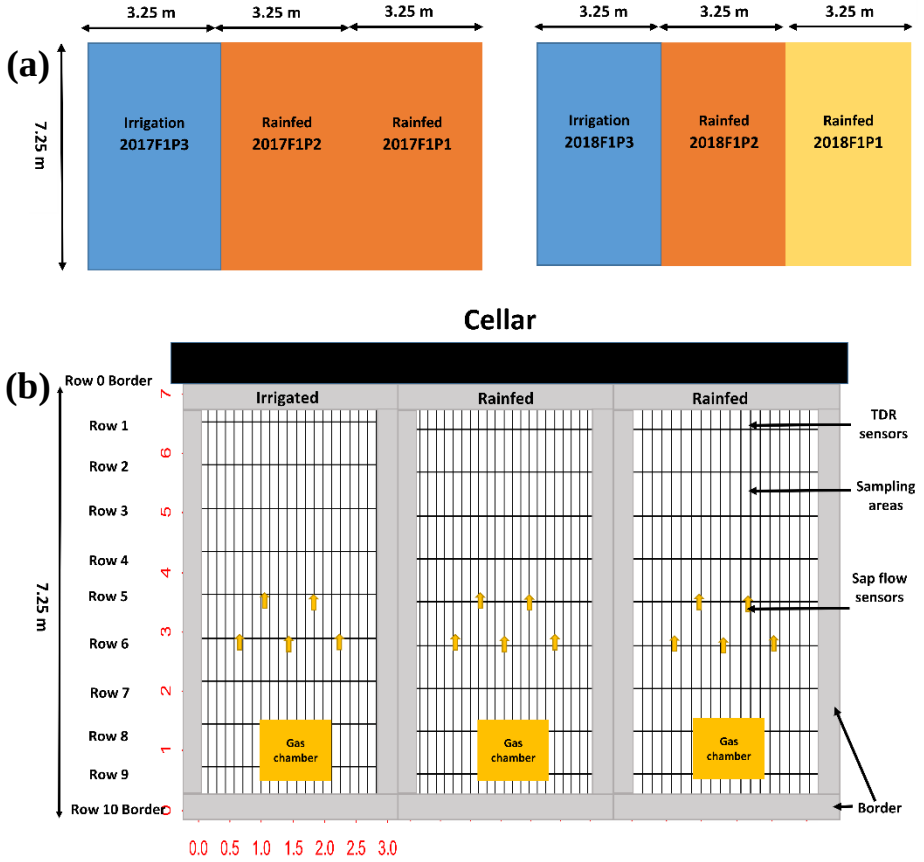

Figure 3.1: Description of (a) field experimental set-up with water treatments and sowing dates in 2017 (left) and 2018 (right) and (b) measurement positions for each treatment (TDR sensors, sap flow sensors, sampling areas, and canopy gas exchange). The "2017F1P3" and "2017F1P2" denote irrigated and rainfed plots in 2017. The "2018F1P3" and "2018F1P2" are the irrigated and rainfed plots with normal sowing dates, respectively while "2018F1P1" is the rainfed plot with late sowing date in 2018.

Table 3.2 Crop phenology and management information in 2017 and 2018.

	2017		2018		
Sowing date (mm/dd/yyyy)	Normal		Normal		Late
	05/04/2017		05/08/2018		05/22/2018
Phenology (mm/dd/yyyy)					
Emergence date	05/09/2017		05/13/2018		05/26/2018
Tasseling date	07/09/2017		07/09/2018		07/21/2018
Silking date	07/14/2017		07/11/2018		07/23/2018
Harvest date	09/12/2017		08/22/2018		09/02/2018
Plot names	2017F1P3	2017F1P2	2018F1P3	2018F1P2	2018F1P1
Growing season (days)¥	136	136	107	107	104
Days without rain	66	66	77	77	71
Water treatments	Irrigated	Rainfed	Irrigated	Rainfed	Rainfed
Cumulative rainfall (mm)*	248.7	248.7	91.3	91.3	81.9
Assumed cumulative evapotranspiration (mm)**	330	330	385	385	355
Irrigation (mm)	130	0	257.6	66	66
Fertilizer application (mm/dd/yyyy) (per hectare)	05/09/2017:100 kg N + 40kg P_2O_5 07/06/2017: 80 kg N + 40 kg K_2O		05/22/2018: 100 kg N 05/30/2018: 40 kg P_2O_5 + 40 kg K_2O 06/27/2018: 80 kg N		
Cultivar	*Zea mays* cv. Zoey				
Sowing density	10.66 plant m^{-2} or 75 cm x 12.5 cm				

Notes: ¥ from sowing to harvest; * for rainfall for whole growing season; ** is calculated by multiplying the number of days without rain with the assumed evaporative demand of 5 mm d^{-1}.

3.2.2 Weather conditions and irrigation management

The experimental site was characterized by temperate climate conditions with an average annual temperature of 9.9 °C and average annual precipitation of 698 mm (Prolingheuer et al., 2010). In 2017, the maize crop received 248.7 mm of rainfall during the growing period (136 days) (Table 3.2). Seasonal average, minimum, and maximum daily seasonal temperatures during were 17.6, 8.3, and 25.3 °C, respectively. The irrigation demand was estimated based on the precipitation collected from the rain gauge nearby the field and assuming an evaporative demand (evapotranspiration rate) of 5 mm d^{-1} (Table 3.2). Irrigation in the irrigated plots was carried out by dripper lines (T-Tape 520-20-500, Wurzelwasser GbR, Münzenberg, Germany) which were installed with 0.3 m intervals and parallel to the crop rows. In the irrigated plots, water was applied (10 times, 13 mm per irrigation event) from mid-June to the end of August for the irrigated plot (2017F1P3) (Table 3.2). No irrigation was applied in the rainfed plots in 2017. With an exceptionally hot and dry condition during the summertime, the growing season 2018 can be classified as an extreme year for crop growth in our experiments (Buras et al., 2020). Crop received only 91.3 and 81.9 mm of rainfall in the early and late sowing plots in 2018, respectively (Table 3.2). Seasonal average, minimum, and maximum

daily temperatures were 19.2, 10.9, and 27.3 °C, respectively. A total irrigation volume of 257.6 mm was applied (split into 13 applications) from mid-June to the mid of August in the irrigated plot (2018I). The two rainfed plots (2018F1P1 and 2018F1P2) were watered 4 times (13, 22, 13, and 18 mm each time) to prevent the plants from dying due to severe drought.

3.2.3 Measurements

3.2.3.1 Soil water measurement

In each soil depth at 10, 20, 40, 60, 80, and 120 cm, time-domain reflectometer (TDR) probes were installed to measure hourly soil water content (SWC) (see Fig. 3.1b). Soil water measurements were described in detail in Cai et al., (2017) and Nguyen et al., (2020). Soil physical parameters of the stony soil (saturated hydraulic conductivity, saturated and residual SWC, and empirical coefficients affecting the shape of the van Genuchten hydraulic functions) were selected from Cai et al., (2018).

3.2.3.2 Crop growth and gas fluxes measurement

Because of the limited number of plants in each plot, two maize plants were sampled biweekly to determine the leaf area index and aboveground dry biomass during the entire growing seasons (Fig. 3.1b) (in total 07 and 09 observations (including harvest) in 2017 and 2018, respectively). Green and brown leaf area was measured using a leaf area meter (LI-3100C, Licor Biosciences, and Lincoln, Nebraska, USA). At harvest, in addition to the sampling of two plants, five separate replicates (1 m^2 each) were harvested to determine the aboveground dry biomass and leaf area. The aboveground dry biomass was measured using the oven drying method (Nguyen et al., 2020).

Hourly leaf stomatal conductance and leaf hydraulic head (Ψ_{leaf}, m) (-100 m equivalent to -1 MPa) were measured every two weeks under clear and sunny conditions (7-10 measured days, from 8 AM to 5 PM). Stomatal conductance (g_s) of two sunlit leaves (uppermost fully developed leaves) and one shaded leaf were measured at steady-state using a LICOR 6400 XT device (Licor Biosciences, Lincoln, Nebraska, USA) with a reference CO_2 concentration of 400 ppm, flow rate of 500 (μmol s^{-1}), and using real-time records of photosynthetic active radiation, vapor pressure deficit (VPD), and leaf temperature provided by the instrument. The leaves were quickly detached by a sharp knife to measure Ψ_{leaf} with a digital pressure chamber (SKPM 140/ (40-50-80), Skye Instrument Ltd, UK) with the working air pressure with a range of 0-35 bars. In 2018, to capture the full diurnal course, Ψ_{leaf} was determined from predawn at hourly intervals to 7 PM) on three days (two days before irrigation and one day after irrigation).

Based on the LAI measurement, the sunlit leaf area (LAI_{su}) was calculated based on measured LAI, coefficient of light extinction (k), and solar zenith angle (SoZe) (Eqn. 1 and 2) (Moreshet et al., 1990). Solar zenith angle (SoZe) is the angle between the sun's ray and the vertical.

$$LAI_{su} = (1 - e^{-k*LAI})/k \quad (1)$$

$$k = \frac{1}{2\cos(SoZe)} \quad (2)$$

Canopy hydraulic head (Ψ_c - m) was computed as leaf area-weighted average of sunlit and shaded leaf hydraulic heads (Moreshet et al., 1996; Moreshet et al., 1990) assuming that both leaves are transpiring (Petersen et al., 1991) (Eqn. 3).

$$\psi_c = \psi_{su}\frac{LAI_{su}}{LAI} + \psi_{sh}(1 - \frac{LAI_{su}}{LAI}) \quad (3)$$

where Ψ_c is canopy hydraulic head (m); Ψ_{su} is hydraulic head of sunlit leaf (m); Ψ_{sh} is hydraulic head of shaded leaf (m); LAI is measured leaf area index (-); LAI_{su} is leaf area index of sunlit leaf (-);

In 2017, 15 sap flow sensors (SGA13, SGB 16, and SGB 19 types) based on stem diameter size were installed on maize plants from July 7th until harvest (5 sensors in each plot) (Fig. 3.1b). For the 2018 growing season, the same number of sensors were installed from June 28th until the harvest. The plant stem diameter and associated physical indices of each sensor type were entered into data loggers so that the sap flows were automatically calculated by the standard Dynamax program (Dynamax, 2009). The 10 minutes sap flow rate of a single plant (g h^{-1}) was aggregated to hourly intervals then upscaled to canopy transpiration rate (mm h^{-1} or mm d^{-1}) based on the plant density per square meter. The standard deviation of the sap flow measurements in different maize stems was calculated.

The manually closed chamber system (Langensiepen et al., 2012) was employed to measure the hourly canopy gas exchange on the same day with the measurement of the leaf hydraulic head by another customized LICOR 6400 XT (Licor Biosciences, Lincoln, Nebraska, USA) (Fig. 3.1b). Simultaneously, soil respiration was measured manually by LI-8100 (Licor Biosciences, Lincoln, Nebraska, USA) with three replicates in each treatment. Because we focused on the comparison of the hourly instantaneous gross assimilation rate, which was simulated by the crop model, the measured soil respiration was subtracted from the instantaneous canopy CO_2 exchange rate.

3.2.4 Model description

3.2.4.1 Overview of the two coupled root: shoot models

We employed two coupled root: shoot models: “HILLFLOW 1D-Feddes RWU model-SLIMROOT-LINTULCC2” and “HILLFLOW 1D-Couvreur RWU model-SLIMROOT-LINTULCC2” within the modeling framework SIMPLACE (www.simplace.net). These two coupled models were used for winter wheat and described in Nguyen et al., (2020). The HILLFLOW 1D is the physically-based water balance model) (Bronstert and Plate, 1997) which contains Feddes RWU model (hereafter Feddes model) (Feddes et al., 1978) and Couvreur root water uptake model (hereafter Couvreur model) (Couvreur et al., 2014; Couvreur et al., 2012). The SLIMROOT is the root growth model. The LINTULCC2 shoot growth model simulates phenology, photosynthesis, assimilation partitioning, and leaf growth. In the current study, the shoot growth models have been modified by an additional subroutine for the C_4 photosynthesis pathway (Fig. 3.2a). The rest of modeling subroutines were kept the same as in Nguyen et al., (2020).

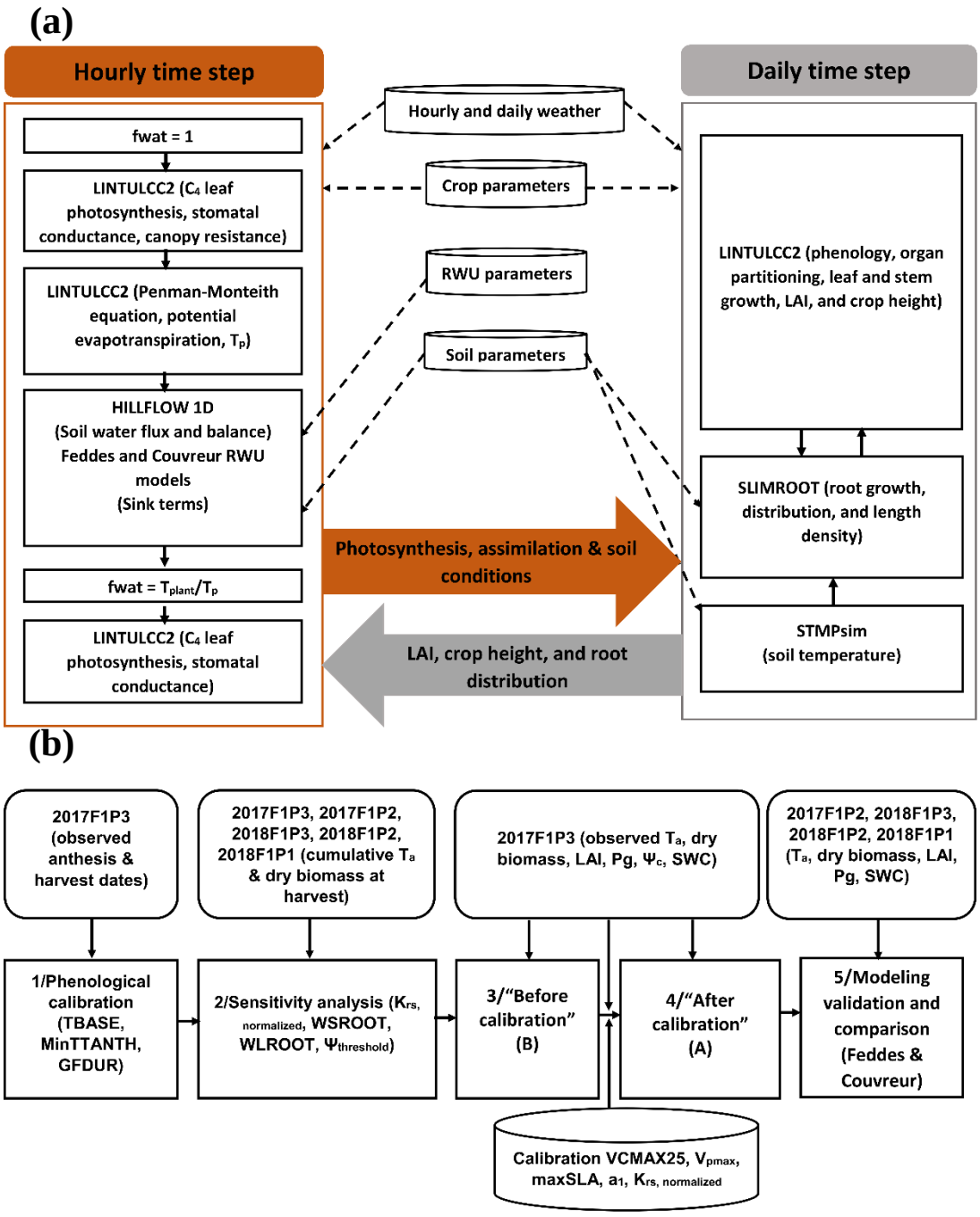

Figure 3.2: Description of (a) the coupled root-shoot models which have been modified with C_4 photosynthesis in this study (adopted from Nguyen et al., 2020) and (b) modeling work flow, used water treatments, simulation outputs, and related parameters. The orange arrow in (a) illustrates the feedbacks from the hourly simulations to daily simulation, while the grey arrow describes the feedbacks from daily simulations to the hourly simulations. The dashed black arrows denote the weather input and parameters to the modeling subroutines. The continuous black arrows in (a) indicate the linkages among the subroutines. The water treatments, variables names, are parameters in (b) are explained in the Table 3.2 and Fig. 3.1, and in the text.

3.2.4.2 Implementation of C4 photosynthesis parameterization for maize

LINTULCC2 (and the coupled root: shoot models in Nguyen et al., 2020) originally developed for wheat, calculates CO_2 uptake for sunlit and shaded leaves based on the Farquhar approach for C_3 photosynthesis. (Farquhar et al., 1980). It uses a numerical iteration approach (Leuning, 1995), which initially assumes that intercellular CO_2 concentration (C_i) equals 0.7 times the ambient atmospheric CO_2 concentration (C_a) (Jones, 1992; Rodriguez et al., 2001). A mechanistic photosynthesis model for maize (C_4 plant) was developed (Yin and Struik, 2009; Caemmerer and Furbank, 2003; Collatz et al., 1992) and introduced into LINTULCC2. The parameters and model variables, as well as sequential equations to mimic the CO_2 pathway in C_4, are described in detail in Appendix A and Appendix B. The C_4 models have rarely been implemented into crop models (Yin and Laar, 2005; Yin and Struik, 2009) because of the complex equations and requirement of high temporal resolution input data at leaf scale (Yin and Struik, 2009). The C_4 model can be parameterized either by numerical iteration approach (i.e Leuning, 1995) or analytical solution (i.e. solving cubic equations Yin and Struik, (2009); Collatz et al., (1992); Zhan et al., (2003)). For the C_4 implementation into the modeling framework (SIMPLACE) (Fig. 2a), we used the numerical iteration approach. We assumed the initial C_i was 0.4 times the C_a (Vico and Porporato, 2008; Jones, 1992; Wong et al., 1979). For the sake of simplification, we used bundle sheath cell conductance of 3 mM m^{-2} s^{-1} (von Caemmerer, 2000).

3.2.4.3 Description of other modeling subroutines

3.2.4.3.1 Potential evapotranspiration and transpiration

The potential evapotranspiration (ETP, mm h^{-1}) was calculated based on the Penman-Monteith equation (see Nguyen et al., 2020) (Fig. 3.2a). The potential transpiration (T_{pot}) was calculated by Equation 4:

$$T_{pot} = ETP(1 - e^{-kLAI}) \quad (4)$$

Where k is the light extinction coefficient. The light extinction coefficient varies depending on maize genotypes, leaf properties, and leaf arrangements. We employed the k = 0.6 in this study for maize (Hay and Porter, 2006). The potential transpiration T_{pot} (mm h^{-1}) implies that the transpiration of the crop is not limited by the root zone water hydraulic head (Fig. 3.2a).

3.2.4.3.2 Root growth model

The maize root system of maize is composed of primary, seminal, crown, and lateral roots. Crown roots could have greater water uptake due to their higher axial conductivity in the proximal parts as compared with younger seminal roots (Ahmed et al., 2018). For simplification, the crown roots (nodal roots) were not explicitly included in the root growth model (SLIMROOT) used in our study. SLIMROOT simulates the vertical extension of the seminal roots and the distribution of lateral roots within soil profiles (Williams & Izaurralde, 2005). Lateral roots are simulated when the assimilates supplied by the shoot to the roots is greater than the assimilate demand of seminal roots. Thus, the omission of explicit growth of crown roots in SLIMROOT is compensated by larger amount of simulated lateral roots. The extension of lateral and seminal roots was simulated based on the root biomass, the soil bulk density, the SWC from the HILLFLOW water balance model, and the computed soil temperature from STMPsim (Nguyen et al., 2020) (Figure 3.2a). Maize roots start to die after silking.

3.2.4.3.3 Physically-based soil water balance model

The water balance model HILLFLOW 1D (Bronstert and Plate, 1997) calculates soil water content and water fluxes by numerically solving the Darcy equation for unsaturated water flow in porous media (Bronstert and Plate, 1997). To express the relations between soil water hydraulic head, soil water content, and hydraulic conductivity, the Mualem-van Genuchten models were employed (van Genuchten, 1980). (Section 3.2.3.1). In this study, the soil profile with a depth of 1.5 m was vertically discretized into 50 layers. The mixed upper boundary condition represents the flux at the soil surface by the precipitation and evaporation rates as long as the soil pressure heads are not higher or lower critical heads. For the bottom boundary, free drainage was implemented.

3.2.4.3.4 Feddes' and Couvreur's root water uptake models

The Feddes RWU model (Feddes et al., 1978) was implemented in the HILLFLOW 1D (Bronstert and Plate, 1997). The root water uptake of each soil layer is calculated from normalized root length density (NRLD) in that layer and a water stress function α which depends on the soil water pressure head (ψ_m, m) in that soil layer and potential transpiration rate T_p (mm h^{-1}) (Feddes et al., 1978).

$$RWU_i = \alpha(\psi_{m,i}, T_p) T_p NRLD_i \Delta z_i \quad (5)$$

Where RWU_i is root water uptake in the soil layer i. The $NRLD_i$ is computed from the root length density, RLD (m m^{-3}) and discretized soil thickness, Δz_i (m):

$$NRLD_i = RLD_i / \sum_{i=1}^{N} RLD_i \, \Delta z_i \quad (6)$$

The parameters of the stress functions for specific crops like maize were selected from (Wesseling et al., 1991).

The approach to estimate root hydraulic conductance and the Couvreur RWU model from winter wheat was implemented for maize. The root hydraulic conductance ($K_{rs,\ doy}$) and the root system conductance for compensatory water uptake (K_{comp} - d^{-1}) were computed based on the total length of the root system below a unit surface area $TRLD_{doy}$ (cm cm^{-2}) (Eqn. 7) at a given day of the year (DOY) which is the output from SLIMROOT (Fig. 3.2).

$$TRLD_{doy} = \sum_{i}^{N} RLD_i \, \Delta z_i \quad (7)$$

Where RLDi is root length density at layer i (cm cm^{-3}) and Δz_i is the thickness of the layer (cm). The normalized root hydraulic conductance $K_{rs,\ normalized}$ (d^{-1} cm^{-1} cm^2) was taken from Nguyen et al., (2020) and Cai et al., (2018) to calculate the daily root hydraulic conductance.

$$K_{rs,\ doy} = K_{rs,\ normalized} TRLD_{doy} \quad (8)$$

The original model from Couvreur et al., (2014) considered the hydraulic conductance from the roots to the plant collar by assuming that the hydraulic resistance from plant collar to leaf was minor and could be neglected as compared to the root system resistance. The shoot hydraulic resistance could be large as reported in some crop plants (Gallardo et al., 1996) or trees (Domec and Pruyn, 2008). To simulate the leaf hydraulic head, the whole-plant hydraulic conductance (K_{plant}) needs to be estimated. The whole-plant hydraulic conductance can be estimated from different plant organs (soil to root, stem to leaf, for instance in the study from (Saliendra et al., 1995) or a more complex approach based on plant architecture in Janott et al., (2011). The hydraulic conductance data from plant collar to leaf, which depends on environmental conditions and plant species, are often rare and difficult to obtain (Meunier et al., 2018; Chunfang et al., 1999; Sunita et al., 2014). We followed the simple approach in (Nguyen et al., 2020), the root hydraulic conductance ($K_{rs,\ doy}$) (d^{-1}) was used to calculate the whole plant hydraulic conductance (K_{plant} - d^{-1}) based on a constant fraction β (Eqn. 9)

$$K_{plant,\ doy} = \beta K_{rs,\ doy} \quad (9)$$

where β (unitless) is a fraction to upscale root hydraulic conductance to whole-plant hydraulic conductance ($K_{plant,\ doy}$).

The Couvreur RWU model is based on a mechanistic description of water flow in the coupled soil-plant system. The root water uptake (RWU) in a certain soil layer is related to the water potentials and RWU in other soil layers so that compensatory uptake is considered in this model. The RWU (mm h^{-1}) in a certain soil layer i is obtained from:

$$RWU_i = T_{plant} NRLD_i \Delta z_i + K_{comp}(\psi_i - \psi_{sr}) NRLD_i \Delta z_i \quad (10)$$

where ψ_i (m) is the total water potential head in layer i, ψ_{sr} (m) is the average hydraulic head in the root zone, K_{comp} (d^{-1}) is root system conductance for compensatory water uptake, and NRLD (unitless) is normalized root length density. The average root zone hydraulic head is calculated as the weighted average of the hydraulic heads in the different soil layers as:

$$\psi_{sr} = \sum_{i=1}^{N} \psi_i NRLD_i \, \Delta z_i \quad (11)$$

The plant transpiration rate is the minimum of the potential transpiration rate T_p (mm h^{-1}) and the transpiration rate $T_{threshold}$ (mm h^{-1}) when the hydraulic head in the canopy reaches a threshold value, $\psi_{threshold}$, which triggers stomatal closure:

$$T_{plant} = \max(0, \min(T_p\ , T_{threshold})) \quad (12)$$

$T_{threshold}$ is calculated from the difference between the root zone hydraulic head and the threshold hydraulic head of the canopy that is multiplied by the plant hydraulic conductance, K_{plant} as:

$$T_{threshold} = K_{plant}(\psi_{sr} - \psi_{threshold}\ ) \quad (13)$$

The coupled models employ a water stress index (fwat, Eqn. 14) as the ratio of T_{plant} and potential transpiration to consider the down-regulation effects of water stress on maximum carboxylation rate and stomatal conductance (Appendix A and Appendix B).

$$\text{fwat} = \frac{T_{plant}}{T_p} \quad (14)$$

Where fwat is the water stress factor (-); T_{plant} and T_p are the actual and potential transpiration rate, respectively (mm h^{-1}).

The photosynthesis and stomatal conductance, water balance, root water uptake, and Penman-Monteith subroutines run at the hourly resolution, while the remaining subroutines calculate in a daily time step (Fig. 3.2a). For a further description of the water balance model,

root growth model, Feddes' and Couvreur's RWU models, crop model, Penman-Monteith subroutines, and modeling configuration we refer the readers to the detailed model description and parameterization from Nguyen et al., (2020). In summary, we will compare the performance of two coupled root: shoot models with two different RWU subroutines in simulating CO_2 and H_2O fluxes and crop growth of maize (Fig. 3.2a):

- HILLFLOW1D-Couvreur's RWU-SLIMROOT-LINTULCC2 (Co)
- HILLFLOW1D-Feddes' RWU-SLIMROOT-LINTULCC2 (Fe)

3.2.4.4 Modeling workflow

3.2.4.4.1 Model sensitivity analysis

Before performing the sensitivity analysis, the Fe and Co models were calibrated with maize phenology parameters. The base temperature was set to 8 °C, while the minimal temperature sum from sowing to anthesis were varied from 500 to 900 °Cd (see Table 3.3, phenology parameters) until the simulated anthesis date is matched to the observed silking date. The model was further calibrated by changing the temperature sum from anthesis to harvest parameter to fit the simulated and the observed harvest dates (see Table 3.3, Fig. 3.2b).

Table 3.3 Key parameters used in modeling sensitivity analysis and calibration for maize (variables in italic were used for calibration)

Subroutines	Parameters	Explanation (unit)	Value range for maize	Source	Maize (2017F1P3)	
					Before	After
Phenology	TBASE	Base temperature (°C)	8	White, 2001	8	
	MinTTANTH	Minimum thermal sum from sowing to anthesis (°C d))	500-900		630	
	GFDUR	Thermal sum from anthesis to maturity/harvest (°C d))	500-900		600	
Assimilation	*maxSLA*	Maximum specific leaf area (m^2 g^{-1})	0.018-0.06	Amanullah et al., (2007); Miner and Bauerle (2019); Zhou et al., (2020)	*0.03*	*0.04*
	VCMAX25	The maximum carboxylation rate of Rubisco at 25 °C (μM m^{-2} s^{-1})	30-60	Miner and Bauerle (2019); Pomodo et al., (2016); von Caemmerer (2000)	*30*	*41*
	V_{pmax}	The maximum PEP carboxylation rate (μM m^{-2} s^{-1})	38-182	Miner and Bauerle (2019); Pomodo et al., (2016); Massad et al., (2007)	*80*	*120*
	a_1	Slope of coupled photosynthesis and stomatal conductance model (-)	4-11	Oleson et al., (2013); Wang and Leuning (1998)	*6*	*4.5*
Couvreur RWU model	$\Psi_{threshold}$	Canopy water potential threshold (m)	(-120) – (-200)	Cochard (2000); Tuzet et al., (2003); Tardieu and Simonneau (1998)	-200	-200
	$K_{rs,\ normalized}$	Normalized root hydraulic conductance (cm d^{-1})		Cai et al., (2018)	*0.2554 x 10^{-5}*	*0.37 x 10^{-5}*
	β	Fraction to upscale from K_{rs} to K_{plant} (-)	0-1	Nguyen et al., 2020	0.55	
Feddes RWU model	hlim1	Soil water pressure head at anaerobic limit (m)		Wesseling et al., 1991; Simunek et al., 2009	0	
	hlim2	Upper limit of pressure head range for optimal transpiration (m)			-0.03	
	hlim3h	Lower limit of pressure head range for optimal transpiration for high transpiration rate, T_{pot3h} (m)			-3.25	
	hlim3l	Lower limit of pressure head range for low transpiration rate, T_{pot3l} (m)			-6	
	hlim4	Soil water pressure head at wilting point (m)			-80	
	T_{pot3h}	High transpiration rate (m d^{-1})			0.0048	
	T_{pot3l}	Low transpiration rate (m d^{-1})			0.00096	
Root growth	MaxDEP	Maximum root depth (m)			1.5	
	RINPOP	Number of emerged plant per square meter (number m^{-2})			10.66	
	RSROOT	Maximum elongation rate of seminal root (m d^{-1})	0.03-0.035	Watt et al., (2006)	0.03	
	NRSPP	Number of seminal root per plant (number $plant^{-1}$)	3-5	Lynch (2013)	3	
	WLROOT	Specific weight for lateral root (g m^{-1})		Nguyen et al., (2020)	0.0061	
	WSROOT	Specific weight for seminal root (g m^{-1})		Nguyen et al., (2020)	0.02	

In our work, the crop-water-related parameters in the Co model ($K_{rs,\ normalized}$ and critical canopy hydraulic head threshold ($\Psi_{threshold}$) and SLIMROOT root growth model were adopted from the literature. However, the parameters for maize such as $K_{rs,\ normalized}$ are rarely reported. Cai et al., (2017a) and Cai et al., (2018) reported that $K_{rs,\ normalized}$ ranges from 0.03 x 10^{-5} to 0.48 x 10^{-5} d^{-1} cm^{-1} cm^2. The $\Psi_{threshold}$ characterizes the specific stomatal behavior. The isohydric response with higher $\Psi_{threshold}$ was initially defined at the species level (Tardieu and Simonneau, 1998), nevertheless, this behavior shows a continuum even within species (Klein, 2014; Franks et al., 2007; Schultz, 2003). The use of $\Psi_{threshold}$ and its values are different among modeling approaches. The $\Psi_{threshold}$ of -260 m was the reference leaf hydraulic head for species with insensitive stomatal regulation such as anisohydric (Tuzet et al., 2003). In contrast, the reference leaf water hydraulic head for isohydric was -120 m (Tuzet et al., 2003). Various authors used the $\Psi_{threshold}$ of -160 m for both winter wheat and maize (Cai et al., 2018; Couvreur et al., 2012; Couvreur et al., 2014). Moreover, the root growth parameters can vary among maize cultivars and soil types. In SLIMROOT, parameters such as specific weight for lateral root (WLROOT, g m^{-1}), and specific weight for seminal root (WSROOT, g m^{-1}) are required. Because the specific weights of roots in cereal crops vary with the soil strength (Colombi et al., 2017; Hernandez-ramirez et al., 2014), we selected the specific weights of roots for the stony soil from the range that was reported by Noordwijk and Brouwer, (1991) for the modeling sensitivity analysis for maize.

For the Co model, the sensitivity of cumulative RWU and total aboveground dry biomass at harvest was tested with the step-wise change of four plant-water relations parameters ($K_{rs,\ normalized}$, specific weight of seminal and lateral root, and $\Psi_{threshold}$), while the photosynthesis parameters of maize (Table 3.3, “before calibration”) were the same for all simulations. From Cai et al., (2018) and Nguyen et al., (2020), the $K_{normalized}$ was taken as 0.2554 x 10^{-5} d^{-1} cm^{-1} cm^2. In the first set of simulations, the $K_{normalized}$ was sequentially changed to 0.04, 0.15, 0.2554, 0.372, 0.48, 0.59, and 0.81 x 10^{-5} d^{-1} cm^{-1} cm^2. For the second part, the specific weight of seminal roots varied sequentially to 0.005, 0.0075, 0.01, 0.0125, 0.015, 0.0175, 0.02, and 0.0225 g m^{-1} while the specific weight of lateral roots was the same (0.02 g m^{-1}) for all simulations. For the third set of simulations, the specific weight of lateral roots was kept at 0.0061 g m^{-1}, while the specific weight of lateral roots was sequentially changed to 0.002, 0.003, 0.0035, 0.004, 0.005, 0.006, and 0.007 g m^{-1}. In the last set of simulations, the critical leaf hydraulic head ($\Psi_{threshold}$) was changed between -120 and -290 m.

3.2.4.4.2 Model calibration, validation, and comparison

Criteria for model evaluation

The model performance in simulating aboveground dry biomass, LAI, actual transpiration (referred also as RWU), gross assimilation rate, and soil water content in different soil depths was assessed via (i) the root mean square errors (RMSE) (Eqn. 15); (ii) correlation coefficients (r) (Eqn. 16); (iii) index of agreement (I, the degree to which simulated values approached the observations) (Eqn. 17). This value varies from 1 (for perfect agreement) to 0 (for no agreement);

$$RMSE = \sqrt{\frac{\sum_{i=1}^{n}(Sim_i - Obs_i)^2}{n}} \quad (15)$$

$$r = \frac{\sum_{i=1}^{n}\left(Sim_i - \overline{Sim}\right)\left(Obs_i - \overline{Obs}\right)}{\sqrt{\left[\sum_{i=1}^{n}\left(Sim_i - \overline{Sim}\right)^2\right]\left[\sum_{i=1}^{n}\left(Obs_i - \overline{Obs}\right)^2\right]}} \quad (16)$$

$$I = 1 - \left[\frac{\sum_{i=1}^{n}(Sim_i - Obs_i)^2}{\sum_{i=1}^{n}\left(\left|Sim_i - \overline{Obs}\right| + \left|Obs_i - \overline{Obs}\right|\right)^2}\right] \quad (17)$$

Where Sim and Obs are simulated and measured variables, respectively; i is the index of a given variable; $\overline{Obs}$ and $\overline{Sim}$ are the mean of the simulated and measured data, respectively; and n is the number of observations.

Model calibration

We used the irrigated plots in 2017 (2017F1P3) for calibration. The C_4 photosynthesis parameters, the parameters for α stress functions, and root parameters such as specific weights of lateral (0.0061 g m^{-1}) and seminal root (0.02 g m^{-1}), $K_{rs,\ normalized}$ of 0.2554 10^{-5} cm d^{-1}, $\Psi_{threshold}$ of -200 m, β of 0.55 were used for performing simulations (Fig. 3.2b and Table 3.3, "before calibration"). These referred as "before calibration" results (FeB and CoB for Feddes and Couvreur models, respectively). We calibrated the Fe and Co model by varying the following parameters: specific leaf area (SLA, m^2 g^{-1}), maximum carboxylation rate of Rubisco at 25 °C (VCMAX25, µM m^{-2} s^{-1}), maximum PEP carboxylation rate (V_{pmax}, µM m^{-2} s^{-1}), the slope of coupled photosynthesis and stomatal conductance model (a_1, (-)), and $K_{rs,\ normalized}$. The RMSE (Eqn. 15), correlation efficiency (r) (Eqn. 16), and I (Eqn. 17) were calculated using the R software (R core development teams, 2018) and used to compare the simulated and

observed LAI, gross assimilation rate, aboveground dry biomass, and actual transpiration. The best parameter set was identified manually by choosing a simulation with the lowest RMSE and the highest r and I. These chosen parameters and output results are referred as “after calibration” (FeA and CoA for Feddes and Couvreur models, respectively (Fig. 2b). The parameters after calibration were listed in Table 3.3.

Modeling validation and comparison

The parameter set from the “after calibration” step was used for model validation and comparing the Co and Fe models (Table 3.3 and Fig. 3.2b). Based on the criteria for model evaluation (r, RMSE, and I), we examined the model capacity for simulating the aboveground dry matter, LAI, RWU, SWC, and gross assimilation rate for the remaining water treatments. The remaining treatments were used for this last stage: the rainfed plot in 2017 (2017F1P2), the irrigated plot with normal sowing date in 2018 (2018F1P3), the rainfed plot with normal sowing date in 2018 (2018F1P2), and the rainfed plot with a late sowing date in 2018 (2018F1P1) (cf. Table 3.2, Fig. 3.1a, and Fig. 3.2b).

3.3 Results and discussions

3.3.1 Model sensitivity analysis

The sensitivity of RWU and biomass to the changing $K_{rs,\ normalized}$, specific weights of the seminal and lateral root, and critical hydraulic head $\Psi_{threshold}$ were illustrated in Figure 3.3. The change of $K_{rs,\ normalized}$ and specific weight of seminal and lateral roots directly affects total root hydraulic conductance (thus whole-plant hydraulic conductance, K_{plant}) because they depend on total root length and hydraulic conductance of root segments. Among these parameters, the change of $K_{rs,\ normalized}$ resulted in a larger change in RWU and biomass than those due to the change of root growth parameters (Fig 3.3a, b, c, d, e, and f). The reduction of $K_{rs,\ normalized}$ leads to a stronger decrease in RWU and biomass in 2018 as compared to 2017. This is due to less soil water availability in 2018 than those in 2017. However, the increased $K_{rs,\ normalized}$ by the same magnitude had a smaller relative effect on RWU and biomass than decreasing values of $K_{rs,\ normalized}$. A larger increase of RWU and biomass was observed in the more severe water stress plots (i.e. the two rainfed plots in 2018) as compared to the other less severe water stress plots (i.e irrigated and rainfed plots in 2017). This indicates that increasing water uptake capacity by plants would increase the uptake of water and crop growth in maize.

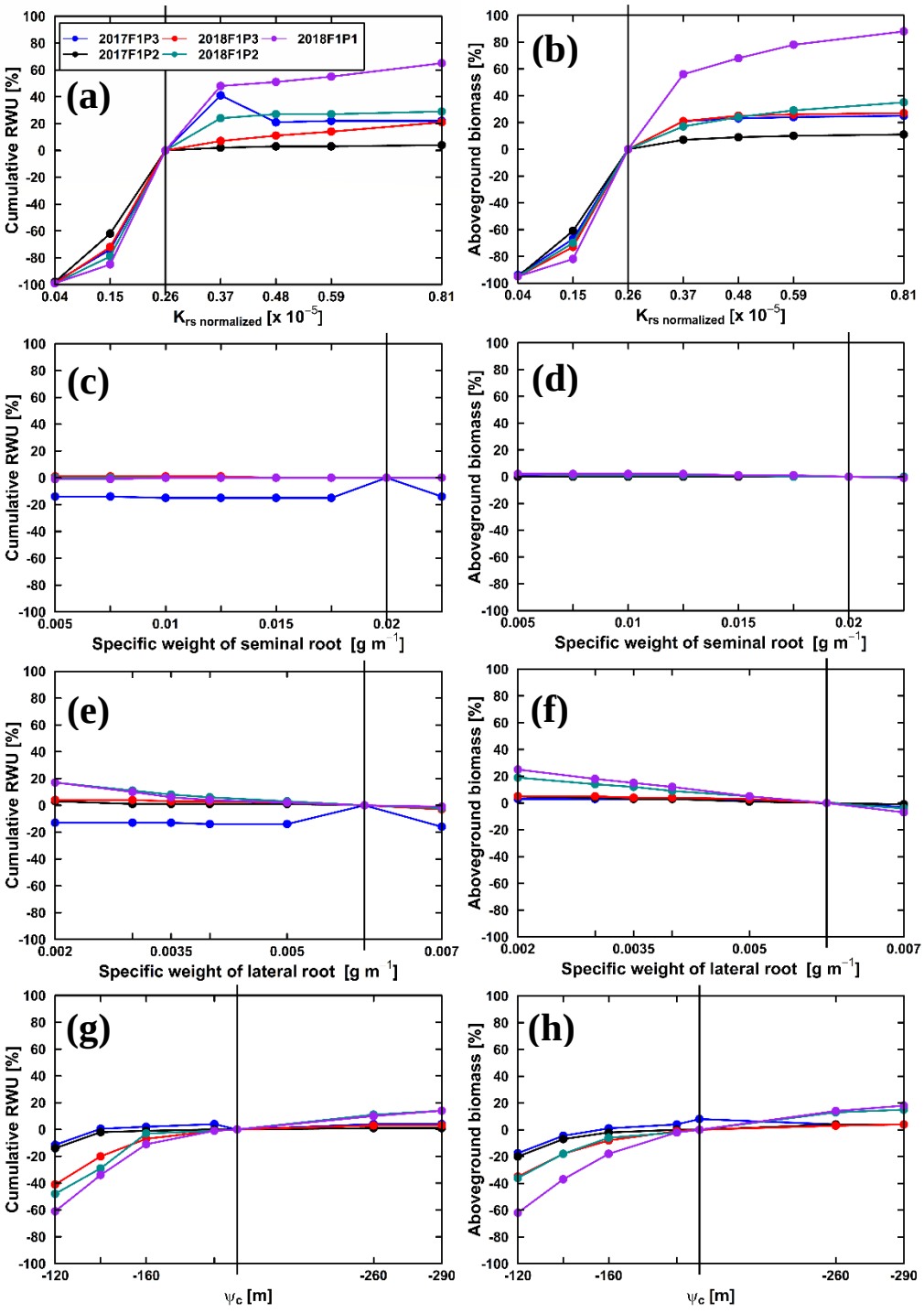

Figure 3.3: Relative changes of (a, c, e, g) simulated cumulative RWU and (b, d, f, h) simulated aboveground biomass to the reference of cumulative RWU and aboveground biomass at harvest by changing $K_{rs,\ normalized}$, specific weights of seminal (WSROOT) and lateral (WSLROOT) roots, and canopy pressure head threshold ($\Psi_{threshold}$) at the irrigated in 2017 (2017F1P3), rainfed plot in 2017 (2017F1P2), irrigated plot with normal sowing date in 2018 (2018F1P3), rainfed plot with normal sowing date in 2018 (2018F1P2), and rainfed plot with late sowing date (2018F1P1). The reference of simulated cumulative RWU and biomass (vertical lines) for each treatment based on the plant water relation parameters ($K_{rs,\ normalized}$, WSROOT, WLROOT, and $\Psi_{threshold}$) from winter wheat (Nguyen et al., 2020) and C_4 photosynthesis parameters in Table 3.3 ("before calibration").

Decreasing the specific weight of lateral and seminal roots increases the total root length, thus the whole-plant hydraulic conductance. However, there was a minor change in aboveground biomass and RWU for the considered range of specific weights of root. Use of $\Psi_{threshold}$ at -120 m and -140 m resulted in a substantial reduction of RWU and biomass as compared to those $\Psi_{thresholds}$ below -160 m (Fig. 3.3g and 3.3h), especially in the rainfed plots in 2018. The use of a high $\Psi_{threshold}$ leads to tight control Ψ_c and stomatal conductance that consequently reduces transpiration and photosynthesis because plants keep Ψ_c close to its threshold value (Olioso et al., 1996). An increase of the $\Psi_{threshold}$ means that water stress occurs earlier which finally causes more reduction of RWU and biomass. When $\Psi_{threshold}$ varies from -160 m to -200 m, the change in RWU and biomass is less pronounced as compared to those changes of $\Psi_{threshold}$ from -120 and -140 m (Fig. 3.3g and 3.3h). These findings are well corroborated with findings from Nguyen et al., (2020) where higher $\Psi_{thresholds}$ i.e. -120 or -140 m could overestimate water stress (thus lower biomass and RWU) in winter wheat.

3.3.2 Crop model calibration

There was a relatively large deviation in the observed aboveground dry biomass and LAI between two measured replicates which indicates the crop heterogeneity within the treatment (Fig. 3.4). The seasonally simulated growth curves of LAI and biomass were satisfactorily captured after calibration in both Co and Fe models (Fig 3.4a, 3.4b & Appendix 3D). The RMSE of the Fe model before calibration was 0.97 kg m^{-2} and 1.72 (-) for biomass and LAI, respectively, while the corresponding RMSEs after calibration were 0.36 kg m^{-2} and 0.69 (Table 3.4). In the Co model, the RMSE of biomass and LAI before calibration were 1.01 kg m^{-2} and 1.83, respectively which got improved after calibration having the value of 0.24 kg m^{-2} and 0.66 for biomass and LAI, respectively (Table 3.4).

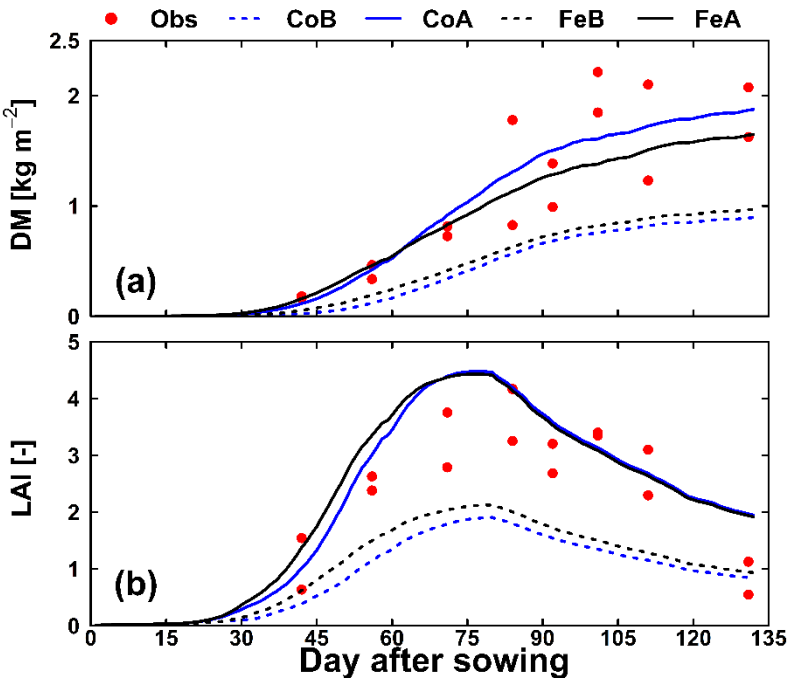

Figure 3.4: Comparison of measured data and simulated (a) aboveground dry biomass (DM), (b) LAI by Couvreur before calibration (CoB, blue dotted lines), Couvreur after calibration (CoA, blue solid lines), Feddes before calibration (FeB, dark dotted lines), Feddes after calibration (FeA, black solid lines) in the irrigated plot in 2017 (2017F1P3). Two red dots in (a) and (b) mean two measured replications.

Table 3.4 Root mean square error (RMSE), coefficient of correlation (r), and agreement index (I) of aboveground dry biomass, leaf area index (LAI), daily root water uptake (RWU or T_a), and hourly gross assimilation rate (Pg) before and after modeling calibration for 2017F1P3 and modeling validation for 2017F1P2, 2018F1P3, 2018F1P2, and 2018F1P1 treatments (cf. Fig. 3.1 and Table 3.2)

		Before Calibration		After calibration		Validation									
		2017F1P3				2017F1P2		2018F1P3		2018F1P2		2018F1P1		Overall*	
		Co	Fe	Co	Fe	Co	Fe	Co	Fe	Co	Fe	Co	Fe	Co	Fe
Dry biomass	RMSE	1.01	0.97	0.24	0.36	0.31	0.28	0.52	0.55	0.19	0.25	0.15	0.18	0.29	0.32
	r	0.96	0.96	0.95	0.95	0.89	0.9	0.96	0.95	0.89	0.85	0.91	0.96	0.91	0.92
	I	0.67	0.66	0.9	0.91	0.93	0.92	0.85	0.83	0.93	0.83	0.88	0.79	0.90	0.84
	n	8	8	8	8	8	8	10	10	10	10	10	10	38	38
LAI	RMSE	1.83	1.72	0.66	0.69	0.75	0.63	0.94	0.96	0.87	0.84	0.65	0.53	0.80	0.74
	r	0.89	0.9	0.89	0.88	0.85	0.85	0.8	0.81	0.76	0.78	0.71	0.74	0.78	0.80
	I	0.6	0.73	0.89	0.88	0.83	0.85	0.76	0.75	0.85	0.85	0.74	0.78	0.80	0.81
	n	8	8	8	8	8	8	10	10	10	10	10	10	38	38
RWU	RMSE	1.62	1.41	0.67	0.78	0.54	0.38	1.27	1.29	1.17	1.13	0.92	0.91	0.98	0.93
	r	0.91	0.94	0.94	0.95	0.91	0.95	0.73	0.74	0.74	0.73	0.74	0.76	0.78	0.80
	I	0.81	0.85	0.96	0.94	0.94	0.97	0.85	0.84	0.72	0.77	0.72	0.74	0.81	0.83
	n	64	64	64	64	66	66	54	54	54	54	54	54	228	228
Pg	RMSE	12.85	12.59	7.83	7.96	7.35	7.44	7.55	7.38	8.29	8.15	8.21	8.20	7.85	7.79
	r	0.72	0.63	0.78	0.75	0.75	0.76	0.77	0.78	0.67	0.68	0.65	0.66	0.71	0.72
	I	0.48	0.6	0.81	0.82	0.72	0.70	0.68	0.69	0.72	0.74	0.64	0.64	0.69	0.69
	n	61	61	61	61	56	56	41	41	45	45	44	44	186	186

The unit of RMSE for RWU (mm d^{-1}), Pg (μM m^{-2} s^{-1}), aboveground dry biomass (kg m^{-2}), and LAI (-); n is number of samples/ measurement points. * indicates the average values from all validated plots (2017F1P2, 2018F1P3, 2018F1P2, and 2018F1P1).

The water supply (precipitation and irrigation), daily root water uptake (RWU or T_a), and soil water content were displayed in Fig. 3.5. Both models were able to represent the seasonal fluctuation of RWU and SWC (Fig. 3.5a). After calibration, the Feddes model simulated higher RWU than the Co model from sowing to DAS 48 which was consistent with the lower estimated SWC of the Fe model than the Co model. After calibration, the simulated RWU of the Co was almost similar to those from the Fe model after DAS 48. Both models underestimated RWU from DAS 75 to DAS 112 that led to lower simulated cumulative RWU as compared to cumulative sap flow (Fig. 3.5a, Appendix 3C & Appendix 3E). The correlation efficiency (r) and I were relatively similar before and after calibration for both models. Both

models slightly underestimated the SWC after calibration, especially in the later growing season at the 60 and 80 cm soil depths (Fig. 3.5b, Appendix 3F).

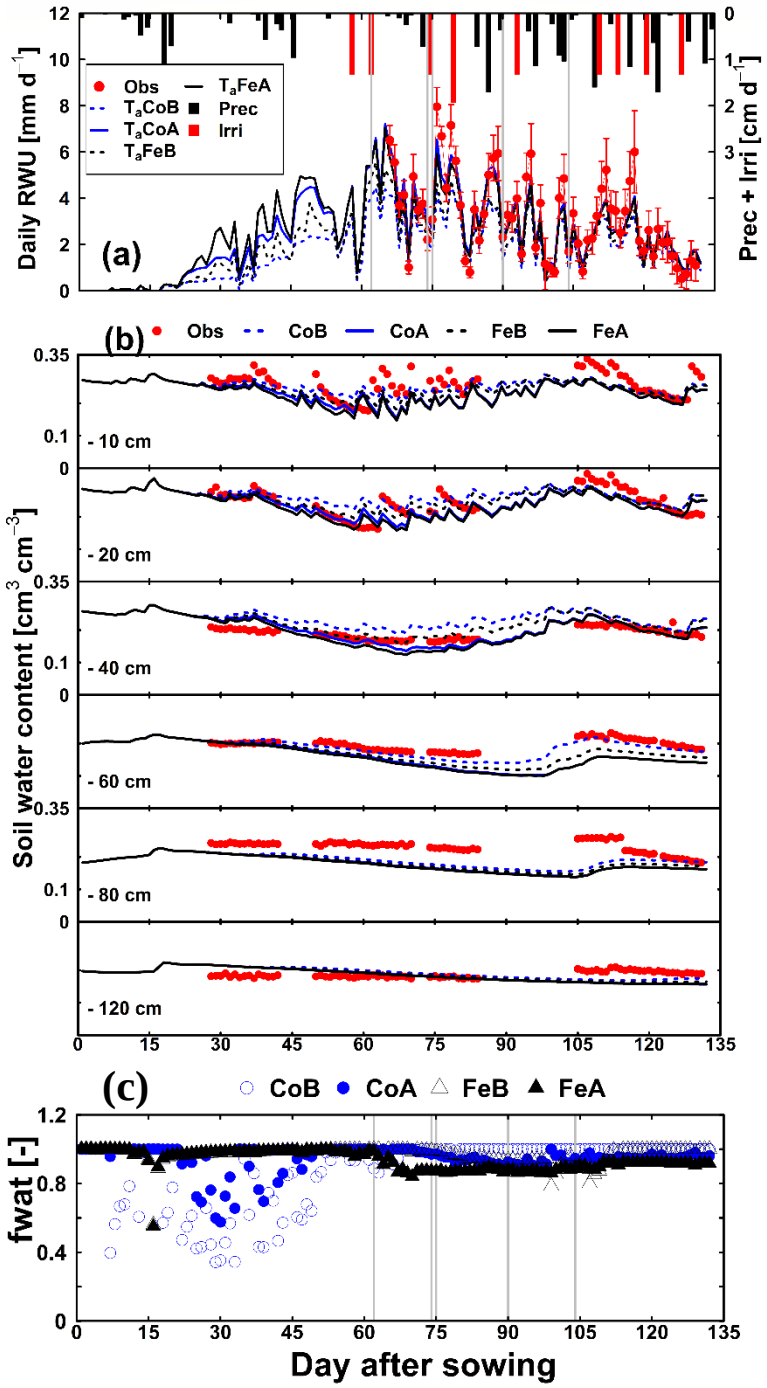

Figure 3.5: Comparison between observed (red) and (a) daily actual transpiration (RWU or T_a), (b) soil water content at different soil depths, and (c) daily transpiration reduction factor (fwat) simulated by Couvreur before calibration (CoB), Couvreur after calibration (CoA), Feddes before calibration (FeB), and Feddes after calibration (FeA) in the irrigated plot in 2017 (2017F1P3). The black and red bars in (a) denote precipitation (Prec) and irrigation (Irri), respectively. The error bars in (a) indicate standard error for 5 sap flow sensors. Vertical grey lines in (a & c) show days with the measured and simulated diurnal courses of root water uptake (RWU), canopy hydraulic head (ψ_c), stomatal conductance (g_s), and gross assimilation rate (Pg) as used in Figure 3.6.

The transpiration reduction was also shown in Fig. 3.5c. Before calibration, the water stress (fwat < 1) was appeared already from DAS 8 to DAS 68 in the Co model. The water stress also occurred in period from DAS 8 to DAS 45 for the Co model after calibration, however it was less pronounced which was opposite to the Fe model. This caused the lower simulated biomass and LAI in the Co model as compared to the Fe model. The Co model simulated less transpiration reduction (less water stress) than in the Feddes model at the late growing season (after DAS 68). This could explain the higher simulated biomass and LAI from the Co model in comparison to the Fe model after calibration.

Diurnal courses of RWU, ψ_c, g_s, and gross assimilation rate (Pg) followed the observed values in the selected days (Fig. 3.6). Root water uptake was slightly lower than measured sap flow in the morning (i.e. 9-10 AM) but the opposite was the case in the afternoon (4-6 PM). Root water uptake started later than transpiration because the stored water in the plant is used for transpiration. The plant hydraulic capacitance of plant tissues (Kramer and Boyer, 1995; Langensiepen et al., 2009) (Fig. 3.6b) can delay the change of ψ_c that derives water uptake which was not considered in our model. However, the differences between simulated RWU and sap flow in the morning and afternoon due to the plant hydraulic conductance was canceled out when the hourly sap flow and RWU were aggregated (Fig. 3.6c). Both models were able to simulate the diurnal courses of transpiration, stomatal conductance of sunlit leaves, and gross assimilated rate (Table 3.4 and Appendix 3E) comparable to the measured data. The canopy pressure head (Ψ_c) of the Co model matched fairly well with the observed ones after calibration.

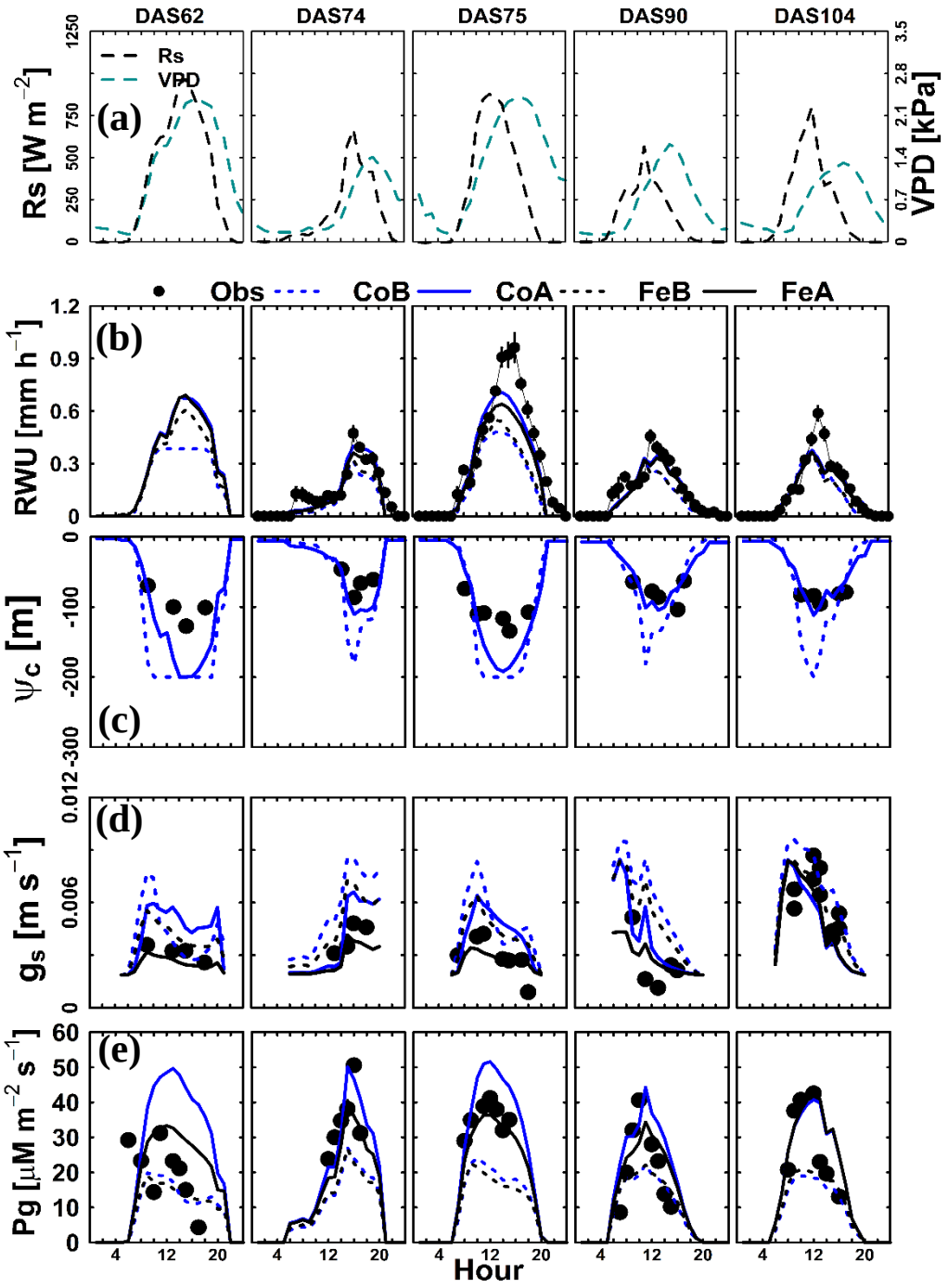

Figure 3.6: Diurnal courses of 5 selected measurement days: 05 July (DAS 62), 17 July (DAS 74), 18 July (DAS 75), 02 August (DAS 90), and 16 August 2017 (DAS 104) (a) global radiation (Rs, black long dash lines) and vapor pressure deficit (VPD, cyan long dash lines), (b) actual transpiration (RWU or T_a), (c) canopy hydraulic head (ψ_c), (d) stomatal conductance to water vapor (g_s), and (e) gross assimilation rate (Pg) at the irrigated plot in 2017 (2017F1P3). The black dots denote the observed. The lines denote simulated output by Couvreur before calibration (CoB, blue dotted lines), Couvreur after calibration (CoA, blue solid lines), Feddes before calibration (FeB, dark dotted lines), Feddes after calibration (FeA, black solid lines). Sap flow sensors were installed on 08 July 2017. Simulated stomatal conductance is from sunlit leaves. Vertical black bars in (b) represent the standard deviation of the flux measurements in the five different stems.

3.3.3 Crop model validation and comparison between the Feddes and Couvreur RWU models

3.3.3.1 Aboveground dry biomass and leaf area index

The development of aboveground dry biomass and LAI when applying the calibrated model for different treatments are illustrated in Figure 3.7. The Couvreur model predicted lower biomass and LAI than the Fe model in the early growth stages across all treatments in both years. Whereas, more biomass and LAI were simulated by the Co model than the Fe model at the later crop growth stages. The biomass from Fe and Co models was satisfactorily simulated in the rainfed plot in 2017 (2017F1P2), the rainfed plot with normal sowing date (2018F1P2), and the rainfed plot with a late sowing date (2018F1P1). At the 2018F1P3 plot, the biomass and LAI from both models have a good match with the observed before the silking time. However, afterward, the models underestimated biomass and LAI. The RMSEs of LAI were 0.94 and 0.96 for Co and Fe models, respectively in this plot. In the drought plot (i.e. 2018F1P2), both models overestimated LAI from DAS 65 to harvest (Fig. 3.7f) with RMSEs of 0.87 and 0.84, respectively. In these plots, leaf started rolling when the leaf hydraulic head at around -150 m (equivalent to -1.5 MPa) and completely curling and rolling occurred when the leaf hydraulic head was around -200 m in our field coinciding with days having severe drought, high temperature, and high VPD. This was in agreement with another observation of leaf-rolling at leaf pressure heads of -100 m with its maximum around -200 m in a study on maize from Moulia (1994). Low leaf water hydraulic head could result in a reduction of leaf elongation rate and leaf area under water-limited conditions (Westgate and Boyer, 1985; Munns et al., 2000; Salah and Tardieu, 1997). Our leaf growth model is based on assimilate partitioning, specific leaf area parameters, and air temperature at a daily time scale, thus it is not able to capture the instant effects of leaf water status on leaf area variability.

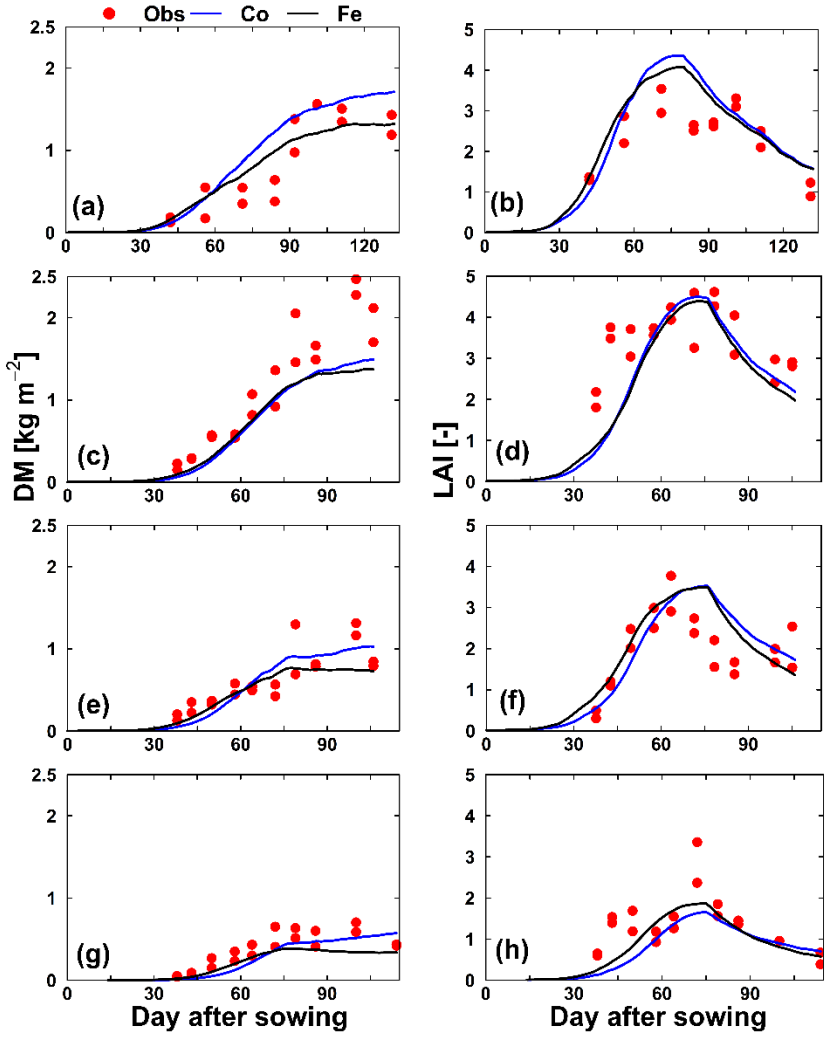

Figure 3.7: Comparison between observed (red dot) and simulated (a, c, e, g) aboveground dry biomass and (b, d, f, h) LAI by Couvreur (Co, blue solid line) and Feddes (Fe, black solid line) at the rainfed plot in 2017 (2017F1P2) (a, b), irrigated plot with normal sowing date in 2018 (2018F1P3) (c, d), rainfed plot with normal sowing date in 2018 (2018F1P2) (e, f), and rainfed plot with late sowing date (2018F1P1) (g, h). Two red dots means two measured replications.

3.3.3.2 Transpiration reduction

The transpiration reduction (fwat) from the four validated plots was displayed in Fig. 3.8. The Couvreur model displayed water stress in all plots at the beginning of growing seasons (DAS 8 to DAS 45 for the normal sowing plots and DAS 17 to DAS 52 for the late sowing plot) which is opposite to the Fe model. After this period, the Fe model predicted more severe water stress than the Co model. Both models were able to simulate the severe water stress during severe

soil water depletion (from DAS 56 to DAS 105 in 2018F1P2; from DAS 60 to the end of the growing season in 2018F1P1) (Fig 3.8c & 3.8d).

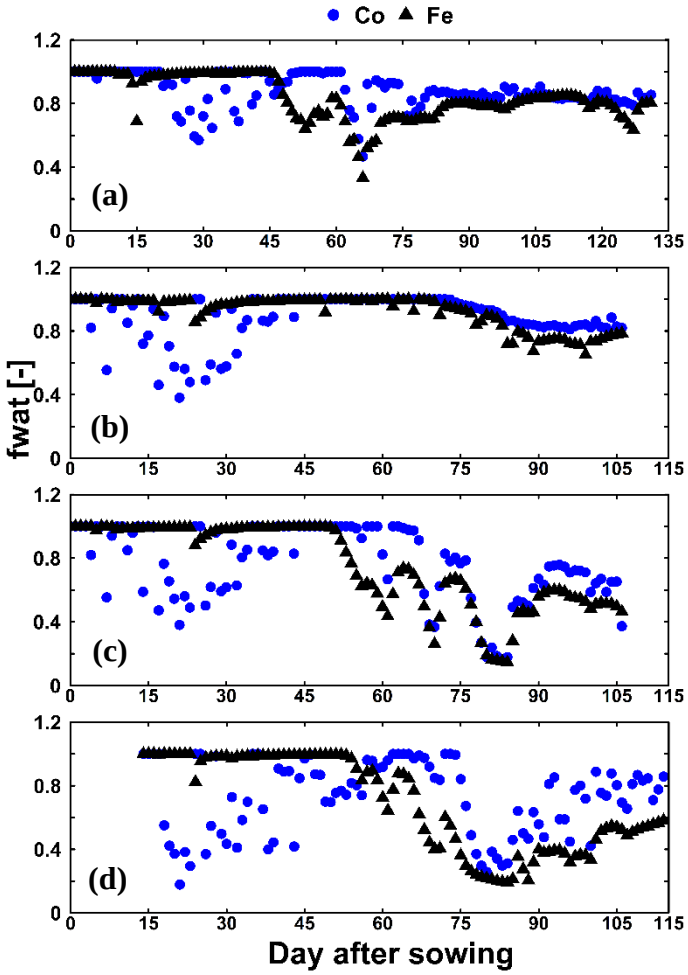

Figure 3.8: Daily transpiration reduction (fwat) simulated by Couvreur (Co, blue dot) and Feddes (Fe, black triangle) at the (a) rainfed plot in 2017 (2017F1P2), (b) irrigated plot with normal sowing date in 2018 (2018F1P3), (c) rainfed plot with normal sowing date in 2018 (2018F1P2), and (d) rainfed plot with late sowing date (2018F1P1).

3.3.3.3 Root water uptake and soil water content

Simulated T_p, RWU, and SWC were presented in Figure 3.9 for the rainfed plot in 2017 (2017F1P2) and the irrigated plot with a normal sowing date in 2018 (2018F1P3). The Couvreur model simulated lower RWU and SWC than the Fe model in the earlier growing phases. However, it calculated slightly higher RWU and SWC than the Fe model in the later growing period. Both models simulated fairly well the dynamics of RWU at the 2017F1P2 (Fig. 3.9a, 3.9b) with RMSEs of 0.54 and 0.38 mm d^{-1} for the Co and Fe model, respectively. In the irrigated plot 2018F1P3, the simulated T_{act} and measured sap flow were much higher than those in 2017F1P2 (also in 2017F1P3). Our measured sap flow for some days at the irrigated

plot 2018F1P3 went to 10.6 mm d^{-1} where a daily maximum f VPD and temperature were up to 3.8 kPa and 37° C, respectively. Such high sap flow values at the 2018F1P3 have been reported in a semi-arid climate and irrigated soil conditions in maize (Langensiepen et al., 2009). However, our measured sap flow was higher than those reported in Germany (i.e. Langensiepen et al., (2009); Heinlein et al., (2017)). The air temperature and VPD were high in the main crop growing period, while soil water was relatively sufficient due to irrigation could explain the high values of sap flow in the 2018F1P3 (see Section 3.2.2). The dynamics of predicted SWC from the two models followed the measured values over different soil depths for both water treatments (Fig. 3.9b, 3.9d & Appendix 3F).

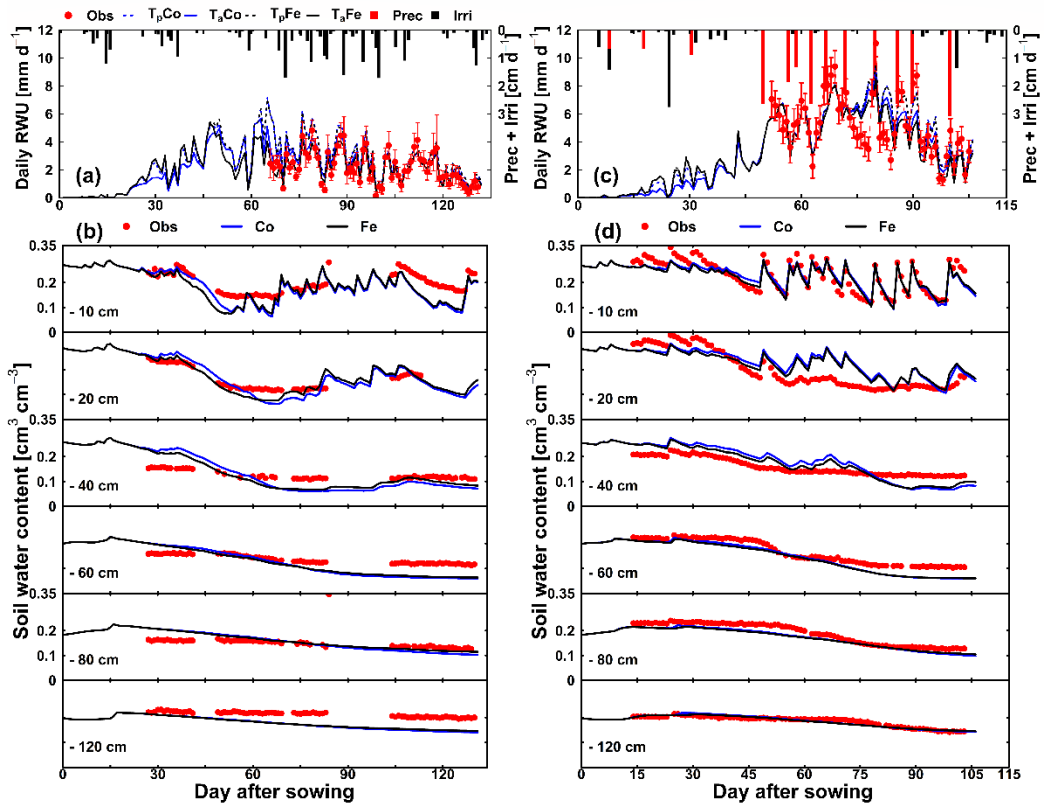

Figure 3.9: Comparison between measured sap flow (red) and simulated (a, c) root water uptake (RWU or T_a) and potential transpiration (T_p) and (b, d) soil water content by Couvreur (Co, blue line), and Feddes (Fe, black line) from sowing to harvest at the rainfed plot with normal sowing date in 2017 (2017F1P2) (a, b) and at the irrigated plot with normal sowing date in 2018 (2018F1P3) (c, d). Time series of precipitation (Prec) and irrigation (Irri) are given in the panels. Vertical red bars in (a) and (c) represent the standard deviation of the flux measurements in the five different stems.

The comparison of simulated T_p, RWU, and SWC from two models to the measured data at the remaining rainfed plots in 2018 with normal (2018F1P2) and late sowing dates (2018F1P1) was shown in Fig. 3.10. Comparing with the measured sap flow, both models overestimated

RWU from DAS 52 to DAS 70 at the 2018F1P2 and from DAS 52 to DAS 73 at the 2018F1P1. The overestimated RWU by both models in these periods in two plots was consistent with their overestimated SWC at corresponding times at the topsoil layers (10, 20, and 40 cm depths). However, after these periods, the simulated RWU from the two models matched relatively well. Soil is a heterogeneous substrate, while it is also spatially different within the plot. Thus, it is rather difficult to find a representative set of soil characteristics valid for a whole plot in our study which can explain the deviations of simulated RWU and SWC in two models.

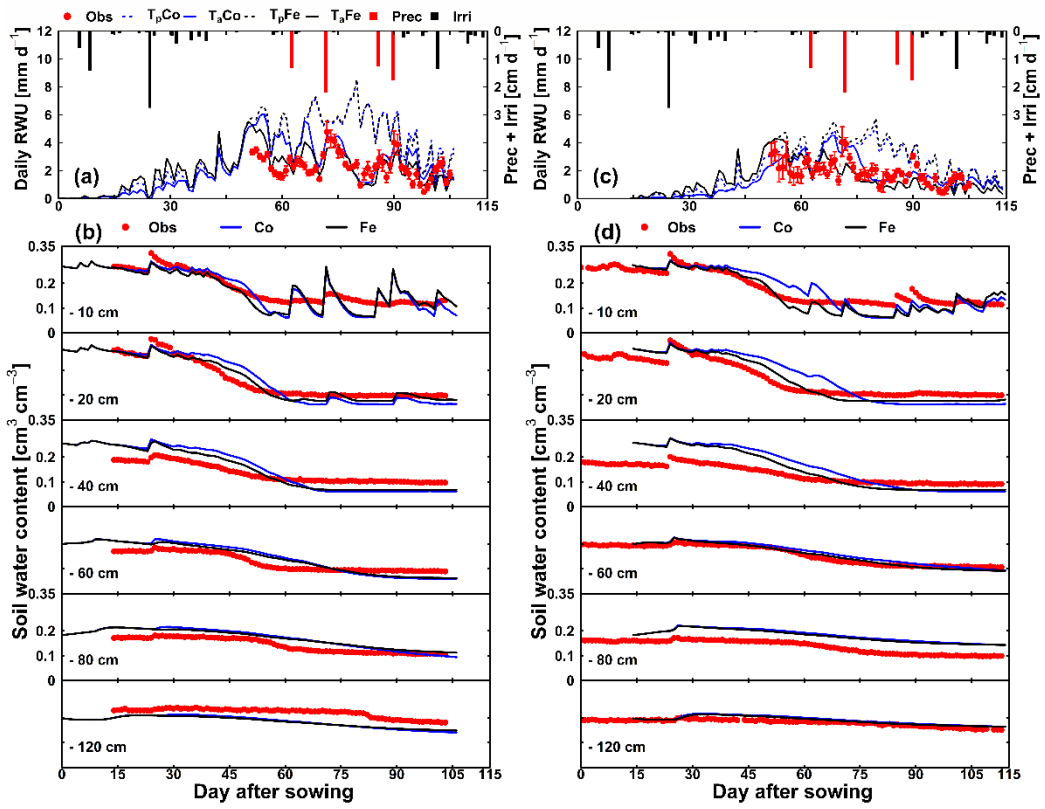

Figure 3.10: Comparison between measured sap flow (red) and simulated (a, c) root water uptake (RWU or T_a) and potential transpiration (T_p) and (b, d) soil water content by Couvreur (Co, blue line), and Feddes (Fe, black line) from sowing to harvest at the rainfed plots in 2018 with normal sowing date (2018F1P2) (a, b) and with late sowing date (2018F1P1) (c, d). Time series of precipitation (Prec) and irrigation (Irri) are given in the panels. Vertical red bars in (a) and (c) represent the standard deviation of the flux measurements in the five different stems.

3.3.3.4 Overall performance of the coupled models with Couvreur and Feddes RWU models

Numerous studies applied the common Feddes RWU model with HYDRUS water balance model (Simunek et al., 2009) in simulating soil water flux and nutrient flow under different

water regimes (Gonzales et al., 2015), the interaction of water and salt content (He et al., 2017; Wang et al., 2015) or nitrogen levels and irrigation methods (Tafteh et al., 2012). Few studies coupled crop models (i.e. WOFOST crop model) with the Feddes RWU model and HYDRUS model to simulate crop growth and water uptake in maize (Li et al., 2012; Yang et al., 2017). Note that the coupling work of LINTULCC2 crop model with the Feddes RWU model in this study considers the more mechanistic C_4 assimilation routines and stomatal conductance model. Moreover, these subroutines link with soil water flux at the hourly step which is not represented in these abovementioned studies. The coupled model with the Feddes RWU model simulated well the transpiration reduction, assimilate, RWU, and crop growth for maize in both years.

The modeling approach using $\Psi_{threshold}$ as a trigger for stomatal control and involving plant hydraulic conductance has received increasing attention in improvements and applications of the soil-plant-atmosphere model. However, most work so far investigates water response behavior in crops such as soybean (Olioso et al., 1996) or spring wheat (Jensen et al., 1993). Comparison of modeling performance between Feddes RWU model and Couvreur RWU model has been done in winter wheat (Nguyen et al., 2020; Cai et al., 2018; Cai et al., 2017). The Couvreur model uses a stomatal regulation model which assumes that stomatal conductance is not influenced by Ψ_c as long as the Ψ_c is above $\Psi_{thresholds}$. The Ψ_c was kept constant by changing stomatal conductance when the $\Psi_{thresholds}$ are reached. In fact, this is a perfectly isohydric system. Thus, from the theoretical point of view, this approach should be able to represent stomatal regulation of maize because it maintained its Ψ_c at certain $\Psi_{thresholds}$ (Tardieu and Simonneau, 1998; Cochard, 2002). To our best of knowledge, this is the first study where the performance of the Couvreur RWU model is evaluated and compared with the Feddes model for maize under field scale. Our results showed that both models simulated rather similarly the crop growth, CO_2, and H_2O gas flux exchanges of maize in the main growing season.

The Couvreur model displayed water stress in all plots during the initial growth stages (14 to 45 DAS in 2017, 3 to 45 DAS in the normal sowing plots in 2018, and 2 to 37 DAS for the late sowing plot in 2018). In contrast, the Feddes model simulated water stress only on few days (14 and 15 DAS in 2017 and 23 DAS at the normal sowing plots in 2018 and 8 DAS for the late sowing plot in 2018) during the initial growth stages. The inaccurate simulation of water stress in the Couvreur model could be related to the low simulated K_{plant} in the earlier growing period. This explains the slightly lower simulated biomass and LAI from the Couvreur model as compared with the Feddes model and the observed data in this period. After this period, the

Couvreur model predicted water stress and crop growth better than the Feddes model when K_{plant} increased (Appendix 3G). The root and plant hydraulic conductance in the Couvreur model is a function of the total root length system. Because the Feddes model did not consider the root hydraulic property, it was not sensitive to the low estimates of root system conductance (in the earlier growth of root), which is opposite to the Couvreur model. A sensitivity analysis was carried out by changing either $K_{init,normalized}$ or β to examine the effect on transpiration reduction and biomass (data not shown). The increase of $K_{init,normalized}$ or β improved the prediction of water stress at the earlier growth stage of the crop; however, it led to an underestimation of water stress (thus overestimation of RWU and biomass growth) at the later growth stage. The supply of assimilates from shoot to root is given by a partitioning table based on the thermal time. This approach probably was not sufficient to capture dynamic changes in carbon allocation to the root over the cropping season (thus dynamic root hydraulic conductance), especially under the condition of drought stress.

In this study, the coupled model was calibrated using data from the irrigated plot in 2017 based on the value ranges of parameters that were taken from other modeling studies and literature. The calibrated parameters worked fairly well for both the water-stressed and non-water-stressed plots. This could be related to the choice of initial parameter values. However, it is still questionable whether the derived parameters are suitable to describe water uptake and crop growth also under conditions of lower soil water availability. Further studies might be required to derive crop stress parameters from inverse modelling (i.e., in G. Cai et al., 2018) when data from water-stressed treatments are used for maize. Modeling and understandings the effect of varying soil moisture and evaporative conditions on crop growth, CO_2, and H_2O gas flux exchange at field conditions often requires comprehensive and expensive measurements to capture the soil–plant–atmosphere continuum. The modeling study and the presented data, to the best of our knowledge, are unique. Due to the associated complex and expensive construction of underground rhizotrone facilities, the experimental sites did not allow to involve replicates in water treatments (Nguyen et al., 2020). The limited size of the subplot did not allow for a larger sample of biomass, leaf-cutting, and LAI, which can become noisy due to the soil and water heterogeneity within the subplots. The spatial variability of stomatal reactions over leaves, plants, and stands of plants can be large (Rochette et al., 1991). However, despite these shortcomings, the data illustrated the difference and variability among water regimes and two growing seasons that are still valid for model calibration, validation, and for comparing the two model approaches in the present study.

3.2 Conclusion

We extended and evaluated two different RWU approaches within a coupled soil water balance and crop growth model for maize. One of the RWU models was the recently developed Couvreur RWU approach, which simulates the water potential gradient from soil to root and to leaves based on whole-plant hydraulic conductance, whereas the other approach was the commonly used Feddes model that does not explicitly include plant hydraulic conductance.

For the coupled model with the Couvreur RWU approach, the effect of the change of the root segment conductance, specific weight of roots, and the leaf pressure head threshold at which stomata close on RWU and aboveground biomass is amplified by the positive feedback between the aboveground biomass, the root biomass, the total root length, the root system hydraulic conductance, and plant hydraulic conductance. For instance, decreasing the specific weight of lateral and seminal roots increases the total root length, and thus the K_{plant} that led to an increase in RWU and biomass. The coupled model, which considers plant hydraulic conductance and links root system properties to plant water uptake, water stress, and crop growth in a more mechanistic way, could be able to describe the effects of specific crop characteristics (change of root segment conductance, specific root lengths of seminal and lateral root, or leaf critical pressure head) on crop performance under different conditions of soil moisture and evaporative demand.

Overall, the biomass, leaf area development, SWC, canopy pressure heads, leaf stomatal conductance, and transpiration rate were relatively well predicted for maize by both models. However, the coupled Couvreur model simulated inaccurately water stress in the first 45 d of the crop season, resulting in slightly underestimated biomass and LAI, which was opposite to the results from the Feddes model. Nevertheless, the coupled Couvreur model simulated slightly better transpiration reduction, water uptake, assimilation, and crop growth than the Feddes model in the late growing period.

Future application of the more mechanistic Couvreur approach in predicting the crop responses to different soil water conditions should pay attention to an accurate estimate of K_{plant}. A root growth model, which considers changes in carbon allocation to the root system that are triggered by stress through a more mechanistic representation of root–shoot partitioning, would improve accuracies in the simulation of whole-plant hydraulic conductance in different growth stages. Using a dynamic parameterization of the normalized root system conductance (i.e., different $K_{rs,normalized}$) could further improve the estimation of whole-plant hydraulic conductance.

4 Chapter: Responses of winter wheat and maize to varying soil moisture: from leaf to canopy

Abstract

Drought is a serious constraint to crop growth and production of important staple crops such as winter wheat and maize. Understanding of how crops respond to drought can support crop breeding and crop choice and management to minimize its negative impacts and can further improve crop modelling. Plants may respond to drought through immediate stomatal regulation and through altering their morphological characteristics over longer periods, with many degrees and combinations of short- and long-term responses depending on the intensity and duration of drought and crop type. However, the availability of detailed field observations for different crop types that provide information on crop responses at short- and longer term time scales and for different organizational levels is still limited. We examine the effects of different water treatments on the short-term changes of leaf water potential (LWP) and gas exchange at the leaf level together with the seasonal change of canopy photosynthesis, transpiration, and crop growth of winter wheat and maize based on field data collected in 2016, 2017, and 2018. The long-term morphological changes, such as reduction of leaf area and tiller number, in response to drought in winter wheat was more important for regulating transpiration and assimilation rate than stomatal control. Maize (grown in 2017 and 2018) showed seasonal variations in minimum LWP with a complete stomatal closure at LWP between -1.6 and -2 MPa. While stomata progressively closed with increasing drought, the physiological advantages of C_4 photosynthesis systems as well as morphological adjustments in leaf area size and leaf-rolling strongly influenced crop growth and canopy gas exchange in maize in the drought plots as compared with the irrigated plot. Observations highlight that improvements of soil-vegetation-atmosphere models in simulating gas exchange and crop growth should emphasize not only stomatal regulations but also dynamically reducing leaf area under water stress.

Keywords: anisohydric, drought, crop growth, isohydric, photosynthesis, stomatal conductance, transpiration

Abbreviations: VPD: vapor pressure deficit (kPa); Rs: global radiation (W m^{-2}); PAW: plant available water (m^3); SWC: soil water content (cm^3 cm^{-3}); DM: dry matter (g m^{-2} or kg m^{-2}); LAI: leaf area index (-); Gs: leaf stomatal conductance to water vapor (M m^{-2} s^{-1}); An: net photosynthesis (µM m^{-2} s^{-1}); E: leaf transpiration rate (mM m^{-2} s^{-1}); C_i: intercellular CO_2 concentration (M M^{-1}); LUE: light use efficiency (g DM MJ^{-1}); WUE: water use efficiency (µM CO_2 M^{-1} H_2O or mM CO_2 M^{-1} H_2O); LWP: leaf water potential (MPa).

4.1 Introduction

Globally, crop drought stress is a serious constraint limiting agricultural production (IPCC, 2007). Plant responses to drought are complex involving adaptive changes (Chaves et al., 2002) operating at a range of time scales (Tardieu et al., 2018). The various responses, generally grouped into short-term and long-term, are determined by the crop type as well as the intensity, duration, and rate of progression of the imposed stress (Pinheiro and Chaves, 2011). Stomatal control is considered an immediate and effective response to water stress in the field to prevent excessive water loss and desiccation (Tyree and Sperry, 1988; Brodribb and McAdam, 2011). The short-term regulation of stomata that control water flow between soil and the atmosphere (Taiz and Zeiger, 2006) can be classified into two broad categories based on the degree of stomatal closing upon sensing water stress. This strategy is observed in isohydric plants which close their stomata to maintain leaf water potential (LWP) above critical levels. The second strategy is found in anisohydric plants which have a looser stomatal control with the result that LWP will decrease in response to soil drying and/or increasing evaporative demand. As a result, LWP in anisohydric plants experiencing drought stress will be much lower than well-watered plants (Tardieu and Simonneau, 1998). A continuum exists in the degree to which stomata regulate the LWP for trees (Domec and Johnson, 2012; Klein, 2014) or in grape-vine (Schultz, 2003). Also, cultivars of grape vine show large differences in minimum LWP indicating differing degrees of isohydric behavior (Coupel-Ledru et al., 2014). Comparing different herbaceous species, Turner et al., (1984) showed that there was a range from isohydric to increasingly anisohydric behavior in terms of the response to increasing vapor pressure deficit (VPD) under sufficient soil moisture.

Identification of whether or how stomatal controls differ among species and genotypes is studied with experimental observation of minimum LWP or the analysis of genetic variability in terms of stomatal control to variation of soil moistures. Maize (Zea mays L.) and winter wheat (Triticum aestivum) are generally considered as isohydric and anisohydric, respectively (Tardieu and Simonneau, 1998). Tardieu and Simonneau (1998) reported that maize limits its LWP to values higher than -1.8 MPa regardless of soil water condition under high evaporative demand. LWP tended to maintain at a value close to -1.6 MPa in both drought tolerant and sensitive maize genotypes (Cochard, 2002). However, analysing measurements of LWP from 400 lines of maize from the tropical and European origins under greenhouse and growth chamber, Welcker et al., (2011) reported different values of minimum LWP from -0.8 to -1.5 MPa, indicating their links with genomic regions and genetic variability of stomatal responses.

Few reports described anisohydric behaviour in wheat. Moreover, such reports were from wheat that are grown in pots (Tardieu and Simonneau, 1998; Henson et al., 1989; Gallé et al., 2013). Different responses of stomatal conductance to VPD indicate a large genetic variability of stomatal responses in winter wheat which depended on its genome architecture (Schoppach et al., 2016). Given the potentially large variation in stomatal responses, it is important to better understand how stomata function in maize and winter wheat, with resulting implications for LWP, tissue expansion and water use under field conditions.

Understanding plant water use under drought, requires knowledge of various processes from leaf to whole plant and canopy levels (Chaves et al., 2003). Stomatal responses to soil moisture deficit drive subsequent gas exchange and growth process (Chaves et al., 2002). For instance, because of earlier stomatal closure of isohydric plants, on the one hand, this response limits carbon assimilation from photosynthesis limitation whereas the stomatal control limits the rate of water use and onset of more severe drought conditions. In the case of a pronounced anisohydric behaviour, one could hypothesize that the limited degree of stomatal regulation could lead to higher total carbon assimilation. Progress in understanding how isohydric versus anisohydric responses effect photosynthesis capacity and plant growth rate under drought has been primarily in woody species (i.e. poplar and grapevine) (Sade et al., 2012; Attia et al., 2015; Poni et al., 2014; Roman et al., 2015; Pou et al., 2012). Relatively little is known about the roles of stomatal regulations on gas exchange at leaf and canopy scales as well as crop growth for important annual crops such as maize and wheat.

The effects of soil water deficit on photosynthesis and transpiration due to stomatal regulation should be considered together with the longer term changes in canopy structure and morphology. These consist of a diverse range of intermediate or long-term adaptations to varying soil water (Ramalho and Chaves, 1991; Rodrigues et al., 1995; Chaves et al., 2003; Chaves et al., 2002; Aroca, 2012). For example, when exposed to soil water deficit, wheat morphology can be altered via a reduction in tiller number, leaf area expansion, and internode lengths (Miralles and Slafer, 1997). Leaf-rolling is observed in maize when LWP falls below -1 MPa and plants change their leaf angle to reduce the leaf surface area exposed to sunlight (Moulia, 1994; Tardieu et al., 2018). These structural canopy changes reduced canopy transpiration and photosynthesis fluxes in both crops (Abd Allah, 2009; Cai et al., 2018; Baldocchi, 1994; Perdomo et al., 2015; Kupisch et al., 2015; Miralles and Slafer, 1997). Understanding such canopy changes is complex as changes in canopy structure could be the cumulative results of altered stomatal conductance. For instance, soil water depletion causes stomal closure which can reduce water loss, but it also increases leaf termperature that

consequently leads to quicker leaf rolling (Jones, 1998). Cultivars with high vigor or rapid leaf growth have earlier soil water depletion with earlier stomatal closure than cultivars with lower vigor or slower leaf growth (Tardieu and Simmoneau, 1998), though the later may be prone to execessive soil water evaporation in early growth periods (Bourgault et al., 2020). The disentanglement of the relative importance of stomatal and non-stomatal longer term effects (i.e. leaf area growth) has rarely been performed due to the need to examine both stomatal responses and changes in canopy characteristics (i.e. LAI) associated with gas exchange because they require extensive measurements at both leaf and canopy level (Hay and Porter, 2006).

This study intends to provide more insight into how these two modes of stomatal regulations function and finally affect crop growth under field conditions. The overall aim is to analyze and understand how maize and winter wheat respond to different soil moisture treatment under field conditions from the leaf to the canopy level. The research questions addressed are: (i) what are the stomatal strategies of winter wheat and maize under different water supply conditions in the field? (ii) how do photosynthesis and transpiration from leaf to canopy levels as well as crop growth rate and LAI differ among different water regimes associated with the finding stomatal regulations? (iii) what is the relative contribution of short-term stomatal regulation vs longer term adjustments (i.e. LAI) to gas exchange and crop biomass production? The study does not intend to compare photosynthesis and crop growth characteristics between winter wheat and maize. We rather investigate the stomatal functions and crop growth processes for each crop separately over different soil water conditions. This study is based on the analysis of field experiments on winter wheat (one year) and maize (two years), under contrasting water supply conditions over three years.

4.2 Materials and Methods

4.2.1 Location and experimental set-up

The field experiment was conducted in Selhausen, North Rhine-Westphalia, Germany (50°52’N, 6°27’E). The field is slightly inclined with a slope of around 4°. The experiment site was located upslope with stony soil with 60% (by weight) fluvial gravel deposits.

The experimental site was divided into three subplots (P1, P2, and P3). The subplot size was 7.25 m x 3.25 m. The experiment was performed from 2016 to 2018, with winter wheat being tested in 2016 and maize tested in 2017 and 2018. In 2016, three water treatments were assigned to three subplots: a plot with a rainout shelter (2016P1), a rainfed plot (2016P2), and

an irrigated plot (2016P3) (Table 4.1). Winter wheat (*Triticum aestivum* cv. Ambello) was sown with a density of 350-370 seed m^{-2} on the 26th of October 2015 and harvested on 26th of July 2016 (Table 4.1).

Table 4.1 Summary of experimental set-up from 2016 - 2018

Year	Water treatments	Sowing density (seed m^{-2})	Sowing dates (dd/mm/yy)	Plot names
2016	Sheltered	350	26/10/2015	2016P1
	Rainfed			2016P2
	Irrigated			2016P3
2017	Rainfed	10.66	04/05/2017	2017P1
	Rainfed			2017P2
	Irrigated			2017P3
2018	Rainfed	10.66	22/05/2018	2018P1
	Rainfed		08/05/2018	2018P2
	Irrigated			2018P3

In 2017, using the same experimental site, only two treatments were tested: rainfed plots (2017P1/ 2017P2) and irrigation (2017P3) (Table 4.1). Silage maize (*Zea may* cv. Zoey) was sown on 4th May 2017 with a density of 10.66 seeds m^{-2} for all treatments. In 2018, using the same cultivar and sowing density, plants were sown on 8th May 2018 on the same site for one rainfed plot (2018P1) and one irrigated plot (2018P3). In 2018, one of the rainfed plots (2018P2) was sown two weeks after the other plots on 22nd May 2018. The key phenology dates and fertilizer applications are summarized in Table 4.2.

Table 4.2 Key phenological dates and fertilizer applications (dd/mm/yy)

Years	Plot names	Phenology	Fertilizer applications
2016	2016P1 2016P2 2016P3	Sowing: 26/10/15 Emergence: 11/11/15 Anthesis: 03/06/16 Harvest: 26/07/16	03/15/16: 80 kg N + 60 kg K_2O + 30 kg P_2O_5 02/05/16: 60 kg N 07/06/16: 50 kg N
2017	2017P1 2017P2 2017P3	Sowing: 04/05/17 Emergence: 09/05/17 Tasseling: 09/07/17 Silking: 14/07/17 Harvest: 16/09/17	09/05/17: 100 kg N + 40kg P_2O_5; 06/07/17: 80 kg N + 40 kg K_2O
2018	2018P1	Sowing: 22/05/18 Emergence: 26/05/18 Tasseling: 21/07/18 Silking: 23/07/18 Harvest: 02/09/18	22/05/18: 100 kg N; 30/05/18: 40 kg P_2O_5 + 40 kg K_2O 27 /06/18: 80 kg N
	2018P2 2018P3	Sowing: 08/05/18 Emergence: 13/05/18 Tasseling: 09/07/18 Silking: 11/07/18 Harvest: 22/08/18	

4.2.2 Weather conditions and water applications

Weather variables (global radiation, temperature, relative humidity, precipitation, and wind speed) were recorded every 10 minutes by the nearby weather station (around 100 m away from the experiment). To measure canopy temperature, in each treatment, one infrared radiometer sensor (model Apogee SI-121, UP Umweltanalytische Produkte GmhH) was mounted on the wooden polar at 2 m above soil surface with a viewing angle of 45°. Canopy temperature was measured every 30 minutes using C1000 data logger (Campbell Scientific, Utah, USA).

The irrigation demand was estimated based on the precipitation collected from the rain gauge nearby the field and assuming an evaporative demand (evapotranspiration rate) of 5 mm d^{-1}. Drip lines (T-Tape 520-20-500, Wurzelwasser GbR, Müzenberg, Germany) were installed at 0.3 m intervals parallel to the crop rows. In 2016, wheat plants grown in the irrigated plot (2016P3) were irrigated twice (23 mm each time) (Fig. 4.1c, red bars). The sheltered plots were manually covered using a plastic rain-out shelter during precipitation events (11 times) to induce drought stress (Fig. 4.1a). Daily maximum canopy temperature in each plot, air temperature and vapor pressure deficit in 2016 are shown in Fig. 4.2a.

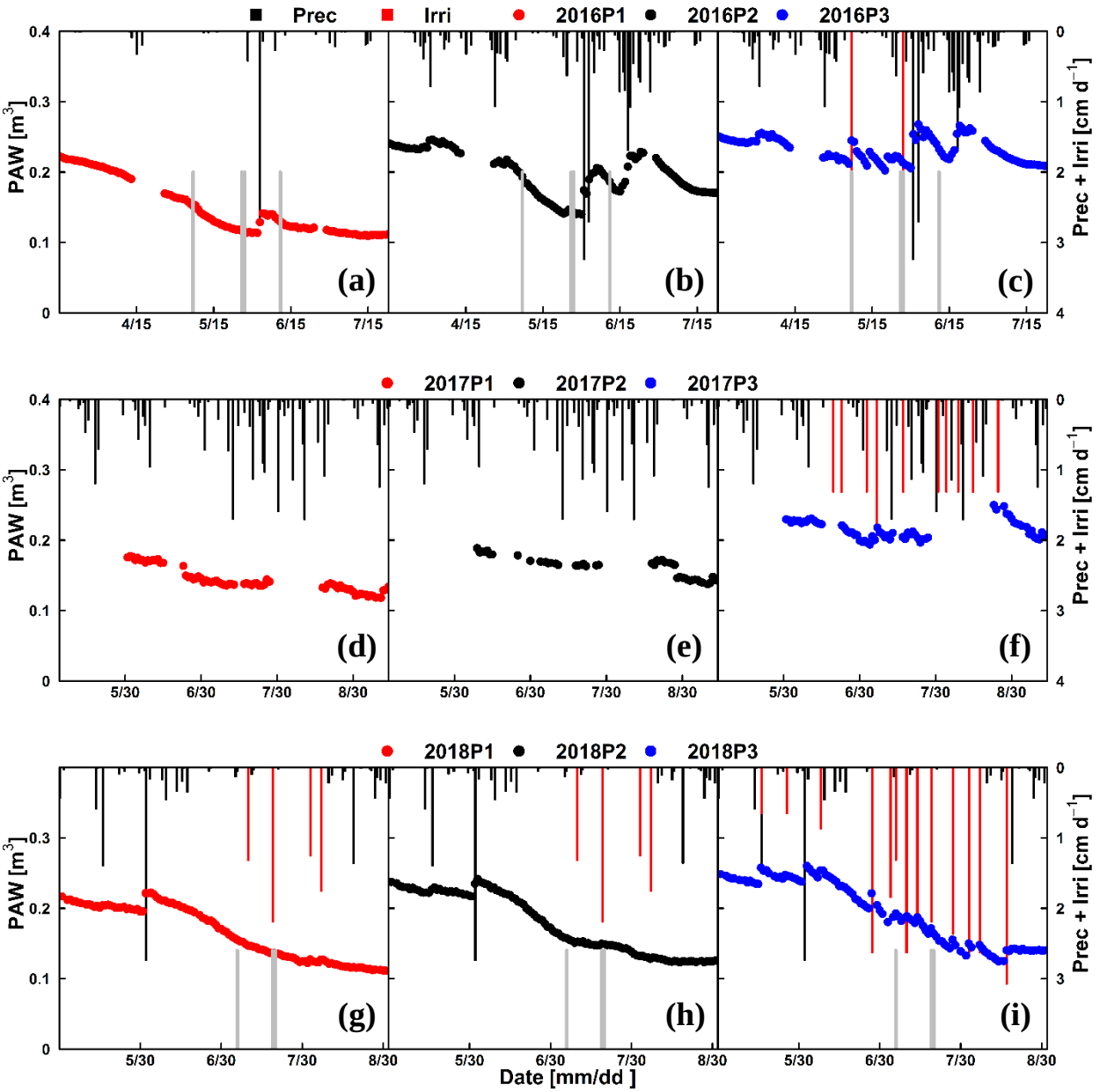

Figure 4.1: Daily plant available water (PAW) during three growing seasons for different water treatments: (a-b-c) in winter wheat in 2016 from March 30 to harvest July 23 with sheltered plot (2016P1 – red dots), rainfed plot (2016P2 – black dots), and irrigated plot (2016P3 – blue dots), (d-e-f) in maize in 2017 from April 30 to harvest in 2017 with two rainfed plots (2017P1 – red dots and 2017P2 – black dots), and irrigated plot (2017P3 – blue dots), and (g-h-i) in maize 2018 from April 30 to harvest in 2018 with two rainfed plots (2018P1 – red dots and 2018P2 – black dots), and irrigated plot (2018P3 – blue dots) (cf. Table 4.1). The red and black bars indicate precipitation (Prec) + irrigation (Irri), respectively. Grey bars in (a-b-c) indicate the four measured days that are shown in Fig. 4.3. Grey bars in (g-h-i) indicate the measured days that are shown in Fig. 4.4, Fig. 4.5, and Fig. 4.6.

In 2017, maize received a total amount of 230 mm precipitation during the growing period (136 days). Average, minimum and maximum daily air temperature were 17.6, 8.3, and 25.3 °C, respectively (Fig. 4.2b). The crop was irrigated 10 times using an amount of 13 mm between

mid of June to end of August for the irrigated plot (2017P3) (Fig. 4.1f). Characterized by exceptionally hot and dry weather conditions during the summer season, 2018 can be classified as an extreme year with respect to plant growth at our site (Buras et al., 2020). Maize experienced high temperature and VPD, especially around tasseling and silking time. While in 2017 a precipitation sum of 122 mm was recorded within the growing period (116 days), only 92 mm were recorded in the growing period of 2018 (116 days). Average, minimum, and maximum daily air temperature exceeded those of 2017 with 19.2, 10.85, and 27.3 °C, respectively (Fig. 4.2c). A total amount of irrigation of 257 mm was applied (13 times) between mid of June and mid of August on the irrigated plot (2018P3) (Fig. 4.1i). Contrary to 2017, the two rainfed plots (2018P2 and 2018P2) had to be watered 4 times (using 13, 22, 13, and 18 mm, respectively) to avoid a complete crop failure due to severe drought (Fig. 4.1g & 4.1h).

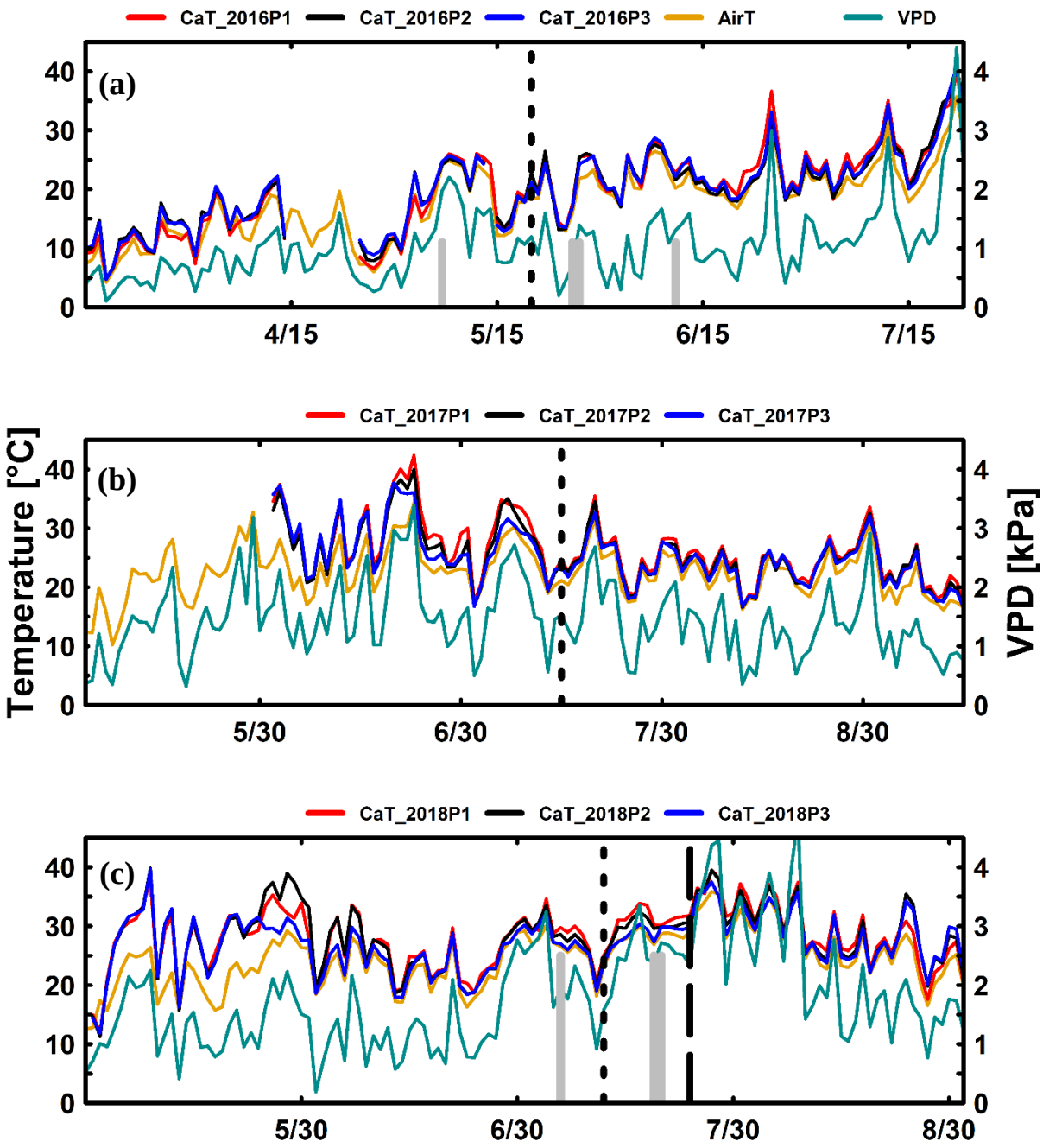

Figure 4.2: Daily maximum canopy temperature (CaT, °C), air temperature (AirT, °C) and daily maximum air vapor pressure deficit (VPD) (kPa) in three growing seasons for (a) winter wheat in 2016 from March 30 to harvest 23 July (b) maize in 2017 from April 30 to harvest, and (c) maize 2018 from April 30 to harvest in 2018. Different CaT line colors indicate the applied water treatments (cf. Table 4.1). The black dotted vertical lines indicate anthesis times of winter wheat in 2016, silking time in all plots in maize 2017, and in the rainfed and irrigated plots with normal sowing date plot (2018P2 and 2018P3) in 2018. The black dashed vertical line indicates silking time in the late sowing plot in 2018 (2018P1). Grey bars in (a) indicate the four measured days that are shown in Fig. 4.3. Grey bars in (c) indicate the measured days that are shown in Fig. 4.4, Fig. 4.5, and Fig. 4.6.

4.2.3 Measurements

4.2.3.1 Soil water measurement and plant available water

In each soil depth at 10, 20, 40, 60, 80, and 120 cm, time domain reflectometer probes (TDR) and soil temperature sensors (Decagon Devices Inc., UMS GmbH München, Germany) were installed to measure hourly volumetric soil water content (SWC) and soil temperature, respectively. A detailed description of sensor installation, calibration, data post processing can be found in (Cai et al., 2016). The SWC data from three years is presented in Nguyen *et al.*, (2020) and Nguyen *et al*., (2022).

Plant available water was calculated as the difference between actual (measured) SWC and SWC at wilting point (Kirkham, 2005) over the rooting zone. The SWC at wilting point was derived from soil texture information and soil organic matter content which were measured in three different layers (0-30 cm, 30-60 cm, and 60-90 cm) (Stadler et al., 2015). As the SWC was measured at 10, 20, 40, 60, 80, and 120 cm soil depths, measured SWC data represent volumetric content for the layers 0-15 cm, 15-30 cm, 30-45 cm, 45-65 cm, 65-85cm, and 85-125 cm. The SWC at wilting point of the 0-30 cm layer was used for the first two layers (0-15 cm and 15-30 cm), while the SWC at wilting point of 30-60 cm layers was employed for 30-45 cm and 45-65 cm. The SWC at wilting point for the 60-90 cm layer was used for the 65-85 cm, and 85-125 cm layers.

4.2.3.2 Leaf gas exchange and leaf water potential

Hourly leaf stomatal conductance (Gs), net photosynthesis (An) and leaf transpiration (E) were measured every two weeks under clear sky and sunny conditions. There were seven observation days with measurements from 7 AM to 8 PM and 3 observation days from 10 AM to 4 PM in 2016 (Table 4.3). Four observation days from 8 AM to 5 PM and six days from 10 AM to 4 PM were carried out in 2017. In 2018, 6 days from 8 AM to 7 PM and 5 days from 10 AM to 4 PM were carried out (Table 4.3). In 2016, for winter wheat, Gs of three to four uppermost fully developed leaves were measured at steady-state using a LICOR 6400 XT device (Licor Biosciences, Lincoln, Nebraska, USA) with a reference CO_2 concentration of 400 ppm, flow rate of 500 (µmol s^{-1}), and using real-time records of photosynthetic active radiation, vapor pressure deficit (VPD), and leaf temperature provided by the instrument. In 2017 and 2018, for maize, two sunlit leaves (uppermost fully developed leaves) and one shaded leaf were measured. After leaf gas exchange measurements, leaves were quickly detached using a

sharp knife to measure leaf water potential (LWP) with a digital pressure chamber (SKPM 140/ (40-50-80), Skye Instrument Ltd, UK) with the working air pressure ranging from 0 to 35 bars. To study the diurnal course of LWP under dry and re-wetted soil conditions, in 2018, three additional days with predawn measurements at two days before irrigation and one day after irrigation. The intrinsic water use efficiency (WUE) is calculated as the ratio of photosynthesis and stomatal conductance (An/Gs) while the instantaneous WUE describes the photosynthesis rate per unit of transpired water (An/E).

Table 4.3 Summary of measurement days with leaf gas exchange and leaf water potential for three growing seasons

Years	Measurement days (mm/dd)
2016	April 20, **May 6**, **May 25**, **May 26**, June 7, **June 9**, June 20, **June 23**, **June 29**, and **July 8**
2017	July 5, July 17, **July 18**, August 2, **August 4**, August 7, **August 13**, August 16, **August 23**, and September 5
2018	June 15, June 20, June 27, **July 3**, **July 5**, **July 8**, July 9, **July 10**, **July 17**[**], **July 18**[**], **July 19**[**], **July 26**, August 2, and **August 16**

[*] Bold days indicate measurement from 7 AM to 8 PM in 2016 and 8 AM to 5 PM in 2017, and from 8 AM to 7 PM in 2018. The remaining days was from 10 AM to 4 PM.

[**] Leaf water potential was measured predawn.

4.2.3.3 Crop growth measurement

The crop growth information included bi-weekly observations of phenology, leaf greenness, tiller number (winter wheat), plant height, tiller/plant diameter, green and brown leaf area, dry matter of different organs, and total aboveground dry matter. Leaf greenness was randomly determined from 12 leaves using SPAD Chlorophyll-meter (Konica Milta, Inc., Japan). Plant height was measured randomly from 5 and 15 plants in winter wheat and maize, respectively. Five random main tillers (winter wheat) and stems (maize) were measured to determine stem diameter in both crops. Due to the limited number of plants in each plot, two rows (measuring 1 meter each) in winter wheat in 2016 and two plants in maize in 2017 and 2018 were sampled for determining total aboveground dry matter and leaf area (8, 7, and 8 times for 2016, 2017, and 2018, respectively). Green and brown leaf area was measured by LI-3100C (Licor Biosciences, Lincoln, Nebraska, USA). At harvest, in addition to sampling of two rows, three replicates (one-meter square each) were harvested for winter wheat to determine dry matter and grain yield. Five separate replicates ($1m^2$ each) were harvested from maize in 2017 and

2018. The dry matter of separate organs was determined by the oven method (Nguyen et al., 2020).

4.2.3.4 Sap flow and canopy chamber measurement

In 2016, five, three, and five sap flow sensors (SAG3) (Dynamax Inc., Houston, USA) were installed from 25 May to harvest (wheat stem diameter between 3-5 mm) on plants grown in the irrigated, rainfed, and sheltered plots, respectively. Sensor data, in particular the partitioning of energy, electricity supply, sap flow, and the temperature difference between upper and lower thermocouples (dT) of each sensor were recorded at 10 minute intervals using a CR1000 data logger and two AM 16/32 multiplexers (Campbell Scientific, Logan, Utah). The 10 minute data (dT °C) were aggregated to hourly values and used to estimate sap flow (g h^{-1} $tiller^{-1}$) following the approach of Langensiepen et al., (2014). Sap flow of single tillers was upscaled to canopy transpiration based on bi-weekly recorded tiller number (in 2016). In 2017 (from 7th July 2017 until harvest) and 2018 (from 28th June 2018 until harvest), 15 sap flow sensors (SGA 13, SGB 16, and SGB 19 types) were installed on 5 maize plants per plot based on stem diameter size. The sap flow in the plant (g h^{-1}) was calculated directly by the data loggers (Dynamax, 2009) and used as a surrogate for canopy transpiration based on the number of plants per square meter.

Canopy gas exchange was measured hourly on the same days as leaf gas exchange and LWP measurements. The closed chamber system (Langensiepen et al., 2012) was used to determine the time series of CO_2 change using an infrared gas analyzer (LICOR 6400 XT, Licor Biosciences, Lincoln, Nebraska, USA). The instantaneous canopy CO_2 exchange rate measured by the closed chamber was estimated based on the regression approach by (Langensiepen et al., 2012). The sap flow and canopy gas exchange measurements are described elsewhere in detail for winter wheat (Nguyen et al., 2020) and for maize in 2017 and 2018 (Nguyen et al., 2022).

4.2.4 Light use efficiency

Intercepted photosynthetic active radiation (PAR_{int}) at instantaneous level is calculated based on Lambert-Beer equation ($PAR_{int} = PAR * (1 - e^{-k*LAI})$) with the extinction coefficient k = 0.6 for both crops (Hay and Porter, 2006). The instantaneous PAR_{int} was integrated over the day and over the period with measurement of aboveground dry matter. The hourly instantaneous CO_2 gas exchange was used to integrate over the whole day assuming the rates of dark respiration

was constant during night and depended on daily maximum photosynthesis rate (20% during day time, Geijn and Goudriaan, (1996)). Based on the CO_2 gas flux (g CO_2 m^{-2} d^{-1}), the light use efficiency (LUE_{Flux}) is derived by fitting daily CO_2 flux with the daily PAR_{int}. The resulting of LUE was multiplied by the mass ratio of C: CO_2 and divided by the mass faction of carbon (0.459 gC gDM^{-1}). The final unit of LUE_{Flux} is in g DM MJ^{-1}. Based on aboveground dry matter, the light use efficiency (LUE_{DM}) (g DM MJ^{-1}) is estimated from fitting the aboveground dry matter and accumulated PAR_{int}.

4.2.5 Statistical analysis

To test for significant differences between the An, E, Gs, LWP, An/Gs, An/E, and instantaneous canopy CO_2 flux of the different water treatments (cf. Table 4.1), we applied the Tukey HSD test and a multiple comparison test which provided within the "multcompView" R-package (Grave et al., 2019). All data processing and analysis were conducted using the R statistical software (R Core Team, 2018).

4.3 Results

4.3.1 Plant available water, leaf gas exchange, and leaf water potential under different water supplies

4.3.1.1 Plant available water

Soil water status and water supply throughout the growing seasons are illustrated in Figure 4.1. The PAW clearly differed among the three water treatments in winter wheat in 2016. PAW was highest in the irrigated plots, followed by the rainfed and the sheltered plots over the whole season (Fig 4.1c, 4.1b, and 4.1a, respectively). The PAW dropped considerably from April and May, then slightly increased in the first week of June and decreased again around the end of the grain filling period in the sheltered plot. In 2017 missing measured SWC data and noisy data due to the malfunction of sensors were discarded. The remaining data differ among treatments but the magnitudes of the differences were generally less pronounced as compared to 2016. Despite the same rainfall, PAW of the rainfed plot 2017P2 was larger than PAW from the rainfed plot 2017P1 throughout the growing season. This may be explained by the carry-over effects of the sheltering of 2016P1 in 2016 which may have caused the decrease of SWC in 2017. In 2018, the differences of PAW were obvious in the three treatments. Plant available water was higher on June 15 but then decreased rapidly from the middle of the elongation phase until harvest.

4.3.1.2 Diurnal course of leaf gas exchange and water potential

The diurnal dynamics of stomatal conductance of water vapor (Gs), leaf net photosynthesis (An), transpiration (E), and LWP from winter wheat on four observation days in 2016 are shown in Fig. 4.3. Leaf gas exchange and LWP differed among water treatments, especially in May 25 and 26. The highest rates of An, E, Gs, and LWP were observed for the irrigated plot, followed by the rainfed plot and finally the sheltered plot. The differences in leaf gas exchange and LWP were consistent with the differences in PAW between the three levels of water supply (Fig. 4.1a-c). In the sheltered plot, when PAW was decreased from 0.151 m^3 (May 6) to 0.115 m^3 (May 25) (2016P1 in Fig. 4.1a), LWP decreased from -1.65 MPa to -2.5 MPa, respectively. On May 26, LWP was approximately -2 MPa while stomatal conductance was very low (Fig. 4.3k) due to the increasing evaporative demand (Fig. 4.3c). Despite increased PAW following subsequent precipitation events, LWP on June 9 remained low at approximately -2 MPa at midday for all plots. Stomatal conductance was highest in the morning, before decreasing sharply in the afternoon including in the irrigated plot for instance May 6 and May 26 when VPD was increasing. Photosynthesis and E also decreased, but to a lesser extent than Gs.

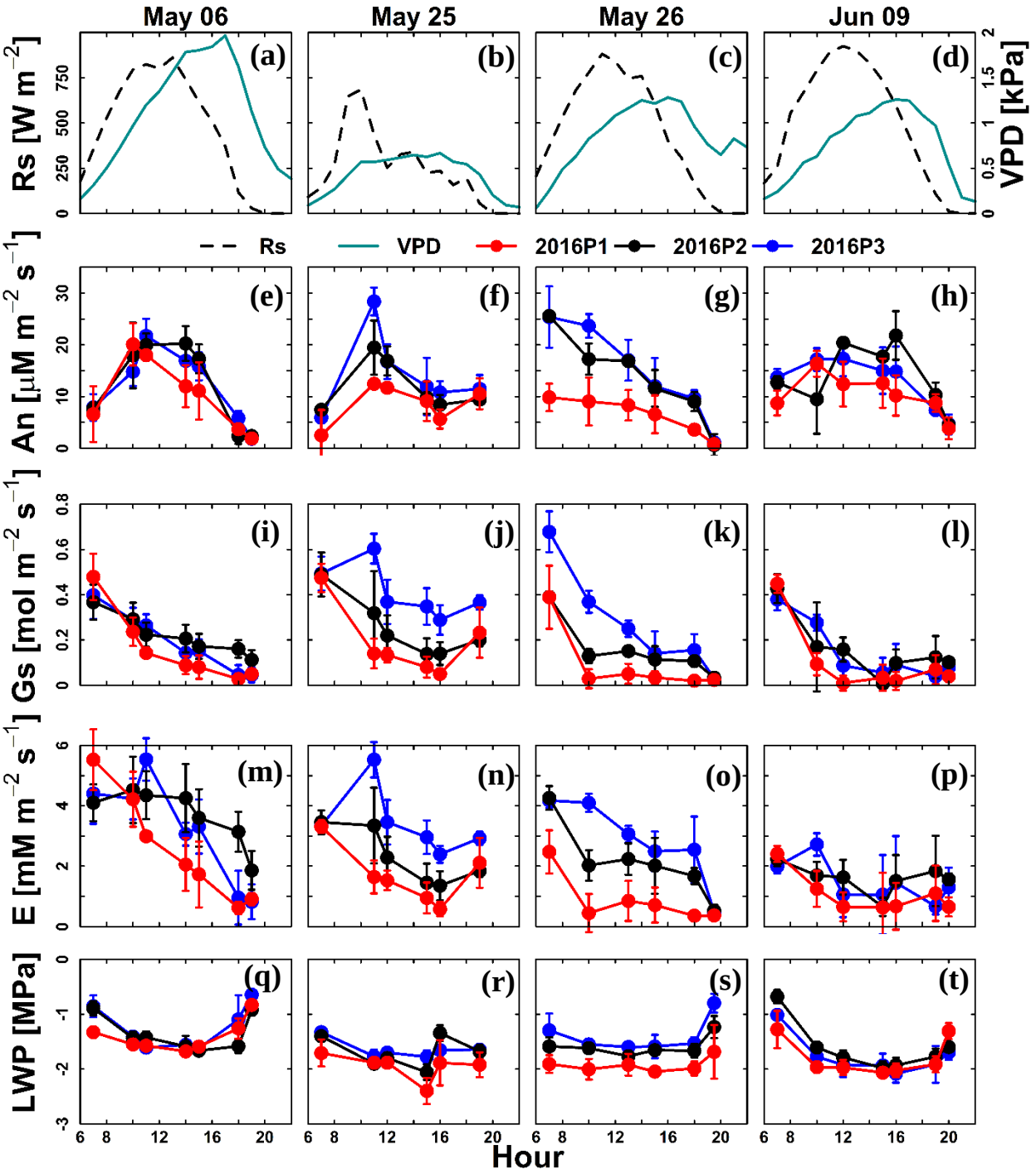

Figure 4.3: Diurnal course of four days of measurement in winter wheat in 2016: (a-d) global radiation (Rs) and vapor pressure deficit (VPD); (e-h) leaf net photosynthesis, (i-l) leaf stomatal conductance (Gs), (m-p) leaf transpiration (E), and (q-t) leaf water potential (LWP)) at the sheltered plot (F1P1 – red dots), rainfed plot (F1P2 – black dots), and irrigated plot (F1P3 – blue dots). Error bars indicate the standard deviation of measurement which was carried out from 3-4 upmost fully developed leaves.

In 2018, the hourly Gs and LWP measurements in maize on July 05 in the irrigated and rainfed plots were obtained separately for sunlit and shaded leaves (Fig. 4.4). There were significant differences in Gs, An, E, and LWP between sunlit and shaded leaves except only the rainfed with normal sowing date in 2018 (2018P2) (Appendix 4a). The differences between two leaves were pronounced in terms photosynthesis and transpiration rates, especially in the irrigated plots. The lower gas exchange and LWP is related to lower levels of intercepted radiation by shaded leaves as compared to sunlit ones. Leaf gas exchange and LWP was lower in the rainfed plots as compared to the irrigated plot. LWP of sunlit leaves in the rainfed plots was around -1.8 MPa, while it was approximately -1.5 MPa in the irrigated plot. The progressive stomatal closure in the rainfed plots resulted in the plateau of LWP (at around -1.6 MPa) from 10 AM to 4 PM on July 5 (Fig. 4.4k-m).

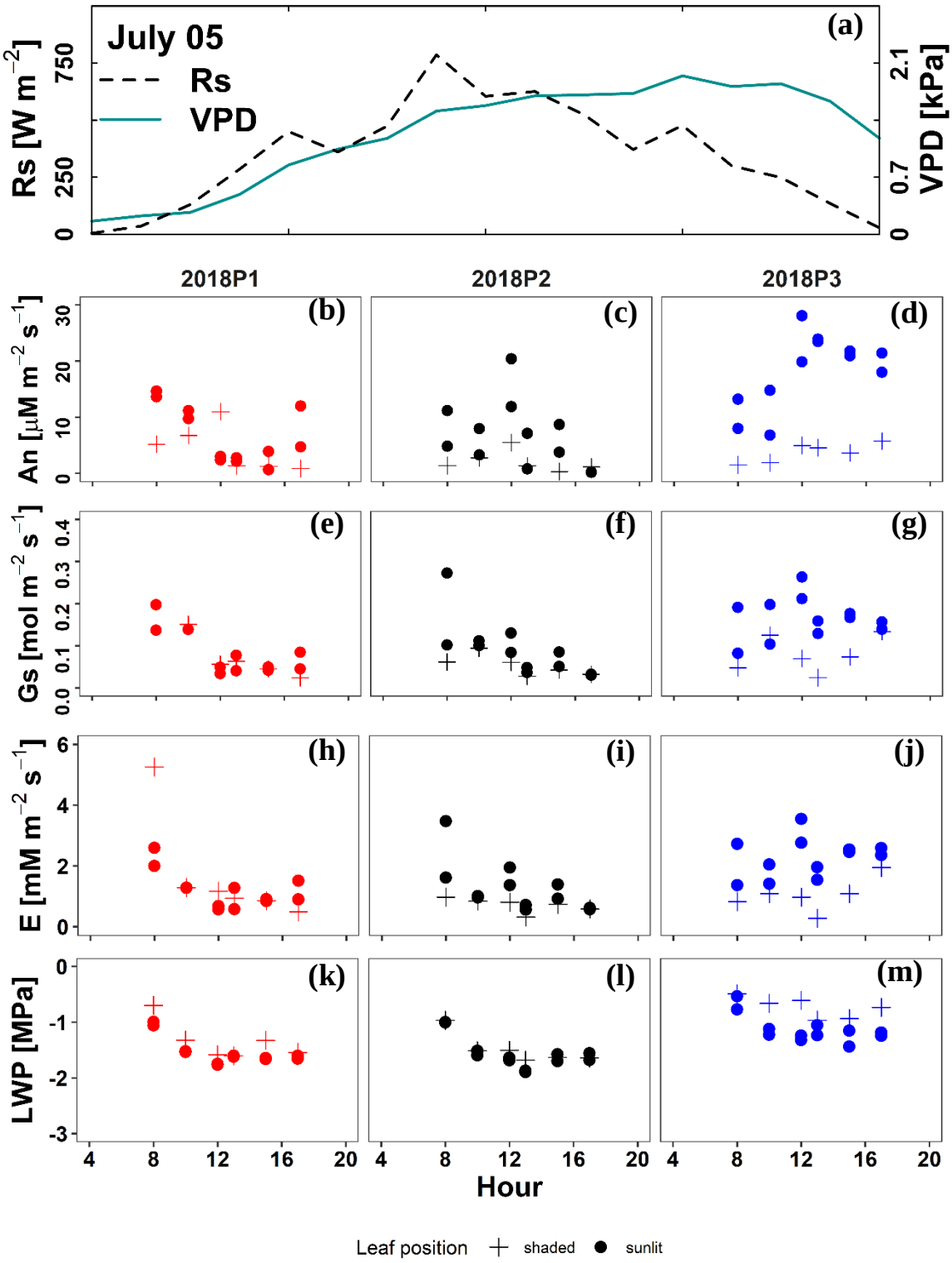

Figure 4.4: Diurnal course of (a) global radiation (Rs) and vapor pressure deficit (VPD), (b-d) leaf net photosynthesis (An), (e-g) leaf stomatal conductance (Gs), (h-j) leaf transpiration (E), and (k-m) leaf water potential (LWP) on July 05, 2018 in maize at the rainfed plot with late sowing date (2018P1–red), rainfed plot with normal sowing date (2018P2 – black), and irrigated plot with normal sowing date (2018P3 – blue) (cf. Table 4.1). Measurement was carried out from shaded leaf (plus symbol) and two sunlit leaves (solid dots).

Diurnal course of leaf gas exchange and LWP under conditions characterized by lower PAW in the rainfed plots at high evaporative demand (July 18) was shown in Figure 4.5. Stomatal conductance (Gs), An, and E showed a drop around midday, even in the irrigated plot indicating the combined effects of high VPD and severe soil water deficit. Predawn LWP was around -1.66 MPa in both rainfed plots with late (2018P1) and normal sowing date (2018P2), while it was around -1 MPa for the irrigated plot (2018P3). Midday LWP decreased to -2.5 MPa with very low Gs and severe leaf rolling symptoms in the two rainfed plots, while the lowest LWP value of the irrigated plot was still around at -2 MPa. Irrigation water was applied in the afternoon for all plots. This could explain the slight increase in gas exchange (Gs, An, and E), and LWP after water application.

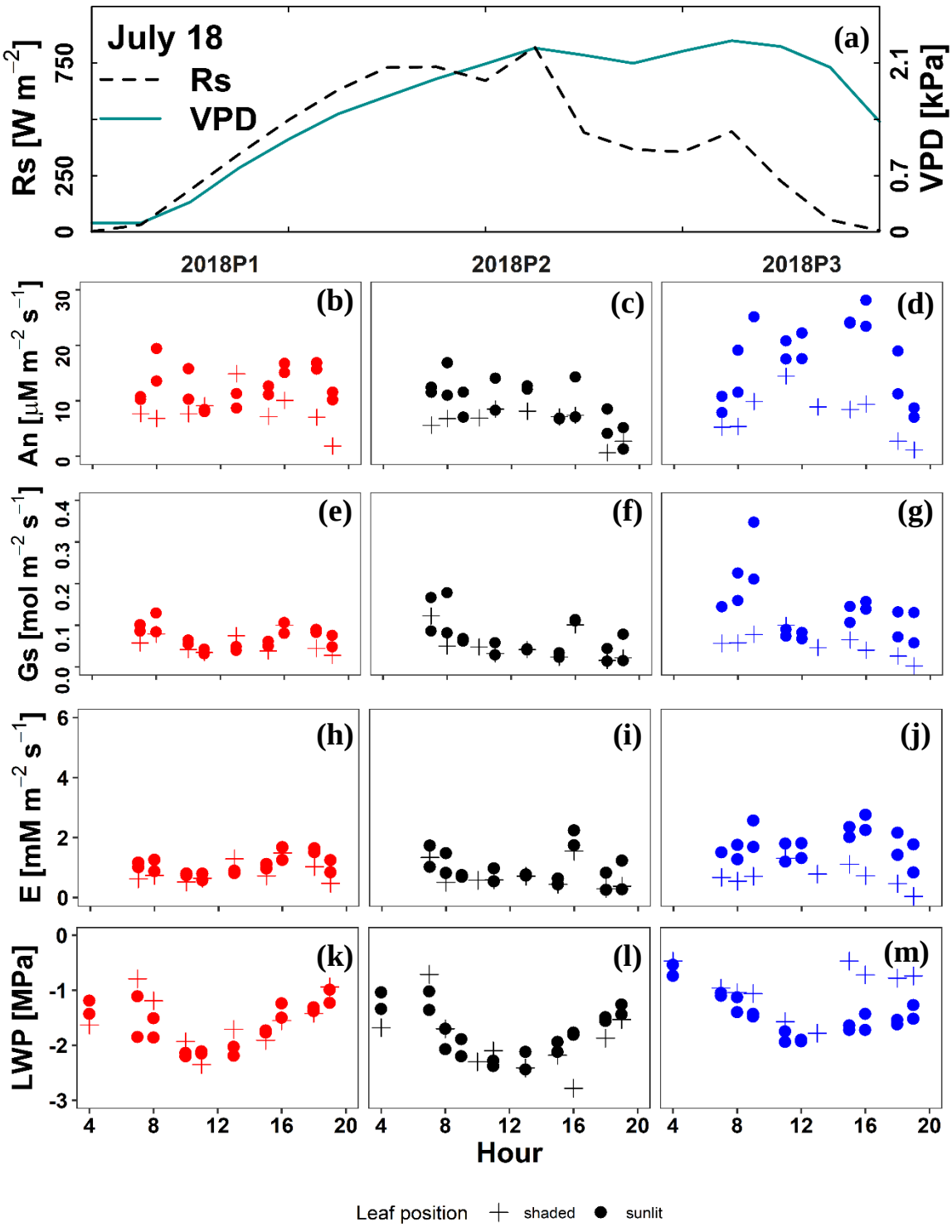

Figure 4.5: Diurnal course of (a) global radiation (Rs) and vapor pressure deficit (VPD), (b-d) leaf net photosynthesis (An), (e-g) leaf stomatal conductance (Gs), (h-j) leaf transpiration (E), and (k-m) leaf water potential (LWP) on July 18 in maize in 2018 before irrigation at the rainfed plot with late sowing date (2018P1– red), rainfed plot with normal sowing date (2018P2 – black), and irrigated plot with normal sowing date (2018P3 – blue) (cf. Table 4.1). Measurement was carried out from shaded leaf (plus symbol) and two sunlit leaves (solid dots). Crop was irrigated at 2 PM, 3.20 PM, 4.45 PM for 2018P3, 2018P2, and 2018P1, respectively (22 mm for each plot) (Fig. 4.1g-i).

After irrigation, increases for An, Gs, and E on July 19 were recorded (Fig. 4.6), as compared to the previous day despite higher VPD values. This illustrates the recovery of plant when PAW increases, particularly for the two rainfed plots (2018P1 and 2018P2). The decrease in leaf gas exchange was observed in the rainfed plot with late sowing date (2018P1) when VPD was highest (after 12 PM). However, this did not occur in the irrigated and rainfed plot with normal sowing date. Predawn LWP was essentially the same in all plots at approximately -0.45 MPa. The lowest LWP did not fall below -2 MPa in three plots.

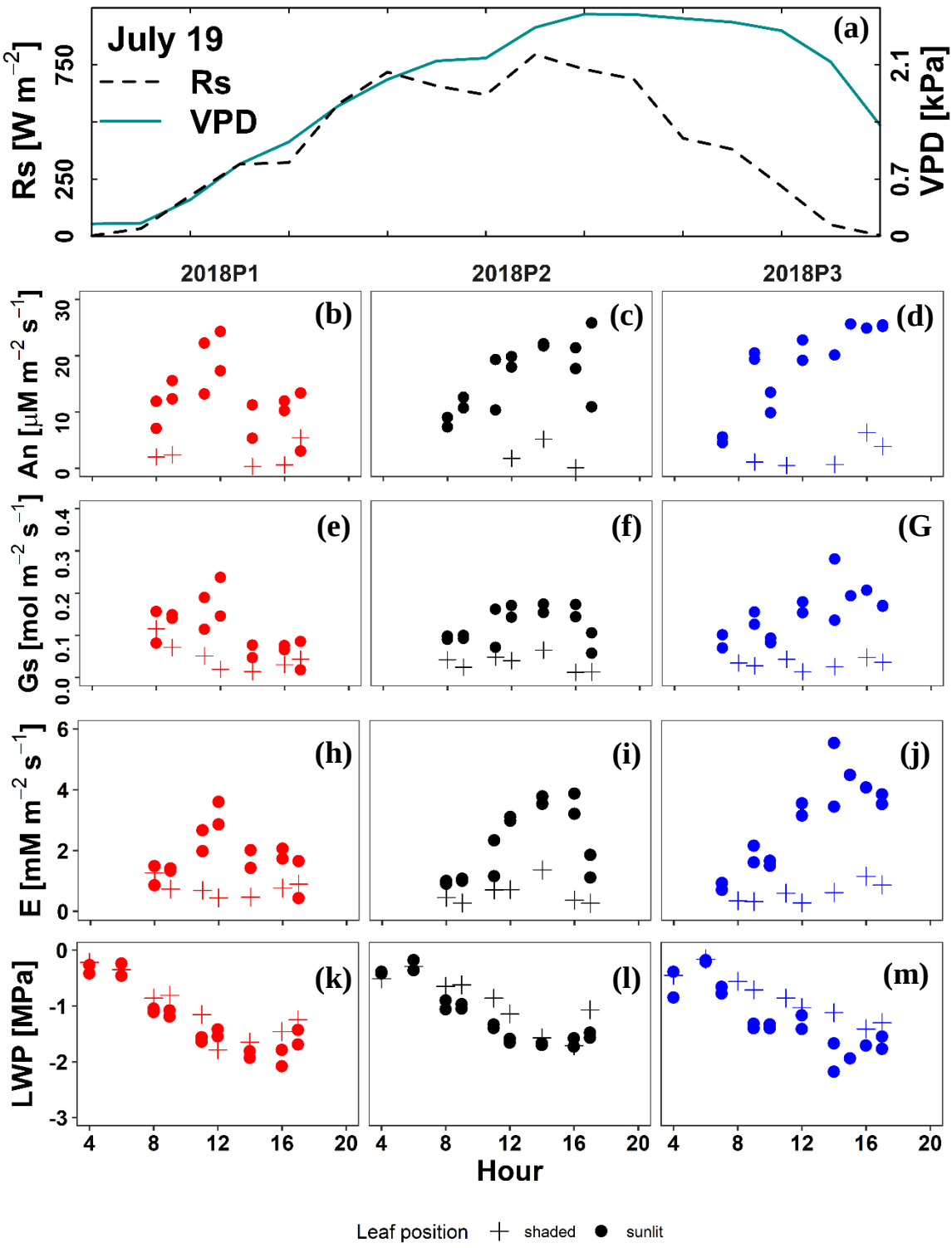

Figure 4.6: Diurnal course of (a) global radiation (Rs) and vapor pressure deficit (VPD), (b-d) leaf net photosynthesis (An), (e-g) leaf stomatal conductance (Gs), (h-j) leaf transpiration (E), and (k-m) leaf water potential (LWP) on July 19 in maize in 2018 after irrigation at the rainfed plot with late sowing date (2018P1– red), rainfed plot with normal sowing date (2018P2 – black), and irrigated plot with normal sowing date (2018P3 – blue) (cf. Table 4.1). Measurement was carried out from shaded leaf (plus symbol) and two sunlit leaves (solid dots).

4.3.1.2 Seasonal leaf gas exchange and water potential

Further analysis of how the leaf gas exchange and LWP differed across levels of water supply are presented in Fig. 4.7 and Table 4.4. In 2016, net photosynthesis, Gs, E, and LWP of the sheltered plot (2016P1) were significantly lower as compared to the remaining plots (irrigated - 2016P3 and rainfed - 2016P2) (Fig. 4.7a, 4.7d, 4.7g & 4.7j). There was no significant difference in leaf gas exchange and LWP in the rainfed (2016P2) and irrigated plot (2016P3) in winter wheat in 2016. In 2017, all measured variables were significantly lower in the rainfed plot (2017P1) compared to the irrigated plot (Fig. 4.7b, 4.7e, 4.7h & 4.7k). Compared to the other rainfed treatment (2017P2), 2017P1 showed significantly different Gs rates, but this was not true for An, E, and LWP. There were no significant difference between the late sowing rainfed (2018P1) and normal rainfed plot (2018P2). However, leaf gas exchange and LWP of these both plots were significantly lower than the irrigated plot in 2018 (Fig. 4.7c, 4.7f, 4.7i & 4.7l).

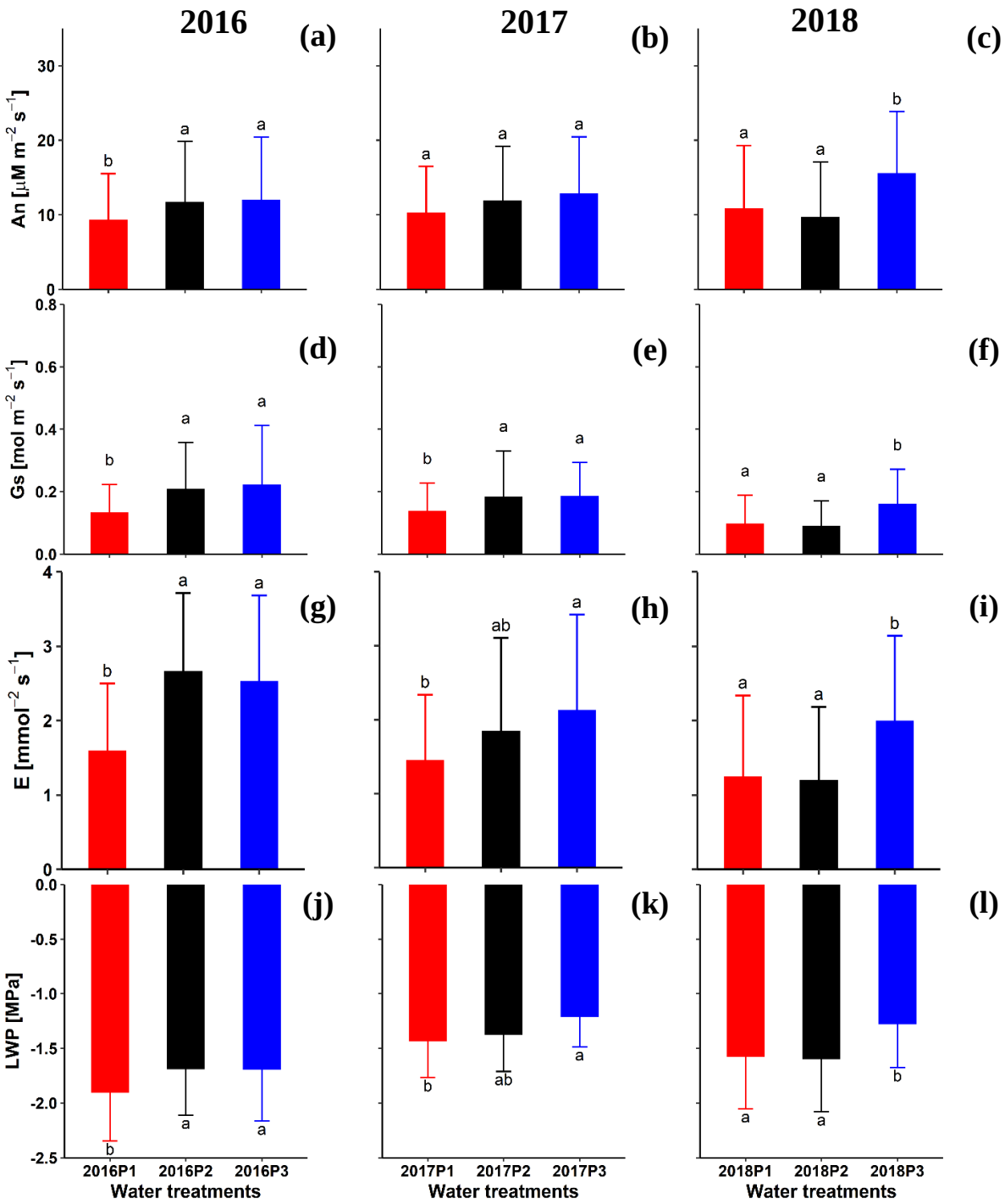

Figure 4.7: Barplots of measurement data for each observation year and treatment: (a-b-c) net photosynthesis (An), (d-e-f) stomatal conductance to water vapor (Gs), (g-h-i) transpiration rate (E), and (j-k-l) leaf water potential (LWP). The left panel refers to winter wheat in 2016 at the sheltered plot (2016P1 – red), rainfed plot (2016P2 – black), and irrigated plot (2016P3 – blue). The middle panel refers to maize in 2017 at the two rainfed plots (2017P1 – red and 2017P2 – black), and irrigated plot (2017P3 – blue). The right panel refers to maize in 2018 at the rainfed plot with late sowing date 2018P1– red, rainfed plot with normal sowing date (2018P2 – black) and irrigated plot with normal sowing date (2018P3 – blue) (cf. Table 4.1). Data from 2017 and 2018 only includes observations from sunlit leaves. Error bars indicate the standard deviation with the number of leaves n = 115, 79, and 177 for 2016, 2017, and 2018, respectively. Small letters (a, b, and ab) indicate a significant difference between water treatments according to Tukey's HSD test ($p < 0.001$). Treatments share the same letter mean that the difference between treatments are not significantly different (cf. Table 4.4).

Table 4.4 Summary of leaf and canopy gas exchange, leaf water potential, and crop growth characteristics in different water treatments.

	2016 - wheat			2017 - maize			2018 - maize		
	2016P1	2016P2	2016P3	2017P1	2017P2	2017P3	2018P1	2018P2	2018P3
An ($\mu M\ m^{-2}\ s^{-1}$)	9.3(5.2)b	11.8	12.0(7.4)a	10.3(6.2)a	11.9(7.3)a	12.9(7.6)a	10.9(6.5)a	9.7(7.4)a	15.6(7.2)b
Gs ($M\ m^{-2}\ s^{-1}$)	0.13(0.09)b	0.21(0.1)a	0.22(0.12)a	0.14(0.09)b	0.18(0.08)a	0.19(0.11)a	0.1(0.17)a	0.09(0.05)a	0.11(0.07)b
E ($mM\ m^{-2}\ s^{-1}$)	1.6(0.5)b	2.7(1.1)a	2.5(1.0)a	1.5(0.7)b	1.8(1.1)ab	2.1(1.0)a	1.2(0.9)a	1.2(0.9)a	2.0(1.1)b
An/Gs ($\mu M\ CO_2\ M^{-1}\ H_2O$)	86(55)a	79(41)a	74 (41)a	78(36)a	70(34)a	72(35)a	114(41)a	103(45)a	111(41)a
An/E ($mM\ CO_2\ M^{-1}\ H_2O$)	5.0(2.6)a	5.0(2.3)a	4.7(2)a	6.3(2.1)a	5.9(2.4)a	6.1(2.3)a	6.7(2.4)a	6.2(2.8)a	6.9(2.1)a
Ci ($M\ M^{-1}$)	229(102)b	247(81)a	254(84)a	221(59)b	220(63)ab	231(52)a	164(72)a	173(70)a	166(73)b
LWP (MPa)	-1.9(0.4)b	-1.7(0.4)a	-1.7(0.5)a	-1.4(0.3)b	-1.4(0.3)ab	-1.2(0.27)a	-1.6(0.5)a	-1.6(0.5)a	-1.3(0.5)b
Canopy CO_2 flux ($\mu M\ m^{-2}\ s^{-1}$)	12.2(5.7)b	16.7(10)a	18.3(12)a	9.05(6.4)b	10.1(8.2)b	20.3(11)a	12.5(8.9)b	13.8(9.7)b	34(17)a
Cumulative transpiration (mm)	55	144	132	117	145	216	101	126	281
SPAD values	48.7(3.57)	48.2(3.53)	49.3(2.95)	25(8.70)	29.0(6.74)	37.5(8.45)	33.5(6.74)	34.8(6.07)	52.26(6.43)
Plant height (cm)	68.2(5.25)	74.7(3.89)	73.3(3.45)	121.6(16.12)	119.8(19.12)	164.6(27.83)	125(10.74)	162.9(15.14)	165.1(16.84)
Tiller (or plant) diameter (mm)	3.11(0.07)	3.52(0.19)	3.63(0.26)	15.2(0.49)	16.2(1.1)	16.5(0.53)	14.98(0.42)	19.59(0.63)	19.24(0.48)
Tiller (or plant) density (m^{-2})	375(13)	524(14)	580(7.46)	10.66	10.66	10.66	10.66	10.66	10.66
LAI/tiller (or plant) density (m^2)	0.0046	0.0051	0.0049	0.2665	0.2579	0.3480	0.1918	0.2398	0.3678
Total dry matter at harvest ($g\ m^{-2}$)	675(109)	1228(179)	1361(155)	1529(83)	1656(231)	1884(199)	580(198)	880(121)	2045(137)
Grain yield at harvest ($g\ m^{-2}$)	265(45)	604(52)	628(31)	-	-	-	-	-	-
Dry cob weight at harvest ($g\ m^{-2}$)	-	-	-	1113(63)	1153(179)	1300(133)	72(20)	261(65)	1234(61)

Abbreviation: An: Net leaf photosynthesis, Gs: stomatal conductance, E: leaf transpiration, Ci: intercellular CO_2 concentration, LWP: leaf water potential. Data for An, Gs, E, Ci, LWP, and canopy CO_2 fluxes were from all measurements (see Figure 7 and Figure 9). Values in the brackets mean the standard deviation of all measurement points. Different small letters (a, b, and ab) indicate a significant difference between water treatments according to Tukey's HSD test ($p < 0.001$). For winter wheat, the SPAD, plant height, tiller, and LAI of were measured on May 25, 2016. For maize in 2017, the SPAD, plant height, and LAI were measured on July 14, while stem diameter was measured on July 7. For maize in 2018, the SPAD, plant height, and LAI were measured on July 19, while stem diameter were measured on June 28. Grain yield was not available for maize due to the harvest of silage in 2017 and 2018. Values in the brackets mean the standard deviation of sampling replicates.

4.3.2 Crop growth, canopy gas exchange, transpiration, and light use efficiency under different water treatments

4.3.2.1 Crop growth

The dynamic development of aboveground dry matter and leaf area index (LAI) for the different water regimes are presented in Figure 4.8. In 2016, the aboveground dry matter was initially similar across the water treatment levels. However, starting at the end of May, differences between treatments were measured which persisted until the end of the growing season. Drought stress in the sheltered plot substantially reduced the dry matter as compared to the irrigated and rainfed plot (Fig. 4.8a). The effect of water amount supplied was visible in the LAI by the end of April and persisted, relative to the irrigated treatment, until harvest, illustrating the effects of soil water deficit on LAI (Fig. 4.8d). The aboveground dry matter of three subplots in maize in 2017 was similar between the water supply levels before June 30, though the aboveground dry matter and LAI of the irrigated plot was higher than both rainfed plots throughout most of the growing season. Aboveground dry matter and LAI were similar in the two rainfed plots for the entire growing season (Fig. 4.8b & 4.8e). The deviation between treatments in terms of aboveground dry matter and LAI was much clearer and pronounced in 2018 as compared to 2017 (Fig. 4.8c & 4.8f). Aboveground dry matter and LAI of the irrigated plot were much larger than the rainfed plot with the same sowing date. Leaf area and dry matter were substantially smaller in the late sowing date rainfed plot.

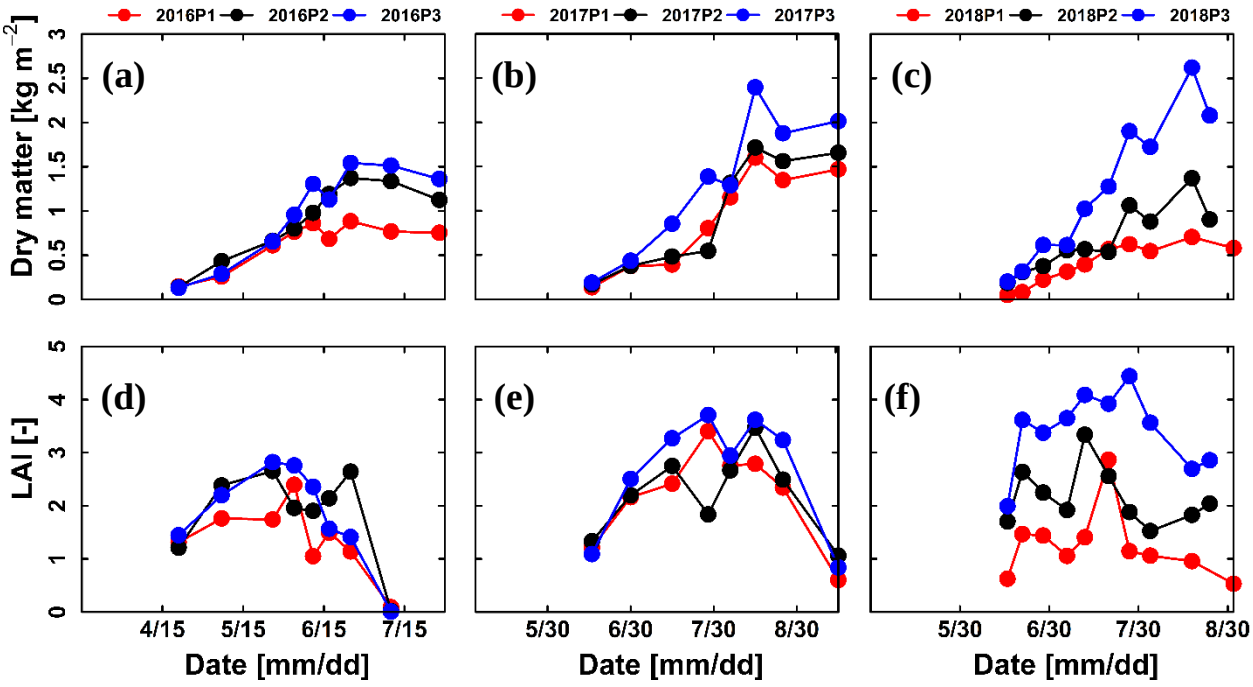

Figure 4.8: Dynamics of (A-B-C) aboveground dry matter and (D-E-F) leaf area index (LAI) in different water treatments levels. The left panel refers to winter wheat in 2016 at the sheltered plot (2016P1 – red dots), rainfed plot (2016P2 – black dots), and irrigated plot (2016P3 – blue dots). The middle panel refers to maize in 2017 at the two rainfed plots (2017P1 – red dots and 2016P2 – black dots), and irrigated plot (2017P3 – blue dots). The right panel refers to maize in 2018 at the rainfed plot with late sowing date (2018P1– red dots), rainfed plot with normal sowing date (2018P2 – black dots) and irrigated plot with normal sowing date (2018P3 – blue) (cf. Table 4.1). Each point represents the average of two sampling replicates, except the last points at harvest (see section 4.2.3.3 and Table 4.4).

Additional crop growth characteristics are presented in Table 4.4. Leaf greenness was largely similar between plots in 2016. However, water deficit in the sheltered plots resulted in considerably reduced plant height, number of tillers, and tiller diameters as compared to the non-sheltered plots. Thus, winter wheat reduced both number of tillers and leaf area. The leaf area index per tiller density was lower in sheltered plots as compared to unsheltered plots. Grain yield was highest in the irrigated and rainfed plots which were almost three times higher than in the sheltered plot. Leaf greenness and plant height of maize were remarkably lower in the rainfed plots than the irrigated plots in both years. Stem diameters were similar in the rainfed plots as compared to the irrigated plots in 2017 and 2018, except in the late sowing plot. With higher LAI and similar plant density, the LAI per plant density was higher in the irrigated plots than rainfed plots.

4.3.2.2 Canopy CO_2 fluxes and transpiration

The average and maximum amounts of CO_2 uptakes were considerably different among water treatments and between seasons (2017 and 2018) (Table 4.4 and Fig. 4.9). In 2016, the lowest

maximum flux was at the sheltered plot (2016P1) (15.3 µM m^{-2} s^{-1}) (Fig. 4.9a) because of the reduction in the number of tillers and leaf area due to earlier senescence at around DOY 127 and more pronounced at DOY 147. The highest daily maximum net CO_2 fluxes were observed at the irrigated plot (2016P3) (42.5 µM m^{-2} s^{-1}, Fig 4.9c), following by the rainfed plot (2016P2) (31.2 µM m^{-2} s^{-1}). In 2017, the net CO_2 flux in the irrigated plot was much higher than the remaining rainfed plots (Fig. 4.9d, 4.9e & 4.9f and Table 4.4). This pattern also is found in 2018. However, the highest daily maximum CO_2 flux in the irrigated plot in 2018 (2018P3) was around 63.7 µM m^{-2} s^{-1} while it is 41.1 µM m^{-2} s^{-1} in the irrigated plot in 2017 (2017P3). The CO_2 flux in the rainfed plots in both years (2017 and 2018) was not significantly different (Table 4.4).

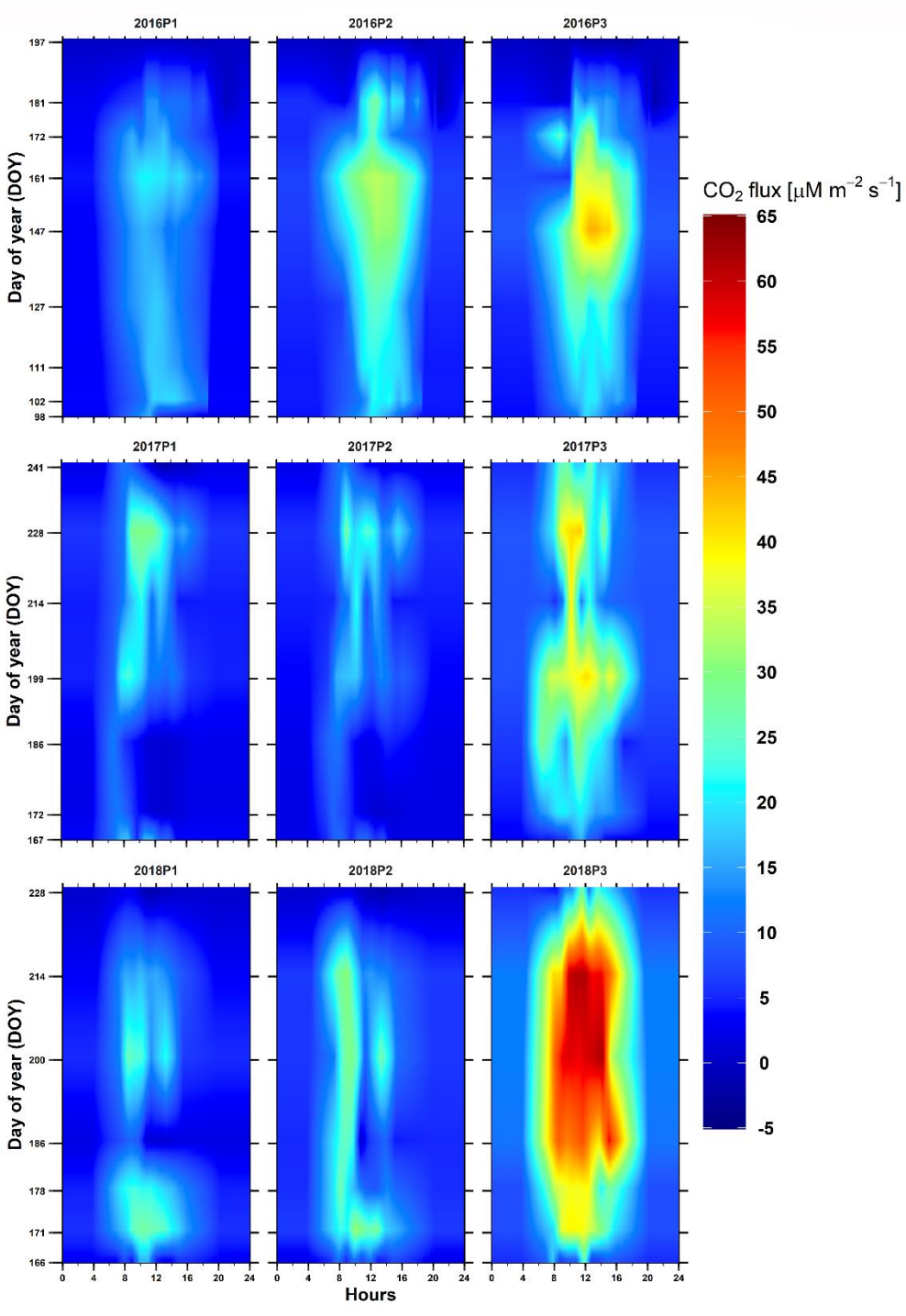

Figure 4.9: Daily cycles of instantaneous canopy CO_2 gas fluxes: the top panel - winter wheat (2016) at the sheltered plot (2016P1), rainfed plot (2016P2), and irrigated plot (2016P3); the middle panel - maize (2017) at the two rainfed plots (2017P1 and 2017P2), and irrigated plot (2017P3); and the bottom panel - maize (2018) at the rainfed plot with late sowing date (2018P1), rainfed plot with normal sowing date (2018P2) and irrigated plot with normal sowing date (2018P3) (cf. Table 4.1).

The seasonal variability of crop transpiration as measured by sap flow sensors and expressed on per tiller (winter wheat) or per plant (maize) basis and per unit LAI are shown in Figure 4.10. Transpiration per tiller and per LAI of the sheltered plot were in general lower than for the rainfed and irrigated plots (Fig. 4.10a and 4.10b). Sap flow per tiller and LAI in the sheltered plot was increased during a couple of days in the second week of June with heavy rainfall. Sap flow per tiller of the rainfed plot was very similar to the irrigated plot in the last week of May. However, it was higher than the irrigated in the last two weeks of June (Fig. 4.10a) which is in contrast to sap flow per unit of LAI where it was lower than irrigated plot in this period. Both sap flow per plant and sap flow per unit of LAI were not much different among the three treatments in maize in 2017 (Fig. 4.10c and 4.10d). Sap flow in the irrigated plot was slightly higher than in the rainfed plots this year. Sap flow per plant from the irrigated plot in 2018 was considerably larger as compared to the irrigated plot in 2017. Mean sap flow per single plant in the irrigated plot was around 480 g d^{-1}, while only 312 g d^{-1} was observed in 2017 (Fig. 4.10c). Contrary to 2017, sap flow per plant for the irrigated plot was considerably higher than sap flow per plant from the two rainfed plots, particularly from June 30 to August 9 in 2018 (Fig. 4.10e). The deviation of sap flow per unit LAI for the irrigated plot in 2018 and the two rainfed plots was less pronounced than the deviation of sap flow per plant (Fig. 4.10f).

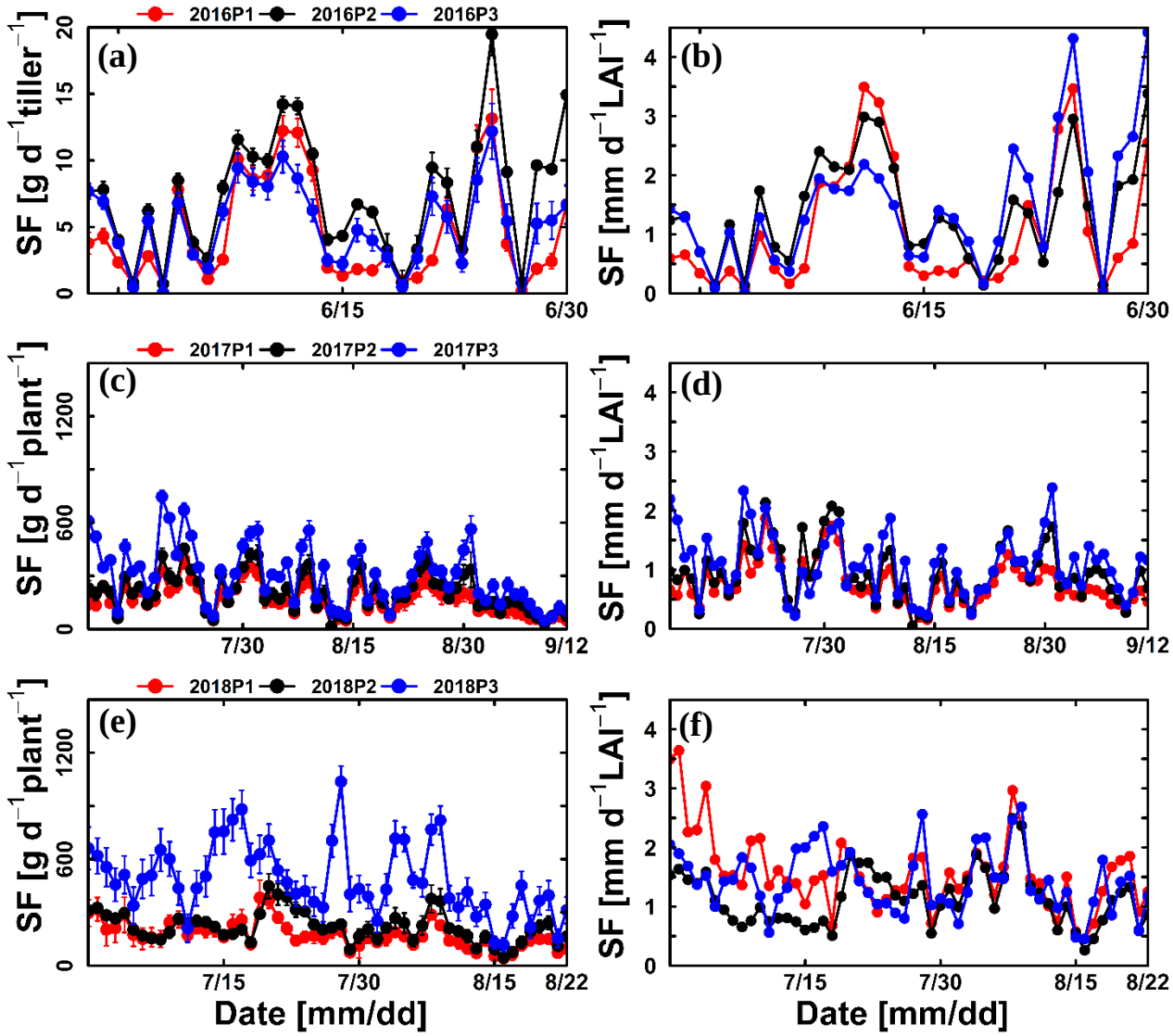

Figure 4.10: Sap flow (SF) per tiller or plant (a-c-e) and SF per unit leaf area index (LAI) (b-d-f) in different water treatments levels. The top panel refers winter wheat in 2016 at the sheltered (2016P1 – red dots), rainfed (2016P2 – black dots), and irrigated plot (2016P3 – blue dots). The middle panel refers to maize in 2017 at the two rainfed plots (2017P1 – red dots and 2017P2 – black dots), and irrigated plot (2017P3 – blue dots). The bottom panel refers to maize in 2018 at the rainfed plot with late sowing date (2018P1 – red dots), the rainfed plot with normal sowing date (2018P2 – black dots), and the irrigated plot with normal sowing date (2018P3 – blue dots). Data is shown from May 24 to June 30, 2016 for winter wheat; from July 9 to September 12, 2017 and from June 30 to August 22, 2018 for maize. Error bars in (a-c-e) indicate the standard deviation of the sap flow measurements in the five different tillers (winter wheat) or five plants (maize).

4.3.2.3 Light use efficiency

The slope of fitting functions between daily CO_2 fluxes and aboveground dry matter over the intercepted PAR (PAR_{int}) are shown in Fig. 4.11. The light use efficiency was slightly different if

being calculated based on daily CO2 fluxes or aboveground dry matter (Table 4.5), particularly for the rainfed plot (2017P1) and the rainfed plot with the late sowing date in 2018 (2018P2). The LUEs in general were remained high in the stress plots in two crops. The LUEs from the irrigated plots were higher than those in the remaining plots, especially in maize.

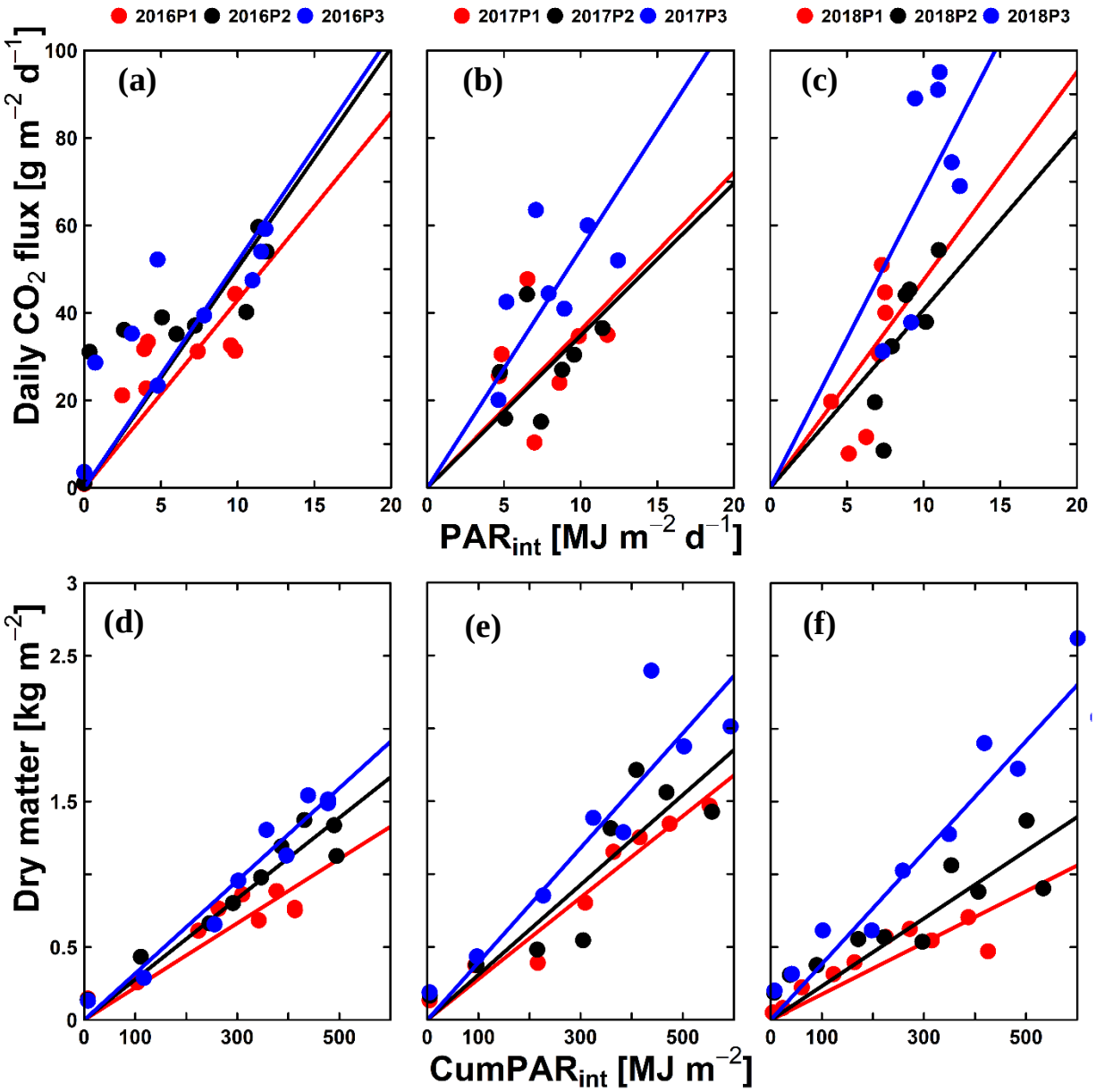

Figure 4.11: Daily CO_2 fluxes fitted against daily intercepted PAR (PAR_{int}) (a-b-c) and aboveground dry matter fitted against cumulated intercepted PAR ($CumPAR_{int}$) (d-e-f) to derive LUE (see Table 4.5). The left panel refers to winter wheat in 2016 at the sheltered plot (2016P1 – red dots), rainfed plot (2016P2 – black dots), and irrigated plot (2016P3 – blue dots). The middle panel refers to maize in 2017 at the two rainfed plots (2017P1 – red dots and 2017P2 – black dots), and irrigated plot (2017P3 – blue dots). The right panel refers to maize in 2018 at the rainfed plot with late sowing date (2018P1– red dots), rainfed

plot with normal sowing date (2018P2 – black dots) and irrigated plot with normal sowing date (2018P3 – blue) (cf. Table 4.1).

Table 4.5 Light use efficiency (LUE) of different water treatments in winter wheat (2016) and in maize (2017 and 2018) calculated based on daily CO_2 fluxes (LUE_{Flux}) and aboveground dry matter (LUE_{DM})

Water treatments	LUE_{Flux} (g DM MJ^{-1})		LUE_{DM} (g DM MJ^{-1})	
	Values	R^2	Values	R^2
2016P1	2.548	0.79	2.212	0.96
2016P2	2.986	0.58	2.777	0.98
2016P3	3.078	0.51	3.184	0.99
2017P1	2.140	0.63	2.796	0.98
2017P2	2.070	0.58	3.086	0.92
2017P3	3.241	0.73	3.932	0.96
2018P1	2.765	0.54	1.766	0.92
2018P2	2.359	0.52	2.322	0.94
2018P3	4.050	0.73	3.831	0.98

Leaf temperature did not differ among three water treatments in winter wheat in 2016 (Fig. 4.12a) but maize showed differences (Fig. 4.12b & 4.12c). Temperature at the irrigated plot was up to 3-4 °C higher than for the rainfed plots in both years. Canopy temperature was generally higher than air temperature for both crops (Fig. 4.2). Canopy temperature in the sheltered plot deviated from those in non-sheltered plots in wheat from June 9th (Fig. 4.2a and Fig. 4.12d) when crop was starting with leaf senescence. In contrast to leaf temperatures, the canopy temperature in maize under rainfed conditions was 1-2 °C higher than the under irrigation.

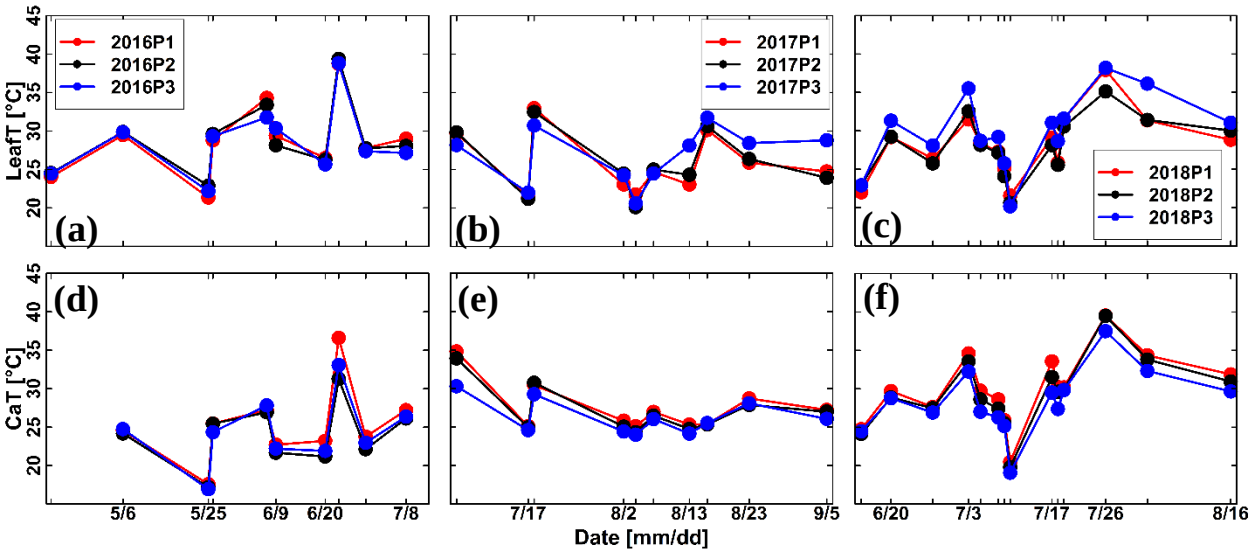

Figure 4.12: Daily maximum leaf temperature (LeafT) (a-b-c) and canopy temperature (CaT) (d-e-f) in the day with leaf gas exchange and LWP measurements. The left panel refers to winter wheat in 2016 at the sheltered plot (2016P1 – red dots), rainfed plot (2016P2 – black dots), and irrigated plot (2016P3 – blue dots). The middle panel refers to maize in 2017 at the two rainfed plots (2017P1 – red dots and 2016P2 – black dots), and irrigated plot (2017P3 – blue dots). The right panel refers to maize in 2018 at the rainfed plot with late sowing date (2018P1– red dots), rainfed plot with normal sowing date (2018P2 – black dots) and irrigated plot with normal sowing date (2018P3 – blue) (cf. Table 4.1). The y axes start from 15 °C.

4.4 Discussion

4.4.1 Stomatal conductance and leaf water potential of winter wheat and maize

4.4.1.1 Winter wheat

The lower leaf gas exchange and LWP in the sheltered plot as compared to the rainfed and irrigated plots indicated that soil water levels strongly affected stomatal conductance, photosynthesis, transpiration and LWP in winter wheat. A more negative LWP in wheat under water stress as compared to non-stress conditions have been observed in several studies (Singh and Kumar, 1979; Turner and Henson, 1989; Brisson and Casals, 2005) and are consistent with our observations of pronounced LWP differences among water regimes. Wheat is a crop with known anisohydric stomatal regulation when grown in pots (Henson et al, 1989; Tardieu and Simonnaeu, 1998). However, detailed field-based reports and data showing the anisohydric behavior of winter wheat are rare. Observed differences of stomatal conductance and LWP among the irrigated, rainfed, and sheltered plots (i.e. May 25 and 26, Fig. 4.3) were similar to the observation in sunflower (anisohydric) in Tardieu and Simonneau, (1998). This suggests that, also under field conditions, winter wheat exhibits anisohydric stomatal behavior. However, the difference in midday LWP among water treatment levels in our study (i.e. May 25 and 26, Fig. 4.3) was not as large as reported for sunflower (Tardieu and Simonneau, 1998).

These authors did not find a response of stomata to VPD in well-watered sunflower under field conditions in their study. However, it should be noted that there were only two irrigation applications in the irrigated plot for our study in 2016. The observed decrease of stomatal conductance during the afternoon in the irrigated plots on that day could be due to the combined effects of VPD and mild water stress in the irrigated plot as it contained a high stone content, and low available water capacity (Fig. 4.3). LWP levels on these two days (May 25 and 26) reflect the difference in PAW between treatments. A hydropassive stomatal closure in wheat is as a result of direct loss of water through evaporation due to increasing atmospheric demand (VPD). Moreover, the deficit of soil moisture triggers chemical production in dehydrated root (i.e. abscisic acid) such that root signaling induces hydroactive stomatal closure in anisohydric plants (Davies and Zhang, 1991; Tardieu and Simonneau, 1998).

4.4.1.2 Maize

Maize is known to typically maintain LWP in response to decreasing soil water potential and increasing VPD at levels similar to well-watered plants (Tardieu and Simonneau, 1998). In our work, LWP plateaued from 10 AM to 4 PM with minimal differences among water treatment levels (Fig. 4.4). The LWP plateau corresponds with the low Gs. Predawn LWP differed among water treatments (July 17, Appendix 4d), however LWP was maintained around -2 MPa from 12 to 4 PM during this day, as well. These results are consistent with the observations of maize from Tardieu and Simonneau (1998). Our field results confirm isohydric stomatal behavior of maize under field conditions.

The seasonal response of stomatal conductance to different VPDs was reported in cowpea (Bates and Hall, 1981; Shackel and Hall, 1983), a plant with clear isohydric behavior. The leaf water potential from eucalyptus, a plant rather characterized as having anisohydric behavior, can decrease to very low values and vary with the fluctuations of soil moisture whereas the difference between soil water potential and midday Ψ_{leaf} is maintained constant over a season which is defined as “isohydrodynamic” (Franks et al., 2007). Large variability of minimum LWP has been reported for maize genotypes. Leaf water potential can be limited at quite high values, for instance -0.8 MPa in some lines of maize, while values as low as -1.5 MPa have also been recorded (Welcker et al., 2011). Some drought-tolerant maize genotypes exhibited higher minimum LWP under soil water depletion than more sensitive ones, which is associated with their ability to avoid xylem embolism and hydraulic failure (Cochard, 2002; Tyree et al., 1986; Li et al., 2009) Note that the constant LWP level (around -1.8 MPa) under different soil water regimes reported in Tardieu and Simonneau (1998) and Tardieu et al., (2017) that was

associated with high VPD values was based on observations from a single day. Measurements on LWPs and Gs for different days and growing seasons have been rarely reported for maize. The results of our study with two year of maize with contrasting evaporative demand and levels of soil moisture (Table 4.4; Fig. 4.4, Fig. 4.5, Fig. 4.6, Fig. 4.7, and Appendix 4c) reveals that maize appears to maintain its LWP around -1.6 to -2 MPa. Stomatal closure is complete between -1.6 and -2 MPa as was also reported by Cochard, (2002). In our study, the observed LWP was below -2 MPa for several days. Similar values were also reported by Li et al., (2002) for field-grown maize in semiarid conditions. In our study leaf water potential dropped below -2 MPa in the rainfed plots to levels much lower than those observed in the irrigated plots in 2018. This could imply different degrees of isohydry in maize. However, any conclusions concerning contrasting minimum LWPs between 2017 and 2018 should not be overemphasized. Observed extremely low LWPs correspond with extremely low Gs and were further accompanied by complete leaf curling in both rainfed treatments in 2018 (Fig. 4.5) due to the extremely dry and hot weather and severe dry soil, in this record year of widespread crop yield failures due to drought across Germany (Webber et al., 2020).

4.4.2 Gas exchange and crop growth and the relative roles of stomatal regulations and canopy adjustments under different water regimes

4.4.2.1 Winter wheat

Water stress strongly reduced canopy CO_2 flux, transpiration, and crop growth in the sheltered plots. Winter wheat displayed different responses to water stress at the canopy scale. The reduction of tiller number and leaf area of wheat in response to drought stress has been reported by several authors, e.g. Musick and Dusek, (1980), Trillo and Fernández (2005), Innes et al., (1981) and Cai et al., (2018). These phenomena were also observed in our study (Table 4.4). Reduced LAI (Fig. 4.8d) saves plant available water and postpones desiccation which enhances the ability of tissue hydration. The relatively high LUE at low PAW (Table 4.5 and Fig. 4.1a) and higher canopy temperature (Fig. 4.12d) as compared to the non-sheltered plots is an indication of drought tolerance and processes of early canopy senescence (Fig. 4.8d) which can be explained as a drought escape mechanism (Chaves et al., 2003). Lower LWP and a greater sensitivity of tissue growth to depleted soil water relative to gas exchange has been reported for different crops (Sadras and Milroy, 1996). The reduction of leaf tissue growth is typically an early responses to limited soil water because it strongly depends on osmotic regulation and turgor pressure (Kramer and Boyer, 1995). The reduction of biomass and LAI in the sheltered plot

showed an earlier start of canopy senescence when soil moisture was depleted (Fig. 4.8a & 4.8d). The induced leaf abscission in wheat is understood as a result of an increase in synthesis and responsiveness to ethylene (Wright, 1977).

While the PAW was low from flowering until the end of growing season and air temperature and VPD were both higher (Fig. 4.2a), the LUE values calculated were not markedly lower from the sheltered plot as compared to the non-sheltered plots. The leaf temperature differences between the three water treatments was minor (Fig. 4.12a) while there were significant differences in Gs, E, and LWP (Fig. 4.8d, 4.8g, & 4.8j), indicating anisohydric control for winter wheat. Stomatal opening allows leaf transpiration that enhances leaf cooling effects while CO_2 uptakes occur. In contrast to leaf temperature, the canopy temperature at the sheltered plot was 2-4 °C higher than those at the non-sheltered plots (Fig. 4.12d). The variability of canopy temperature within farmer fields with varying soil water was also reported in Kupisch et al., (2015). Our result demonstrates that there was an interaction between soil water supply and crop response which emphasizes that for wheat transpiration adjustments driven by reduced LAI are more important than the stomatal regulation under water stress. Transpiration rates per tillers and per LAI were relatively similar (Fig. 4.10a & 4.10b) while transpiration of the whole canopy (Nguyen et al., 2020a) and cumulative canopy transpiration (Table 4.5) showed considerable differences (due to the differences of tiller number and LAI). In the non-sheltered plots, higher LAI and tiller number resulted in higher canopy transpiration as compared to the sheltered plot which in turn led to different microclimatic patterns such as the resulting lower canopy temperature in these treatments.

4.4.2.2 Maize

Effects of soil water stress on maize have been investigated in numerous studies focusing on soil plant relations, stomatal regulations and associated eco-physiological mechanisms (see most work from Tardieu et al., 1998; Tardieu et al., 2017). Other studies have concentrated more on crop growth and gas exchange processes of old and modern hybrid cultivars (Nissanka et al., 1997), radiation use efficiency and yield loss if plants were exposed to water stress at different growing stages (Abrecht and Carberry, 1993; Earl and Davis, 2003; Çakir, 2004), combined effects of water and heat stress on leaf physiology and plant growth (Perdomo et al., 2016) or on water and nitrogen stress effects on canopy gas exchange (Jones et al., 1986). Fewer studies directly compare observations of water stress effects on stomatal regulations and canopy exchange and on dynamic crop growth processes in the same analysis as presented in this study.

Drought resistance involves different mechanism such as the ability to maintain tissue hydration or to function while dehydrated as well as avoiding drought through adaptations of the plant life cycle. Each of these mechanisms was observed in our study for maize. Progressive stomatal closure led to a constant LWP at a certain threshold, thus, indicating an isohydric strategy to maintain a certain level of tissue hydration (Fig. 4.4, Fig. 4.5, Fig 4.6 and Appendix 4b & 4c). Comparatively higher instrinsic WUEs (An/Gs) and instantanous WUEs (An/E) (Table 4.4) and high LUE (Table 4.5), associated with higher leaf temperatures (Fig. 4.12b & 4.12c), in the stress plots versus non-stressed plots illustrate the capacity of maize in photosynthesis functioning despite leaf dehydration. Leaf rolling was observed in both rainfed plots in the second week of June 2017 and from the beginning of June until the end of the growing period in 2018, indicating a dehydration avoidance mechanism resulting from morphological adjustments. Leaf rolling is an effective mechanisms for delaying senescence (Richards *et al.*, 2002; Aparicio-Tejo and Boyer, 1983). Bullying-form cells which are located in the upper epidermis and hydrodermis cells under epidermis of leaf near the midrib and vascular bundles of leaves caused rolling in *Gramineae* species (Kadioglu and Terzi, 2007). When these cells shrink, they cause leave rolling but when they are turgid, the leaves are flat and more in parallel with soil surface. Interaction of plant hormone regulator such as abscisic acid (ABA) signaling from dehydrated root and hydraulic signal could account for mediating cell division and the change of leaf elongation of drought in maize (Salah and Tardieu, 1997).

Soil water depletion causes stomal closure which can reduce water loss, but it also increases leaf termperature that consequently leads to quicker leaf rolling (Jones, 1998). This contrasts with our result where higher leaf temperatures (up to +3-4 °C) were found in the irrigated plots, but not in the water stress plots (Fig. 4.12b & 4.12c). Changes in leaf temperature during leaf rolling differs among species (Kadioglu and Terzi, 2007). For example, leaf folding in *Vigna unguiculata* causes a reduction up to 5.5 °C (Schakel and Hall, 1979). Stomata are closed in completely rolled leaves, thus, leaf curling has a minor effects on total leaf conductance (Heckathorn and Delucia, 1991). However, leaf rolling reduces transpiration and strongly affects the energy balance due to lower intercepted incident irradiances which in turn causes lowering leaf temperature (Heckathorn and Delucia, 1991). Such differences have not always been observed, as an example Matthews et al. (1990) found no temperature differences in sorghum between plants with and without leaf rolling (Matthews et al., 1990). Further, our result constrasts with the findings from (Fernandez and Castrillo, 1999) in maize that the initiation of leaf rolling under pot-growing conditions is related with a higher leaf temperature. Higher leaf temperature in the irrigated plots in our work could be explained due to higher intercepted

radiation (Fig. 4.11b, 4.11c, 4.11e & 4.11f) that can increase heat of the leaf while stomata mostly close under isohydric strategy.

The lower temperature at the leaf level did not result in lower canopy temperature in maize at the rainfed plots as compared to the irrigated plots (Fig. 4.12e & 4.12f). The difference in canopy temperature was not as large as the difference in leaf temperature, illustrating effects of canopy structure on the microclimate of vegetation canopies. Canopy temperature for the rainfed plots was slightly higher than for the irrigated ones as expected. This corresponds with differences in canopy transpiration (Fig. 4.10c & 4.10e) while the deviations of transpiration per unit of LAI (Fig. 4.10d & 4.10f) was not pronounced at canopy level. This emphasizes the importance of LAI and transpiration adjustments per ground area together with the isohydric stomatal regulation in maize in response to water stress. Maize is a widely-spaced crop, such that each plant acts as "stand-alone" canopy. Increase of canopy temperature in the rainfed plots could potentially be explained by the progressively increased degree of stomatal closure which resulted in lower canopy transpiration. Also, the reduction of LAI due to leaf rolling and crop size (height and diameter) of single maize plants (Table 4.4) led to larger exposure of the soil surface to radiation because of sparse canopy (Reicosky et al., 1980). Leaf rolling allows the light to penetrate into the lower layers of the canopy. An increase of the heat within the canopy (resulting in lower temperatures of shaded leaves in the irrigated than in the rainfed plots (data not shown)) could surpass the heat reduction from less intercepted light due to leaf rolling, which consequently results in higher canopy temperatures in the rainfed plots.

Isohydric responses are hypothesized to lead to reduced photosynthesis rates due to their pronounced stomatal control. However, contradicting results on the photosynthesic capacity of plants with isohydric behavior have been reported for grapvines and trees (Sade et al., 2012; Attia et al., 2015; Poni et al., 2014; Roman et al., 2015; Pou et al., 2012). In our study, stomatal closure in maize was associated with sigificantly lower intercellular CO_2 concentration (Table 4.4). Leaf greenness (as proxy of chlorophyll content and availability of Rubisco enzymes) was reduced in the water stress plots. However, instrinsic WUEs (An/Gs) and instantaneous WUEs (An/E) (Table 4.4) did not differ among treatments while LUEs was relatively high in the rainfed plots (Table 4.5). Maize is a C_4 plant having the Kranz bundle sheath cells surrounding xylem and phloem, where mesophyll cells surrounding the Kranz cells show large numbers of well-developed chloroplasts (Keeley and Rundel, 2003). This particular arrangement of Kranz cells around the vascular bundles within a leaf facilitates high CO_2 concentration at bundle sheath cell that could suppress oxygenase of Rubisco. Moreover, in maize, a special CO_2 acceptor which has higher affinity to CO_2 that could minimize the photorespiration (von Caemmerer, 2000).

These physiological advantages of photosynthetic system in maize (Ghannoum, 2009) could explain the overall high LUEs even though lower internal CO_2 levels and more negative LWPs (from -1.6 to -2 MPa) were observed under water stress (i.e. 2018). The light use efficiency in the rainfed plots were lower than in the irrigated plot which is due to the reduction of LAI and intercepted PAR (Fig. 4.8e & 4.8f and Fig. 4.11b, 4.11c, 4.11e & 4.11f). This is consistent with the work from Baldocchi (1994), where incremental increases in LAI enhanced maize's ability to absorb photosynthetic active radiation and enlarged the crop's sink strength for CO_2. Vitale et al., (2007) also reported that reduced net ecosystem photosynthesis under water stress in maize was not attributed to photodamage of the photosynthesis apparatus, but rather to limited LAI development.

4.4.3 Limitation of the study

Our study presented the measured gas fluxes data from leaf to canopy and crop growth for winter wheat and maize under different water regimes. To the best of our knowledge, such data and comprehensive measurements have rarely been reported together in a comparative analysis. However, we acknowledge a lack of field replicates for the water treatments which is related to the use of complex and expensive construction of underground rhizotrone facilities at our site (see Nguyen et al., 2020 for further details). The limited size of the subplots did not allow for an extensive sampling of aboveground dry matter and destructive LAI measurements which in some instances causes high standard deviations due to small-scale soil heterogeneity even within the subplots. The spatial variability of stomatal reactions over leaves, plants, and the crop stand levels can be large (Rochette et al., 1991). The variability of stem growth and stem-stem variability of sap flux can result in a large variation of crop transpiration in winter wheat (Langensiepen et al., 2014). However, these measurement issues did not affect the relative differences between dates, treatments, crops and years shown in this study.

4.5 Conclusion

In this study, we evaluated the response of winter wheat and maize to variable water supply at the leaf and the canopy scale by investigating leaf stomatal and canopy morphological characteristics. For both crops drought stress strongly reduced the gas exchange and water status of leaves as well as the crop growth. Winter wheat showed anisohydric stomatal regulation. Despite significant reductions of the leaf water potential (LWP) and stomatal conductance (Gs) at the leaf level, we found a relatively high light use efficiency (LUE) under drought stress. A reduction of leaf area and tiller number as desiccant tolerance thus has a more

important role than stomatal regulation for wheat canopy gas exchange and crop growth. Maize displayed isohydric stomatal behavior and maintained a minimum LWP around -1.6 to -2 MPa. Total effects of the more aggressive stomatal regulation on canopy gas exchange and LUE were however modulated by the canopy structure (i.e. the variable response of sunlit and shaded leaves), and prominent leaf rolling/plant size adjustments. The isohydric stomatal regulation in maize is not necessary resulting in limitation of the photosynthesis capacity under water stress due to the special leaf anatomy and physiological advantages of the photosynthesis system which apparently overrules the role of stomatal control of water loss.

The inclusion of such stomatal regulations in the soil-vegetation-atmospheric models (SVAT) and land surface model schemes (Verhoef and Egea, 2014), as well as soil-plant models (Tardieu et al., 2015) has received a lot of attention. To consider stomatal functions, one approach is to use minimum LWP as proxy of stomatal regulation that can be sufficient in modelling applications (Tardieu et al., 2017; Couvreur et al., 2012; Huber et al., 2014; Cai et al., 2018; Nguyen et al., 2020; Tuzet et al., 2003; Olioso et al., 1996). The critical LWP thresholds in these studies were from -1.2 to -2.9 MPa depending on crop types and the used water stress functions on stomatal conductance models. The minimum of LWP from -1.6 to -2 MPa for winter wheat and maize with very low stomatal conductance from our study could add the reference basis for these modeling approaches. However, clarity about distinct anisohydric and isohydric behavior and possible continuum is still challenged by experimental evidences on variable LWP thresholds for different cultivars of the same species (Welcker et al., 2011; Schultz, 2003; Coupel-Ledru et al., 2014; Schoppach et al., 2016; Hochberg et al., 2013; Hochberg et al., 2018) as also confirmed in this study. The underlying mechanisms for this possible continuum for stomatal behaviors of the two crops in this study are still unclear and require further research. Further, results from this study show that SVAT models and process-based crop simulation models should focus not only on simulating stomatal regulations to capture the response to drought stress, but also require adequate representations of leaf and canopy growth as well as morphological adjustments affecting the energy balance.

5 Chapter: General discussion and outlook

5.1 General discussion

This thesis is based on a comprehensive data set obtained using a unique experimental set-up. The CO_2 and H_2O gas fluxes were measured at soil, leaf, and canopy scales. The associated crop growth was observed and simulated for different soil types and water regimes and seasonally and annually contrasting weather conditions. The field trial and the complex measurement design did not only allow for a comprehensive studies of soil/water-plant relation processes but facilitated the parameterization and validation of improved crop modeling approaches.

The first aim of this thesis was to understand responses of stomata, patterns of CO_2 and H_2O gas flux exchange, and crop growth to varying soil water status through combined modelling studies and field experiments. The second aim was to improve the simulation of CO_2 and H_2O gas fluxes and crop growth (biomass, LAI, root growth) by implementing equations for a more detailed simulation of eco-physiological stomatal responses, physically based soil water flux simulation, and soil hydraulic properties in an existing crop model. To achieve these two main aims, in Chapter 2, data collected for winter wheat in 2016 was used. The existing crop model was coupled with the Couvreur RWU model and a physically based WB model, thereby allowing for representing whole plant hydraulic conductance and leaf water potential for simulating crop stomatal conductance. This was possible for both, isohydric and anisohydric stomatal responses. A comparative study was then performed between this new coupled modeling approach and the coupled modeling approach that is based on the Feddes RWU model where plant hydraulic conductance is not considered. In addition, for the new coupled model, the sensitivity of biomass and root water uptake to the changes of important soil-plant related parameters (critical leaf water head threshold, root hydraulic parameter, and specific root weights) was investigated. Chapter 3 described the extension and application of both coupled modeling approaches for maize, thus for a plant with isohydric stomatal regulation and C_4 photosynthesis pathway, using data from 2017 and 2018. In the Chapter 4, all measured data of leaf water potential, gas fluxes (photosynthesis and transpiration), temperature from leaf and canopy levels, and crop growth (aboveground dry biomass, LAI, plant height etc.) from stony soil in 2016, 2017, and 2018 were presented and analyzed together with soil water status. This Chapter disentangled the stomatal strategies for winter wheat and maize, the relative roles of stomatal regulations and longer-term adjustment (leaf growth) to gas exchange and crop growth among different water treatments. In this final chapter, I firstly discuss to which extent the new coupled model, that allows for consideration of both isohydric and anisohydric stomatal

behavior, improves the model performance in simulating CO_2 and H_2O gas fluxes and crop growth for maize and wheat. Secondly, an integrated discussion of how the results from field measurements (Chapter 4) compare with the insights from the modelling studies (Chapter 2 and 3) and on the importance to consider and distinguish between isohydric and anisohydric responses is provided. Finally, the limitations of the study and scientific gaps which have not been covered by this thesis will be discussed. This leads to suggestions for further research and outlooks in the future.

5.1.1 Model performance in winter wheat and maize

5.1.1.1 Root water uptake, transpiration reduction, and soil water content

The simulated RWU from the coupled model which considered plant hydraulic conductance and leaf water hydraulic threshold (Couvreur RWU), were relatively similar to those predicted by the coupled model using the Feddes approach in simulations for winter wheat (Chapter 2, Section 2.3.1.2, Table 2.1). These findings were in line with results of Cai et al., (2018) and Cai et al., (2017) on winter wheat grown in the same field. However, a more pronounced and earlier reduction in transpiration rates and biomass growth was predicted by the Feddes model for the irrigated and rainfed plots in silty soil with high soil water availability (compared to stony soil) in comparison to the results from the Couvreur model. This result contrasts to simulation work by Cai et al., (2018) and Cai et al., (2017), which found no reduction in transpiration in the silty soil when using the Feddes approach. Our results indicated that using the single parameter set in the Feddes RWU method for both soil types to adapt the water stress function following potential transpiration might not work for all treatments and soil types in winter wheat. Cai et al., (2018) and Vandoorne et al., (2012) suggested adjusting the parameters for the Feddes RWU model when applying this method for heterogeneous soils and crop types. For the Couvreur RWU model, however, we successfully used a single set of the initial parameter of $K_{rs,normalized}$ for all soil types and water treatments. This suggests that the Couvreur model could represent the effects of soil heterogeneity on root and shoot growth without the need for adapting parameters.

With regard to simulated SWC, the coupled model with the Couvreur approach was able to simulate both dynamics and magnitude of SWC in different soil depths and for different water treatments (Chapter 2, section 2.3.1.2, Fig. 2.8, and Appendix 2G). The SWC simulated by the Couvreur model was almost similar to that simulated by the Feddes approach for winter wheat. Both models underestimated water contents in deeper soil layers during the late growing season (i.e., in depths of 80 and 120 cm) (Fig. 2.8). This could be due to the free drainage bottom

boundary condition in the HILLFLOW water balance model, which implies that the water can only leave the soil profile but no water can flow in it. This is in line with findings from Sulis et al., (2019) using terrestrial systems simulation with the inclusion of hydraulic architecture approach which was carried out for winter wheat in the same field site. Capillary rise in the soil can keep the lower layers relatively wet (Vanderborght et al., 2010). The shallower water table and seasonal variability of the groundwater table strongly affect soil water content in the silty soil (Groh et al., 2020a; Groh et al., 2020b; Klotzsche et al., 2019; Cai et al., 2017). The soil was hardly dried out in the lower rhizotrone (Klotzsche et al., 2019; Cai et al., 2017; Cai et al., 2018). In our simulation, the use of a soil depth of 1.5 m may not be deep enough to capture this effect. The larger RWU simulated by the Couvreur model than by the Feddes model in the silty soil in May resulted in slightly lower simulated water contents by the Couvreur model. However, the differences in simulated water contents by the two models were much smaller than the deviations from the observed water contents.

Chapter 3 described the application of the two coupled models on maize for stony soil conditions in 2017 and 2018. Both models performed similar in simulating RWU and SWC across seasons and treatments. Simulated variation of RWU and SWC in the irrigated and rainfed plots in the stony soil in 2017 and the irrigated plot in 2018 agreed well with field observations when soil water was sufficient, either due to irrigation or adequate rainfall amounts (Chapter 3, Section 3.3.3.3, Fig. 3.9d and 3.9d). However, both models overestimated RWU from DAS 52 to 70 at the drought stress plots in 2018 (early growing season), while they predicted RWU throughout the remaining observation period rather well. The overestimation was consistent with the overestimated topsoil layer SWC during this period (Fig. 3.10b and 3.10d). This illustrates the challenge for representing the three-dimensional heterogeneity of the soil substrate within the observation plots using a single set of soil characteristics (Cai et al., 2021; Herbrich et al., 2018). These difficulties in the soil parametrization could explain the deviations of simulated RWU and SWC from field observations.

Chapter 3 further highlighted the less accurate estimates in transpiration reduction by the Couvreur model for early growing stage regardless of water treatments and years (from sowing to DAS 45) (Fig 3.5c and Fig. 3.8) compared with the Feddes model. However, by considering the increase in K_{plant} starting from DAS 45 until harvest led to a more realistic simulation of the transpiration reduction by the Couvreur model as compared to the Feddes approach. The sensitivity analysis showed that the increase in $K_{init,\ normalized}$ could improve the simulation of transpiration reduction in the earlier growth stages. However, the increase of $K_{init,\ normalized}$ resulted in too high K_{plant} values for later growing stages, consequently causing an

underestimation of simulated water stress in the Couvreur model. The Couvreur model used the root length and root segment conductance for estimating total root system conductance and K_{plant}. The Feddes model did not represent this feature, thus, was not sensitive to estimates of total root conductance. In case few data for an accurate parametrization are available (i.e. root growth data and $K_{intial,\ normalized}$) for maize, the Couvreur approach might lead to a higher bias in simulating water stress, and thus crop biomass and LAI growth.

5.1.1.2 Leaf water hydraulic head, gross assimilation rate, and stomatal conductance

Chapter 2 described the capacity of the Couvreur model in simulating the gross CO_2 assimilation rate for winter wheat (Fig. 2.7). The model was able to simulate the effect of water stress on the reduction of assimilation (DOY 147 on the sheltered plot in the upper field, Fig. 2.9) when Ψ_{leaf} reaches to $\Psi_{threshold}$ = -2 MPa. Since the evaporative demand was not high with a noon vapor pressure deficit (VPD) around 1.2 kPa, the sharp drop of photosynthesis around midday in our study was associated with a plateau of Ψ_{leaf} under water stress (Fig. 2.9e). This diurnal variation in assimilation was not captured using the Feddes model although a similar type of water stress function was employed (as T_{act}/T_{pot}). The simulation result indicated that the effects of declined soil water and leaf water pressure head on photosynthesis were captured through using the critical leaf water pressure head threshold. The pattern of diurnal photosynthesis in our simulation was similar to the modeling results from Olioso et al., (1996) for soybean. With regard to the sheltered plot located in the lower field with loamy soils, on DOY 147 (Fig. 2.9j), the Feddes model agreed with the observation data. In contrast, there was a considerable underestimation of gross assimilation during this day by the coupled model that used the Couvreur approach, thus, with the inclusion of plant hydraulic and stomatal regulation dynamics. This was due to the underestimation in simulated Ψ_{leaf}. The simulated Ψ_{leaf} dropped to the $\Psi_{threshold}$ even though the measured Ψ_{leaf} did not. Underestimated root growth (Fig. 2.4) and soil water content (Fig. 2.8) in the deeper soil layers in this sheltered plot caused the lower estimated soil root leaf water potential (Ψ_{sr}), K_{rs}, and K_{plant}. These consequently resulted in much lower calculated Ψ_{leaf}. This revealed that the performance of the coupled model with the Couvreur approach is strongly dependent on realistic estimates of the soil to root water pressure head which, in turn, is a result of simulations of root growth and soil water pressure head. Thus, in this case the more mechanistic model like Couvreur model led to higher uncertainty in simulation results. This illustrates that crop models are optimized for simulating aboveground processes (Tao et al., 2020; Boote et al., 2013) and still have deficiencies in representing belowground processes (Maurel and Nacry, 2020; Boote et al., 2013; Gayler et al., 2013).

However, that might change if the observation data of root length density and root biomass is available for root modeling parameterization (Gayler et al., 2013).

Inclusion of C_4 photosynthesis (Chapter 3, Section 3.3, Fig. 3.2) in both Couvreur and Feddes models allowed to simulate gross photosynthesis rates in maize (Section, Fig. 3.6, Appendix 3E, and Table 3.4). The considerable soil water depletion and extremely hot weather (high VPD and temperature) in 2018 caused more negative Ψ_c and a strong reduction of stomatal conductance, RWU, and photosynthesis (i.e DAS 70 and 86 in the rainfed plot with normal sowing date in 2018 (2018F1P2) (Appendix 3H) and late sowing date plot (and 2018F1P1, data not shown). Advancement of land surface model through considering plant hydraulic conductance has received a lot of attention in recent years (Li et al., 2021; Kennedy et al., 2019; Sulit et al., 2019; Roman et al., 2015). Recent work from Li et al (2021) has included plant hydraulic conductance to NOAH-MP land surface model which has been tested for trees (i.e. oark). Sulis et al., (2019) introduced the Courveur model into Community land surface model (CLM 4.0) and validated for winter wheat. In our work, the Co model captured the asymmetrical patterns of gross assimilation rate and RUW when simulated leaf water potential was lower than critical leaf water potential threshold that was consistent to the reports from Tuzets et al., (2003) and Li et al., (2020). The Couvreur model was able to capture leaf water hydraulic head, stomatal conductance, and photosynthesis under water stress and non-stress (after irrigation) by using the $\Psi_{threshold}$ = -2 MPa for maize (Appendix 3H and 3I). The Co model in our work represented the reported leaf water potential in maize (around -1.6 to -2 MPa). Kennedy et al., (2019) introduced the plant hydraulic system into Community Land Surface model (CLM version 5.0). However, the stem-to-leaf resistance was not fully considered in this model which underestimated isohydricity (i.e. minimum leaf water potential dropped to -2.5 MPa during drought). The different levels of water deficit created by rainout shelters in winter wheat in 2016 and especially the 2018 growing season were representative years for drought periods. These drought stress condition might be expected under predicted climate change scenarios. The coupled models (Co and Fe) considering the two-way feedback overall performed well for both winter wheat and maize in our thesis.

5.1.1.3 Aboveground biomass, leaf area index, and root growth

The dynamic growth of biomass and leaf area index in winter wheat was simulated well by the newly coupled model for plots located in the lower field while the model underestimated biomass in the upper field, characterized by stony soil (this was also found if using the Feddes approach)

(Chapter 2, Section 2.3.1.1, Fig. 2.3, and Table 2.1). This result indicates that there are some environmental factors influencing crop growth that could not be captured in our model. The effects of soil strength and lower soil temperature on crop development in the stony field were not captured by the model. For maize, both coupled Co and Fe models simulated satisfactorily the biomass and LAI growth for different water treatments and two contrasting growing seasons (2017 and 2018) (Chapter 3, Fig. 3.4, Fig. 3.7). Both models had relatively similar performance in simulating biomass and LAI (Chapter 3, and Table 3.4). The inaccurate estimate of the transpiration reduction by the Courveur model in the earlier growth stages was consistent with the lower biomass and LAI as compared to the Feddes model. Also, the accurate prediction of water stress in the later growing season led to better simulation in biomass and LAI in the Couvreur model.

Under drought conditions, an increase in rooting depth and root length facilitates the access to water from deeper soil layer and has direct effects on biomass accumulation in winter wheat (Manschadi et al., 2006) in maize (Zhang et al., 2015). The model underestimated drought-induced root growth, particularly at deeper soil layers in the lower field for winter wheat (Chapter 2, Fig. 2.4). Combined with the sensitivity of the Couvreur model to the simulation of total root length (thus total root hydraulic system) this led to an inadequate estimate of water stress during the growing season, thus, simulation errors could be attributed to the root growth model (Chapter 2, Fig. 2.5). When soil water was depleted, the change of root: shoot ratio (more biomass for root development) is a sign that roots grew deeper to facilitate an water uptake from deeper soil layers (Peng et al., 2020; Cai et al., 2018; Raynolds et al., 2007; Jamieson et al., 1998) and, thus, an increased crop WUE (Yang et al., 2019; Lynch, 2013; Walter and Schurr, 2005). A fixed root-shoot ratio in simulation models, e.g., based on the use of partitioning tables for a given growth period as well as the simulation of root growth as a purely source-driven process (supply from assimilates) (Goudriaan and Van Laar, 1994), may not allow for capturing the shift in the carbon allocation to roots (for more root growth) in response to water stress. However, observed imaged root data from rhizotubes (Chapter 2, Fig. 2.4, and Appendix 2F) that was used for deriving the absolute root length density might have potential errors and uncertainties (Morandage et al., 2021; Cai et al., 2018).

5.1.1.4 Plant hydraulic conductance

The coupled model with the Couvreur RWU model approach explicitly calculated K_{rs} based on the root segment of the individual root. The K_{rs} was then extrapolated to estimate K_{plant}. The

calculated K_{plant} was in the range of the K_{plant} which was estimated from sap flow, leaf water potential, and soil to root water potential for winter wheat (1.5 10^{-5} to 11.2 10^{-5} d^{-1} from all plots) (Chapter 2, Section 2.3.1.3, and Fig. 2.10). The K_{plant} was highest at 1 week around anthesis then gradually reduced at the end of the growing season due to root aging and death. Our results were in line with the reported K_{plant} values (between 5.7 x 10^{-5} d^{-1} and 20 x 10^{-5} d^{-1}) for ryegrass (Feddes and Raats, 2004). Our estimated K_{plant} was consistent in both magnitude and temporal dynamic of K_{rs} in studies from Cai et al., (2017) and Cai et al., (2018), which used inverse modeling while using data from the same winter wheat cultivar and soil types as in this study but based on a different observation period. Our measured and simulated K_{plant} was in line with the reported root conductance values in Meunier et al., (2018).

The model simulations overestimated the total root length in the upper irrigated and rainfed field plots whereas the root densities in the lower rainfed and sheltered plots were underestimated (Appendix 2F). Nevertheless, despite these over- and underestimations of total root length, the simulated K_{plants} reproduced the measured ones in the different treatments quite well. For the sheltered plot of the lower field, based on the root density measurements (Fig. 2.4), one would expect to observe the highest K_{plant} of all treatments. However, this was not shown in the measurements. Also, based on the measured total root lengths, one would expect that K_{plant} of the sheltered plot in the upper field should be similar to K_{plant} in the other plots of the upper field. But, K_{plant} was clearly lower in the sheltered plot of the upper field than in the other treatments in the upper field. In the model simulations, the lower K_{plant} in the sheltered plots compared to the other plots in the same field locations was due to a lower simulated total root length. Since the differences in observed total root lengths were smaller (upper field) or even opposite (lower field) to the differences in simulated total root lengths, the smaller observed K_{plant} in the sheltered plots have probably causes that were not considered in the model. A potential candidate is the resistance to water flow from the soil to the root in the soil, which increases considerably when the soil dries out (Carminati and Javaux, 2020; Koebernick et al. 2018; Caminati et al., 2009), as was the case in the sheltered field plots.

For maize, a further analysis of the simulated K_{plant} of the Couvreur model for this treatment before and after calibration was included in Appendix 3G. Reported values of K_{plant} are rare for maize, thus, their interpretation and discussion in a larger context is only possible to a limited extent. Sunita et al., (2014) reported measured K_{plant} values in the range of 6.9 x 10^{-5} d^{-1} to 12.96 x 10^{-5} d^{-1} during the main growing season for pot-grown maize. Meunier et al., (2018) measured the different components of root hydraulic conductance (axial and radial) from

different root types in maize growing in containers, ranging from 0.1 x 10^{-5} to 5 x 10^{-5} d^{-1}. Nguyen et al., (2020) and Cai et al., (2018) reported that K_{plant} of winter wheat can range from 3.6 x 10^{-5} d^{-1} to 10 x 10^{-5} d^{-1} in the same field and the same soil type under irrigated conditions. Note that we used a fraction of 0.55 for upscaling of root hydraulic conductances to the plant level (K_{plant}) in the simulation. Our simulated K_{plant} was also in line with those reported ranges. The Couvreur model was able to capture the differences in K_{plant} among water regimes and weather conditions in maize. The adjustment of a root segment hydraulic conductance ($K_{init, normalized}$) allows for realistic estimates of K_{plant} in maize, however, the simulated results has to be tested with the corresponding data (i.e. K_{plant} estimated from sap flow, root counts, and measured leaf hydraulic head, see Chapter 2 Fig. 2.10 in winter wheat). Closing the gap between physically based approaches used in hydrologic modes and empirical approaches in crop models more data on $K_{init, normalized}$ and K_{plant} for maize would be required.

5.1.2 Distinction of isohydric and anisohyric stomatal behaviors in field observations and modeling studies

A separation of iso-and anisohydric behaviors (constant and variable leaf water potential (Ψ_{leaf}), respectively) is generally suspected to be at the species level (Tardieu and Simonneau, 1998). In this thesis the distinction in daytime Ψ_{leaf} was observed among different water treatments (irrigated, rainfed, and sheltered plots) for stony soil soil conditions and on days with high evaporative demand of the atmosphere (DOY 146 and DOY 147) (Chapter 4, Section 4.3.1.2, and Fig. 4.3). Results confirmed the anisohydric stomatal regulation in winter wheat described by Tardieu and Simonneau (1998). For maize, the results of our study with two years with contrasting evaporative demand and levels of soil moisture (Chapter 4, Table 4.4, Fig. 4.4, Fig. 4.5, Fig. 4.6, Fig. 4.7, and Appendix 4B and 4C) revealed that maize appears to maintain its Ψ_{leaf} around -1.6 to -2 MPa. In both crops, overall, stomatal conductance is very low when Ψ_{leaf} was between -1.6 and -2 MPa. This illustrates that there was no clear separation in terms of Ψ_{leaf} between plants with isohydric and anisohydric behaviors in our work. Variable degrees of isohydry in stomatal control have been reported in other studies as well. The *Eucalyptus gomphocephala*, an eucalyptus plant that is commonly being characterized as having an anisohydric behavior, can downregulate evapotranspiration and stomatal conductance to very low values and dynamically adapt to the fluctuations of soil moisture whereas the difference between soil water pressure head and midday Ψ_{leaf} is maintained constant over a season stomatal regulation. This rather unusual behavior was therefore reported and classified as isohydrodynamic by Franks et al., (2007). There is also an ongoing discussion on the consequences of the results from studies illustrating that there is no clear separation between

isohydricity and anisohydricity in trees (Hochberg et al., 2018; Meinzer et al., 2014; Klein, 2014; Domec and Johnson, 2012; Sade et al., 2012; Franks et al., 2007) or in grape-vine (Levin et al., 2019; Coupel-Ledru et al., 2014; Schultz, 2003), poplar (Zhang et al., 2020; Attia et al., 2015), and herbaceous species (Turner et al., 1984). Tree plants adjusted their water use across years demonstrating that there is interannual variability in isohydricity which was drived by their environmental dryness (Wu et al., 2021; Gou et al., 2020; Ratzmann et al., 2019). A like-anisohydric behavior was observed under high evaporative demand but can change within species to a like-isohydric behavior under lower evaporative demand in grapevine (Rogiers et al., 2012; Zhang et al., 2012; Schulze, 2003).

Chapter 2 for winter wheat and Chapter 3 for maize discussed model performances when representing corresponding isohydric and anisohydric behaviors. The Couvreur model with the same $\Psi_{threshold}$ of -2 MPa was able to simulate the CO_2 and H_2O gas flux exchange and crop growth for both crops. The coupled model developed within this thesis uses a stomatal regulation model which assumes that stomatal conductance is not influenced by Ψ_{leaf} as long as the Ψ_{leaf} is above $\Psi_{threshold}$. The Ψ_{leaf} was kept constant by changing stomatal conductance (reducing) when the $\Psi_{thresholds}$ were reached. In fact, this represents a perfectly isohydric system. The ambiguous separation between maize and winter wheat in terms of minimum Ψ_{leaf} shown in our field data explained why the Couvreur model performed fairly well for both crops despite using the same $\Psi_{threshold}$ (-2 MPa). Moreover, model sensitivity analyses for winter wheat (Chapter 2, Section 2.3.2, and Fig. 2.11) and maize (Chapter 3, Section 3.3.1, Fig. 3.3, Appendix 3H, and Appendix 3I), performed by changing the $\Psi_{thresholds}$, and indicated that using $\Psi_{thresholds}$ higher than -1.5 MPa resulted in lower simulated biomass and RWU. The use of a higher $\Psi_{threshold}$ (above -1.5 MPa) caused earlier and more pronounced water stress which consequently reduced photosynthesis (Fig 3.3 and Appendix 3H and 3I). Our work showed that simulations with $\Psi_{threshold}$ = -2 MPa yielded better biomass and LAI predictions than the simulations with $\Psi_{threshold}$ = -1.5 MPa. In other studies, a $\Psi_{threshold}$ of -1.2 MPa has been set to represent an isohydric behavior, while the use of $\Psi_{threshold}$ of -1.9 and -2.6 MPa were found suitable for simulating an anisohydric behavior (Tuzet et al., 2003). However, it is worth noting that Tuzet et al., (2003) did not consider the effect of high relative humidity/VPD on the stomatal model, thus their simulated results are expected to differ from our results. The high atmospheric demand in the European drought year 2018 (i.e., high VPD and air temperature) caused much lower Ψ_{leaf}, photosynthesis, and stomatal conductance in the data presented in this thesis (Chapter 4, Section 4.3.1.2). Moreover, the work from Tuzet et al., (2003) has not been validated under field conditions, where plants are subjected to more severe water deficit and

high evaporative demand. Minimum Ψ_{leaf} thresholds ranging from -1.6 to -2 MPa for winter wheat and maize with very low stomatal conductance levels derived from field measurements and simulation results can be used as reference values in future modeling studies. Both, modeling studies and field observations, suggested that an isohydric and anisohydric behaviour can be captured by using single $\Psi_{threshold}$ (i.e. -2 MPa). However, this finding needs to be verified based on longer time series and under different environmental conditions.

Improvement of simulations of gas fluxes and crop growth could be only successfully achieved when considering both stomatal regulations at leaf level and other relevant processes, especially (i) photosynthesis processes at the leaf level, (ii) leaf growth, (iii) root growth, and (iv) the accurate representation of soil water over the complete soil profile. Regarding point (i), in fact, Chapter 4 has shown that light use efficiency (LUE) in maize was not much affected in the drought stress plots (Section 4.3.2.3, Fig. 4.11 and Table 4.5) when the stomata were mostly closed due to isohydric stomatal control. The photosynthesic capacity was not limited although aggressive stomatal behavior was found for maize. This could be explained by a complex combination of both well-known biochemical and anatomical specializations of C_4 plants, which result in an elevated CO_2 concentration at the site of Rubisco (von Caemmerer et al., 2003). This special anatomical and biochemical arrangement added advantages for maize in terms of CO_2 assimilation that overruled the role of stomatal functions. Both tested coupled modeling approaches were successfully extended to include the C_4 photosynthesis pathway for simulating maize growth (Chapter 3). This included the simulation of the CO_2 diffusive mechanisms from leaf surface to intercellular space cells, and bundle sheath cells. Thus, realistic simulations of leaf photosynthesis and stomatal conductance at the leaf scale and photosynthesis levels at the canopy scale were achieved. In other words, improving the simulation of CO_2 and H_2O gas flux exchanges at leaf and canopy levels, requires the consideration of both stomatal regulation strategies and biochemical photosynthesis processes. In terms of points (ii) and (iii), model results and field observations indicated that accurate simulations of dynamic leaf area index and root growth are very important in addition to the simulation of stomatal regulations, especially under water stress. Leaf area reduction and tiller number decrease in winter wheat and leaf rolling/ plant size adjustments in maize are crucial mechanisms to avoid drought stress which strongly influenced the canopy transpiration and photosynthesis, and LUE (Chapter 4, Section 4.3.2.2, Fig. 4.9 and Fig. 4.10). An underestimation of root growth in deeper soil layers in the silty soil (Chapter 2, Section 3.1.1, Fig 2.4, and Appendix 2F) led to an underestimation of soil water fluxes and soil to root water potential (in the Couvreur model), and, in consequence, to an underestimation of photosynthesis, transpiration and leaf water potential in winter wheat. The

simulation of root growth and total root length over the different growing stages (earlier and later growing stages) also play crucial roles in simulating root hydraulic conductance and whole plant hydraulic conductance in maize in the case of the Couvreur model. The Couvreur model represents more detailed crop characteristics. However, it is sensitive to the output and accuracies of the root growth simulation (Chapter 2 and 3). The sensitivity of biomass and RWU to the change of root hydraulic conductance was higher than to the changes of $\Psi_{threshold}$ for both crops (Chapter 2, Figure 2.11 and Chapter 3, Fig. 3.3). In other words, the accurate simulation of root growth, total root hydraulic conductance, and thus whole plant hydraulic conductance was critical for the final performance of the Couvreur model. This was a common issue of soil-plant models that based on hydraulic principles and root system hydraulic conductance (Maurel and Nacry, 2020; Sulis et al., 2019). A better integration of root functions and their relations to soil and growing stages in crop models would certainly aid improvements of crop growth and water use simulations (Maurel and Narcy 2020). Concerning the last point (iv), a realistic simulation of water fluxes requires the consideration of complex processes from soil to soil compartment, soil to root process, and water uptakes (representing sink terms like in the Couvreur and Feddes models). The small-scale three-dimensional heterogeneity of soil characteristics could affect simulations of the crop growth, soil water flux, and thus, compromise the performances of crop models (Chapter 2 and Chapter 3). Thus, finding representative values for characterizing soil hydraulic properties is still a major challenge when aiming for a realistic simulations of the processes involved in gas flux exchanges and crop growth at the plot scale (Cai et al., 2021; Xiong and Nadal, 2020; Moraes et al., 2019; Herbich et al., 2018). At the study site, dynamic changes in the groundwater table throughout the growing season can markedly affect water fluxes and crop growth (Groh et al., 2020a; Klotzsche et al., 2019; Cai et al., 2018; Cai et al., 2016; Vanderborght et al., 2010). The underestimated soil water content for the silty soil during winter wheat cultivation was therefore most likely only partly explained by errors in the root growth simulation but also by the strong influence of the groundwater table which could not be captured by the tested models.

5.2 Limitations and Outlook

5.2.1 Limitations of experimental designs and field measurements

This thesis presented detailed measurements of gas fluxes (CO_2 and H_2O) at leaf and canopy scales and high resolution crop growth data for winter wheat and maize grown under contrasting water regimes and variable soil characteristics. Such comprehensive field-based flux and crop measurements, covering a wide range of water stress conditions, have rarely been reported and

used for modeling parameterization, calibration, and validation or for the development of model extensions. A lack of field replicates for the water treatments is acknowledged and can be explained by the use of complex and expensive underground rhizotrone facilities at our site (for further details referred to Nguyen et al., 2020). The limited size of the subplots did not allow for an extensive sampling of aboveground dry matter and destructive LAI measurements which in some instances causes high standard deviations due to small-scale soil heterogeneity even within the subplots although the measurements themselves are accurate. The spatial variability of stomatal reactions over leaves, plants, and crop stand levels can be large (Vilà-Guerau De Arellano et al., 2020; Rochette et al., 1991). The variability of stem growth and stem-stem variability of sap flux can result in a large variation of crop transpiration in winter wheat (Langensiepen et al., 2014). However, these measurement issues did not affect the relative differences between dates, treatments, crops, and years shown in this thesis.

For the observations of the root development using horizontal rhizotubes, further investigations are required on how root counts (counts cm^{-2}) or root length (cm cm^{-2}) can be accurately translated for instance into root length densities (cm cm^{-3}) that can be compared and validated the simulated root length density from the models (Morandage et al., 2021; Cai et al., 2018). Also, an offset and higher measured sap flow as compared to simulated RWU from both models in winter wheat (Chapter 2, Section 2.3.1.2, and Fig. 2.7) and maize (Chapter 3, Fig. 3.5a, 3.9a, and 3.10a, Appendix 3E) suggested that measurements of sap flow and data quality need to be further investigated and checked.

5.2.2 Outlook for further understandings of plant-water (soil) relations

Clarity about distinct anisohydric and isohydric behavior and possible continuum is still challenged by experimental evidence on variable LWP thresholds for different cultivars of the same species (Levin et al., 2020; Hochberg et al., 2018; Schoppach et al., 2016; Welcker et al., 2011; Schultz, 2003; Coupel-Ledru et al., 2014; Hochberg et al., 2013). The underlying mechanisms for this possible continuum for stomatal behaviors of the two crops in this study are still unclear and require further research.

5.2.3 Outlook for improvements of modeling of CO_2 and H_2O gas flux exchange and crop growth

5.2.3.1 Representation of dynamic leaf growth

Leaf area index (LAI) is an integrative measure of the carbon and water balance in plants because it describes the potential surface area available for leaf gas exchange (CO_2 & H_2O)

(Fang et al., 2019; Cowling and Field, 2003). Despite the importance of LAI simulation in simulating gas fluxes, it is still receiving less attention than work on improving the stomatal functions in the crop models and SVAT schemes (Park and Jeong, 2021; Ewert, 2004; Cowling and Field, 2003; Damour et al., 2011). Inadequate LAI could result in inaccurate estimates of intercepted radiation, and the energy balance, thus affects photosynthesis, potential evapotranspiration, and actual transpiration. This thesis focused on including more eco-physiological characteristics of stomatal regulation and water fluxes in crop modeling routines. However, it was shown, that the reductions of leaf area and tiller number in winter wheat and leaf rolling maize observed in the measurement data (Chapter 4) and highlighted in the modeling studies (Chapter 2 and 3) play important roles in regulating CO_2 & H_2O gas fluxes and final biomass. Chapter 3 revealed how the LAI of maize was much more dynamic through leaf rolling when the plant is exposed to water stress, with leaf expansion causing a quick recovery after soil rewetting (Tardieu et al., 2018; Kramer and Boyer, 1995). Stomatal closure occurs in parallel with leaf curling and thus photosynthesis and transpiration are strongly reduced (Baret et al., 2018; Tardieu and Parent, 2017). Stomatal regulations and leaf rolling also determined the differences in canopy temperature (Fig 4.12). Leaf elongation and leaf width could change quickly after an increase in the soil water potential and vapor pressure deficit (Tardieu and Simonneau, 1998; Lacube et al., 2017). Curling of the upper leaves towards the midrib, as a clear indication of water stress in drought plots, was observed for maize in the European drought year 2018. Modeling of LAI still did not satisfactorily capture differences due to changes in soil type for winter wheat (Chapter 2) and due to annual growing season conditions for maize. Although tested coupled model approaches allowed to simulate water flux, photosynthesis, and stomatal conductance at hourly intervals, the leaf area simulation, implemented in the main crop growth module (LINTULCC), was still operated at a daily scale and thus could not capture leaf elasticity during the day. The coupled model applied the function of leaf weight and daily average temperature while the direct effect of diurnal changes in leaf and soil water variation was not included. A more realistic simulation of leaf growth via improved representations of assimilation allocation to leaf growth needs to be considered. A more complex approach for simulating the processes of leaf expansion in response to changes in leaf water and evaporative conditions within short time periods has successfully been introduced in some studies (Lacube et al., 2020; Lacube et al., 2017; Salah and Tardieu, 1997; Tardieu and Davies, 1993; Chenu et al., 2008). Further research to transfer this knowledge and modeling parameterization is required.

5.2.3.2 Representation of dynamic root growth

Because roots provide an important basis to sustain water and nutrient flow for a plant, a reliable root growth simulation is crucial in soil-plant modeling schemes. Chapter 2 in this study showed that the root growth model might need to be improved in order to capture the root growth dynamics in the deeper soil layers (i.e., in silty soil). Chapter 3 illustrated the importance of accurate simulations of root hydraulic conductance in the earlier and later growing stages in the case of the coupled model using the Couvreur approach. Under drought, the root: shoot ratio is increased to devote more assimilate for root growth to lower soil layers (Du et al., 2020; Cai et al., 2018; Lynch, 2013). The opposed phenomenon might be observed, for instance water deficit inhibited RLD and root: shoot ratio at dry soil but specific root length and root surface increased with depths (Peng et al., 2019). To account for this dynamic root growth, a more dynamic (over time and soil depths) root response to water stress has been suggested in the Conclusion sections of Chapters 2 and 3. The sink-source relation between root and shoot should be improved based on the function of soil water. Coupling a 3D root growth model to crop models could enhance the simulation of root growth and root extension over different soil depths (Cho et al., 2018). A 3D functional-structural plant model of root and shoot driven by radiative transfer, photosynthesis, and soil hydraulics has been used to simulate effects of water limitation on plant biomass (Braghiere et al., 2020). However, the use of a 3D root growth model or both 3D shoot and root models might face complex parametrization, an increasingly large number of parameters, and high computational costs that are difficult to use at broader scales (Vanderborgth et al., 2021; Morandage et al., 2019; Couvreur et al., 2014). Moreover, any improvement of the root growth model requires the availability of measured root growth data (in different soil depths or different cultivars) under different soil/water conditions which are often unavailable in soil-plant modeling research. Additional studies for root data are required which could support further understanding root growth traits in responding to soil/water stress and improving root growth simulation (Tracy et al., 2020; Yang et al., 2020)

5.2.3.3 Consideration of plant hydraulic conductance and underlying signals in soil-plant models

Because the applied model assumed a constant whole plant hydraulic conductance during the day that solely depends on root length, xylem embolisms due to soil water depletion or the decline in root hydraulic conductance of root-soil contact were not represented. Strong transpiration or severe soil water stress causes a decline in plant xylem hydraulic conductance

when xylem cavitation occurs (Brodersen et al., 2019; Cardoso et al. 2018; Cochard, 2002). The air gap reduces the contact area between soil and roots and induce a strong increase of the hydraulic resistance to radial water flow between them which, in turn, could result in early water stress (Koebernick et al. 2018; Couvreur et al., 2014a). In addition, the hydraulic conductance of the root-soil interface would decline as soil water potential decreases or as a consequence of root shrinkage due to root-soil contact loosening (Rodriguez-Dominguez and Brobribb, 2020; Koebernick et al. 2018; Carminati et al., 2009; Sperry et al. 2002; Herkelrath et al., 1977). The variation of plant hydraulic conductance due to effects of ABA through aquaporin channels has been reported in maize (Ding and Chaumont, 2020; Maurel and Narcy, 2020; Rodriguez-Gamir et al., 2019; Caldeira et al., 2014; Parent et al., 2012; Couvreur et al., 2014). The roles of plant capacitance are also important and affect plant transpiration and leaf water status over a short period in maize (Xiong and Nadal 2020; Vogel et al., 2017; Hartzell et al., 2017; Tardieu et al., 2015; Langensiepen et al., 2009; Meinzer, 2002; Kramer and Boyer, 1995). The soil-root contact processes (effect of air-gap/soil-root contact loosening or positive of aquaporin on root hydraulic conductance) (see work from Couvreur et al., 2014 and Lei et al., 2021 at plant scale) could be implemented and translated to the field scale for future applications of the coupled model presented in this thesis.

5.2.3.4. Future applications of coupled models in other environments

One of the main applications of crop models is the prediction of future crop yields under conditions of climate change (Peng et al., 2020; Tao et al., 2009; Riitter and Keuled, 1997) or for climate risk assessments (Webber et al., 2020; Webber et al., 2018; Ewert et al., 2015; Ewert et al., 2009). Some studies also employ crop models to simulate yields of crops at large spatial scales (Bondeau et al., 2007; Challinor et al., 2004). The newly coupled crop model presented in this thesis, with an explicit consideration of the plant hydraulic conductance and related stomatal regulations, can be used for such studies for providing more reliable predictions of gas exchange rates and crop yield, i.e., under water stress. However, further testing of the model is required. Firstly, the estimate of the water potential within the continuum pathway strongly depends on the estimate of soil water potential, which is considerably affected by the availability, quality and choice of soil hydraulic model parameters (Sulis et al., 2019; Montzka et al., 2017; Vereecken et al., 2016; Verhoef and Egea, 2014; Wöhling et al., 2008). The root growth and root architecture were strongly influenced by soil strength (Morandage et al., 2021) and soil compactions (Xiong et al., 2020; Moraes et al., 2019), and different for eroded soil (Herbich et al., 2018) which reflects the importance of soil heterogeneity for crop growth and the needs to

consider them in soil plant models and earth system models (Fatichi et al., 2020). Model validations at field scales under different soil and climatic conditions as used in this study will be helpful in assessing model performance in other regions. Secondly, the groundwater table could strongly influence the simulation of water fluxes and crop growth (Groh et al., 2020a; Groh et al., 2020b) which suggests that this should be considered and investigated in more detail in follow-up studies. Thirdly, the coupled models were only applied under optimum nutrient conditions. Fertilisers (i.e. nitrogen and potassium) remarkably varied and strongly influenced crop growth (Qi et al., 2019; Chi et al., 2020; Shahzad and Amtmann, 2017). Thus, the model needs to be able to simulate the effects of the limited nutrient and fertilizer variability on crop growth processes through links with corresponding fertilization modeling routines. This will allow the model to simulate crop growth under both, water and nutrient limited conditions. Finally, the model should be validated with different cultivars from winter wheat and maize because of the variation in leaf water status (Gallé et al., 2013; Welcker et al., 2011) and the difference in root hydraulic conductivity (Zhao et al., 2005; Siddique et al., 1990).

5.3 Conclusion

The thesis firstly aimed at better understandings the responses of leaf stomatal, gas fluxes, crop growth, and their interrelationships under different soil moistures through both modeling work (Chapter 2 and 3) and the experimentation study (Chapter 4). The second aim was to improve the simulation of gas fluxes exchange and crop growth through the representation of more detailed eco-physiological soil-plant processes in the existing crop model. We can conclude that:

(a) Consideration of plant hydraulic conductance can improve the simulation of CO_2 and H_2O fluxes, and crop growth in biomass, roots, and leaf area index in winter wheat.

(a1)

- The Couvreur and Feddes models showed relatively similar performance in the simulation of dry matter, leaf area index (LAI), root growth, RWU, gross assimilation rate, and soil water content.
- The Feddes model predicts more stress and less growth in the silty soil than in the stony soil, which is opposite to the observed growth.

(a2)

- The newly coupled Couvreur model was also able to simulate the dynamics and magnitude of whole plant hydraulic conductance over the growing season.

(a3)

- A mechanistic model that is based on plant hydraulics and links root system properties to RWU, water stress, and crop development can evaluate the impact of certain crop properties (change of root segment conductance, specific weights of root, or leaf pressure head thresholds) on crop performance in different environments and soils.

(b) The coupled model with the Couvreur RWU model is generic enough to simulate the effects of soil water availability on the CO_2 and H_2O gas fluxes and crop growth of maize with varying weather conditions under stony soil.

(b1)

- For the Couvreur model, the RWU and dry biomass were more sensitive to the root hydraulic conductance parameters than to $\Psi_{thresholds}$ and root growth parameters.

(b2)

- Overall, both Couvreur and Feddes models performed similarly for biomass, LAI, root water uptake, and gross assimilation rate
- The Feddes model simulated accurately the plant water stress in the first 45 days of the growing season whereas the Couvreur model resulted in a lower agreement with observations.
- Considering more specific crop properties, the Couvreur model becomes more error-prone in comparison to the Feddes model if the dynamic root growth and total root system conductance (thus whole-plant hydraulic conductance) were inadequately simulated.

(c) Winter wheat and maize had various adaptive responses to maintain leaf and canopy photosynthesis capacity and a relatively high light use efficiency under decreasing soil moisture.

(c1)

- Winter wheat showed anisohydric stomatal regulation.
- Maize displayed isohydric stomatal behavior and maintained a minimum leaf water potential of around -1.6 to -2 MPa.

(c2)

- For both crops, drought stress strongly reduced the gas exchange and water status of leaves as well as the crop growth
- Despite significant reductions of the leaf water potential and stomatal conductance at the leaf level, there was a relatively high light use efficiency (LUE) in both crops under drought stress.

(c3)

- A reduction of leaf area and tiller number as desiccant tolerance has a more important role than stomatal regulation for wheat canopy gas exchange and crop growth.
- The isohydric stomatal regulation in maize is not necessary resulting in limitation of the photosynthesis capacity under water stress due to the special leaf anatomy and physiological advantages of the photosynthesis system which overrules the role of stomatal control of water loss.
- Total effects of the more aggressive stomatal regulation on canopy gas exchange and LUE were however modulated by the canopy structure (i.e. the variable response of sunlit and shaded leaves), and prominent leaf rolling/plant size adjustments.

In conclusion, the two-way feedbacks between growth and root water uptake is very important for predicting the crop response to different soil water conditions. Using one single critical leaf water potential threshold is sufficient to characterize stomatal regulation whereas it is also important to represent long-term responses of root and leaf for both winter wheat and maize for field-scale modeling applications. The coupled model developed within this thesis provides a promising approach that should be evaluated for further crops, soils, and climate conditions to be applied for modeling studies at larger spatial scales.

Appendix

Appendix 2A: Leaf photosynthesis and stomatal conductance calculation (wheat)

$$AMAX_{l,t} = \frac{VCMAX_{l,t}(\,Ci_{l,t} - \Gamma^*)}{Ci_{l,t} + KMC\left(1 + \frac{O_2}{KMO}\right)}\text{fwat} \quad \text{(A1)}$$

$$EFF_{l,t} = \frac{J}{2.1}\frac{Ci_{l,t} - \Gamma^*}{4.5(Ci_{l,t} + 2\Gamma^*)} \quad \text{(A2)}$$

$$FGR_{l,t} = AMAX_{l,t}\left(1 - e^{-I_{l,t}\frac{EFF_{l,t}}{AMAX_{l,t}}}\right) \quad \text{(A3)}$$

$$Ci_{l,t} = Ca - \left(FGR_{l,t}\frac{1}{gs_{l,t}}\right) \quad \text{(A4)}$$

$$gs_{l,t} = a_1 + \frac{b_1 FGR_{l,t}}{\left(Ci_{l,t} - \Gamma^*\right)(1 + \frac{DS_{l,t}}{D_0})}\text{fwat} \quad \text{(A5)}$$

AMAX is light saturated leaf photosynthesis (μM CO_2 m^{-2} s^{-1}); VCMAX is maximum carboxylation rate of Rubisco enzyme (μM m^{-2} s^{-1}); Ci is intercellular CO_2 concentration (μM mol^{-1}); Ca is atmospheric CO_2 concentration (μM mol^{-1}); KMC is Michaelis-Menten constant for CO_2 (μM mol^{-1}); KMO is Michaelis-Menten constant for O_2 (μM mol^{-1}); O_2 is atmospheric oxygen concentration (μM mol^{-1}); Γ* is CO_2 compensation point (μM mol^{-1}); EFF is quantum yield (μM CO_2 MJ^{-1}); J is conversion energy from radiation to mole photon (mole photons MJ^{-1}); FGR is leaf photosynthesis rate (μM CO_2 m^{-2} s^{-1}); I is the total absorbed flux of radiation (MJ m^{-2} s^{-1}); gs is bulk stomatal conductance (mol m^{-2} s^{-1}); a_1 is residual stomatal conductance (mol m^{-2} s^{-1}) when FGR = 0; b_1 is fitting parameter (-); DS is the vapor pressure deficit at the leaf surface (Pa); D_0 is empirical coefficient reflecting the sensitivity of the stomata to VPD (Pa); l is sub-indices indicates canopy layer (sunlit and shaded leaf) (-); t is sub-indices indicates time of the day (-); fwat is water stress factor for stomatal conductance and maximum carboxylation rate (-);

Appendix 2B: Scale up leaf stomatal conductance to canopy resistance in hourly simulation

To scale up from leaf stomatal conductance to canopy and for computation efficiency, we approximate the integrals

$$\int_0^{LAI} f(l)dl$$

By Gaussian quadrature $LAI\sum_{j=1}^{5} w_j * f(LAI * x_j)$ where x_j are the nodes and w_j the weights of the 5-point gaussian quadrature (Goudriaan and van Laar, 1994). LAI is the leaf area index and f is a

function dependent on leaf area for instance gsH2O.The above mentioned bulk stomatal conductance to CO_2 ($gs_{l,t}$ - mol m^{-2} s^{-1}) of sunlit and shaded leaf to stomatal conductance was converted to stomatal conductance to H_2O (m s^{-1}) based on the molar density of air.

$$gsH2O_{sun} = 1.56 * gs_{sun}/41.66 \quad \text{(B1)}$$

$$gsH2O_{shade} = 1.56 * gs_{shade}/41.66 \quad \text{(B2)}$$

Leaf stomatal conductance to H_2O (m s^{-1}) was calculated based on fraction of sunlit leaf area FSLLA

$$gsH2O_{leaf} = gsH2O_{sun} * FSLLA + gsH2O_{shade}\,(1 - FSLLA) \quad \text{(B3)}$$

The hourly canopy conductance HourlyGSCropH2O (m s^{-1}) was calculated in Eq. (B4)

$$HourlyGSCropH2O = LAI * \sum_{j=1}^{5} w_j\, gsH2O_{leaf} \quad \text{(B4)}$$

Hourly canopy resistance (s m^{-1}) was the reciprocal of hourly canopy conductance

$$Hr_s = 1/\mathrm{HourlyGSCropH2O} \quad \text{(B5)}$$

Hourly aerodynamic resistance (r_a) was calculated as Equation 4 in the Chapter 2 in the FAO Irrigation and Drainage Paper No. 56, (Allen et al., 1998). Assuming the leaf cuticle resistance and soil surface resistance were minor and neglected, the calculated canopy resistance (Hr_s) with fwat = 1 was directly used to calculate hourly crop evapotranspiration (ETP) using Penman-Monteith (Eq. B6) (See Equation 3, Chapter 2 in the FAO Irrigation and Drainage Paper No. 56, Allen et al., (1998)).

$$\mathrm{ETP} = \frac{\Delta(R_n - G) + \rho_a c_p \frac{(e_s - e_a)}{r_a}}{\lambda\left(\Delta + \gamma\left(1 + \frac{Hr_s}{r_a}\right)\right)} \quad \text{(B6)}$$

R_n is net radiation (MJ m^{-2} h^{-1}) ; G is soil heat flux (MJ m^{-2} h^{-1}); e_s is saturation vapor pressure at the air temperature (kPa); e_a is actual vapor pressure at the air temperature (kPa); ρa is mean air density at constant pressure(kg m^{-3}); c_p is the specific heat at constant pressure of the air (1.013 10^{-3} MJ kg^{-1} ◦C^{-1}); Δ is slope of the saturation vapor pressure-temperature relationship (kPa ◦C^{-1}); γ is the psychrometric constant of instrument (kPa ◦C^{-1}), Hr_s is canopy resistance (s m^{-1}); r_a is the aerodynamic resistance (s m^{-1}); λ is the latent heat of vaporization (2.45 MJ kg^{-1}).

Appendix 2C: Crop parameters used in the modelling work (wheat)

Sub-models	Parameters	Explanation (unit)	Stony	Silty	Reference
LINTULCC2	VCMAX25	Maximum carboxylation rate of Rubisco at 25°C (μM m^{-2} s^{-1})	62.1		Yin et al., (2009)
	Ca	Atmospheric CO_2 concentration (μM mol^{-1})	410		
	RGRL	Relative growth rate of leaf area during exponential growth $(°Cd)^{-1}$	0.007		van Laar et al., (1997)
	LAICR	Critical leaf area index (-)	5		van Laar et al., (1997)
SLIMROOT	$RSROOT_{max}$	Maximal elongation rate of seminal roots per day (m d^{-1})	0.03		Watt et al., (2006)
	DRRATE	Daily fraction of dying roots (-)	0.008		
	RINPOP	Number of emerged plants per square meter (number m^{-2})	350		
	MAXDEP	Maximum root depth (m)	1.5		
	NRSPP	Number of seminal root per plant (number $plant^{-1}$)	3		Shorinola et al., (2019); Huang et al., (1991)
	WLROOT	Specific weight for lateral root (g m^{-1})	0.0061	0.004	Jamieson and Ewert, (1999); Noordwijk and Brouwer (1991)
	WSROOT	Specific weight of seminal root (g m^{-1})	0.02	0.015	Jamieson and Ewert, (1999); Huang et al., (1991)
Feddes	hlim1	Soil water pressure head at anaerobic limit (m)	0		Cai et al., (2018)
	hlim2	Upper limit of pressure head range for optimal transpiration (m)	-0.01		Cai et al., (2018)
	hlim3h	Lower limit of pressure head range for optimal transpiration for high transpiration rate, T_{pot3h} (m)	-2.79		Cai et al., (2018)
	hlim3l	Lower limit of pressure head range for low transpiration rate, T_{pot3l} (m)	-7.47		Cai et al., (2018)
	hlim4	Soil water pressure head at wilting point (m)	-160		Cai et al., (2018)
	T_{pot3h}	High transpiration rate (m d^{-1})	0.0048		Cai et al., (2018)
	T_{pot3l}	Low transpiration rate (m d^{-1})	0.00096		Cai et al., (2018)
Couvreur	$\Psi_{threshold}$	Critical leaf hydraulic head for specific plant (m)	-200		Cochard, (2002); Tardieu and Simonneau, (1998)
	$K_{rs,\ normalized}$	Initial normalized root hydraulic conductance (cm d^{-1})	0.2544	10^{-5}	Cai et al., (2018)
	$K_{comp,\ normalized}$	Initial normalized compensatory hydraulic conductance (cm d^{-1})	0.0636	10^{-5}	Cai et al., (2018)
	□	Fraction to upscale from K_{rs} to K_{plant} (-)	0.55		

Appendix 2D: Soil physical parameters at the top (0-30 cm) and subsoil (30-150 cm)

Soil types	Layers	α	n	l	θ_r	θ_s	ks
		(m^{-1})	(-)	(-)	($m^3 m^{-3}$)	($m^3 m^{-3}$)	(m s^{-1})
Stony	Top soil	3.61	1.386	3.459	0.0430	0.3256	$10.7*10^{-6}$
	Sub soil	4.95	1.534	3.459	0.0543	0.2286	$5.83*10^{-8}$
Silty	Top soil	2.31	1.292	1.379	0.1392	0.4089	$1.16*10^{-6}$
	Sub soil	0.50	1.192	1.379	0.1304	0.4119	$1.73*10^{-6}$

The θ_r and θ_s are residual and saturation soil water content, respectively; α, n, l are empirical coefficients affecting the shape of the van Genuchten hydraulic functions ; ks is saturated hydraulic conductivity of the soil

Appendix 2E: Feddes root water uptake model

The root water uptake in HILLFLOW 1D model which is limited by soil water content in the root zone calculated by reduction of potential transpiration (T_{pot}). The semi-empirical reduction function $\alpha(\Psi_{m,i})$ is derived from soil pressure head (Feddes et al., 1978). The $\alpha(\psi_{m,i})$ also depends on T_{pot} because ψ_3 (soil pressure head where optimum condition for transpiration) is calculated via piecewise linear function of T_{pot} (Wesseling and Brandyk, 1985). The root water uptake was calculated based on relative root length density which is output from the SLIMROOT root growth model.

$$\alpha\left(\psi_{m,i}\right) = \begin{cases} 0 & \psi_{m,i} \geq \psi_1, \psi_{m,i} \leq \psi_4 \\ (\psi_{m,i} - \psi_1)/(\psi_2 - \psi_1) & \psi_2 \leq \psi_{m,i} \leq \psi_1 \\ 1 & \psi_3 \leq \psi_{m,i} \leq \psi_2 \\ (\psi_{m,i} - \psi_4)/\psi_3 - \psi_4) & \psi_4 \leq \psi_{m,i} \leq \psi_3 \end{cases} \quad \text{(F1)}$$

$$\psi_3 = \begin{cases} \psi_{3h} & T_{pot} > T_{3h} \\ \psi_{3h} + \dfrac{(\psi_{3l} - \psi_{3h})\left(T_{3h} - T_{pot}\right)}{(T_{3h} - T_{3l})} & T_{3l} < T_{pot} < T_{3h} \\ \psi_{3l} & T_{pot} < T_{3l} \end{cases} \quad \text{(F2)}$$

$\alpha(\Psi_{m,i})$ transpiration reduction as function of soil pressure head (-); Ψ_1 is soil water pressure head at anaerobic limit (m); Ψ_4 is soil pressure head at wilting point (m); Ψ_2 and Ψ_3 are upper and lower limits of pressure head for optimal transpiration (m), respectively; T_{pot} is potential transpiration (m d^{-1}); Ψ_{3h} is lower limit of pressure head range for optimal transpiration for high transpiration rate, T_{pot3h} (m); T_{3h} is high potential transpiration rate (m d^{-1}); Ψ_{3l} is lower limit of pressure head range for low transpiration rate, T_{pot3l} (m); T_{3l} is low potential transpiration rate (m d^{-1}).

Appendix 2F:

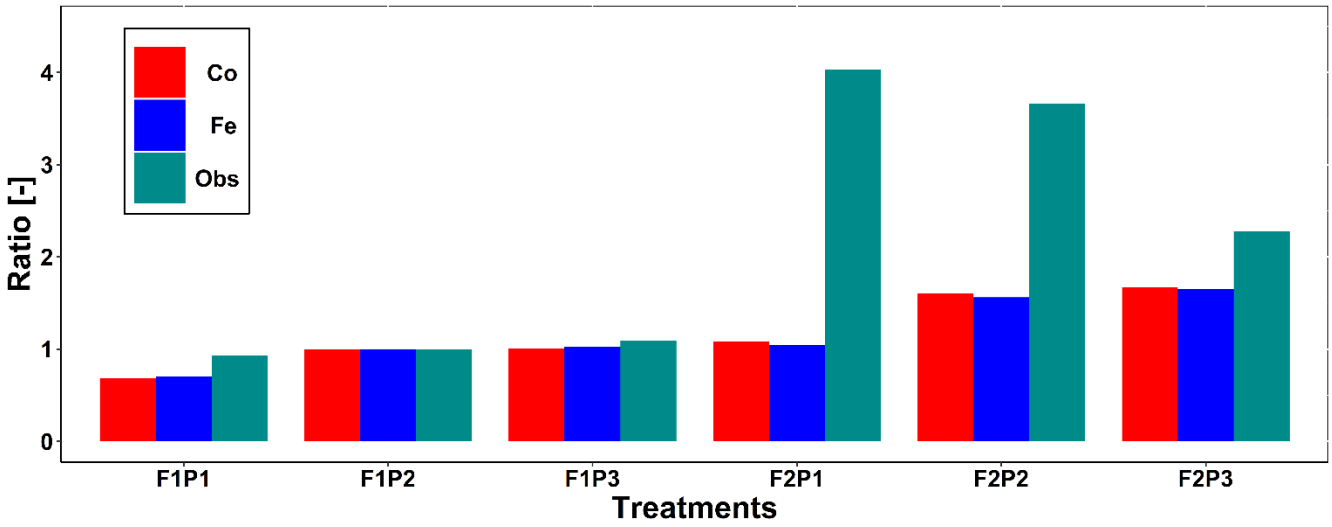

Appendix 2F: Comparison ratio of the observed total root length from minirhizotubes to observed total root length from F1P2 (green line with squares) and ratio of simulated total root length to the simulated total root length from F1P2 on 11 July 2016 (DOY 193) from Couvreur (Co, solid red, dots), and Feddes (Fe, solid blue, triangles) model at the sheltered (P1), rainfed (P2), and irrigated (P3) plots of the stony soil (F1) and the silty soil (F2)

Appendix 2G: Statistic RMSEs of soil water content simulated by the two models: the Couvreur (Co) and Feddes (Fe) in the sheltered (P1), rainfed (P2), and irrigated (P3) plots of the stony soil (F1), and the silty soil (F2). RMSE is $cm^3\,cm^{-3}$

		F1		F2	
	Depth (cm)	Co	Fe	Co	Fe
P1	10	0.09	0.09	0.08	0.08
	20	0.08	0.08	0.06	0.05
	40	0.04	0.04	0.07	0.07
	60	0.07	0.07	0.03	0.03
	80	0.08	0.08	0.03	0.03
	120	0.03	0.03	0.06	0.05
P2	10	0.10	0.10	0.09	0.08
	20	0.10	0.10	0.07	0.07
	40	0.06	0.06	0.07	0.06
	60	0.06	0.06	0.05	0.05
	80	0.05	0.04	0.06	0.06
	120	0.06	0.06	0.06	0.05
P3	10	0.11	0.12	0.10	0.11
	20	0.12	0.12	0.08	0.08
	40	0.08	0.08	0.09	0.08
	60	0.07	0.07	0.06	0.05
	80	0.05	0.06	0.06	0.06
	120	0.03	0.03	0.07	0.07

Appendix 3A: List of main variables used in the photosynthesis models and their units

Variables	Explanation	Unit
VCMAX	Maximum carboxylation rate	μM m^{-2} s^{-1}
J_{max}	Maximum electron transport rate	μM electrons m^{-2}
J	Electron transport rate	μM electrons m^{-2}
C_a	Atmospheric CO_2 concentration	μM mol^{-1}
C_i	Intercellular CO_2 concentration	μM mol^{-1}
C_m	Mesophyll CO_2 concentration	μM mol^{-1}
C_{bs}	Bundle-sheath CO_2 concentration	μM mol^{-1}
O2	Atmospheric O_2 concentration	mM mol^{-1}
rCiCa	Ratio of intercellular CO_2 to atmospheric CO_2 concentration	(-)
g_{bd}	Boundary layer conductance	m s^{-1}
g_s	Stomatal conductance	mol m^{-2} s^{-1}
g_{bs}	Bundle-sheath conductance to CO_2	mM m^{-2} s^{-1}
g_m	Mesophyll conductance to CO_2	mol m^{-2} s^{-1}
g_0	Residual stomatal conductance when irradiance approaches zero	mol m^{-2} s^{-1}
α_m	Fraction relates stomatal conductance and mesophyll	(-)
DS	Leaf to air vapor pressure deficit (VPD)	kPa
D_0	Parameters reflect the sensitivity of stomatal conductance to VPD	kPa
Γ^*	CO_2 compensation point in the absence of day respiration	μM mol^{-1}
a_1	Empirical coefficient relates photosynthesis and stomatal	(-)
R_d	Day respiration rate	μM m^{-2} s^{-1}
R_m	Mesophyll mitochondrial respiration rate	μM m^{-2} s^{-1}
KMC	Michaelis-Menten constant for CO_2	μM mol^{-1}
KMO	Michaelis-Menten constant for O_2	mM mol^{-1}
EAVCMX	Energy activation for maximum carboxylation rate	J mol^{-1}
A_n	Net photosynthesis rate	μM m^{-2} s^{-1}
A_c	Rubisco activity limited net photosynthesis rate	μM m^{-2} s^{-1}
A_j	RuBp limited photosynthesis rate	μM m^{-2} s^{-1}
L_{bs}	Rate of CO_2 leakage from bundle-sheath to mesophyll	μM m^{-2} s^{-1}
V_p	The PEP carboxylation rate	μM m^{-2} s^{-1}
V_{pmax}	The maximum PEP carboxylation rate	μM m^{-2} s^{-1}
K_p	The Michaelis-Menten constant for CO_2 of PEP	μM mol^{-1}
V_{pr}	The PEP regeneration rate	μM m^{-2} s^{-1}
I_2	The absorbed irradiance	μM m^{-2} s^{-1}
θ	Empirical curvature parameter of hyperbolic function	(-)
fwat	Water stress index	(-)

Appendix 3B: Description of photosynthesis approach for maize (C_4)

The CO_2 transfers along the path from atmospheric CO_2 concentration (C_a) to intercellular CO_2 concentration (C_i) according to Fick's law of diffusion:

$$C_i = C_a - A_n\left(\frac{1}{g_{bd}} + \frac{1}{g_s}\right) \quad \text{(C1)}$$

Where C_a and C_i are atmospheric and intercellular CO_2 concentration (μmol mol^{-1}). The $1/g_{bd}$ and $1/g_s$ are boundary layer resistance and stomatal resistance, respectively. The width of sunlit and shaded maize leaves was assumed 0.01 m and their boundary layer resistance were computed following (Campbell and Norman, 1998):

$$\frac{1}{g_{bd}} = 300\sqrt{0.01/u} \quad \text{(C2)}$$

Where u is wind speed (m s^{-1}). Air diffusion from intercellular space to mesophyll cell is given:

$$C_m = C_i - A_n/g_m \quad \text{(C3)}$$

In addition to stomatal conductance, the non-stomatal limitations (here mesophyll conductance) appear to be co-regulated under water stress (Flexas et al., 2004). Stomatal conductance and internal conductance (or mesophyll conductance) were both proportionally decreased under soil water deficit (Warren, 2008). In our work, due to the absence of detailed data, we assumed g_m is proportional to g_s, namely $g_m = \alpha_m * g_s$. The proportionality differed among species that α_m is ranging from 0.77 to 2.31 (Ouyang et al., 2017; Warren, 2008).

Stomatal conductance was simulated based on the Leuning approach (Leuning, 1995) with consideration of water stress (fwat), the effect of leaf to air vapor pressure deficit ($1+ DS/D_0$), intercellular CO_2 concentration (C_i), Γ^* is CO_2 compensation point in the absence of day respiration (R_d).

$$g_s = g_0 + \frac{a_1 A_n}{(C_i - \Gamma^*)(1 + \frac{DS}{D_0})} fwat \quad \text{(C4)}$$

Following the approach from Farquhar et al., (1980) and von Caemmerer, (2000), the Rubisco limited rate of photosynthesis rate is given by

$$A_c = \frac{VCMAX(\ C_{bs} - \Gamma^*)}{C_{bs} + KMC\left(1 + \frac{O2}{KMO}\right)} fwat - R_d \quad \text{(C5)}$$

Where C_{bs} and O_2 are the CO_2 and O_2 concentration at the site of photosynthesis activities which is bundle sheath cell in maize; VCMAX is the maximum catalytic activity of Rubisco at leaf temperature; Γ^* is CO_2 compensation point at the absence of R_d; KMC and KMO are Michaelis-Menten kinetics for CO_2 and O_2.

The photosynthesis can be limited by the RuBp regeneration rate which is driven by ATP and NAPDH that supplied by the electron transport rate J. The rate of RuBp-limited CO_2 assimilation was computed by:

$$A_j = J\frac{C_{bs} - \Gamma^*}{4.5C_{bs} + 10.5\Gamma^*} - R_d \quad \text{(C6)}$$

Where C_{bs} is the CO_2 concentration at the bundle sheath cell. The electron transport J was estimated based on the absorbed irradiance (I_2), empirical curvature parameter of hyperbolic function (θ) (von Caemmerer, 2000):

$$J = \frac{I_2 + J_{max} + \sqrt{(I_2 + J_{max})^2 - 4\theta I_2 J_{max}}}{2\theta} \quad \text{(C7)}$$

The leaf net photosynthesis (A_n) was the function of both A_c and A_j

$$A_n = \min(A_c, A_j) \quad \text{(C8)}$$

C_4 photosynthesis involves both the mesophyll and bundle sheath cells of the leaves which characterized a high CO_2 concentrating mechanism that allows Rubisco at this location to fix CO_2. This process inhibits the oxygenation reaction and reduces the photorespiration rate. The supply of CO_2 due to the PEP carboxylation (V_p) can be formulated as a function of CO_2 assimilation (A), the rate of CO_2 leakage from bundle-sheath to mesophyll (L_{bs}), and mitochondrial respiration (R_m).

$$V_p = \mathrm{A} + L_{bs} + R_m \quad \text{(C9)}$$

The rate of PEP carboxylation (V_p) is given by a Michaelis-Menten equation (von Caemmerer, 2000):

$$V_p = \min\left(\frac{C_m V_{pmax}}{C_m + K_p}, V_{pr}\right) \quad \text{(C10)}$$

Where C_m is CO_2 concentration in the mesophyll; V_{pmax} is the maximum PEP carboxylation rate and K_p is the Michaelis-Menten constant for CO_2; V_{pr} is a constant and upper-bound PEP regeneration rate (von Caemmerer, 2000).

The CO_2 leakage from bundle-sheath cell back to the mesophyll cell was driven by the CO_2 concentration gradient difference and the conductance (g_{bs}) between them:

$$L_{bs} = g_{bs}(C_{bs} - C_m) \quad \text{(C11)}$$

Appendix 3C: Cumulative precipitation and irrigation (Prec+Irri), simulated potential evapotranspiration (ETP), potential transpiration (T_p), and actual transpiration (RWU or T_a)

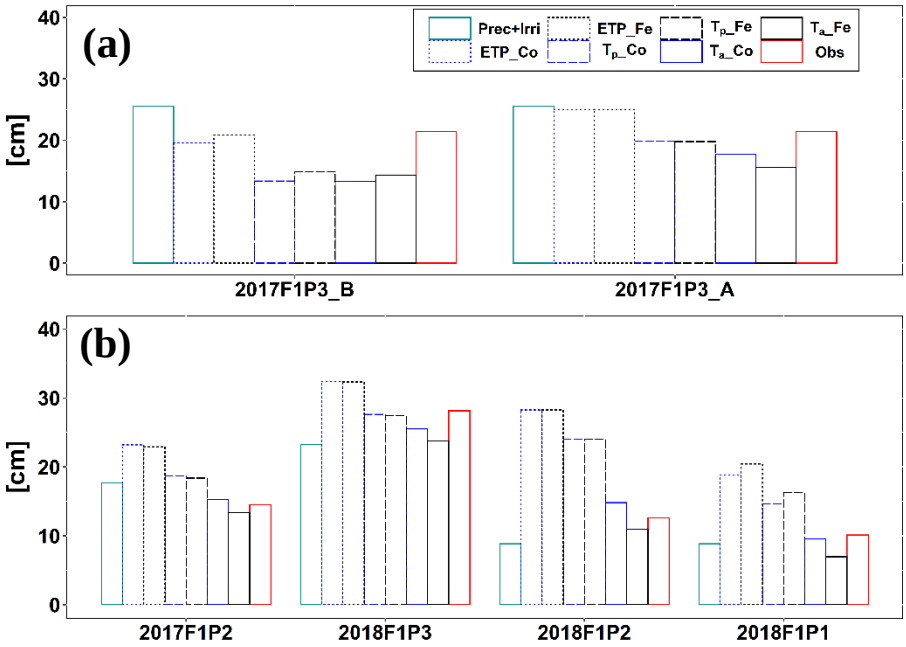

Appendix 3C. Cumulative precipitation and irrigation (Prec+Irri), simulated potential evapotranspiration (ETP), potential transpiration (T_p), and actual transpiration (RWU or T_a) by Couvreur (Co) and Feddes (Fe), and measured transpiration by sap flow sensors (Obs) (a) at the irrigated plot in 2017 (2017F1P3) for before calibration (2017F1P3_B) and after calibration (2017F1P3_A) and (b) at the rainfed plot in 2017 (2017R1), the irrigated plot with normal sowing date (2018F1P3), rainfed with normal sowing date (2018F1P2) and rainfed plot with late sowing date (2018F1P1). Data was shown from 08 July to harvest 12 September in 2017, while it was from 29 June to 21 August in 2018.

Appendix 3D: Comparison between simulated from the Couvreur (Co) and Feddes (Fe) RWU models and observed dry biomass (kg m^{-2}) at harvest before and after modeling calibration for 2017F1P3 and modeling validation for 2017F1P2, 2018F1P3, 2018F1P2, and 2018F1P1 treatments (cf. Fig. 3.1 and Table 3.2).

	2017F1P3		2017F1P2	2018F1P3	2018F1P2	2018F1P1
	Before calibration	After calibration	Validation			
Measured	1.884 (0.199)		1.656 (0.231)	2.045 (0.137)	0.880 (0.121)	0.580 (0.198)
Simulated Co	0.895	1.875	1.711	1.492	1.025	0.574
Simulated Fe	0.969	1.649	1.320	1.371	0.728	0.337

Numbers in the brackets indicate the standard deviation of 7 measured replicates.

Appendix 3E

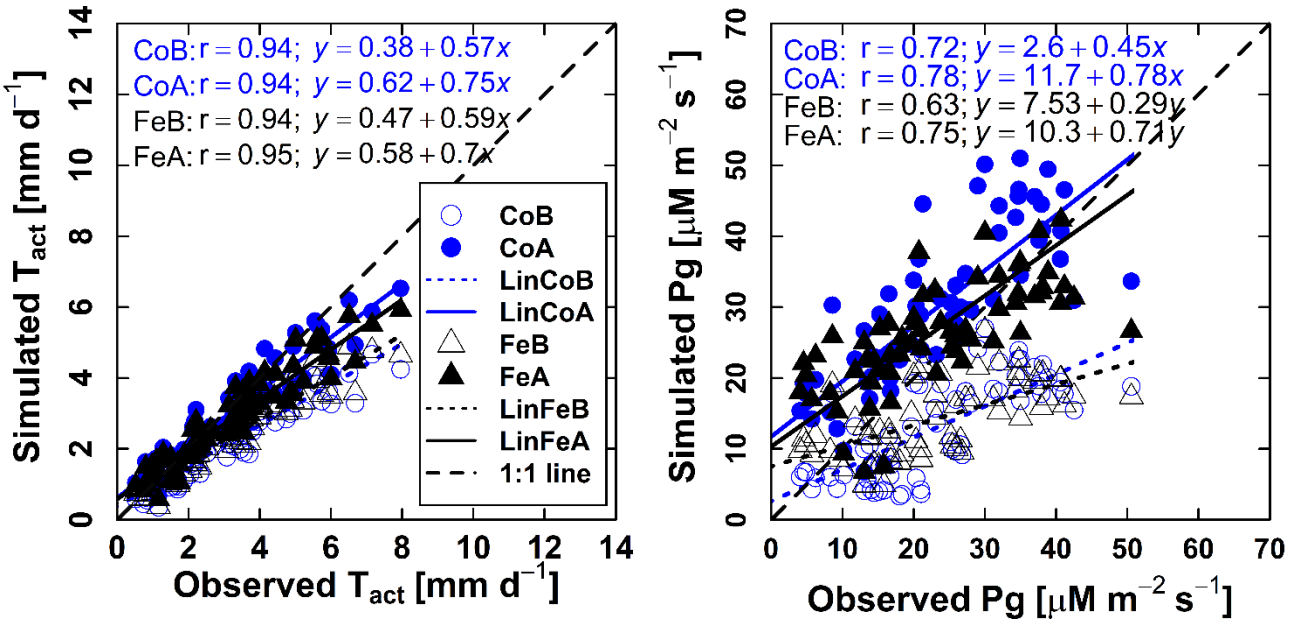

Appendix 3E: Correlation of simulated and observed (a) daily transpiration (RWU or T_a) and (b) gross photosynthesis rate (Pg) from Couvreur model before and after calibration (CoB and CoA, respectively), Feddes before and after calibration (FeB and FeA, respectively) at the irrigated plot in 2017 (2017F1P3). The black dashed lines are 1:1 lines. The solid and dotted lines are the linear regressions lines between simulated and observed data from two models before and after calibration (LinCoB, LinCoA, LinFeB, and LinFeA).

Appendix 3F: Root mean square error (RMSE, $cm^3\ cm^{-3}$), coefficient of correlation (r), and agreement index (I) of soil water content before and after modeling calibration for 2017F1P3 and modeling validation for 2017F1P2, 2018f1P3, 2018F1P2, and 2018F1P1 treatments (cf. Fig. 3.1 and Table 3.2). * means the overall performance of the model from all validated plots (2017F1P2, 2018F1P3, 2018F1P2, and 2018F1P1).

		Before Calibration		After calibration		Validation									
		2017F1P3				2017F1P2		2018F1P3		2018F1P2		2018F1P1		Overall*	
Depth (cm)		Co	Fe	Co	Fe	Co	Fe	Co	Fe	Co	Fe	Co	Fe	Co	Fe
10	RMSE	0.033	0.047	0.038	0.051	0.052	0.051	0.028	0.028	0.038	0.039	0.037	0.033	0.039	0.038
	r	0.7	0.67	0.7	0.68	0.8	0.78	0.9	0.92	0.87	0.84	0.88	0.94	0.86	0.87
	I	0.67	0.65	0.69	0.64	0.76	0.75	0.94	0.94	0.92	0.91	0.92	0.94	0.89	0.89
	n	74	74	74	74	75	75	90	90	90	90	113	113	368	368
20	RMSE	0.036	0.033	0.03	0.035	0.03	0.027	0.055	0.051	0.034	0.021	0.046	0.028	0.041	0.032
	r	0.63	0.73	0.73	0.75	0.95	0.93	0.79	0.81	0.93	0.97	0.9	0.97	0.89	0.92
	I	0.66	0.8	0.8	0.8	0.93	0.94	0.83	0.83	0.96	0.98	0.92	0.97	0.91	0.93
	n	74	74	74	74	57	57	89	89	90	90	114	114	350	350
40	RMSE	0.038	0.022	0.026	0.024	0.047	0.037	0.042	0.033	0.047	0.037	0.057	0.048	0.048	0.039
	r	0.66	0.87	0.85	0.9	0.98	0.96	0.89	0.93	0.96	0.98	0.96	0.99	0.95	0.97
	I	0.52	0.82	0.73	0.81	0.65	0.71	0.83	0.88	0.84	0.89	0.77	0.82	0.77	0.83
	n	74	74	74	74	60	60	90	90	90	90	114	114	354	354
60	RMSE	0.015	0.044	0.032	0.046	0.039	0.036	0.027	0.029	0.032	0.026	0.015	0.01	0.028	0.025
	r	0.89	0.46	0.67	0.49	0.97	0.97	0.98	0.98	0.93	0.94	0.98	0.98	0.97	0.97
	I	0.87	0.48	0.61	0.48	0.69	0.7	0.94	0.93	0.89	0.92	0.97	0.98	0.87	0.88
	n	73	73	73	73	74	74	84	84	90	90	114	114	362	362
80	RMSE	0.048	0.06	0.055	0.061	0.036	0.033	0.02	0.022	0.03	0.028	0.049	0.045	0.034	0.032
	r	0.12	0.24	0.19	0.23	0.42	0.4	0.98	0.98	0.96	0.96	0.96	0.97	0.83	0.83
	I	0.38	0.36	0.37	0.36	0.59	0.58	0.94	0.93	0.84	0.84	0.59	0.62	0.74	0.74
	n	73	73	73	73	69	69	89	89	90	90	114	114	362	362
120	RMSE	0.024	0.027	0.025	0.027	0.052	0.051	0.008	0.007	0.037	0.038	0.014	0.012	0.028	0.027
	r	-0.68	-0.64	-0.65	-0.63	0.31	0.3	0.95	0.95	0.91	0.88	0.92	0.92	0.77	0.76
	I	0.03	0.08	0.06	0.08	0.36	0.36	0.97	0.97	0.61	0.58	0.8	0.85	0.69	0.69
	n	74	74	74	74	75	75	88	88	90	90	112	112	365	365

Appendix 3G: Simulated whole plant hydraulic conductance in different water treatments and sowing dates

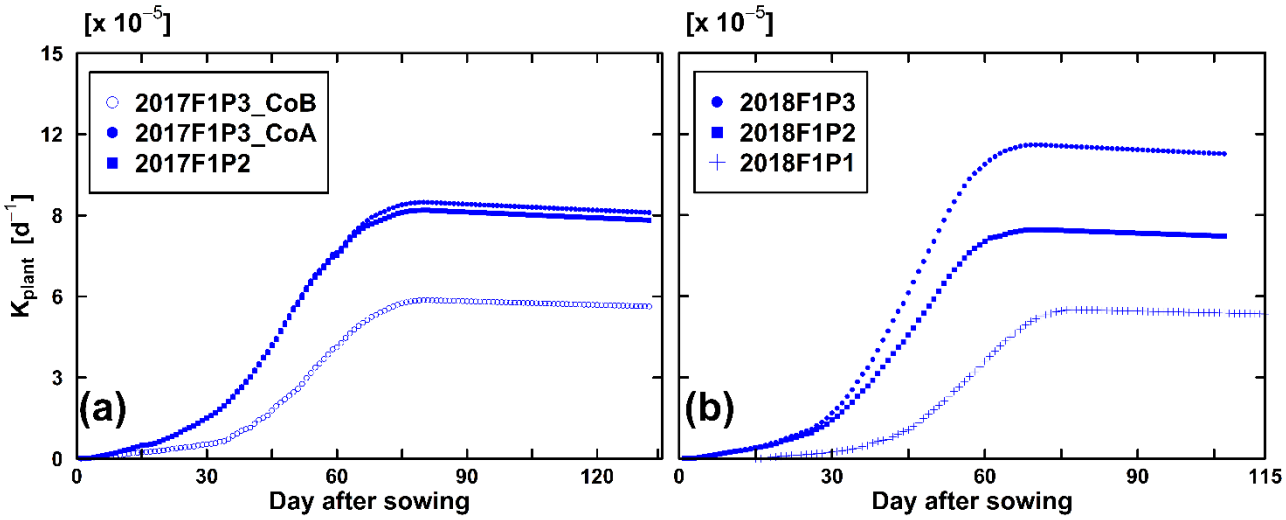

Appendix 3G: Comparison of simulated whole plant hydraulic conductance (K_{plant}) by Couvreur model (Co) from sowing to harvest in different water treatments (a) in 2017 seasons and (b) in 2018. Two plots in 2017 are the irrigated plot – 2017F1P3 and rainfed plot – 2017F1P2. Three plots in 2018 are the irrigated plot with normal sowing date – 2018F1P3, rainfed plot with normal sowing date – 2018F1P2, and rainfed plot with late sowing date – 2018F1P1 (Table 3.2 and Fig. 3.1). The K_{plant} from 2017F1P3 was from Couveur before calibration (CoB) and Couveur after calibration (CoA). The K_{plant} from the validated treatments (2017F1P2, 2018F1P3, 2018F1P2, and 2018F1P1) based on the calibrated parameters (see Table 3.3).

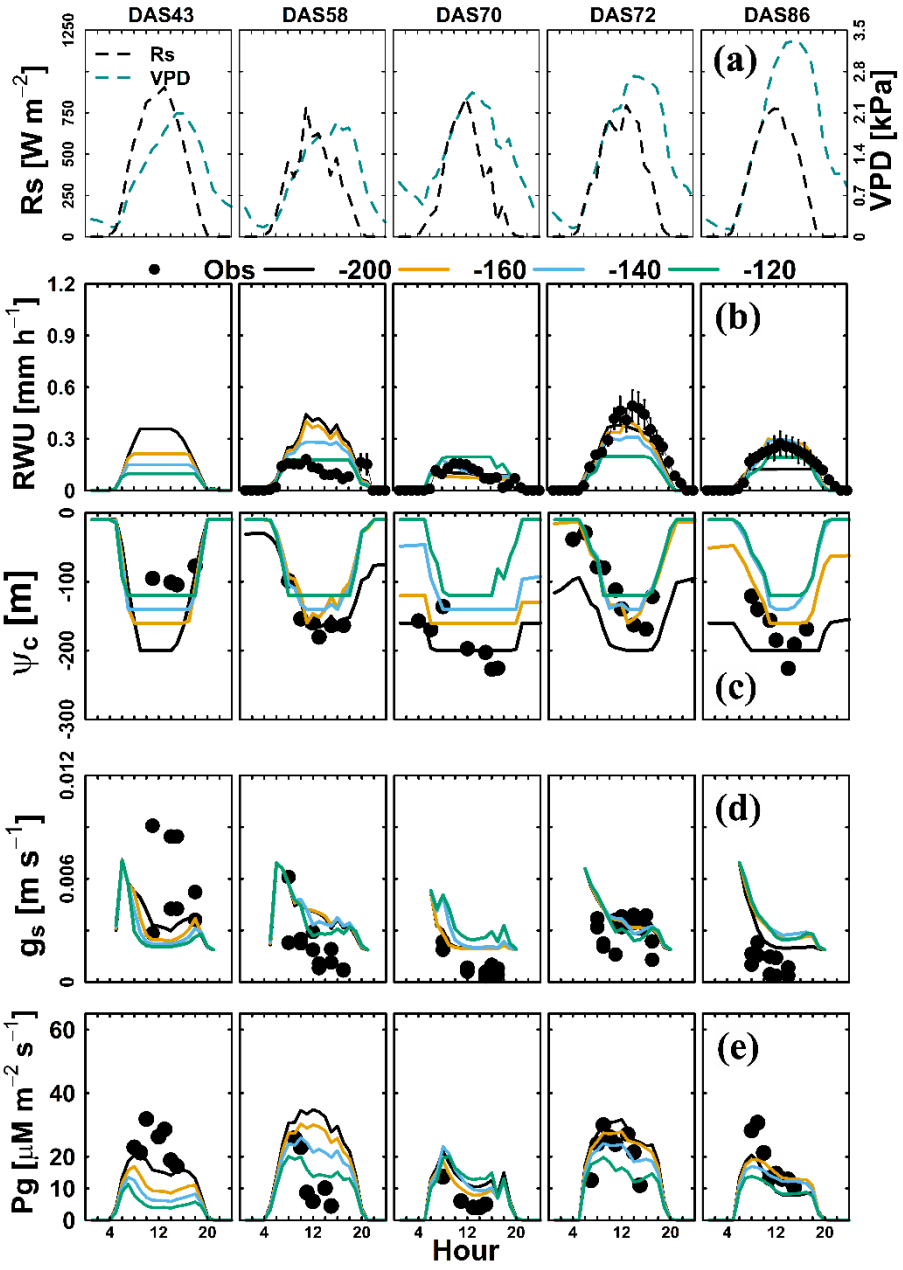

Appendix 3H: Diurnal course of observed data (black dots) and the simulated output from Couvreur model when $\Psi_{thresholds}$ are changing, -200 m (black lines), -160 m (yellow lines), -140 m (blue lines), and -120 m (green lines) of 5 selected days: 20 June (DAS 43), 05 July (DAS 58), 17 July (DAS 70), 19 July (DAS 72), and 02 August 2018 (DAS 86) (a) global radiation (Rs, black dash line) and vapor pressure deficit (VPD, cyan dash line) (b) actual transpiration (RWU or T_a), (c) canopy hydraulic head (ψ_c), (d) stomatal conductance to water vapor (g_s), and (e) gross assimilation rate (Pg) in 2018 with normal sowing date at the rainfed plot (2018F1P2). Sap flow sensors were installed on 29 June 2018. Simulated stomatal conductance are from sunlit leaves. Measurements in DAS 70 and DAS 72 were done from predawn and before and after irrigation, respectively. Vertical black bars in (b) represent the standard deviation of the flux measurements in the different stems. All simulations used the parameter set after calibration (see Table 3.3).

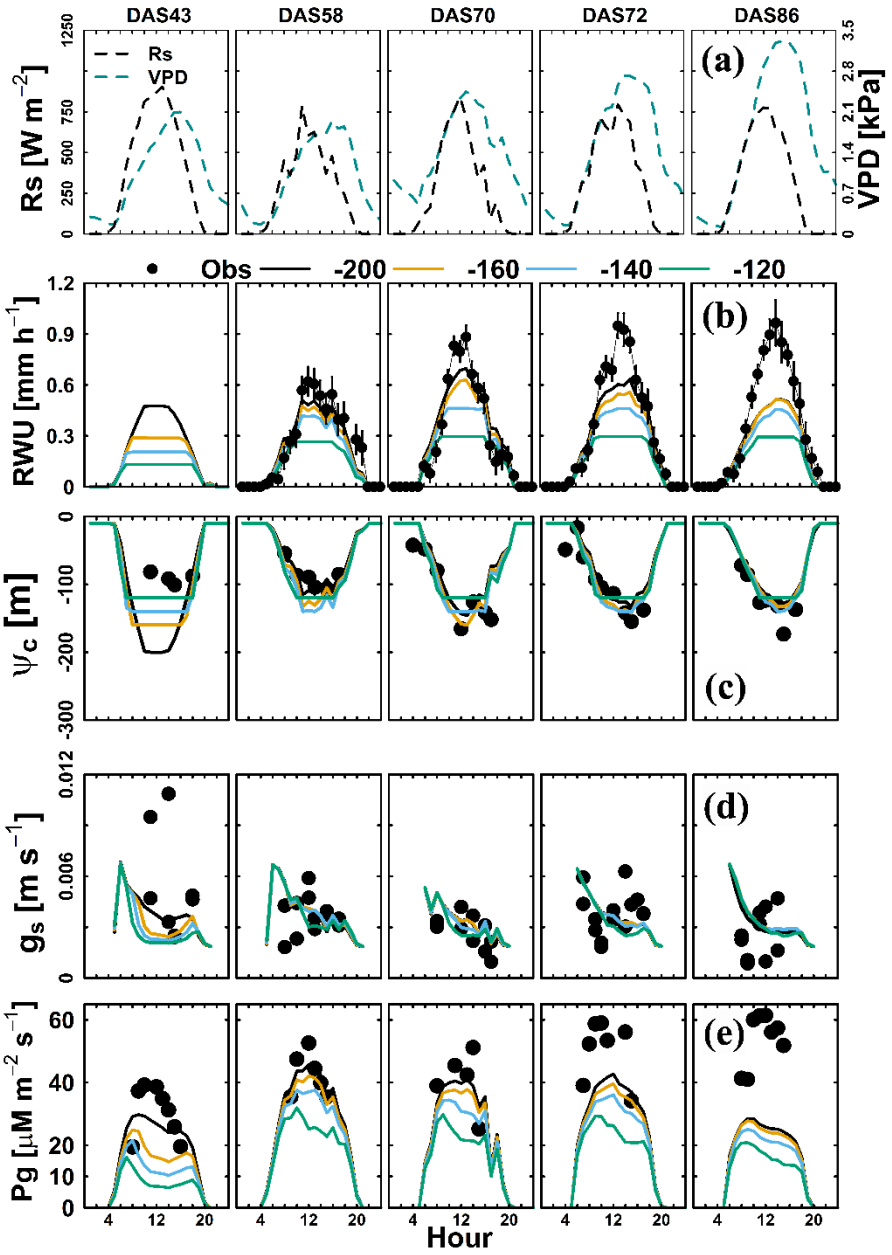

Appendix 3I: Diurnal course of observed (black dots) and the simulated output from Couvreur model when $\Psi_{thresholds}$ are changing, -200 m (black lines), -160 m (yellow lines), -140 m (blue lines), and -120 m (green lines) of 5 selected days: 20 June (DAS 43), 05 July (DAS 58), 17 July (DAS 70), 19 July (DAS 72), and 02 August 2018 (DAS 86) (a) global radiation (Rs, black dash line) and vapor pressure deficit (VPD, cyan dash line) (b) actual transpiration (RWU or T_a), (c) canopy hydraulic head (ψ_c), (d) stomatal conductance to water vapor (g_s), and (e) gross assimilation rate (Pg) in 2018 with normal sowing date at the irrigated plot (2018F1P3). Sap flow sensors were installed on 29 June 2018. Simulated stomatal conductance are from sunlit leaves. Measurements in DAS 70 and DAS 72 were done from predawn and before and after irrigation, respectively. Vertical black bars in (b) represent the standard deviation of the flux measurements in the different stems. All simulations used the parameters after calibration (see Table 3.3).

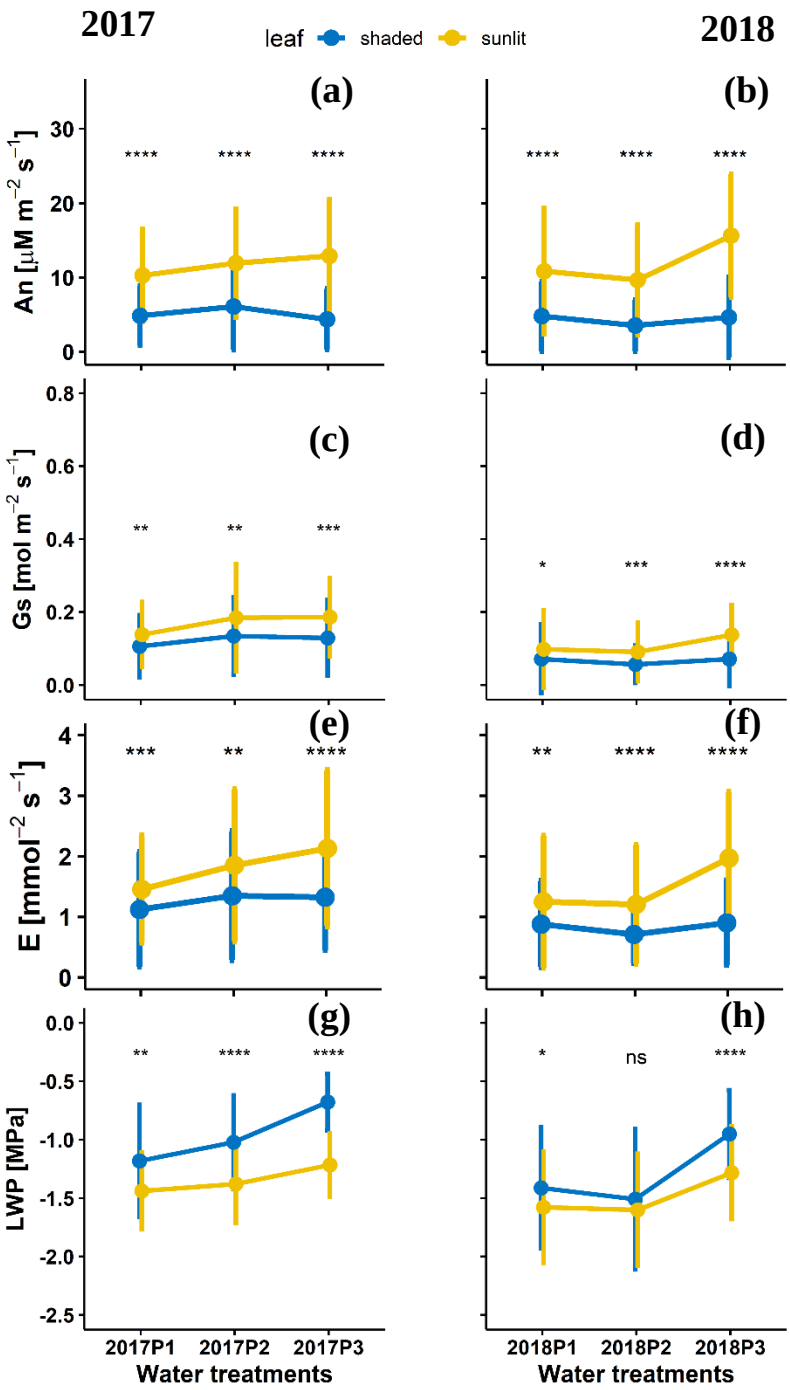

Appendix 4A: Comparison the means from all measured days and hours for shaded leaves (blue color) and sunlit leaves (yellow color) of four variables: (a-b) net photosynthesis (An), (c-d) stomatal conductance to water vapor (Gs), (e-f) transpiration rate (E), and (g-h) leaf water potential (LWP). The left panel refers to maize in 2017 at the two rainfed plots (2017P1 and 2017P2), and irrigated plot (2017P3). The right panel refers to maize in 2018 at the rainfed plot with late sowing date 2018P1, rainfed plot with normal sowing date (2018P2) and irrigated plot with normal sowing date (2018P3) (cf. Table 4.1). Error bars indicate standard deviation of population with n = 42 and 79 measured shaded and sunlit leaves, respectively for each treatment in 2017 while n = 83 and 177 measured shaded and sunlit leaves, respectively for each treatment in 2018. The symbol ns (non-

significant), *, **, ***, and **** indicate the results of T-test with P-value > 0.05, P-value ≤ 0.05, P value ≤ 0.01, P-value ≤ 0.001, and P-value ≤ 0.0001, respectively.

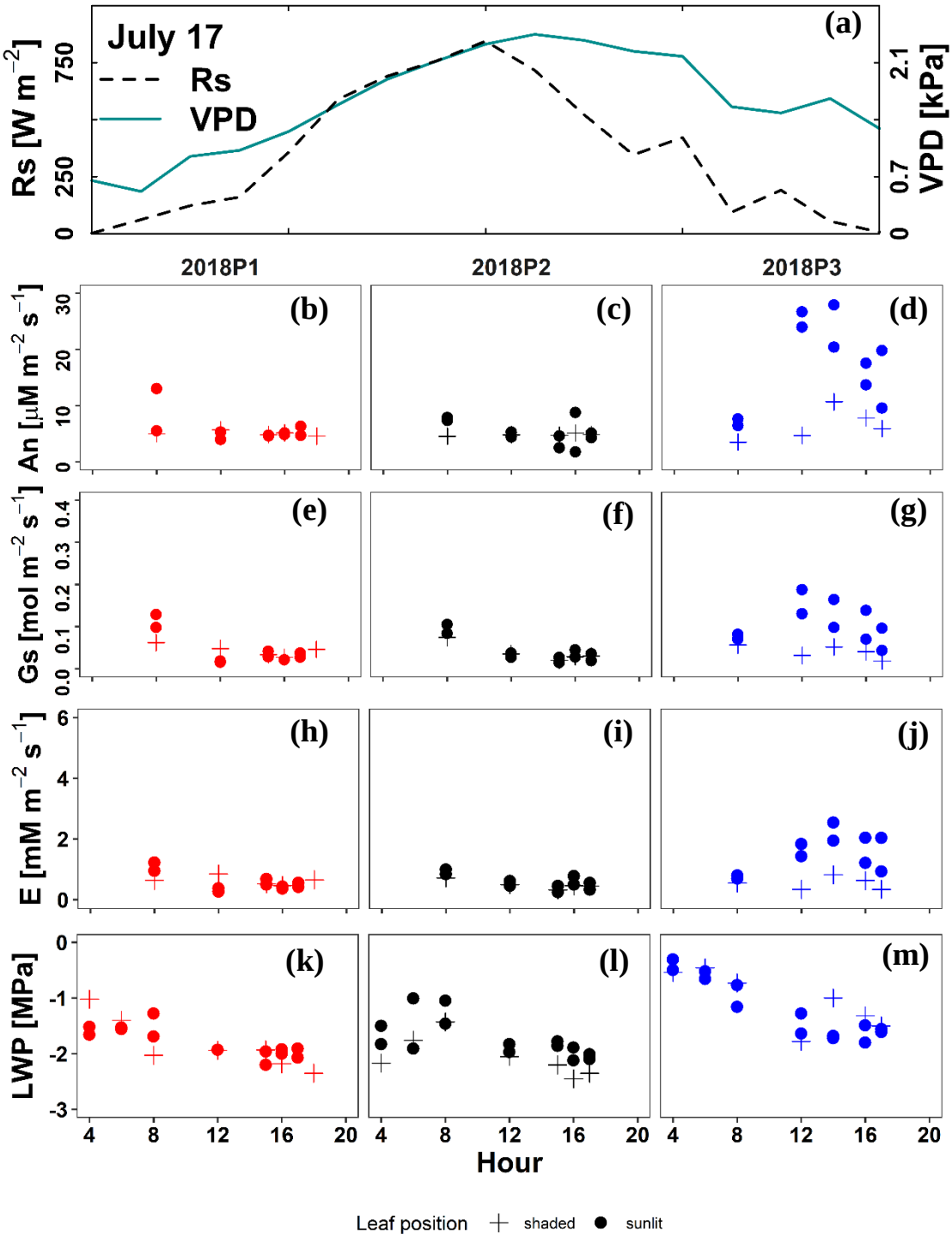

Appendix 4B: Diurnal course of (a) global radiation (Rs) and vapor pressure deficit (VPD), (b, c, d) leaf net photosynthesis (An), (e, f, g) leaf stomatal conductance (Gs), (h, i, j) leaf transpiration (E), and (k, l, m) leaf water potential (LWP) measured on July 17 in maize in 2018 before irrigation at the rainfed plot with late sowing date (2018P1– red), rainfed plot with normal sowing date (2018P2 – black), and irrigated plot with normal sowing date (2018P3 – blue) (cf. Table 4.1). Measurement was carried out from shaded leaves (plus symbol) and two sunlit leaves (solid dots).

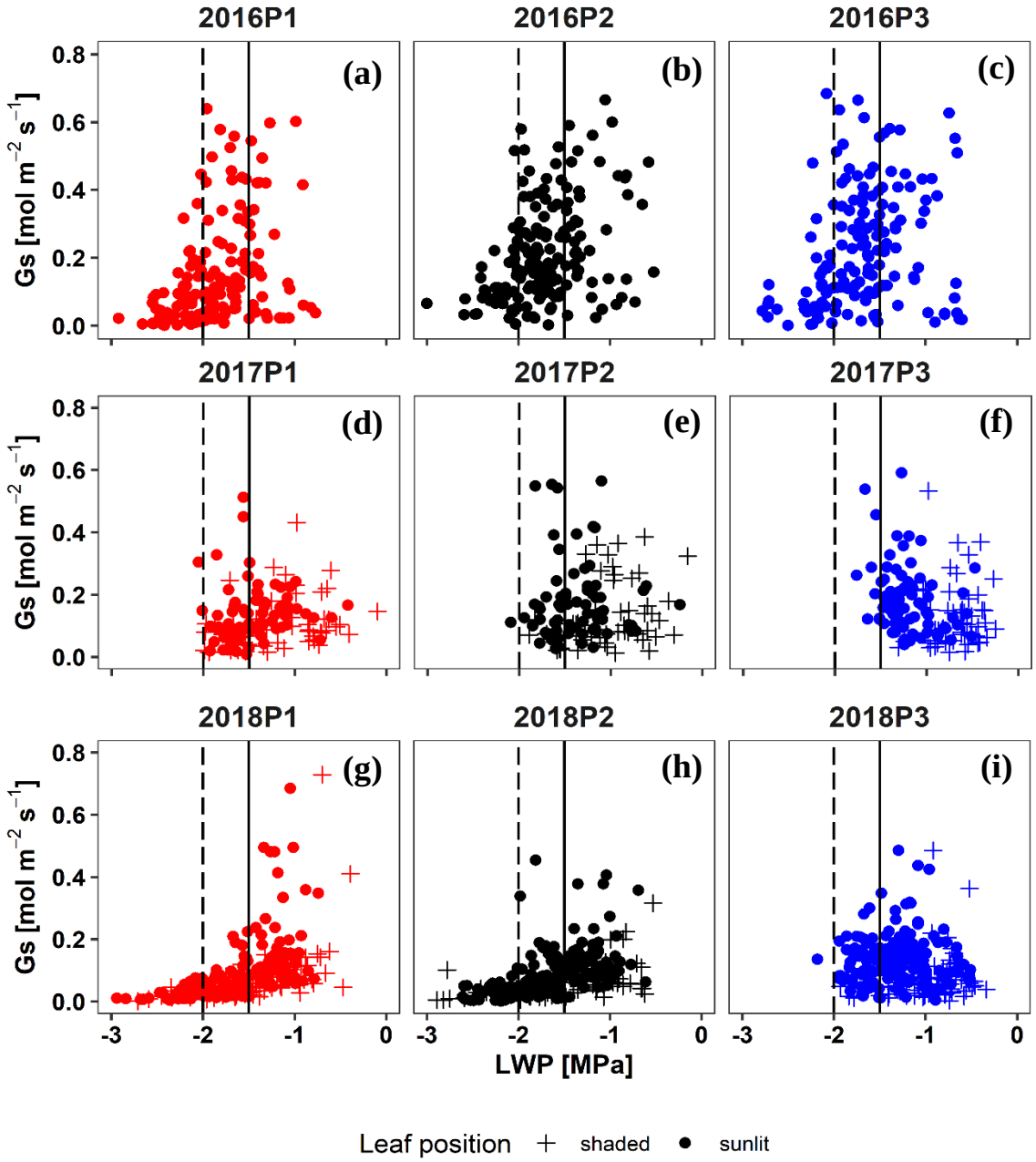

Appendix 4C: Seasonal stomatal conductance to water vapor (Gs) versus leaf water potential (LWP) of different water treatments in (a-b-c) winter wheat in 2016 at the sheltered plot (2016P1 – red), rainfed plot (2016P2 – black dots), and irrigated plot (2016P3 – blue), (d-e-f) in maize in 2017 at the two rainfed plots (2017P1 – red and 2017P2 – black), and irrigated plot (2017P3 – blue), and (g-h-i) in maize 2018 at the rainfed plot with late sowing date 2018P1– red, rainfed plot with normal sowing date (2018P2 – black) and irrigated plot with normal sowing date (2018P3 – blue) (cf. Table 4.1). Vertically continuous and dashed lines indicated LWP at -1.5 and -2 MPa, respectively. Measurement was carried out 3-4 upmost fully developed leaves in 2016, while measurement was carried out from shaded leaf (plus symbol) and two sunlit leaves (solid dots).

References

Abd Allah AA. 2009. Genetic studies on leaf rolling and some root traits under drought conditions in rice (Oryza sativa L.). African Journal of Biotechnology, 6241–6248.

Abrecht DG, Carberry PS. 1993. The influence of water deficit prior to tassel initiation on maize growth, development and yield. Field Crops Research 31, 55–69.

Addiscott, T. M. and Whitmore, A. P.: Simulation of solute in soil leaching of differing permeabilities, Soil Use Manag., 7(2), 94–102, 1991.

Adiredjo, A.L., O. Navaud, T. Lamaze, and P. Grieu. 2014. Leaf carbon isotope discrimination as an accurate indicator of water-use efficiency in sunflower genotypes subjected to five stable soil water contents. J. Agron. Crop Sci. 200(6): 416–424. doi: 10.1111/jac.12079.

Ahmadi, S.H., M.N. Andersen, R.T. Poulsen, F. Plauborg, and S. Hansen. 2009. A quantitative approach to developing more mechanistic gas exchange models for field grown potato: A new insight into chemical and hydraulic signalling. Agric. For. Meteorol. 149(9): 1541–1551. doi: 10.1016/j.agrformet.2009.04.009.

Ahmed, M. A., Zarebanadkouki, M., Meunier, F., Javaux, M., Kaestner, A., & Carminati, A. (2018). Root type matters: Measurement of water uptake by seminal, crown, and lateral roots in maize. Journal of Experimental Botany, **69**(5), 1199– 1206. doi.org/10.1093/jxb/erx439

Allen, R. G., Pereira, L. S., Raes, D. and Smith, M.: FAO Irrigation and Drainage Paper - Crop Evapotranspiration, 1998.

Amanullah, M.J. Hassan, K. Nawab, and A. Ali. 2007. Response of Specific Leaf Area (SLA), Leaf Area Index (LAI) and Leaf Area Ratio (LAR) of Maize (Zea mays L .) To Plant Density , Rate and Timing of Nitrogen Application. World Appl. Sci. J. 2(3): 235–243.

Aparicio-Tejo P, Boyer JS. 1983. Significance of Accelerated Leaf Senescence at Low Water Potentials for Water Loss and Grain Yield in Maize1. Crop Science 23, cropsci1983.0011183X002300060040x.

Aroca R. 2012. *Plant responses to water stress from morphological to molecular features* (R Aroca, Ed.). Springer-Verlag Berlin Heidelberg.

Attia Z, Domec J-C, Oren R, Way DA, Moshelion M. 2015. Growth and physiological responses of isohydric and anisohydric poplars to drought. Journal of Experimental Botany.

Baldocchi D. 1994. A comparative study of mass and energy exchange rates over a closed C3 (wheat) and an open C4 (corn) crop: II. CO2 exchange and water use efficiency. Agricultural and Forest Meteorology 67, 291–321.

Ball, J.T., I.E. Woodrow, and J.A. Berry. 1987. A Model Predicting Stomatal Conductance and its Contribution to the Control of Photosynthesis under Different Environmental Conditions. Prog. Photosynth. Res. (953): 221–224. doi: citeulike-article-id:8423355.

Baret, F., S. Madec, K. Irfan, J. Lopez, A. Comar, et al. 2018. Leaf-rolling in maize crops : from leaf scoring to canopy-level measurements for phenotyping. J. Exp. Bot. 69(10): 2705–2716. doi: 10.1093/jxb/ery071.

Bates LM, Hall AE. 1981. Stomatal closure with soil water depletion not associated with changes in Bulk leaf water status. Oecologia 50, 62–65.

Bourgault M, Webber HA, Chenu K, *et al.* 2020. Early vigour in wheat: Could it lead to more severe terminal drought stress under elevated atmospheric [CO2] and semi-arid conditions? Global Change Biology 26, 4079–4093.

Braghiere, R.K., F. Gérard, J.B. Evers, C. Pradal, and L. Pagès. 2020. Simulating the effects of water limitation on plant biomass using a 3D functional-structural plant model of shoot and root driven by soil hydraulics. Ann. Bot. 126(4): 713–728. doi: 10.1093/aob/mcaa059.

Brisson N, Casals M-L. 2005. Leaf dynamics and crop water status throughout the growing cycle of durum wheat crops grown in two contrasted water budget conditions. Agronomy for Sustainable Development 25, 151–158.

Brodersen, C.R., A.B. Roddy, J.W. Wason, and A.J. McElrone. 2019. Functional Status of Xylem Through Time. Annu. Rev. Plant Biol. 70: 407–433. doi: 10.1146/annurev-arplant-050718-100455.

Bronstert, A. and Plate, E. J.: Modelling of runoff generation and soil moisture dynamics for hillslopes and micro-catchments, J. Hydrol., 198(1–4), 177–195, doi:10.1016/S0022-1694(96)03306-9, 1997.

Buckley, T.N., K.A. Mott, and G.D. Farquhar. 2003. A hydromechanical and biochemical model of stomatal conductance. Plant, Cell Environ. 26: 1767–1786.

Buras A, Rammig A, Zang CS. 2020. Quantifying impacts of the 2018 drought on European ecosystems in comparison to 2003. , 1655–1672.

Caemmerer, S. Von, and R.T. Furbank. 2003. The C4 pathway : an efficient CO2 pump. Photosynth. Res. (77): 191–207.

Cai G, Vanderborght J, Langensiepen M, Schnepf A, Hüging H, Vereecken H. 2018. Root growth, water uptake, and sap flow of winter wheat in response to different soil water conditions. Hydrology and Earth System Sciences 22, 2449–2470.

Cai, G., A. Carminati, M. Abdalla, and M.A. Ahmed. 2021. Soil textures rather than root hairs dominate water uptake and soil-plant hydraulics under drought. Plant Physiol. (2008): 1–15. doi: 10.1093/plphys/kiab271.

Cai, G., J. Vanderborght, A. Klotzsche, J. van der Kruk, J. Neumann, et al. 2016. Construction of Minirhizotron Facilities for Investigating Root Zone Processes. Vadose Zo. J. 15(9): 0. doi: 10.2136/vzj2016.05.0043.

Cai, G., J. Vanderborght, V. Couvreur, C.M. Mboh, and H. Vereecken. 2017a. Parameterization of Root Water Uptake Models Considering Dynamic Root Distributions and Water Uptake Compensation. Vadose Zo. J. 0(0): 0. doi: 10.2136/vzj2016.12.0125.

Cai, Q., Y. Zhang, Z. Sun, J. Zheng, W. Bai, et al. 2017b. Morphological plasticity of root growth under mild water stress increases water use efficiency without reducing yield in maize. Biogeosciences 14(16): 3851–3858. doi: 10.5194/bg-14-3851-2017.

Çakir R. 2004. Effect of water stress at different development stages on vegetative and reproductive growth of corn. Field Crops Research 89, 1–16.

Campbell, G.S., and J.M. Norman. 1998. An introduction to environmental biophysics (J.M. Norman, editor). 2. ed. Springer, New York u.a. Last access on 01.03. 2016

Carminati, A., and M. Javaux. 2020. Soil Rather Than Xylem Vulnerability Controls Stomatal Response to Drought. Trends Plant Sci. 25(9): 868–880. doi: 10.1016/j.tplants.2020.04.003.

Carminati, A., Vetterlein, D., Weller, U., Vogel, H.-J. and Oswald, S. E.: When Roots Lose Contact, Vadose Zo. J., 8(3), 805–809, doi:10.2136/vzj2008.0147, 2009.

Champeyroux, C., J. Bellati, M. Barberon, V. Rofidal, C. Maurel, et al. 2019. Regulation of a plant aquaporin by a Casparian strip membrane domain protein-like. Plant. Cell Environ. 42(6): 1788–1801. doi: https://doi.org/10.1111/pce.13537.

Chaves MM, Maroco JP, Pereira JS. 2003. Understanding plant responses to drought — from genes to whole plant. Functional Plant Biology 30, 239–264.

Chaves MM, Pereira JS, Maroco J, Rodrigues ML, Ricardo CPP, Osório ML, Carvalho I, Faria T, Pinheiro C. 2002. How plants cope with water stress in the field. Photosynthesis and growth. Annals of Botany 89, 907–916.

Chi, Y., P. Yang, S. Ren, N. Ma, J. Yang, et al. 2020. Effects of fertilizer types and water quality on carbon dioxide emissions from soil in wheat-maize rotations. Sci. Total Environ. 698: 134010. doi: 10.1016/j.scitotenv.2019.134010.

Christmann, A., E. Grill, and J. Huang. 2013. Hydraulic signals in long-distance signaling. Curr. Opin. Plant Biol. 16(3): 293–300. doi: 10.1016/j.pbi.2013.02.011.

Christmann, A., E.W. Weiler, E. Steudle, and E. Grill. 2007. A hydraulic signal in root-to-shoot signalling of water shortage. Plant J. 52(1): 167–174. doi: 10.1111/j.1365-313X.2007.03234.x.

Chunfang, W., M.T. Tyree, and E. Steudle. 1999. Direct measurement of xylem pressure in leaves of intact maize plants. A test of the cohesion-tension theory taking hydraulic architecture into consideration. Plant Physiol. 121(4): 1191–1205. doi: 10.1104/pp.121.4.1191.

Cochard H. 2002. Xylem embolism and drought-induced stomatal closure in maize. Planta 215, 466–471.

Collatz, G.J., M. Ribas-Carbó, and J.A. Berry. 1992. Coupled photosynthesis-stomatal conductance model for leaves of C4 plants. Aust. J. plant Physiol. 19: 519–538.

Colombi, T., Kirchgessner, N., Walter, A. and Keller, T.: Root Tip Shape Governs Root Elongation Rate under, , 174(August), 2289–2301, doi:10.1104/pp.17.00357, 2017.

Coupel-Ledru, A., É. Lebon, A. Christophe, A. Doligez, L. Cabrera-Bosquet, et al. 2014. Genetic variation in a grapevine progeny (Vitis vinifera L. cvs GrenachexSyrah) reveals inconsistencies between maintenance of daytime leaf water potential and response of transpiration rate under drought. J. Exp. Bot. 65(21): 6205–6218. doi: 10.1093/jxb/eru228.

Couvreur, V., J. Vanderborght, X. Draye, and M. Javaux. 2014b. Dynamic aspects of soil water availability for isohydric plants: Focus on root hydraulic resistances. water Resour. Res. 50: 8891–8906. doi: 10.1002/2014WR015608.Received.

Couvreur, V., Vanderborght, J. and Javaux, M.: A simple three-dimensional macroscopic root water uptake model based on the hydraulic architecture approach, Hydrol. Earth Syst. Sci., 16, 2957–2971, doi: 10.5194/hess-16-2957-2012, 2012b.

Couvreur, V., Vanderborght, J., Beff, L. and Javaux, M.: Horizontal soil water potential heterogeneity: Simplifying approaches for crop water dynamics models, Hydrol. Earth Syst. Sci., 18(5), 1723–1743, doi:10.5194/hess-18-1723-2014, 2014.

Damour, G., T. Simonneau, H. Cochard, and L. Urban. 2010. An overview of models of stomatal conductance at the leaf level. Plant, Cell Environ. 33(9): 1419–1438. doi: 10.1111/j.1365-3040.2010.02181.x.

Daryanto, S., L. Wang, and P. Jacinthe. 2016. Global Synthesis of Drought Effects on Maize and Wheat Production. PLoS One 11(5): 1–15. doi: 10.1371/journal.pone.0156362.

Davies WJ, Zhang J. 1991. Drying soil regulation of growth and development of plants in drying soil. Annual review of plant physiology and Plant Molecular biology 42, 55–76.

de Jong van Lier, Q., van Dam, J. C., Metselaar, K., de Jong, R. and Duijnisveld, W. H. M.: Macroscopic Root Water Uptake Distribution Using a Matric Flux Potential ApproachAll rights reserved. No part of this periodical may be reproduced or transmitted in any form or by any means, electronic or mechanical, including photocopying, recording, or , Vadose Zo. J., 7(3), 1065–1078 [online] Available from: http://dx.doi.org/10.2136/vzj2007.0083, 2008.

de Moraes, M.T., H. Debiasi, J.C. Franchini, J. de A. Bonetti, R. Levien, et al. 2019. Mechanical and Hydric Stress Effects on Maize Root System Development at Different Soil Compaction Levels. Front. Plant Sci. 10(October): 1–18. doi: 10.3389/fpls.2019.01358.

De Pury, D.G.G., and G.D. Farquhar. 1997. Simple scaling of photosynthesis from leaves to canopies without the errors of big-leaf models. Plant, Cell Environ. 20(5): 537–557. doi: 10.1111/j.1365-3040.1997.00094.x.

Desborough, C.: The impact of root weighting on the response of transpiration to moisture stress in land surface schemes, Mon. Weather Rev., (1994), 1920–1930, doi:10.1175/1520-0493(1997)125<1920:TIORWO>2.0.CO;2, 1997.

Dewar, R.C. 2002. The Ball-Berry-Leuning and Tardieu-Davies stomatal models: Synthesis and extension within a spatially aggregated picture of guard cell function. Plant, Cell Environ. 25(11): 1383–1398. doi: 10.1046/j.1365-3040.2002.00909.x.

Dickinson, R. E., Henderson-Sellers, A., Rosenzweig, C. and Sellers, P. J.: Evapotranspiration models with canopy resistance for use in climate models, a review, Agric. For. Meteorol., 54(2–4), 373–388, doi:10.1016/0168-1923(91)90014-H, 1991.

Ding, L., T. Milhiet, V. Couvreur, H. Nelissen, A. Meziane, et al. 2020. Modification of the expression of the aquaporin ZmPIP2;5 affects water relations and plant growth. Plant Physiol. 182(4): 2154–2165. doi: 10.1104/PP.19.01183.

Dodd, I.C., G. Egea, C.W. Watts, and W.R. Whalley. 2010. Root water potential integrates discrete soil physical properties to influence ABA signalling during partial rootzone drying. J. Exp. Bot. 61(13): 3543–3551. doi: 10.1093/jxb/erq195.

Domec J, Johnson DM. 2012. Does homeostasis or disturbance of homeostasis in minimum leaf water potential explain the isohydric versus anisohydric behavior of Vitis vinifera L . cultivars ? Tree 32, 245–248.

Domec, J., and M.L. Pruyn. 2008. Bole girdling affects metabolic properties and root , trunk and branch hydraulics of young ponderosa pine trees. Tree Physiol. (28): 1493–1504.

Du, Y., Q. Zhao, L. Chen, X. Yao, W. Zhang, et al. 2020. Effect of drought stress on sugar metabolism in leaves and roots of soybean seedlings. Plant Physiol. Biochem. 146(October 2019): 1–12. doi: 10.1016/j.plaphy.2019.11.003.

Dunbabin, V. M., Postma, J. A., Schnepf, A., Pagès, L., Javaux, M., Wu, L., Leitner, D., Chen, Y. L., Rengel, Z. and Diggle, A. J.: Modelling root-soil interactions using three-dimensional models of root growth, architecture and function, Plant Soil, 372(1–2), 93–124, doi:10.1007/s11104-013-1769-y, 2013.

Dynamax. 2005. Dynagage sap flow sensors manual. 1–107. Last access on March 5th 2015.

Earl HJ, Davis RF. 2003. Effect of Drought Stress on Leaf and Whole Canopy Radiation Use Efficiency and Yield of Maize. Agronomy Journal 95, 688–696.

Egea, G., Verhoef, A. and Vidale, P. L.: Towards an improved and more flexible representation of water stress in coupled photosynthesis-stomatal conductance models, Agric. For. Meteorol., 151(10), 1370–1384, doi:10.1016/j.agrformet.2011.05.019, 2011.

Enders, A., Diekkrüger, B., Laudien, R., Gaiser, T., Bareth, G., 2010. The IMPETUS Spatial Decision Support Systems, in: Speth, P., Christoph, M., Diekkrüger, Bernd (Es.), Impacts of Global Change on the Hydrological Cycle in West and Northwest Africa. Springer Berlin Heidelberg, Berlin, Heidelberg, pp. 360–393.

Ewert, F., Rodriguez, D., Jamieson, P. D., Semenov, M. A., Mitchell, R. A. C., Goudriaan, J., Porter, J. R., Kimball, B. A., Pinter Jr., P, J., Manderscheid, R., Weigel, H. J., Fangmeier, A., Fereres, E. and Villalobos, F.: Effects of elevated CO2 and drought on wheat: testing crop simulation models for different experimental and climatic conditions, Agric. Ecosyst. Environ, 93(1–3), 249–266, 2002.

Fang, H., F. Baret, S. Plummer, and G. Schaepman-Strub. 2019. An Overview of Global Leaf Area Index (LAI): Methods, Products, Validation, and Applications. Rev. Geophys. 57(3): 739–799. doi: 10.1029/2018RG000608.

Faria, R. T. De, Madramootoo, C. A., Boisvert, J. and Prasher, S. O.: Comparison of the versatile soil moisture budget and SWACROP models for a wheat crop in Brazil, Can. Agric. Eng., 36(2), 57–68, 1994.

Farquhar, G. D. and Caemmerer, S. Von: Modelling of Photosynthetic Response to Environmental Conditions, in Physiological Plant Ecology II, edited by O. L. Lange, pp. 550–582, Springer-Verlag Berlin Heidelberg., 1982.

Farquhar, G.D., S. Von Caemmerer, and J.A. Berry. 1980. A biochemical model of photosynthetic CO2 assimilation in leaves of C3 species. Planta 90: 78–90. doi: 10.1007/BF00386231.

Fatichi, S., D. Or, R. Walko, H. Vereecken, M.H. Young, et al. 2020. Soil structure is an important omission in Earth System Models. Nat. Commun. 11(1). doi: 10.1038/s41467-020-14411-z.

Feddes, R. A. and Raats, P. A. C.: Parameterizing the soil - water - plant root system, in Wageningen Frontis Series, vol. 6, pp. 95–141. [online] Available from: citeulike-article-id:4285297%5Cnhttp://209.85.173.132/search?q=cache:9fgslcr1dlgJ:library.wur.nl/frontis/unsaturated/04_feddes.pdf+Parameterizing+the+soil+?+water+?+plant+root+system&#38%5Cncd=1&%2338%5Cnhl=en&%2338%5Cnct=clnk&%2338%5Cngl=us&%2338%5Cnclient=firef, 2004.

Feddes, R. A., Hoff, H., Bruen, M., Dawson, T., De Rosnay, P., Dirmeyer, P., Jackson, R. B., Kabat, P., Kleidon, A., Lilly, A. and Pitman, A. J.: Modeling root water uptake in hy drological and climate models, Bull. Am. Meteorol. Soc., 82(12), 2797–2809, doi:10.1175/1520-0477(2001)082<2797:MRWUIH>2.3.CO;2, 2001.

Feddes, R.A., and P.A.C. Raats. 2004. Parameterizing the soil - water - plant root system. Wageningen Frontis Series. p. 95–141

Feddes, R.A., P.J. Kowalik, and H. Zaradny. 1978. Simulation of Field Water Use and Crop Yield. Wiley.

Fernandez D, Castrillo M. 1999. Maize Leaf Roling Initiation. Photosynthetica 37, 493–497.

Flexas, J., J. Bota, F. Loreto, G. Cornic, and T.D. Sharkey. 2004. Diffusive and metabolic limitations to photosynthesis under drought and salinity in C3 plants. Plant Biol. 6(3): 269–279. doi: 10.1055/s-2004-820867.

Franks PJ, Drake PL, Froend RH. 2007. Anisohydric but isohydrodynamic: Seasonally constant plant water potential gradient explained by a stomatal control mechanism incorporating variable plant hydraulic conductance. Plant, Cell and Environment 30, 19–30.

Gallardo, M., Eastham, J., Gregory, P. J. and Turner, N. C.: A comparison of plant hydraulic conductances in wheat and lupins, J. Exp. Bot., 47(295), 233–239, doi:10.1093/jxb/47.2.233, 1996.

Gallé Á, Csiszár J, Benyó D, Laskay G, Leviczky T, Erdei L, Tari I. 2013. Isohydric and anisohydric strategies of wheat genotypes under osmotic stress : Biosynthesis and function of ABA in stress responses. Journal of Plant Physiology 170, 1389–1399.

Gambetta, G.A., T. Knipfer, W. Fricke, and A.J. McElrone. 2017. Aquaporins and Root Water Uptake BT - Plant Aquaporins: From Transport to Signaling. In: Chaumont, F. and Tyerman, S.D., editors. Springer International Publishing, Cham. p. 133–153

Gao, Q., P. Zhao, X. Zeng, X. Cai, and W. Shen. 2002. A model of stomatal conductance to quantify the\rrelationship between leaf transpiration, microclimate and\rsoil water stress. Plant, Cell Environ. 25: 1373–1381.

Gayler, S., Ingwersen, J., Priesack, E., Wöhling, T., Wulfmeyer, V. and Streck, T.: Assessing the relevance of subsurface processes for the simulation of evapotranspiration and soil moisture dynamics with CLM3.5: Comparison with field data and crop model simulations, Environ. Earth Sci., 69(2), 415–427, doi: 10.1007/s12665-013-2309-z, 2013.

Geijn SC va. de, Goudriaan J. 1996. The Effects of Elevated CO2 and Temperature Change on Transpiration and Crop Water Use. Global climate change and agricultural production, 101–121.

Ghannoum O. 2009. C4 photosynthesis and water stress. Annals of Botany 103, 635–644.

González, M.G., T.B. Ramos, R. Carlesso, P. Paredes, M.T. Petry, et al. 2015. Modelling soil water dynamics of full and deficit drip irrigated maize cultivated under a rain shelter. Biosyst. Eng. 132: 1–18. doi: 10.1016/j.biosystemseng.2015.02.001.

Goudriaan, J. and van Laar, H. H.: Modelling potential crop growth processes. Textbook with exercises, 1994.

Gowing, D.J.G., W.J. Davies, and H. Jones. 1990. A Positive Root-sourced Signal as an Indicator of Soil Drying in Apple, Malus x domestica Borkh.

Grave S, Piepho H-P, Selzer L. 2019. Package ‘multcompView’ Title Visualizations of Paired Comparisons.

Groh, J., E. Diamantopoulos, X. Duan, F. Ewert, M. Herbst, et al. 2020a. Crop growth and soil water fluxes at erosion-affected arable sites: Using weighing lysimeter data for model intercomparison. Vadose Zo. J. 19(1): 1–18. doi: 10.1002/vzj2.20058.

Groh, J., J. Vanderborght, T. Putz, H.-J. Vogel, R. Gruendling, et al. 2020b. Responses of soil water storage and crop water use efficiency to changing climatic conditions: a lysimeter-based space-for-time approach. Hydrol. EARTH Syst. Sci. 24(3): 1211–1225. doi: 10.5194/hess-24-1211-2020.

Guo, J.S., K.R. Hultine, G.W. Koch, H. Kropp, and K. Ogle. 2020. Temporal shifts in iso/anisohydry revealed from daily observations of plant water potential in a dominant desert shrub. New Phytol. 225(2): 713–726. doi: 10.1111/nph.16196.

Gutschick, V.P., and T. Simonneau. 2002. Modelling stomatal conductanceof field-grown sunflower under varying soil water content and leafenvironment: comparison of three models of stomatal response toleaf environment and coupling with an abscisic acid-based modelof stomatal response to soil dryi. Plant. Cell Environ. 25(11): 1423–1434. doi: doi:10.1046/j.1365-3040.2002.00937.x.

Hammer, G.L., Z. Dong, G. McLean, A. Doherty, C. Messina, et al. 2009. Can changes in canopy and/or root system architecture explain historical maize yield trends in the U.S. corn belt? Crop Sci. 49(1): 299–312. doi: 10.2135/cropsci2008.03.0152.

Hartzell, S., M.S. Bartlett, and A. Porporato. 2017. The role of plant water storage and hydraulic strategies in relation to soil moisture availability. Plant Soil 419(1–2): 503–521. doi: 10.1007/s11104-017-3341-7.

Hay, R.K.M., and J.R. Porter. 2006. The Physiology of Crop Yield. 2nd ed. Wiley-Blackwell.

He, K., Y. Yang, Y. Yang, S. Chen, Q. Hu, et al. 2017. HYDRUS simulation of sustainable brackish water irrigation in a winter wheat-summer maize rotation system in the North China Plain. Water (Switzerland) 9(7). doi: 10.3390/w9070536.

Heckathorn SA, Delucia EH. 1991. and Leaf Rolling in Grasses. 152, 263–268.

Heinlein, F., C. Biernath, C. Klein, C. Thieme, and E. Priesack. 2017. Evaluation of Simulated Transpiration from Maize Plants on Lysimeters. Vadose Zo. J. 16(1): vzj2016.05.0042. doi: 10.2136/vzj2016.05.0042.

Henson IE, Jensen CR, Turner NC. 1989. Leaf Gas Exchange and Water Relations of Lupins and Wheat_III_acid absisic and drought indeuced stomata closure. Australian Journal Plant Physiology 16, 429–442.

Henzler, T., Waterhouse, R. N., Smyth, a. J., Carvajal, M., Cooke, D. T., a.R., S., Steudle, E. and Clarkson, D. T.: Diurnal varia- tions in hydraulic conductivity and root pressure can be corre- lated with the expression of putative aquaporins in the roots of Lotus japonicus, Planta, C(210), 50–60, 1999.

Herbrich, M., H.H. Gerke, and M. Sommer. 2018. Root development of winter wheat in erosion-affected soils depending on the position in a hummocky ground moraine soil landscape. J. Plant Nutr. Soil Sci. 181(2): 147–157. doi: 10.1002/jpln.201600536.

Hernandez-ramirez, G., Lawrence-smith, E. J., Sinton, S. M., Schwen, A. and Brown, H. E.: Root Responses to Alterations in Macroporosity and Penetrability in a Silt Loam Soil, doi:10.2136/sssaj2014.01.0005, 2014.

Hirasawa, T., and T.C. Hsiao. 1999. Some characteristics of reduced leaf photosynthesis at midday in maize growing in the field. F. Crop. Res. 62(1): 53–62. doi: 10.1016/S0378-4290(99)00005-2.

Hochberg U, Degu A, Fait A, Rachmilevitch S. 2013. Near isohydric grapevine cultivar displays higher photosynthetic efficiency and photorespiration rates under drought stress as compared with near anisohydric grapevine cultivar. Physiologia Plantarum 147, 443–452.

Hochberg U, Rockwell FE, Holbrook NM, Cochard H. 2018. Iso/Anisohydry: A Plant–Environment Interaction Rather Than a Simple Hydraulic Trait. Trends in Plant Science 23, 112–120.

Hsiao, T. C.: Plant responses to water stress, Annu. Rev. Plant Physiol. Plant Mol. Biol., 24, 519–570, 1973.

Huang, B. R., Taylor, H. M. and McMichael, B. L.: Growth and development of seminal and crown roots of wheat seedlings as affected by temperature, Environ. Exp. Bot., 31(4), 471–477, doi: 10.1016/0098-8472(91)90046-Q, 1991.

Huber K, Vanderborght J, Javaux M, Schröder N, Dodd I, Vereecken H. 2014. Modelling the impact of heterogeneous rootzone water distribution on the regulation of transpiration by hormone transport and/or hydraulic pressures. Plant and Soil, 93–112.

Huntingford, C., D.M. Smith, W.J. Davies, R. Falk, S. Sitch, et al. 2015. Combining the [ABA] and net photosynthesis-based model equations of stomatal conductance. Ecol. Modell. 300: 81–88. doi: 10.1016/j.ecolmodel.2015.01.005.

Innes P, Blackwell RD, Austin RB, Ford MA. 1981. The effects of selection for number of ears on the yield and water economy of winter wheat. The Journal of Agricultural Science 97, 523–532.

IPCC. 2007. Intergovernmental Panel on Climate Change. Fourth Assessment Report. Geneva, Switzerland: Inter-gov- ernmental Panel on Climate Change. Cambridge; UK: Cambridge University Press; 2007. Available from: www. ipcc.ch.

Irmak, S. and Mutiibwa, D.: On the dynamics of canopy resistance : Generalized linear estimation and relationships with primary micrometeorological variables, Water Resour. Res., 46, 1–20, doi:10.1029/2009WR008484, 2010.

J. Šimůnek, M. Šejna, H. Saito, M. Sakai, and M.T. van Genuchten. 2009. The HYDRUS-1D Software Package for Simulating the One-Dimensional Movement of Water, Heat, and Multiple Solutes in Variably-Saturated Media. Version 4.08 January 2009. CALIFORNIA.

Jamieson, P. D. and Ewert, F.: The role of roots in controlling soil water extraction during drought : an analysis by simulation, F. Crop. Res., 60, 267–280, 1999.

Janott, M., Gayler, S., Gessler, A., Javaux, M., Klier, C. and Priesack, E.: A one-dimensional model of water flow in soil-plant systems based on plant architecture, Plant Soil, (341), 233–256, doi:10.1007/s11104-010-0639-0, 2011.

Javot, H. and Maurel, C.: The role of aquaporins in root water uptake, Ann. Bot., 90(3), 301–313, doi:10.1093/aob/mcf199, 2002.

Jensen, C.R., H. Svendsen, M.N. Andersen, and R. L??sch. 1993. Use of the root contact concept, an empirical leaf conductance model and pressure-volume curves in simulating crop water relations. Plant Soil 149(1): 1–26. doi: 10.1007/BF00010759.

Jones HG. 1998. Stomatal control of photosynthesis and transpiration. Journal of Experimental Botany 49, 387–398.

Jones JW, Zur B, Bennett JM. 1986. Interactive effects of water and nitrogen stresses on carbon and water vapor exchange of corn canopies. Agricultural and Forest Meteorology 38, 113–126.

Jones, H.G. 1992. Plants and Microclimate: A Quantitative Approach to Environmental Plant Physiology. Cambridge University Press.

Jones, H.G., and R.A. Sutherland. 1991. Stomatal control of xylem embolism. Plant Cell Environ. 14(April): 607–612.

Kadioglu A, Terzi R. 2007. A Dehydration Avoidance Mechanism : Leaf Rolling Das Einrollen von Blättern als Schutz vor Austrocknung Zusammenfassung. The Botanical Review 73, 290–302.

Kage, H., Kochler, M. and Stützel, H.: Root growth and dry matter partitioning of cauliflower under drought stress conditions: Measurement and simulation, Eur. J. Agron., 20(4), 379–394, doi: 10.1016/S1161-0301(03)00061-3, 2004.

Katerji, N., Rana, G. and Fahed, S.: Parameterizing canopy resistance using mechanistic and semi-empirical estimates of hourly evapotranspiration : critical evaluation for irrigated crops in the Mediterranean, Hydrol. Process, 129(August 2010), 117–129, doi:10.1002/hyp.7829, 2011.

Keeley JE., Rundel PW. 2003. Evolution of CAM and C4 Carbon - Concentrating Mechanisms. International Journal of Plant Sciences 164, 54–77.

Kelliher, F. M., Leuning, R., Raupach, M. R. and Schulze, E. D.: Maximum conductances for evaporation from global vegetation types, Agric. For. Meteorol., 73(1–2), 1–16, doi:10.1016/0168-1923(94)02178-M, 1995.

Kirkham MB. 2005. 8 - Field Capacity, Wilting Point, Available Water, and the Non-Limiting Water Range. In: Kirkham MB, ed. Principles of Soil and Plant Water Relations. Burlington: Academic Press, 101–115.

Klein T. 2014. The variability of stomatal sensitivity to leaf water potential across tree species indicates a continuum between isohydric and anisohydric behaviours. Functional Ecology, 1313–1320.

Klotzsche, A., L. Lärm, J. Vanderborght, G. Cai, S. Morandage, et al. 2019. Monitoring Soil Water Content Using Time-Lapse Horizontal Borehole GPR Data at the Field-Plot Scale. Vadose Zo. J. 18(1): 190044. doi: 10.2136/vzj2019.05.0044.

Koebernick, N., S. Schlüter, S.R.G.A. Blaser, and D. Vetterlein. 2018. Root-soil contact dynamics of Vicia faba in sand. Plant Soil 431(1–2): 417–431. doi: 10.1007/s11104-018-3769-4.

Kramer, P. J. and Boyer, J. S.: Water Relations of Plants and Soils, Academic press, Inc. [online] Available from: http://udspace.udel.edu/handle/19716/2830, 1995.

Kucharik, C.J., and K.R. Brye. 2003. Integrated BIosphere Simulator (IBIS) yield and nitrate loss predictions for Wisconsin maize receiving varied amounts of nitrogen fertilizer. J. Environ. Qual. 32(1): 247–268. doi: 10.2134/jeq2003.2470.

Kupisch M, Stadler A, Langensiepen M, Ewert F. 2015. Analysis of spatio-temporal patterns of CO2 and H2O fluxes in relation to crop growth under field conditions. Field Crops Research 176, 108–118.

Lacube, S., L. Manceau, C. Welcker, E.J. Millet, B. Gouesnard, et al. 2020. Simulating the effect of flowering time on maize individual leaf area in contrasting environmental scenarios. J. Exp. Bot. 71(18): 5577–5588. doi: 10.1093/jxb/eraa278.

Langensiepen M, Kupisch M, Graf A, Schmidt M, Ewert F. 2014. Improving the stem heat balance method for determining sap-flow in wheat. Agricultural and Forest Meteorology 186, 34–42.

Langensiepen M, Kupisch M, Wijk MT Van, Ewert F. 2012. Analyzing transient closed chamber effects on canopy gas exchange for optimizing flux calculation timing. Agricultural and Forest Meteorology 164, 61–70.

Langensiepen, M., Kupisch, M., Graf, A., Schmidt, M. and Ewert, F.: Improving the stem heat balance method for determining sap-flow in wheat, Agric. For. Meteorol, 186, 34–42, doi:10.1016/j.agrformet.2013.11.007, 2014.

Langensiepen, M., M. Fuchs, H. Bergamaschi, S. Moreshet, Y. Cohen, et al. 2009. Quantifying the uncertainties of transpiration calculations with the Penman-Monteith equation under different climate and optimum water supply conditions. Agric. For. Meteorol. 149(6–7): 1063–1072. doi: 10.1016/j.agrformet.2009.01.001.

Lei, G., W. Zeng, T.H. Nguyen, J. Zeng, H. Chen, et al. 2021. Relating Soil-Root Hydraulic Resistance Variation with Stomatal Regulation in the Water Transport Simulation Process Key points : Keywords : Water Resour. Res. Under revi.

Leuning, R. 1995. A critical appraisal of a combined stomatal-photosynthesis model for C3 plants. Plant Cell Environ. 18(4): 339–355. doi: 10.1111/j.1365-3040.1995.tb00370.x.

Levin, A.D., L.E. Williams, and M.A. Matthews. 2019. A continuum of stomatal responses to water deficits among 17 wine grape cultivars (Vitis vinifera). Funct. Plant Biol. 47(1): 11–25. doi: 10.1071/FP19073.

Li Y, Fuchs M, Cohen S, Cohen Y, Wallach R. 2002. Water uptake profile response of corn to soil. Plant Cell and Environment 25, 491–500.

Li Y, Sperry JS, Shao M. 2009. Hydraulic conductance and vulnerability to cavitation in corn (Zea mays L.) hybrids of differing drought resistance. Environmental and Experimental Botany 66, 341–346.

Li, L., Z.L. Yang, A.M. Matheny, H. Zheng, S.C. Swenson, et al. 2021. Representation of Plant Hydraulics in the Noah-MP Land Surface Model: Model Development and Multiscale Evaluation. J. Adv. Model. Earth Syst. 13(4): 1–27. doi: 10.1029/2020MS002214.

Li, X., Feng, Y. and Boersma, L.: Partition of photosynthates between shoot and root in spring wheat (Triticum aestivu, L.) as a function of soil water potential and root temperature, Plant Soil, (164), 43–50 [online] Available from: https://link.springer.com/content/pdf/10.1007/BF00010109.pdf, 1994.

Li, Y., W. Kinzelbach, J. Zhou, G.D. Cheng, and X. Li. 2012. Modelling irrigated maize with a combination of coupled-model simulation and uncertainty analysis, in the northwest of China. Hydrol. Earth Syst. Sci. 16(5): 1465–1480. doi: 10.5194/hess-16-1465-2012.

Lipiec, J., Siczek, A., Sochan, A. and Bieganowski, A.: Geoderma Effect of sand grain shape on root and shoot growth of wheat seedlings, Geoderma, 265, 1–5, doi:10.1016/j.geoderma.2015.10.022, 2016.

Lynch, J.P. 2013. Steep, cheap and deep: An ideotype to optimize water and N acquisition by maize root systems. Ann. Bot. 112(2): 347–357. doi: 10.1093/aob/mcs293.

Mahfouf, J. F., Ciret, C., Ducharne, A., Irannejad, P., Noilhan, J., Shao, Y., Thornton, P., Xue, Y. and Yang, Z. L.: Analysis of transpiration results from the RICE and PILPS workshop, Glob. Planet. Change, 13(1–4), 73–88, doi: 10.1016/0921-8181(95)00039-9, 1996.

Martínez-Vilalta, J., and N. Garcia-Forner. 2017. Water potential regulation, stomatal behaviour and hydraulic transport under drought : deconstructing the iso/anisohydric concept. Plant Cell Environ. 40: 962–976. doi: 10.1111/pce.12846.

Massad, R., A. Tuzet, and O. Bethenod. 2007. The effect of temperature on C4 -type leaf photosynthesis parameters. Plant Cell Environ. 30: 1191–1204. doi: 10.1111/j.1365-3040.2007.01691.x.

Matthews RB, Azam-Ali SN, Peacock JM. 1990. Response of four sorghum lines to mid-season drought. II. Leaf characteristics. Field Crops Research 25, 297–308.

Maurel, C., and P. Nacry. 2020. Root architecture and hydraulics converge for acclimation to changing water availability. Nat. Plants 6(7): 744–749. doi: 10.1038/s41477-020-0684-5.

Maurel, C., Verdoucq, L., Luu, D.-T. and Santoni, V.: Plant Aquaporins: Membrane Channels with Multiple Integrated Functions, Annu. Rev. Plant Biol., 59(1), 595–624, doi:10.1146/annurev.arplant.59.032607.092734, 2008.

Mboh, C. M., Srivastava, A. K., Gaiser, T. and Ewert, F.: Including root architecture in a crop model improves predictions of spring wheat grain yield and above-ground biomass under water limitations, J. Agron. Crop Sci., 205(2), 109–128, doi:10.1111/jac.12306, 2019.

Meinzer, F.C. 2002. Co-ordination of vapour and liquid phase water transport properties in plants. Plant Soil 25: 265–274.

Meinzer, F.C., D.R. Woodruff, D.E. Marias, D.D. Smith, K.A. McCulloh, et al. 2016. Mapping 'hydroscapes' along the iso- to anisohydric continuum of stomatal regulation of plant water status. Ecol. Lett. 19(11): 1343–1352. doi: 10.1111/ele.12670.

Merotto Jr, A. and Mundstock, C. M.: Wheat growth as affected by soil strength, Rev. Bras. Ciênc. Solo, 23(2), 197–202, 1999.

Meunier, F., M. Zarebanadkouki, M.A. Ahmed, A. Carminati, V. Couvreur, et al. 2018. Hydraulic conductivity of soil-grown lupine and maize unbranched roots and maize root-shoot junctions. J. Plant Physiol. 227(February): 31–44. doi: 10.1016/j.jplph.2017.12.019.

Meunier, F., M. Zarebanadkouki, M.A. Ahmed, A. Carminati, V. Couvreur, et al. 2018. Hydraulic conductivity of soil-grown lupine and maize unbranched roots and maize root-shoot junctions. J. Plant Physiol. 227(January): 31–44. doi: 10.1016/j.jplph.2017.12.019.

Miner, G.L., and W.L. Bauerle. 2019. Seasonal responses of photosynthetic parameters in maize and sunflower and their relationship with leaf functional traits. Plant Cell Environ. 42(5): 1561–1574. doi: 10.1111/pce.13511.

Miralles DJ, Slafer GA. 1997. Radiation interception and radiation use efficiency of near-isogenic wheat lines with different height. EUPHYTICA, 201–208.

Mo, X. and Liu, S.: Simulating evapotranspiration and photosynthesis of winter wheat over the growing season, Agric. For. Meteorol, 109, 203–222, 2001.

Morandage, S., A. Schnepf, D. Leitner, M. Javaux, H. Vereecken, et al. 2019. Parameter sensitivity analysis of a root system architecture model based on virtual field sampling. Plant Soil 438(1–2): 101–126. doi: 10.1007/s11104-019-03993-3.

Morandage, S., J. Vanderborght, M. Zörner, G. Cai, D. Leitner, et al. 2021. Root architecture development in stony soils. Vadose Zo. J. (April): 1–17. doi: 10.1002/vzj2.20133.

Moreshet, S., M. Fuchs, Y. Cohen, Y. Cohen, and M. Langensiepen. 1996. Water Transport Characteristics of Cotton as Affected by Drip Irrigation Layout. Agron. J. 88: 717–722. doi: 10.2134/agronj1996.00021962008800050006x.

Moreshet, S., Y. Cohen, G. Green, and M. Fuchs. 1990. The Partitioning of Hydraulic Conductances within Mature Orange Trees. J. Exp. Bot. 41(228): 833–839. http://www.jstor.org/stable/23695061.

Moulia B. 1994. Biomechanics of leaf rolling. Biomimetics 2, 267–281.

Munns, R., J.B. Passioura, J. Guo, O. Chazen, and G.R. Cramer. 2000. Water relations and leaf expansion: Importance of time scale. J. Exp. Bot. 51(350): 1495–1504. doi: 10.1093/jexbot/51.350.1495.

Musick JT, Dusek DA. 1980. Planting Date and Water Deficit Effects on Development and Yield of Irrigated Winter Wheat1. Agronomy Journal 72, 45–52.

Nguyen TH, Langensiepen M, Hüging H, Gaiser T, Seidel S, Ewert F. 2022. Expansion and evaluation of two coupled root-shoot models in simulating CO2 and H2O fluxes and growth of maize. Vadose zone Journal. DOI: 10.1002/vzj2.20181

Nguyen, T.H., M. Langensiepen, J. Vanderborght, H. Hüging, C.M. Mboh, et al. 2020. Comparison of root water uptake models in simulating CO2 and H2O fluxes and growth of wheat. Hydrol. Earth Syst. Sci. (24): 4943–4969. doi: 10.5194/hess-24-4943-2020.

Nissanka SP, Dixon MA, Tollenaar M. 1997. Canopy gas exchange response to moisture stress in old and new maize hybrid. Crop Science 37, 172–181.

Noordwijk, M.V.A.N., and G. Brouwer. 1991. Review of Quantitative Root Length Data in Agriculture. In: McMICHAEL, B.L. and PERSSON, H., editors, Plant Roots and their Environment. Elsevier. p. 515–525

Nye, P.H. 1994. The effect of root shrinkage on soil water inflow. Phi.Trans.R.Soc.Lond. B. 345: 395–402.

Oleson, K.W., D.M. Lawrence, G.B. Bonan, B. Drewniak, M. Huang, et al. 2013. Technical Note _Technical Description of version 4.5 of the Community Land Model (CLM). NCAR/TN-50(July).

Olioso A, Carlson TN, Brisson N. 1996. Simulation of diurnal transpiration and photosynthesis of a water stressed soybean crop. Agricultural and Forest Meteorology 81, 41–59.

Ouyang, W., P.C. Struik, X. Yin, and J. Yang. 2017. Stomatal conductance, mesophyll conductance, and trans piration efficiency in relation to leaf anatomy in rice and wheat genotypes under drought. J. Exp. Bot. 68(18): 5191–5205. doi: 10.1093/jxb/erx314.

P. G. Jarvis. 1976. The interpretation of the variations in the leaf water potential and stomatal conductance found in canopies in the field. Phi.Trans.R.Soc.Lond. B. 273: 593–610.

Parent, B., C. Hachez, E. Redondo, and T. Simonneau. 2012. Drought and Abscisic Acid Effects on Aquaporin Content Translate into Changes in Hydraulic Conductivity and Leaf Growth Rate : A Trans-Scale Approach 1 [W][OA]. Plant Physiol. 149(April 2009): 2000–2012. doi: 10.1104/pp.108.130682.

Park, H., and S. Jeong. 2021. Leaf area index in Earth system models: How the key variable of vegetation seasonality works in climate projections. Environ. Res. Lett. 16(3). doi: 10.1088/1748-9326/abe2cf.

Pawłowicz, I., and K. Masajada. 2019. Aquaporins as a link between water relations and photosynthetic pathway in abiotic stress tolerance in plants. Gene 687: 166–172. doi: https://doi.org/10.1016/j.gene.2018.11.031.

Peng, B., K. Guan, J. Tang, E.A. Ainsworth, S. Asseng, et al. 2020. Towards a multiscale crop modelling framework for climate change adaptation assessment. Nat. Plants 6(4): 338–348. doi: 10.1038/s41477-020-0625-3.

Peng, B., X. Liu, X. Dong, Q. Xue, C.B. Neely, et al. 2019. Root morphological traits of winter wheat under contrasting environments. J. Agron. Crop Sci. 205(6): 571–585. doi: 10.1111/jac.12360.

Perdomo JA, Carmo-silva E, Hermida-carrera C, Flexas J. 2016. Acclimation of Biochemical and Diffusive Components of Photosynthesis in Rice, Wheat, and Maize to Heat and Water Deficit : Implications for Modeling Photosynthesis. Frontiers in Plant science 7.

Perdomo JA, Conesa MÀ, Medrano H, Ribas-carbó M. 2015. Effects of long-term individual and combined water and temperature stress on the growth of rice, wheat and maize : relationship with morphological and physiological acclimation. Physiologia Plantarum 155, 149–165.

Perez, P. J., Lecina, S., Castellvi, F., Mart, A. and Villalobos, F. J.: A simple parameterization of bulk canopy resistance from climatic variables for estimating hourly evapotranspiration, Hydrol. Process, 532(December 2003), 515–532, doi:10.1002/hyp.5919, 2006.

Petersen, K.L., S. Moreshet, and M. Fuchs. 1991. Stomatal Responses of Field-Grown Cotton to Radiation and Soil Moisture. Agron. J. 83: 1059–1065. doi: 10.2134/agronj1991.00021962008300060024x.

Peterson, C. A. and Steudle, E.: Lateral hydraulic conductivity of early metaxylem vessels in Zea mays L. roots, Planta, 189(2), 288–297, doi: 10.1007/BF00195088, 1993.

Pinheiro C, Chaves MM. 2011. Photosynthesis and drought: Can we make metabolic connections from available data? Journal of Experimental Botany 62, 869–882.

Poni S, Galbignani M, Magnanini E, Bernizzoni F, Vercesi A, Gatti M, Merli MC. 2014. Scientia Horticulturae The isohydric cv . Montepulciano (Vitis vinifera L.) does not improve its whole-plant water use efficiency when subjected to pre-veraison water stress. Scientia Horticulturae 179, 103–111.

Pou A, Medrano H, Tomas M, Martorell S, Ribas-Carbó M, Flexas J. 2012. Anisohydric behaviour in grapevines results in better performance under moderate water stress and recovery than isohydric behaviour. Plant and Soil 359, 335–349.

Prolingheuer, N., B. Scharnagl, A. Graf, H. Vereecken, and M. Herbst. 2010. Spatial and seasonal variability of heterotrophic and autotrophic soil respiration in a winter wheat stand. Biogeosciences Discuss 7: 9137–9173. doi: 10.5194/bgd-7-9137-2010.

Qi, D., T. Hu, X. Song, and M. Zhang. 2019. Effect of nitrogen supply method on root growth and grain yield of maize under alternate partial root-zone irrigation. Sci. Rep. 9(1): 1–10. doi: 10.1038/s41598-019-44759-2.

Quijano, J. C. and Kumar, P.: Numerical simulations of hydraulic redistribution across climates: The role of the root hydraulic conductivities, Water Resour. Res., 51(10), 8529–8550, doi: 10.1002/2014WR016509, 2015.

Ramalho JDC, Chaves MM. 1991. Drought effects on plant water relations and carbon gain in two lines of Lupinus alpus L. European Journal of Agronomy 1, 271–280.

Ratzmann, G., F.C. Meinzer, and B. Tietjen. 2019. Iso/Anisohydry: Still a Useful Concept. Trends Plant Sci. 24(3): 191–194. doi: 10.1016/j.tplants.2019.01.001.

Reicosky DC, Deaton DE, Parsons JE. 1980. Canopy air temperatures and evapotranspiration from irrigated and stressed soybeans. Agricultural Meteorology 21, 21–35.

Richards RA, Rebetzke GJ, Condon AG, van Herwaarden AF. 2002. Breeding Opportunities for Increasing the Efficiency of Water Use and Crop Yield in Temperate Cereals. Crop science 42, 111–121.

Rochette P, Pattey E, Desjardins RL, Dwyer LM, Stewart DW, Dubé PA. 1991. Estimation of maize (Zea mays L.) canopy conductance by scaling up leaf stomatal conductance. Agricultural and Forest Meteorology 54, 241–261.

Rodrigues ML, Pacheco CM a, Chaves MM. 1995. Soil-plant water relations, root distribution and biomass partitioning in Lupinus albus L .under drought conditions. 46, 947–956.

Rodriguez, D., Ewert, F., Goudriaan, J., Manderscheid, R., Burkart, S. and Weigel, H. J.: Modelling the response of wheat canopy assimilation to atmospheric CO2 concentrations, New Phytol., 150(2), 337–346, doi:10.1046/j.1469-8137.2001.00106.x, 2001.

Rodriguez-Dominguez, C.M., and T.J. Brodribb. 2020. Declining root water transport drives stomatal closure in olive under moderate water stress. New Phytol. 225(1): 126–134. doi: 10.1111/nph.16177.

Rodríguez-Gamir, J., J. Xue, M.J. Clearwater, D.F. Meason, P.W. Clinton, et al. 2019. Aquaporin regulation in roots controls plant hydraulic conductance, stomatal conductance, and leaf water potential in Pinus radiata under water stress. Plant Cell Environ. 42(2): 717–729. doi: 10.1111/pce.13460.

Roman DT, Novick KA, Brzostek ER, Dragoni D, Rahman F, Phillips RP. 2015. The role of isohydric and anisohydric species in determining ecosystem-scale response to severe drought. Oecologia 179, 641–654.

Sade N, Gebremedhin A, Moshelion M. 2012. Risk-taking plants Anisohydric behavior as a stress-resistance trait. Plant singaling & Behavior 7, 767–770.

Sadras VO, Milroy SP. 1996. Soil-water thresholds for the responses of leaf expansion and gas exchange : A review. Field Crops Research 47, 253–266.

Salah BHH, Tardieu F. 1997. Control of Leaf Expansion Rate of Droughted Maize Plants under Fluctuating Evaporative Demand' A Superposition of Hydraulic and Chemical Messages ? Plant Physiology 114, 893–900.

Saliendra, N., J. Sperry, and J. Comstock. 1995. Influence of leaf water status on stomatal response to humidity, hydraulic conductance, and soil drought in *Betula occidentalis*. Planta 196(2): 357–366. doi: 10.1007/BF00201396.

Schakel K, Hall A. 1979. Reversible Leaflet Movements in Relation to Drought Adaptation of Cowpeas, Vigna unguiculata (L.) Walp. Functional Plant Biology 6, 265–276.

Schoppach R, Taylor JD, Majerus E, Claverie E, Baumann U, Suchecki R, Fleury D, Sadok W. 2016. High resolution mapping of traits related to whole-plant transpiration under increasing evaporative demand in wheat. Journal of Experimental Botany 67, 2847–2860.

Schultz HR. 2003. Differences in hydraulic architecture account for near-isohydric and anisohydric behaviour of two field-grown Vitis vinifera L. cultivars during drought. Plant, Cell and Environment 26, 1393–1405.

Shackel KA, Hall AE. 1983. Comparison of Water Relations and Osmotic Adjustment in Sorghum and Cowpea Under Field Conditions. Functional Plant Biology 10, 423–435.

Shahzad, Z., and A. Amtmann. 2017. Food for thought: how nutrients regulate root system architecture. Curr. Opin. Plant Biol. 39: 80–87. doi: 10.1016/j.pbi.2017.06.008.

Shorinola, O., Kaye, R., Golan, G., Peleg, Z., Kepinski, S. and Uauy, C.: Genetic screening for mutants with altered seminal root numbers in hexaploid wheat using a high-throughput root phenotyping platform, G3 Genes, Genomes, Genet., 9(9), 2799–2809, doi:10.1534/g3.119.400537, 2019.

Singh KP, Kumar V. 1979. Influence of irrigation on the leaf water potentials and yield of wheat and barley at two dates of sowing. Field Crops Research, 117–124.

Sperry, J. S., Stiller, V. and Hacke, U. G.: Xylem Hydraulics and the Soil–Plant–Atmosphere Continuum: Opportunities and Unresolved Issues, Agron. J., 2003(95), 1362–1370, 1998.

Sperry, J. S.: Hydraulic constraints on plant gas exchange, Agric. For. Meteorol, 104(1), 13–23, doi: 10.1016/S0168-1923(00)00144-1, 2000.

Srivastava, R. K., Panda, R. K., Chakraborty, A. and Halder, D.: Comparison of actual evapotranspiration of irrigated maize in a sub-humid region using four different canopy resistance based approaches, Agric. Water Manag., 202(February), 156–165, doi:10.1016/j.agwat.2018.02.021, 2018.

Stadler A, Rudolph S, Kupisch M, Langensiepen M, van der Kruk J, Ewert F. 2015. Quantifying the effects of soil variability on crop growth using apparent soil electrical conductivity measurements. European Journal of Agronomy 64, 8–20.

Sulis, M., M. Langensiepen, P. Shrestha, A. Schickling, C. Simmer, et al. 2015. Evaluating the influence of plant-specific physiological parameterizations on the partitioning of land surface energy fluxes. J. Hydrometeorol. 16(2): 517–533. doi: 10.1175/JHM-D-14-0153.1.

Sulis, M., V. Couvreur, J. Keune, G. Cai, I. Trebs, et al. 2019. Incorporating a root water uptake model based on the hydraulic architecture approach in terrestrial systems simulations. Agric. For. Meteorol. 269–270(July 2018): 28–45. doi: 10.1016/j.agrformet.2019.01.034.

Sunita, C., T.R. Sinclair, C.D. Messina, and M. Cooper. 2014. Hydraulic conductance of maize hybrids differing in transpiration response to vapor pressure deficit. Crop Sci. 54(3): 1147–1152. doi: 10.2135/cropsci2013.05.0303.

Tafteh, A., and A.R. Sepaskhah. 2012. Application of HYDRUS-1D model for simulating water and nitrate leaching from continuous and alternate furrow irrigated rapeseed and maize fields. Agric. Water Manag. 113: 19–29. doi: 10.1016/j.agwat.2012.06.011.

Taiz L, Zeiger E. 2006. *Plant Physiology*. 4th ed. Sinauer Associates, Inc. Publishers, Massachusetts.

Tao, F., T. Palosuo, R.P. Roetter, C.G. Hernandez Diaz-Ambrona, M. Ines Minguez, et al. 2020. Why do crop models diverge substantially in climate impact projections? A comprehensive analysis based on eight barley crop models. Agric. For. Meteorol. 281. doi: 10.1016/j.agrformet.2019.107851.

Tardieu F, Draye X, Javaux M. 2017. Root Water Uptake and Ideotypes of the Root System: Whole-Plant Controls Matter. Vadose Zone Journal 16, 0.

Tardieu F, Simonneau T, Muller B. 2018. The Physiological Basis of Drought Tolerance in Crop Plants: A Scenario-Dependent Probabilistic Approach. Annual Review of Plant Biology 69, 733–759.

Tardieu F, Simonneau T, Parent B. 2015. Modelling the coordination of the controls of stomatal aperture, transpiration, leaf growth, and abscisic acid: Update and extension of the Tardieu-Davies model. Journal of Experimental Botany 66, 2227–2237.

Tardieu F, Simonneau T. 1998. Variability among species of stomatal control under fluctuating soil water status and evaporative demand: modelling isohydric and anisohydric behaviours. Journal of Experimental Botany 49, 419–432.

Tardieu, F. 2016. Too many partners in root – shoot signals . Does hydraulics qualify as the only signal that feeds back over time for reliable stomatal. New Phytol. 212: 802–804.

Tardieu, F., and B. Parent. 2017. Predictable 'meta-mechanisms' emerge from feedbacks between transpiration and plant growth and cannot be simply deduced from short-term mechanisms. Plant Cell Environ. 40(6): 846–857. doi: 10.1111/pce.12822.

Tardieu, F., and W.J. Davies. 1993. Integration of hydraulic and chemical signalling in the control of stomatal conductance and water status of droughted plants. Plant. Cell Environ. (16): 341–349. doi: 10.1111/j.1365-3040.1993.tb00880.x.

Tardieu, F., Parent, B., Caldeira, C. F. and Welcker, C.: Genetic and Physiological Controls of Growth under Water Deficit, Plant Physiol., 164(4), 1628–1635, doi:10.1104/pp.113.233353, 2014.

Tim J. Brodribb; Scott A. M. McAdam. 2011. Passive Origins of Stomatal Control in vascular plants. Science (80). 331(6017): 582–585. doi: 10.1126/science.1197985.

Tracy, S.R., K.A. Nagel, J.A. Postma, H. Fassbender, A. Wasson, et al. 2020. Crop Improvement from Phenotyping Roots: Highlights Reveal Expanding Opportunities. Trends Plant Sci. 25(1): 105–118. doi: 10.1016/j.tplants.2019.10.015.

Trillo N, Fernández RJ. 2005. Wheat plant hydraulic properties under prolonged experimental drought: Stronger decline in root-system conductance than in leaf area. Plant and Soil 277, 277–284.

Tsuda, M. and Tyree, M. T.: Whole-plant hydraulic resistance and vulnerability segmentation in Acer saccharinum, Tree Physiol., (17), 351–357, 1997.

Turner NC, HENSON IE. 1989. Comparative water relations and gas exchange of wheat and lupins in the field. Str.and Func.Resp.To Env.Str., 293–304.

Turner NC, Schulze ED, Gollan T. 1984. The responses of stomata and leaf gas exchange to vapour pressure deficits and soil water content - I. Species comparisons at high soil water contents. Oecologia 63, 338–342.

Tuzet A, Perrier A, Leuning R. 2003. A coupled model of stomatal conductance, photosynthesis. Plant, Cell and Environment 26, 1097–1116.

Tyree MT, Fiscus EL, Wullschleger SD, Dixon MA. 1986. Detection of Xylem Cavitation in Corn under Field Conditions. Plant Physiology 82, 597–599.

Tyree MT, Sperry JS. 1988. Do Woody-plants Operate Near the Point of Catastrophic Xylem Dysfunction Caused By Dynamic Water-stress - Answers From A Model. Plant Physiology 88, 574–580.

Tyree, M.T., E.L. Fiscus, S.D. Wullschleger, and M.A. Dixon. 1986. Detection of Xylem Cavitation in Corn under Field Conditions. Plant Physiol. 82(2): 597–599. doi: 10.1104/pp.82.2.597.

Vadez, V.: Root hydraulics : The forgotten side of roots in drought adaptation, F. Crop. Res., 165, 15–24, 2014.

van Dam, J. C.: Field-scale water flow and solute transport. SWAP model concepts, parameter estimation and case studies. [online] Available from: http://www.pearl.pesticidemodels.eu/pdf/swap_thesis.pdf, 2000.

van Genuchten, M. T.: A Closed-form Equation for Predicting the Hydraulic Conductivity of Unsaturated Soils, Soil Sci. Soc. Am. J., 4, 892–898, 1980.

van Laar, H. H., Goudriaan, J. and Van Keulen, H.: SUCROS97 : Simulation of crop growth for potential and water-limited production situations., 1997.

Vanderborght, J., Graf, A., Steenpass, C., Scharnagl, B., Prolingheuer, N., Herbst, M., Franssen, H. H. and Vereecken, H.: Within-Field Variability of Bare Soil Evapora Ɵ on Derived from Eddy Covariance Measurements, Vadose Zo. J., 9, 943–954, doi:10.2136/vzj2009.0159, 2010.

Vanderborght, J., V. Couvreur, F. Meunier, A. Schnepf, H. Vereecken, et al. 2021. From hydraulic root architecture models to macroscopic representations of root hydraulics in soil water flow and land surface models. Hydrol. Earth Syst. Sci. Discuss. (January): 1–37. doi: 10.5194/hess-2021-14.

Vandoorne, B., Beff, L., Lutts, S. and Javaux, M.: Root Water Uptake Dynamics of var. Under Water-Limited Conditions, Vadose Zo. J., 11(3), 0, doi:10.2136/vzj2012.0005, 2012.

Vereecken, H., A. Schnepf, J.W. Hopmans, M. Javaux, D. Or, et al. 2016. Modeling Soil Processes: Review, Key Challenges, and New Perspectives. Vadose Zo. J. 15(5): vzj2015.09.0131. doi: 10.2136/vzj2015.09.0131.

Verhoef, A. and Egea, G.: Agricultural and Forest Meteorology Modeling plant transpiration under limited soil water : Comparison of different plant and soil hydraulic parameterizations and preliminary implications for their use in land surface models, Agric. For. Meteorol, 191, 22–32, doi:10.1016/j.agrformet.2014.02.009, 2014.

Vico, G. and Porporato, A.: Modelling C3 and C4 photosynthesis under water-stressed conditions, Plant Soil, 313(1–2), 187–203, doi: 10.1007/s11104-008-9691-4, 2008.

Vilà-Guerau De Arellano, J., P. Ney, O. Hartogensis, H. De Boer, K. Van Diepen, et al. 2020. CloudRoots: Integration of advanced instrumental techniques and process modelling of sub-hourly and sub-kilometre land-Atmosphere interactions. Biogeosciences 17(17): 4375–4404. doi: 10.5194/bg-17-4375-2020.

Visentin, I., M. Vitali, M. Ferrero, Y. Zhang, C. Ruyter-Spira, et al. 2016. Low levels of strigolactones in roots as a component of the systemic signal of drought stress in tomato. New Phytol. 212(4): 954–963. doi: 10.1111/nph.14190.

Vitale L, Di Tommasi P, Arena C, Fierro A, Virzo De Santo A, Magliulo V. 2007. Effects of water stress on gas exchange of field grown Zea mays L. in Southern Italy: An analysis at canopy and leaf level. Acta Physiologiae Plantarum 29, 317–326.

Vogel, T., J. Votrubova, M. Dohnal, and J. Dusek. 2017. A Simple Representation of Plant Water Storage Effects in Coupled Soil Water Flow and Transpiration Stream Modeling. Vadose Zo. J. 16(5): vzj2016.12.0128. doi: 10.2136/vzj2016.12.0128.

von Caemmerer S. 2000. Biochemical models of leaf photosynthesis. In: Caemmerer S von, ed. Techniques in plant sciences. CSIRO publishing, 176.

Wang, J., Yu, Q. and Lee, X.: Simulation of crop growth and energy and carbon dioxide fluxes at different time steps from hourly to daily, Hydrol. Process, 21, 2267–2274, doi: 10.1002/hyp.6414, 2007.

Wang, Q., Z. Huo, S. Feng, C. Yuan, and J. Wang. 2015. Comparison of Spring Maize Root Water Uptake Models Under Water and Salinity Stress Validated with Field Experiment Data. Irrig. Drain. 64(5): 669–682. doi: 10.1002/ird.1939.

Wang, Y.P., and R. Leuning. 1998. A two-leaf model for canopy conductance, photosynthesis and partitioning of available energy I: Model description and comparison with a multi-layered model. Agric. For. Meteorol. 91(1–2): 89–111. doi: 10.1016/S0168-1923(98)00061-6.

Watt, M., Silk, W. K. and Passioura, J. B.: Rates of Root and Organism Growth, Soil Conditions, and Temporal and Spatial Development of the Rhizosphere, an, 97, 839–855, doi:10.1093/aob/mcl028, 2006.

Webber H, Lischeid G, Sommer M, Finger R, Nendel C, Gaiser T, Ewert F. 2020. No perfect storm for crop yield failure in Germany. Environmental Research Letters 15.

Webber, H., G. Lischeid, M. Sommer, R. Finger, C. Nendel, et al. 2020. No perfect storm for crop yield failure in Germany. Environ. Res. Lett. 15(10). doi: 10.1088/1748-9326/aba2a4.

Welcker C, Sadok W, Dignat G, Renault M, Salvi S, Charcosset A, Tardieu F. 2011. A common genetic determinism for sensitivities to soil water deficit and evaporative demand: Meta-analysis of quantitative trait loci and introgression lines of maize. Plant Physiology 157, 718–729.

Wesseling, J. G. and Brandyk, T.: Introduction of occurrence of high groundwater levels and surface water storage in computer program SWATRE, (1636), 1:48, 1985.

Wesseling, J. G., Elbers, J. A., Kabat, P. and B. J. van den Broek: SWATRE: instructions for input, Internal Note, Winand Staring Centre, Wageningen, the Netherlands, , 1991, 1991.

Westgate, M.E., and J.S. Boyer. 1985. Osmotic adjustment and the inhibition of leaf, root, stem and silk growth at low water potentials in maize. Planta 164: 540–549.

Wilkinson, S., and W.J. Davies. 2002. ABA-based chemical signalling: The co-ordination of responses to stress in plants. Plant, Cell Environ. 25(2): 195–210. doi: 10.1046/j.0016-8025.2001.00824.x.

Wilkinson, S., J.E. Corlett, L. Oger, and W.J. Davies. 1998. Effects of xylem pH on transpiration from wild-type and flacca tomato leaves: A vital role for abscisic acid in preventing excessive water loss even from well-watered plants. Plant Physiol. 117(2): 703–709. doi: 10.1104/pp.117.2.703.

Williams, J., and R. Izaurralde. 2005. The APEX model. Watershed Model. doi: 10.1201/9781420037432.ch18.

Willmott, C. J.: ON THE VALIDATION OF MODELS, Phys. Geogr., 2(2), 184–194, doi:10.1080/02723646.1981.10642213, 1981.

Wöhling, T., Gayler, S., Priesack, E., Ingwersen, J., Wizemann, H. D., Högy, P., Cuntz, M., Attinger, S., Wulfmeyer, V. and Streck, T.: Multiresponse, multiobjective calibration as a diagnostic tool to compare accuracy and structural limitations of five coupled soil-plant models and CLM3.5, Water Resour. Res., 49(12), 8200–8221, doi: 10.1002/2013WR014536, 2013.

Wong, S.C., R. Cowan, and G.D. Farquhar. 1979. Stomatal conductance correlates with photosynthetic capacity. Nature 282: 424–426.

Wright STC. 1977. The relationship between leaf water potential ψleaf and the levels of abscisic acid and ethylene in excised wheat leaves. Planta 134, 183–189.

Wu, G., K. Guan, Y. Li, K.A. Novick, X. Feng, et al. 2021. Interannual variability of ecosystem iso/anisohydry is regulated by environmental dryness.

Xiong, D., and M. Nadal. 2020. Linking water relations and hydraulics with photosynthesis. Plant J. 101(4): 800–815. doi: 10.1111/tpj.14595.

Yang, H., P. Grassini, K.G. Cassman, R.M. Aiken, and P.I. Coyne. 2017. Improvements to the Hybrid-Maize model for simulating maize yields in harsh rainfed environments. F. Crop. Res. 204: 180–190. doi: 10.1016/j.fcr.2017.01.019.

Yang, W., H. Feng, X. Zhang, J. Zhang, J.H. Doonan, et al. 2020. Crop Phenomics and High-Throughput Phenotyping: Past Decades, Current Challenges, and Future Perspectives. Mol. Plant 13(2): 187–214. doi: 10.1016/j.molp.2020.01.008.

Yang, W., S. Guo, P. Li, R. Song, and J. Yu. 2019. Foliar antitranspirant and soil superabsorbent hydrogel affect photosynthetic gas exchange and water use efficiency of maize grown under low rainfall conditions. J. Sci. Food Agric. 99(1): 350–359. doi: 10.1002/jsfa.9195.

Yin, X. and Schapendonk, A. H. C. M.: Simulating the partitioning of biomass and nitrogen between roots and shoot in crop and grass plants, NJAS - Wageningen J. Life Sci., 51(4), 407–426, doi:10.1016/S1573-5214(04)80005-8, 2004.

Yin, X., and H.H. Van Laar. 2005. Crop Systems Dyanamics: An ecophysiological simulation model for genotype-by-environment interactions. 1st ed. Wageningen Academic Publishers.

Yin, X., and P.C. Struik. 2009. C3 and C4 photosynthesis models : An overview from the perspective of crop modelling. Wageningen J. Life Sci. 57: 27–38. doi: 10.1016/j.njas.2009.07.001.

Yin, X., Struik, P. C., Romero, P., Harbinson, J., Evers, J. B., Van Der Putten, P. E. L. and Vos, J.: Using combined measurements of gas exchange and chlorophyll fluorescence to estimate parameters of a biochemical C3 photosynthesis model: A critical appraisal and a new integrated approach applied to leaves in a wheat (Triticum aestivum) canopy, Plant, Cell Environ., 32(5), 448–464, doi:10.1111/j.1365-3040.2009.01934.x, 2009.

Zeng, X., Dai, Y.-J., Dickinson, R. E. and Shaikh, M.: The role of root distribution for climate simulation over land, Geophys. Res. Lett., 25(24), 4533–4536, doi: 10.1029/1998GL900216, 1998.

Zhan, A., H. Schneider, and J.P. Lynch. 2015. Reduced Lateral Root Branching Density Improves Drought Tolerance in Maize. Plant Physiol. 168(4): 1603–1615. doi: 10.1104/pp.15.00187.

Zhan, X., Y. Xue, and G.J. Collatz. 2003. An analytical approach for estimating CO2 and heat fluxes over the Amazonian region. Ecol. Modell. 162(1–2): 97–117. doi: 10.1016/S0304-3800(02)00405-2.

Zhang, L., L. Liu, H. Zhao, Z. Jiang, and J. Cai. 2020. Differences in near isohydric and anisohydric behavior of contrasting poplar hybrids (I-101 (Populus alba L.) x 84K (Populus alba L. x Populus glandulosa Uyeki) under drought-rehydration treatments. Forests 11(4). doi: 10.3390/F11040402.

Zhao, C., Deng, X., Shan, L., Steudle, E., Zhang, S. and Ye, Q.: Changes in Root Hydraulic Conductivity During Wheat Evolution, J. Integr. Plant Biol., 47(3), 302–310, 2005.

Zhou, H., G. Zhou, Q. He, L. Zhou, Y. Ji, et al. 2020. Environmental explanation of maize specific leaf area under varying water stress regimes. Environ. Exp. Bot. 171(November 2019): 103932. doi: 10.1016/j.envexpbot.2019.103932.